SUPRAMOLECULAR DERIVATIVES OF SELECTED BIOACTIVE COMPOUNDS:

A PHYSICOCHEMICAL STUDY

By: HALIMA SAMSODIEN(M.Pharm)

Thesis Presented for the Degree of

DOCTOR OF PHILOSOPHY

in the Department of Chemistry

UNIVERSITY OF CAPE TOWN

December 2010

ACKNOWLEDGEMENTS

I would like to thank:
My supervisors: Professor Mino Caira for his excellent supervision, direction and encouragement and Professor Susan Bourne for her support and motivation. A special thank you for allowing a part-time study within the Centre for Supramolecular Chemistry Research, UCT.

Professor Luigi Nassimbeni for his kindness and for being a constant source of knowledge.

The Supramolecular Chemistry Research group, UCT, for their friendship and camaraderie.

The University of the Western Cape, colleagues and students for providing the time from work since the study was undertaken on a part-time basis.

Karin Badenhorst for her kind assistance and for always keeping me informed regarding activities of the group.

My parents who have always inspired me and guided me with wisdom. And all my family members for their support.

My most precious "Thank you" to my husband, Nizaam, my daughter, Ibtisaam and son, Adam. Without your love, support and constant patience, this would not have been possible.

PUBLICATIONS AND CONFERENCES

RELATED PUBLISHED PAPERS:

Mino R. Caira, Nicole Stieger, Wilna Liebenberg, Melgardt M. De Villiers, and Halima Samsodien, *Solvent inclusion by the Anti-HIV Drug Nevirapine: X-Ray Structures and Thermal Decomposition of Representatives Solvates*, Crystal Growth & Design, 2007, Volume 8, pp. 17-23.

Nicole Stieger, Wilna Liebenberg, Johanna C. Wessels, Halima Samsodien and Mino R. Caira, *Channel Inclusion of Primary Alcohols in Isostructural Solvates of the Antiretroviral Nevirapine: An X-ray and Thermal Analysis Study*, Structural Chemistry, 2010, Volume 21, pp. 771-777.

PARTS OF THIS THESIS HAVE BEEN PRESENTED AT THE FOLLOWING CONFERENCES:

Halima Samsodien, Mino R. Caira Susan A. Bourne and Vincent Smith, *Inclusion of Steroidal Drugs in Cyclodextrins: X-ray Structures of a DIMEB- TRIMEB- and Beta-CD-2-Methoxyestradiol Complex*. The 29th Annual Conference of the Academy of Pharmaceutical Sciences of South Africa, Rustenberg, 2008.

Wilna Liebenberg, Nicole Stieger, Mino R. Caira and Halima Samsodien, *Physico-chemical Properties of Solvated Forms of Nevirapine*, AAPS annual meeting and exposition, USA, 9 November 2009.

ABSTRACT

Halima Samsodien

SUPRAMOLECULAR DERIVATIVES OF SELECTED BIOACTIVE COMPOUNDS: A PHYSICOCHEMICAL STUDY

The author's objective was to prepare new solid phases of three bioactive compounds: the steroidal anticancer agent 2-methoxyestradiol [polymorphs and cyclodextrin (CD) inclusion complexes], its derivative 2-methoxyestradiol-*bis*-sulfamate (polymorphs), and the antiretroviral agent, nevirapine (co-crystals). The solubility and dissolution profiles of the three compounds and those of selected 'supramolecularly-derived' species were also assessed.

Three distinct phases of 2-methoxyestradiol (2ME) were successfully isolated, the most stable form (a polymorph) by the recrystallisation method, an amorph by melt studies and a solvated form by recrystallisation. 2-methoxyestradiol-*bis*-sulfamate (2MES), in the form of a hemihydrate, remained unchanged when recrystallised from various solvents. Several CDs were used for possible 2-methoxyestradiol inclusion; these were α-, β-, γ-CD, and nine derivatised cyclodextrins. Co-precipitation and kneading techniques were employed in attempts to produce inclusion complexes. An inclusion complex of 2ME was isolated with each of the following: β-CD, HPBCD, RAMEB, DIMEB and TRIMEB.

Co-crystallisation of nevirapine was attempted using twelve potential co-formers with GRAS status. Two co-crystals, one with saccharin and one with *rac*-tartaric acid, were isolated by the co-precipitation method.

Physicochemical characterisation techniques used to assess the thermal behaviour of the products included hot stage microscopy, differential scanning calorimetry and thermogravimetric analysis. UV spectrophotometry and elemental analysis were used for host-guest stoichiometric assay and purity determination respectively. X-ray powder diffraction and single crystal X-ray structure determination were used for structural analysis.

The aqueous solubility of the derivative 2MES was found to be twice that of 2ME and this was confirmed by i*n vitro* dissolution studies. The amorphous 2ME preparation had the most promising profile, indicating a dissolution rate double that of untreated 2ME.

Structural elucidation by X-ray diffraction of CD inclusion complexes of a classical steroid, represented by 2ME, was achieved for the first time and the solubility and comparative dissolution profiles of non-toxic oral CD complexes with 2ME versus untreated 2ME and its derivative 2MES were established. A marked increase in the aqueous solubility and dissolution profiles of the CD complexes relative to the untreated 2ME was established.

In the two nevirapine co-crystals, the API molecule retained the usual 'butterfly' conformation, a feature essential for antiretroviral activity. Single crystal X-ray analysis proved that these species were both genuine co-crystals, as opposed to salts.
The aqueous solubility and dissolution rate of nevirapine were significantly enhanced by both co-formers, saccharin and *rac*-tartaric acid.

TABLE OF CONTENTS

Chapter 1

INTRODUCTION

Chapter 1 *presents a literature synopsis of polymorphism, cyclodextrin inclusion and pharmaceutical co-crystallisation. These phenomena are aspects of supramolecular chemistry which is the study of non-covalent interactions between molecules, ions or radicals. More specifically, supramolecular chemistry deals with hydrogen bonding π···π, C-H···π, van der Waals and hydrophobic interactions. Furthermore, Chapter 1 provides the motivation for the study of selected drugs 2-methoxyestradiol, 2-methoxyestradiol-bis-sulfamate and nevirapine.*

1.1 POLYMORPHISM

A polymorph is defined as a 'solid crystalline phase of a given compound resulting from the possibility of at least two different arrangements of the molecules of that compound in the solid state'.[1] These forms are identical in the liquid and vapour states but differ in the way the molecules in each polymorph pack in the solid state. Owing to the differing packing arrangements, resulting physical properties which may differ between polymorphs are solubility, melting point, density, hardness, crystal shape, optical and electrical properties, vapour pressure, hygroscopicity, dissolution rate and ultimately bioavailability. Hence, polymorphs are chemically identical but may be as different in structure and physical properties as the crystals of two different compounds. A very large number of compounds, organic and inorganic, as well as elements themselves, have been shown to crystallise in two or more different crystalline arrangements, depending on conditions under which crystallisation occurs. It appears that many organic materials exist in several polymorphic forms with the number of forms found depending on the effort spent searching for them. Hence, scientists studying the concept of polymorphism emphasise the importance of applying 'due diligence'[1,2] since compounds exhibiting polymorphism demand much time for investigation. Most of these polymorphs, especially the organic ones, do not have special names but are referred to as α, β, γ etc. or I, II, III, etc. The Roman numerals are preferred and by convention Form I represents the most stable form at room temperature. Assignment of the higher numerals proceeds in order of discovery, which in general should follow their order of stability. The possibility of discovery of intermediate forms always exists. Unstable polymorphs, as a result of their greater thermodynamic activity (higher Gibbs free energy), will tend to transform to more stable forms. An intermediate form, the

metastable polymorph, is often the polymorph of choice to be incorporated into pharmaceutical preparations since, in comparison to the stable form, it has a higher solubility. Polymorphism is remarkably common, particularly within certain structural groups: 63% of barbiturates, 67% of steroids and 40% of sulphonamides exhibit polymorphism. Five polymorphs have been identified for progesterone, whereas four polymorphs and three solvates have been identified for the sulphonamide sulphabenzamide.[3] Generally polymorphs are obtained by recrystallisation from various solvents or solvent mixtures. Others can be produced without the presence of solvent by thermal techniques, particularly sublimation and re-crystallisation from the melt. Supercooling of the melt is particularly useful as well in discovering unstable modifications.[3]

Materials in the solid state can be crystalline or amorphous (or a combination of both). The crystalline materials are those in which the molecules are packed in a defined order, and this same order repeats over and over again throughout the particle. In Figure 1.1, (a) represents an ordered packing of a hypothetical molecule; here the shape of the molecule is represented by a 'hockey-stick' style image, illustrating a planar structure with a functional group pointing up at the end; (b) represents an alternative packing arrangement and (c) represents the inclusion of a solvent molecule, to produce a solvated crystalline form.

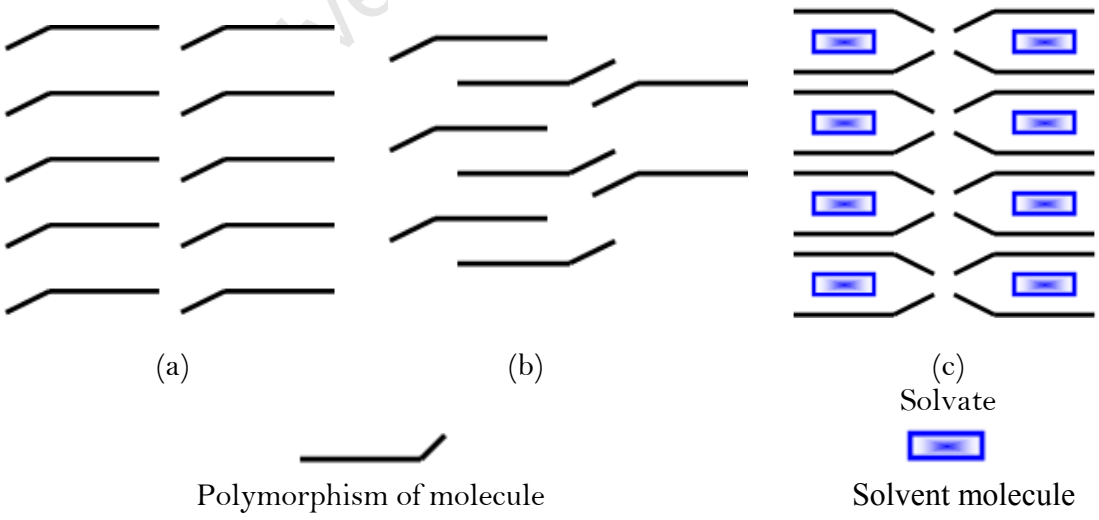

Figure 1.1 Schematic diagram illustrating polymorphism and solvatomorphism.

A characteristic property of a crystal is that it has a distinctive melting point. This is the temperature at which the crystal breaks down, owing to the molecules having gained sufficient energy from the heating process to overcome the attractive forces that hold the crystal together. It follows that crystals with weak forces holding the molecules together (such as paraffins, which only have van der Waals interactions) have low melting points, whereas crystals with strong intermolecular forces (e.g. extensive hydrogen bonding) have high melting points.[3]

If the crystallisation conditions are changed in any way, it is possible that the molecules may start to form crystals with a different packing pattern from that which occurred when the original conditions were used. The change in conditions could be a different solvent, or a change in the stirring rate, or different impurities being present. Figure 1.1(b) shows an alternative packing arrangement from that which occurred for the same molecule in Figure 1.1(a). As both the packing arrangements in Figure 1.1(a) and (b) are repeating ordered systems, they are both crystals; these would be called polymorphic forms.[3]

By looking at the packing arrangements in Figure 1.1 it can be seen that the molecules in (a) are more spaced out than those in (b), which means that the two crystal forms would have different densities (i.e. the same mass of material would be accommodated in different volumes). It looks as though it would be easier to physically pull a molecule off structure (a) than off (b), as the molecules in (b) are more interwoven into the structure. If this were the case then (a) would have a lower melting point than (b) and might dissolve more easily. Also, if an attempt were made to mill the two crystals, it appears that (a) would break easily, as there are natural break lines (either vertically or horizontally), whereas (b) does not seem to have an obvious weak line to allow easy cleavage. This could mean that the milling and compaction (for example: tabletting) properties of the two forms will differ.[3]

Brief Historical Overview

1822 Mitscherlich[4] - first recognition of the phenomenon of polymorphism; discovered that the salt $NaH_2PO_4 \cdot H_2O$ crystallises with different crystal morphologies due to differences in the internal structural arrangements of the constituent ions.

1839 Frankenheim[5] - suggested principles for the transition of one polymorph into a second.

Lehman[6] - coined the irreversible and reversible transitions as monotropic and enantiotropic respectively.

1844 Polarizing microscope invented[5,7]

1897 Ostwald[8] - addressed the relative stabilities of polymorphs using thermodynamics. It was established that the metastable form has the higher solubility and crystallises first, eventually transforming via a solution-mediated process into a more stable form.

1926 Tammann[9] - considered polymorphs as identical molecular species arranged on different lattices using X-ray crystallography.

Preparation and Analysis of Polymorphs

Preparation and investigation of polymorphs is a fundamental step in preformulation studies. Manufacturers of pharmaceuticals are required to prove that potential polymorphism of marketed drugs has been investigated so that an unwanted polymorph does not filter through to the consumer. Thus, it is significant to know which methods are likely to yield polymorphs and to employ them in the search for potential polymorphs.

A number of methods were suggested by Guillory for generating polymorphs, solvates or amorphous forms of a particular compound.[2] Amongst these methods are sublimation, crystallisation from a single or binary solvent system, vapour diffusion, thermal treatment, crystallisation from the melt, rapid pH changes, thermal desolvation of crystalline solvates, growth in the presence of additives, and grinding. Of these methods crystallisation from a variety of solvents is usually the first step in the search for polymorphic forms of a compound and has been very successful in many cases. In

addition, desolvation of crystalline solvates may also be included in these methods since it was reported[10] that the method resulted in the improvement of certain properties such as flowability and uniformity of particle size.

The first step to identifying a polymorph is describing the physical morphology of the crystal or powder. A microscope is employed in this instance. However, different morphologies may not necessarily indicate different forms and therefore we employ further analytical techniques. The second step is to determine the melting points of the various forms generated. A hot stage microscope or a differential scanning calorimeter may be employed in this instance. However, differing melting points may not prove the existence of distinct forms (polymorphs) unequivocally. The third step, which is much more informative, involves application of X-ray diffraction, thermal and spectroscopic techniques, which are respectively used to characterise the polymorphs in terms of their structures, thermodynamic stabilities and spectral energies. Once there is a clear indication that polymorphs of a compound have been found, the several analytical methods employed to characterise their individual properties will provide further information regarding properties related to each other, for example stability relationships. The range of analytical techniques used should be as broad as possible as the information obtained from them is often complementary, as suggested by Bernstein.[1] The reader is referred to Chapter 2 for a more extensive discussion on the preparation of polymorphs and the analytical tools used in their study.

Thermodynamic Stability Relationship[11]

As suggested earlier, with thermal analytical studies, the thermodynamic stability relationships between polymorphs can be established. At specified temperature and pressure, only one polymorph of a given compound is thermodynamically stable (i.e. has the minimum Gibbs free energy), and all other polymorphs are metastable to varying degrees. If this factor alone determined the outcome of crystallisation, then only one polymorph (the most stable) should appear. However, because the nuclei of different polymorphs have unique structural and interfacial properties, their free energies of activation differ, and hence, the nucleation rates of different polymorphs of the same compound generally differ.[11]

Enantiotropy vs Monotropy

Enantiotropy and monotropy are terms used to describe the reversibility or lack thereof of the phase transition between polymorphs.[6] Phase transitions are restricted thermodynamically to occur spontaneously in the direction of the stable form only. Monotropy (irreversible transition) implies that one form is the thermodynamically stable form at all temperatures. Enantiotropy (reversible phase transition) implies the presence of a transition point where the stability order of the polymorphs is reversed. The most widely used thermodynamic relationship for the treatment of stability is:

G = H – TS, where G = Gibbs free energy, H = enthalpy, T = absolute temperature and S = entropy. This relationship is used to construct diagrams that illustrate the variation of G and H with temperature to establish the stability relationship of polymorphs from zero Kelvin to just beyond their melting temperatures. Figure 1.2 illustrates these stability relationships where the subscripts '1' and '2' denote the polymorph to which the function refers, [the lower melting polymorph is denoted '2'], whilst 'L' refers to the supercooled liquid. The subscripts 'f' and 'tr' refer to 'fusion' and 'transition' respectively.

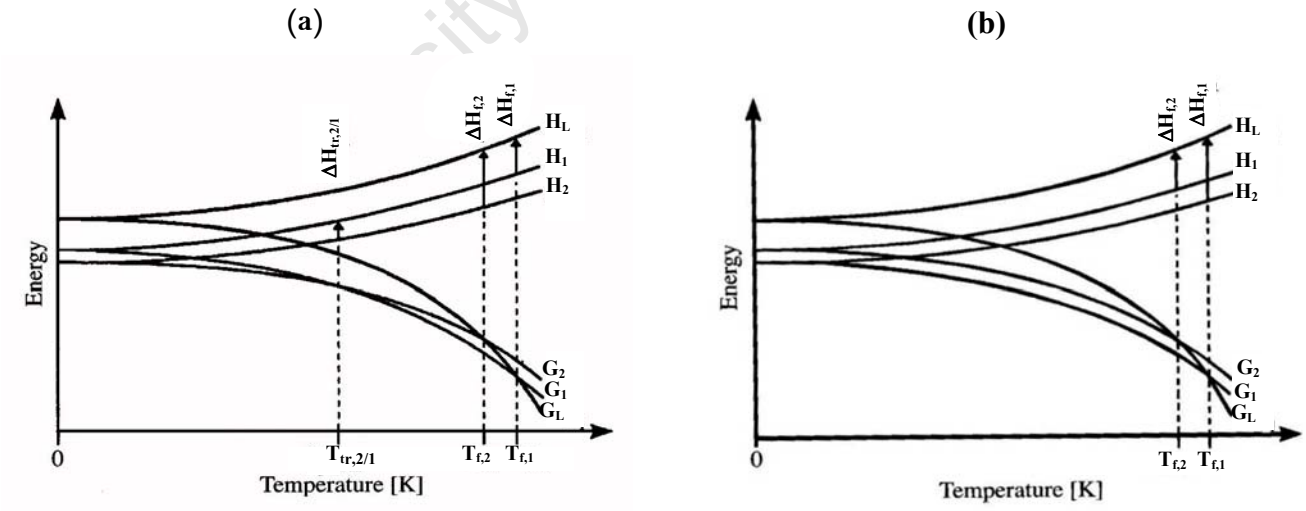

Figure 1.2 Schematic diagrams showing the variation of G and H with temperature for (a) an enantiotropic and (b) a monotropic dimorphic system.

The G curve can only have a negative slope and intersect another curve at most once, whilst the H curves have a positive slope and it is assumed that they never intersect,[1] which leads to one of the Burger and Ramberger rules.[11] which is termed the 'Heat of Transition Rule'. This states that if an endothermic phase change is observed at a particular temperature, the stability relationship is enantiotropic, otherwise it is monotropic.[11]

Other rules suggested by Burger and Ramberger include:

- Heat of fusion rule:
  If the higher melting polymorph has the higher heat of fusion, the stability relationship is monotropic, otherwise it is enantiotropic
- Entropy of fusion rule:
  If the higher melting polymorph has the higher entropy of fusion, the stability relationship is monotropic, otherwise it is enantiotropic
- Heat capacity rule:
  If the higher melting polymorph has the higher heat capacity at a given temperature then the stability relationship is enantiotropic, otherwise it is monotropic
- Density rule:
  The more stable polymorph at the absolute zero of temperature should have the higher density
- Infrared rule:
  For polymorphs with strong hydrogen bonds the one with the larger frequency for the highest frequency infrared absorption band, will have the larger entropy.

The Burger and Ramberger rules are based on statistical mechanical arguments of an ideal model of molecular crystals. Yu[12] used pure thermodynamic arguments to infer the stability relationship from melting data and derived thermodynamic formulae for calculation of ΔG_0, the difference in Gibbs free energy of the polymorphs, and their temperature slopes at the melting point of the lower melting polymorph. Extrapolation of the ΔG_0 temperature slopes to their point of intersection then yields the transition temperature, T_{tr}. The advantage of Yu's treatment is that both the stability relationship

and T_{tr} can be obtained from it. The equations necessary for the determination of the transition temperature for the process

Form 2 ($T_{f,2}$) → Form 1 ($T_{f,2}$) are:

$$\Delta H_o = \Delta H_{f,2} - \Delta H_{f,1} + (C_{p,L} - C_{p,1})(T_{f,1} - T_{f,2})$$

$$\Delta S_o = \Delta H_{f,2}/T_{f,2} - \Delta H_{f,1}/T_{f,1} + (C_{p,L} - C_{p,1}) \ln (T_{f,1}/T_{f,2}) \quad \text{and}$$

$$\Delta G_o = \Delta H_{f,1}(T_{f,2}/T_{f,1}-1) + (C_{p,L} - C_{p,1}) [T_{f,1} - T_{f,2} - T_{f,2} \ln (T_{f,1}/T_{f,2})]$$

where the subscript 0 denotes the function at the melting temperature of the lower melting form and $(C_{p,L} - C_{p,1})$ is the difference between the heat capacities of the supercooled liquid and Form 1 between the temperatures $T_{f,2}$ and $T_{f,1}$. If $\Delta G(T)$ has a linear dependence, then

$$\Delta G(T) = \Delta G_o - \Delta S_o(T-T_{f,2}) \quad \text{and the condition}$$

$$\Delta G(T_{tr}) = 0 \quad \text{yields}$$

$$T_{tr} = \Delta H_o/\Delta S_o$$

All the parameters for these equations are obtained directly from conventional differential scanning calorimetric data, except for the $(C_{p,L} - C_{p,1})$ parameter. Yu estimated the latter from the following derived equation:

$$k = (C_{p,L} - C_{p,1})/\Delta H_{f,1}$$

where the value of k, based on an empirical study of several polymorphic systems, is approximated to 0.003/K.[12]

Kinetic Considerations

Kinetic factors may also determine the polymorphic form that crystallises from solution. Figure 1.3 illustrates the Gibbs free energy vs reaction coordinate graph for a dimorphic system. It shows that even though Form 1 is the thermodynamically stable polymorph, its higher associated Gibbs free energy of activation might prevent its

formation. However, it is the rates of nucleation of the respective polymorphs that determine which one precipitates from solution and the associated Gibbs free energy of activation is merely one of the factors that determine these rates. Competitive kinetic and thermodynamic factors complicate the prediction of the form that will precipitate first. The concept of crystal size is one of the key factors of kinetic nucleation as proposed by Volmer in 1939.[13] According to this concept, a critical size of aggregated molecules must exist in solution before further growth is stabilised. This critical size is usually different for the respective polymorphs, which would thus account for different crystallisation rates. Some of the other factors influencing nucleation rates are molecular volume, surface free energy, temperature, degree of supersaturation and solubility.

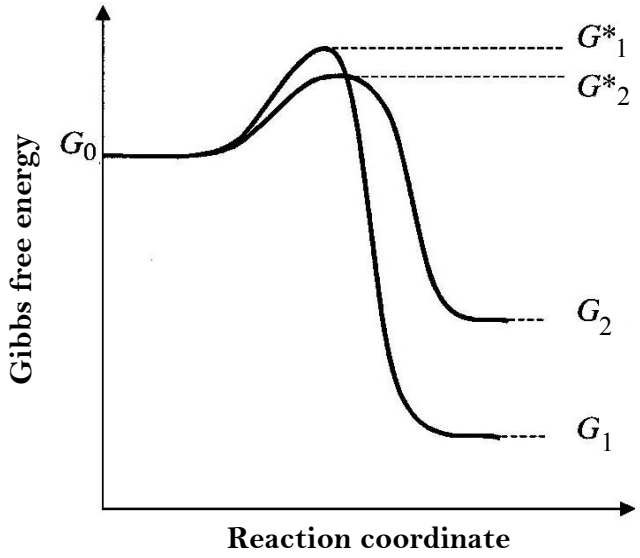

Figure 1.3 Free energy vs reaction coordinate diagrams for two polymorphs illustrating the influence of kinetics on their formation. G*-G$_0$ represents the activation free energy for nucleation.

Structural Features of Polymorphs

The structure of polymorphs of a single compound is a fundamental property as it is this feature that differentiates them. Both X-ray crystallographic techniques and solid-state NMR spectroscopy are key analytical techniques employed for structural elucidation of polymorphs, with X-ray diffraction being the preferred technique. Polymorphic molecules may be classified into 'rigid' molecules or those with conformational 'flexibility'. In cases where different conformations of the molecules are adopted in different crystal structures, the phenomenon is referred to as conformational polymorphism.[14]

There are various methods available for visual comparison of polymorphic structures. For polymorphs with no common unit cell parameters the traditional method was to prepare packing diagrams with a view down an arbitrary crystallographic axis, but this usually conveyed little information about their similarities or differences. It is often more useful to choose a common molecular reference plane and orientate it the same for all the structures. This gives an indication of the immediate environment around the chosen reference plane.[1] Viewing down a common crystallographic axis, i.e. in polymorphic structures that have similar unit cell parameters and/or symmetry elements, may also allow a basis for comparison.

The concept of graph set analysis has in recent years proved to be very useful in comparing polymorphic structures.[15,16] This concept is applied to hydrogen bonds which are very often a common feature of polymorphic structures. In this approach the hydrogen bonding is easily simplified and reduced to four basic patterns, viz. chains (C), rings (R), intramolecular hydrogen-bonded patterns (S) and other finite patterns (D). These designators are superscripted *a* and subscripted *d* for the number of hydrogen-bond acceptors and donors respectively. This is followed by the descriptor (n) which indicates the total number of atoms involved in the pattern. The general graph set descriptor is thus $\mathbf{G_d^a(n)}$ and examples of assignments are given in Figure 1.4.

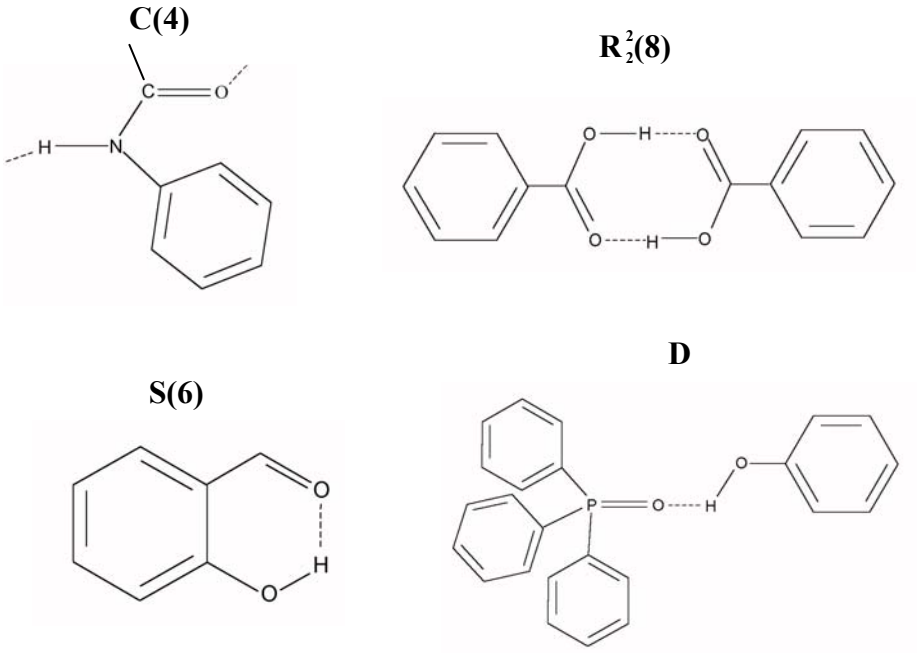

Figure 1.4 Schematic diagrams showing the four basic patterns using graph-set analysis. If no a, d or (n) descriptor is present, the value is assumed to be 1.

Polymorphism in Pharmaceutical Formulations

Careful consideration must be given to the crystal properties and solid state of drugs since practically all drug substances are handled in powder form during their manufacture into dosage forms. Differing crystalline forms can greatly affect formulation, stability and biological activity of the drug. For example, metastable polymorphic forms have higher solubility than stable forms. Even though the more soluble polymorphs are metastable and will eventually convert to the stable form, the rate of such conversion is often slow enough for the metastable form to be employed in the formulation. From a pharmaceutical point of view the degree of conversion should obviously be monitored during storage of the drug product to ensure that its efficacy is not altered significantly. In addition, conversion to the least soluble and most stable polymorph may contribute to the growth of crystals in suspension formulations.[3]

Suspensions: In preparing physically stable dosage forms such as suspensions with aqueous vehicles, if the wrong polymorph is used, phase conversion from the metastable polymorph may occur, producing crystal growth and caking. Crystal growth gives rise to undesirable particle size distribution which can be especially problematic with parenteral suspensions. If caking occurs, the preparation cannot be uniformly suspended.

Solutions: The stability of a drug in its vehicle is the first consideration in formulating a solution. If this information is obtained with regard to a metastable form, it is possible that the concentration of the drug in a solution can exceed the solubility of a less soluble stable form. It is with sparingly water-soluble drugs (e.g. steroids) that solutions, supersaturated with respect to the stable form, may undergo chance nucleation which results in crystallisation and precipitation. One approach to solving this type of problem is to formulate the product in a vehicle containing sufficient co-solvent in order to solubilise the less soluble form.

Creams: In creams, the wrong polymorph suspended in a cream base can undergo phase conversion. The less soluble, stable form will result in crystal growth giving gritty, cosmetically unacceptable creams or products in which the active ingredient is unevenly distributed. The polymorph least susceptible to growth in the cream base should be selected – this is the form least soluble in the base. The greater the solubility of the metastable form suspended in a cream base, the higher the risk of eventual nucleation of the more stable, less soluble form. If the phase conversion is particularly slow in a base, the more soluble metastable form can safely be incorporated to take advantage of the higher therapeutic activity associated with the thermodynamically more active metastable form.

Suppositories: In suppositories, polymorphic transitions affect changes in melting characteristics. Suppository bases often depend on melting at body temperature to release the active ingredients and an increased melting point will mean reduced therapeutic activity. A depressed melting point creates problems with storage and handling. For example, cocoa butter exists in three polymorphic forms and this causes

great difficulty in making suppositories by the fusion method.[3] Cocoa butter melted and brought to a relatively high temperature, say 60-70 °C, then solidified by rapid cooling, will melt below 30 °C. The rapid cooling promotes the formation of only α crystals which melt at too low a temperature (22 °C) to allow normal handling. There is a slow transition from the metastable α form to the β' form (melting point = 28 °C), and finally to the stable β form with highest melting point of 34.5 °C. This transition is fairly slow and suppositories poured from over-heated cocoa butter will only exhibit a normal melting point after several days. Careful melting of the cocoa butter just a few degrees above its melting point allows the crystallisation of nuclei of the β form to remain in the melt, which on cooling favours additional crystallisation of the β form.

Tablets: In tablets, different crystalline forms have different hardness and cohesion properties. When a compound exhibiting polymorphism makes up a large portion of a tabletting mixture, the ease with which the powder is compressed into a tablet can be affected. In general, great care must be taken in the use of raw materials when polymorphism is a physical characteristic of a particular compound.

Polymorphism and Generically Equivalent Dosage Forms

The successful use of a polymorph of significantly greater thermodynamic activity (i.e. higher solubility, higher Gibbs free energy) than the stable form can result in higher blood levels and consequently better therapeutic effects. The amorphous form of the antibiotic novobiocin gives a better therapeutic response than the crystalline form because it is more soluble in the GIT fluids and therefore better absorbed into the bloodstream. Special ingredients (e.g. methylcellulose, PVP, sodium alginate) must be added to suspensions of novobiocin to retard or prevent its transition to the stable crystalline form. The antibiotic chloramphenicol palmitate exists as three crystalline forms (A, B and C) and one amorphous form.[3] The best therapeutic effect is found in those preparations containing only Form B. The presence of the other forms makes the drug less effective and there may therefore be brand to brand variation. Other examples include the anhydrous form of ampicillin which is more efficiently absorbed than the trihydrate forms[3], Form II of methylprednisolone more than Form I and amorphous insulin zinc complex more than the crystalline complex.[17] By varying the ratio

amorphous:crystalline, insulin preparations having different onset and duration of action can be prepared. Hence, the study of polymorphism and its control is vital in the pharmaceutical industry when dealing with a potential new drug during preformulation studies. It is at this stage that the choice of the proper polymorph should be made as this will determine if a pharmaceutical preparation will be chemically and physically stable, or if a powder will tablet well or not, or if the blood level obtained will be the therapeutic level to give the desired pharmacological response.

Polymorphic Control, Structural Elucidation and Crystal Structure Prediction

The decisive need to control the polymorphic forms obtained is of great concern to the pharmaceutical industry and understandably so. The industry may suffer massive financial losses when it fails to manufacture the desired polymorph or an undesired form appears accidentally. Once a particular form has been obtained, a knowledge of the thermodynamics of the polymorphic system, e.g. in the form of energy vs temperature diagrams, is essential to provide information on the storage conditions necessary to prevent any unwanted transformations. The complexity of the practical control of the crystallisation of a desired form may vary between simply reproducing the form with the same protocol as used before, to the rational design of auxiliaries that through selective molecular recognition may inhibit or suppress the growth of the undesired stable form, thus allowing the growth of the desired metastable form.[10] The latter strategy has enjoyed very limited success thus far, but one successful example has been the crystallisation of the metastable form of *N*-(2-acetamido-4-nitrophenyl)pyrrolidine by the addition of a small amount (0.03%) of the designed inhibitor.[18] Between these two extremes there are chemical and physical variations that have been used to produce specific polymorphs.[10] These include, amongst others, examples of polymorphs that have been produced from solutions seeded with the desired form,[19] successive chemical reactions,[20] desolvation of solvates,[21] and successive reheating and cooling strategies to produce a metastable form.

When single-crystal X-ray techniques are not appropriate, such as when the production of microcrystalline particles only is possible, high-resolution powder X-ray diffraction may be employed to elucidate crystal structures. Indexing of the powder diffraction

pattern, optimisation of the molecular unit by modelling methods, generation of trial structures and Rietveld refinement are employed to determine the structure.[22] Optimisation of the method includes the use of synchrotron radiation for rapid data capture, superior treatment of overlapping reflections, more reliable indexing routines, and more flexible methods of obtaining trial structures. Telmisartan[23] is a compound with two polymorphic forms, the structure of one of these having been determined from PXRD data. However the method does prove to have one limitation, namely that while molecular conformations in different polymorphs may be determined with high precision, the same is not true for molecular parameters such as bond lengths and angles.[22]

Ideally, crystal structure prediction is the ultimate objective of supramolecular chemists engaged in the field of polymorphism. However, is it a very complex problem, as acknowledged by Caira[22] in a review article. The problems arise with generating a set of potential polymorphs of the compound, detection of the most stable one at a given temperature and modelling of the nucleation kinetics to determine which phase will actually appear under given conditions. Advancement in this area is growing rapidly and challenges are met with renewed vigour each time. For example, conformationally flexible molecules are especially challenging for crystal structure prediction, not to mention the severe challenge of polymorphic solvates, for which the correct positions and orientations of the drug and solvent molecules must be determined.

To conclude, polymorphs of pharmaceuticals have significant consequences in terms of their performance, e.g. their solubilities may have an impact on their bioavailabilities, their melting points on solubilities, or structures on melting points. The varying physical properties of polymorphs thus command control over the form produced. This, however, can prove costly and with the inclusion of drugs into cyclodextrins, the need for this careful control is effectively eliminated, as 'new chemical entities' are formed and the polymorphic identity of the drug is removed. It should be noted, however, that a given cyclodextrin drug inclusion complex itself may exist in different crystalline forms as proved in 2003.[24] An overview of cyclodextrins in terms of their structure, properties, inclusion complexes and application in the pharmaceutical industry follows.

1.2 CYCLODEXTRINS

Natural Origin of Cyclodextrins

Enzymatic degradation of starch generally results in the production of glucose, maltose, maltotriose and related sugars i.e. a long series of linear or branched chain malto-oligomers, known as dextrins. Dextrins are heterogeneous, amorphous, hygroscopic substances, produced in large quantities for the food, textile, paper and other industries. They are also consumed without prior isolation in such products as e.g. beer and bread. This type of starch degradation is a true hydrolytic process, as the primary product from the splitting of the glycosidic linkage reacts with one molecule of water.[25,26]

If, however, the starch is degraded by the glucosyltransferase enzyme, the primary product of the chain splitting undergoes an intramolecular reaction without the participation of a water molecule. The α-1,4-linked cyclic products are formed; they are known as cyclodextrins (CDs).[26]

CDs are a family of three well known, industrially produced, major cyclic oligosaccharides, and several minor rare ones. The three major cyclodextrins (α-, β- and γ-CD) are crystalline, homogeneous, non-hygroscopic substances, which possess a torus-like macro-ring shape, built up from glucopyranose units.The α-, β- and γ-CD, also known as Schardinger's α-, β- and γ-dextrins, respectively, comprise n = 6, 7 and 8 glucopyranose units respectively[26] (Figure 1.5).

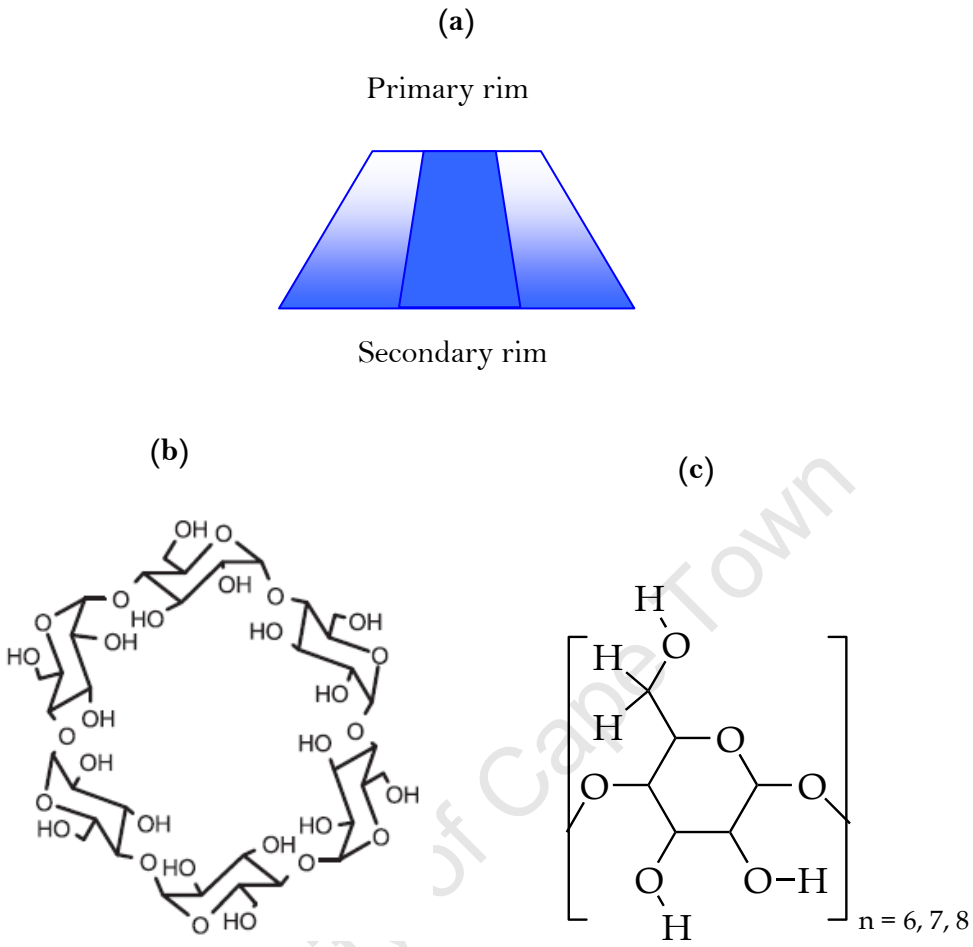

Figure 1.5 (a) The truncated cone representation and (b) the macrocyclic ring of α-CD (as representative) and in parentheses in (c) a α-D-glucopyranose monomer.

Brief Historical Overview

1891	Villiers[27] - first publication of a substance named 'cellulosine' which later proved to be a cyclodextrin.
1904-1911	Schardinger[28-31] – credited with laying down fundamentals of cyclodextin chemistry. Schardinger referred to these compounds as dextrins.
1936	Freudenberg *et al.*[32] – postulated that dextrins contain cyclic α-1,4-glycosidic linkages.
1950s	French[33] and Cramer[34] – were responsible for the enzymatic production of cyclodextrins and characterising their physical and chemical properties.

1960s Ability to form inclusion compounds with improved characteristics, such as solubility and volatility of the included chemical recognised.[26] Toxicological studies of inclusion complexes proved industrial importance in food[35], pharmaceutical, biomedical and analytical industries.[26]

Structural Features of Cyclodextrins

Cyclodextrins consist of glucose monomer units made up of α-D-glucopyranose having the $^4C_1$ chair conformation.[36] When linked, these monomer units are exceptionally rigid. However, they retain sufficient rotational flexibility around the α-(1,4)-linkage C1(n)-O4(n-1)-C4(n-1), (Figure 1.6).

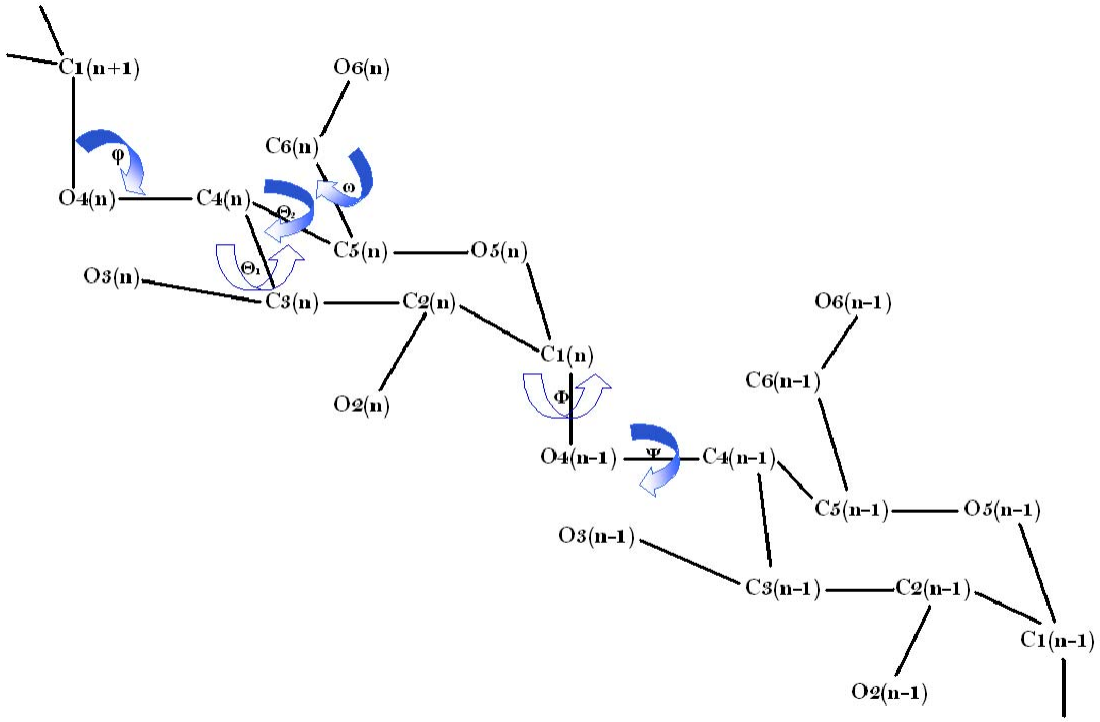

Figure 1.6 Numbering scheme and principal torsion angles of CD structures.

The truncated cone of the cyclodextrin has a hydrophobic cavity and a hydrophilic exterior. The rotational flexibility of the glucopyranose monomer orientates the methine (C3-H and C5-H) and methylene hydrogen atoms (C6-H_2) as well as the lone

pairs of the bridging ethereal oxygen atoms O4(n) towards the interior of the CD cavity. The hydrophobic component of these hydrogens (methine and methylene) plus the additional electron density contributed by the lone pairs imposes some electrically positive character on the cavity.[37] Each rim of the cone has hydroxyl groups attached to it. Each rim is named according to the number and type of hydroxyl groups located there. Thus, the primary rim has a single hydroxyl group (O6-H) per glucose unit while the secondary rim has two hydroxyl groups (O2-H and O3-H) per glucose unit. It follows that the primary rim is the narrower rim while the secondary rim is wider due to the natural tilt of the glucose units. The hydroxyl groups are there to promote/enhance the hydrophilicity of the cyclodextrin.[38] Hydroxyl groups O2-H and O3-H of adjacent glucose units on the secondary rim are hydrogen bonded to each other. The average hydrogen bonding distances O2(n)•••O3(n-1) for α-, β- and γ-CD are in the range 2.98 to 2.82 Å. α-CD has the weakest hydrogen bonds (average distance 2.98 Å) while γ-CD has the strongest (2.82 Å). Only β-CD (2.88 Å) has a complete set of hydrogen bonds which involves all the O2-H and O3-H atoms of the macrocyclic ring. As a consequence, β-CD is the least soluble of the three parent CDs. The solubilities of α-, β- and γ-CD in water are 14.5, 1.85 and 23.2 g per 100 ml at 25 C°, respectively (Table 1.1).[38,39]

Table 1.1 Properties of α-, β- and γ-CDs

Cyclodextrin	Mass (g/mol)	Cavity volume (Å^3)	Outer diameter (Å)	Cavity diameter (Å)		Solubility, g/100 ml in H_2O at 20 °C
				Inner rim	Outer rim	
α, (glucose)$_6$	972	174	15.2	4.5	5.3	14.5
β, (glucose)$_7$	1134	262	16.6	6.0	6.5	1.85
γ, (glucose)$_8$	1296	427	17.7	7.5	8.5	23.2

The principal torsion angles are the primary hydroxyl torsion angle, the glycosidic torsion angle and pyranoid torsion angle (Figure 1.6).

Principal Torsion Angles

Primary Hydroxyl Torsion Angle

The primary hydroxyl or O5-C5-C6-O6 torsion angle (ω) can adopt three orientations namely *(+)-gauche*, *(-)-gauche* or *trans*-conformations. The *(-)-gauche* orientation (ω = -60°) with the O6-H pointing away from the centre of the CD cavity is largely preferred; the *(+)-gauche* (ω = +60°) with the O6-H pointing toward the centre of the CD cavity is observed where a hydrogen bond is formed between the O6 hydroxyl group and an included guest, while the *trans*-orientation (ω = 180°) has not been observed for CD structures, probably due to steric interactions which might occur between O6-H and atoms of the adjacent glucose residue. The mean values of these angles for the parent molecules α-, β-, γ-CD are listed in Table 1.2.[40,41a]

Glycosidic Torsion Angle

The torsion angles around the C1(n)-O4(n-1)-C4(n-1) glycosidic linkage are referred to as the glycosidic torsion angles. They are defined as Φ = O5(n)-C1(n)-O4(n-1)-C4(n-1) and Ψ = C1(n)-O4(n-1)-C4(n-1)-C3(n-1). The mean values of these angles for the parent molecules α-, β-, γ-CD are listed in Table 1.2.[41a,b]

Pyranoid Torsion Angles

The two pyranoid torsion angles Θ_1 (C2-C3-C4-C5) and Θ_2 (C3-C4-C5-O5) can be used to describe the conformational relationships around the C4 atom of each glucose residue. The glucopyranose units generally adopt the $^4C_1$ chair conformation with very small deviations from ideal, undistorted values for the glucose residue (Table 1.2[41a,b]).

Table 1.2 Mean values for principal torsion angles of CDs

CD	|ω| (°)	Φ(°)	Ψ(°)	Θ_1(°)	Θ_2(°)
α	68	108	130	+52	-53
β	64	112	128	+56	-56
γ	68	110	130	+62	-62

O4 Polygon

Polygons, composed of 6, 7 or 8 glycosidic O4 atoms offer a good model for describing the macrocyclic structures of α-, β- and γ-CD.

Figure 1.7 illustrates the various geometrical parameters of the O4 polygon. The side lengths (*l*) of the O4 polygon are the distances between O4(n) and O4(n+1), where O4(n+1) is the O4 atom of the next glucose unit. The radii (r) of the macrocycle are measured from the centre of gravity (C) of all O4 atoms to each O4 atom. The angle (*a*) is the O4(n)•••O4(n+1)•••O4(n+2) angle.

The O4 polygons also offer a means to evaluate (i) the symmetry of the macrocyclic structure and (ii) the planarity of the macrocyclic ring.

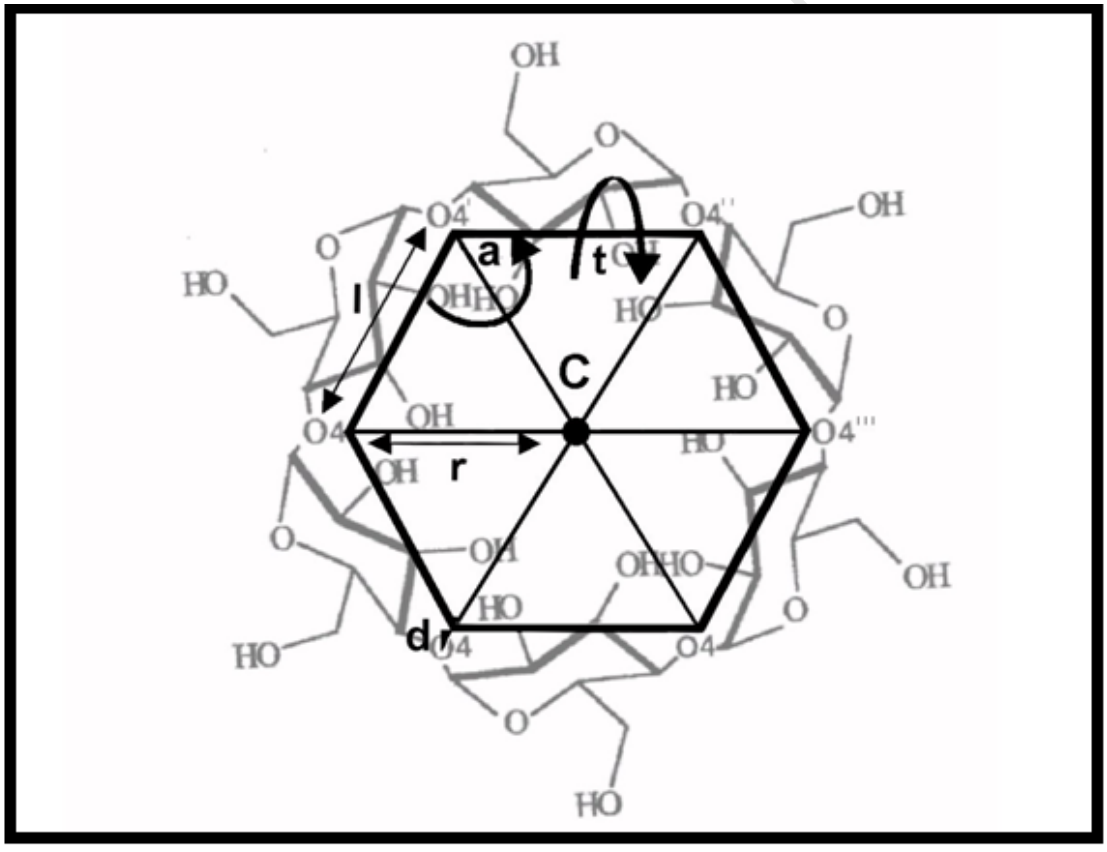

Figure 1.7 Schematic diagram of the O4 polygon for α-CD.

Macrocyclic Symmetry

If the macrocyclic structures of α-, β- and γ-CD showed perfect C_6, C_7, C_8 symmetry then the O4•••O4•••O4 angles would be exactly 120°, 128° and 132° respectively.

Coplanarity of the Glycosidic Oxygen Atoms

This refers to the coplanarity of the O4 linker atoms of the O4 polygon. This can be evaluated by the deviation from planarity (*d*) of each O4 atom from the mean plane of all the O4 atoms, and the O4•••O4•••O4•••O4 torsion angles (*t*) (Figure 1.7). For the planar macrocycle the deviation of each O4 from the mean plane of the macrocycle would be zero and the O4•••O4•••O4•••O4 torsion angles (*t*) would be 0°.

The mean values of the principal geometrical parameters of the O4 polygons for the parent molecules α-, β-, γ-CD are listed in Table 1.3.[41a,c]

Table 1.3 The mean values of the principal geometrical parameters of the O4 polygon

CD	*r* (Å)	*l* (Å)	*a* (°)	*d* (Å)	*t* (°)
α	4.2	4.2	120	0.07	5
β	5.0	4.3	128	0.08	5
γ	5.9	4.5	132	0.02	2

Conformational Descriptors for CDs

Intersaccharidic Bond Angles

The intersaccharidic bond angle (φ) is defined as φ = C1(n+1)-O4(n)-C4(n) (Figure 1.6). The values of φ decrease in the order φ(α-CD) > φ(β-CD) > φ(γ-CD) as the number of glucose residues making up the macrocycle increases (Table 1.4).

Table 1.4 Mean values of the intersaccharidic bond angle, O2(n)···O3(n-1) distances and the tilt angles for α-, β- and γ-CD[41b]

CD	φ(°)	O2(n)···O3(n-1) (Å)	τ_1(°)
α	118.4	2.98	+ 11.4
β	117.7	2.88	+ 9.5
γ	115.0	2.82	+ 14.5

Intramolecular O2(n)···O3(n-1) Hydrogen Bonds

The structural rigidity of the CD seems to be mainly due to a ring of intramolecular hydrogen bonds between the secondary hydroxyl groups (labelled O2-H and O3-H) of adjacent glucose units which are orientated *cis*. These O2(n)•••O3(n-1) hydrogen bonds stabilise the macrocyclic conformation and limit the conformational freedom of the glucosidic bond. The mean O2(n)•••O3(n-1) distances become smaller on increasing the macrocylic ring size from six to seven to eight glucose units (Table 1.4).

Tilt Angle

The tilt angle is a measure of the inclination of the glucose residue with respect to the mean macrocyclic plane defined by the O4 linker atoms. Two definitions of the tilt angle are quoted. The tilt-angle (τ_1) is defined as the angle between the mean plane through the six pyranoid ring atoms (labelled C1, C2, C3, C4, C5 and O5) of each glucose unit and the normal to the O4 mean plane. The tilt angle, τ_1, is schematically illustrated in Figure 1.8 with the glucose residue and appropriate mean planes all viewed edge-on.

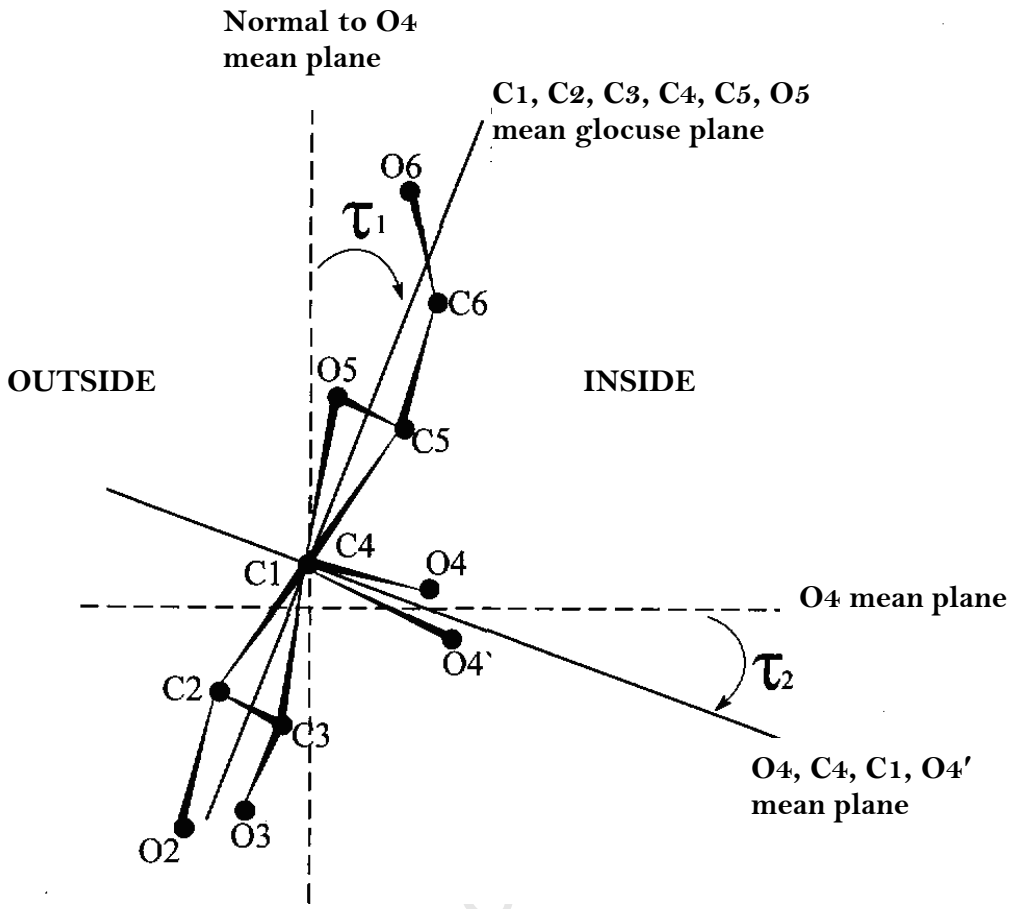

Figure 1.8 Schematic representation of the tilt angles τ_1 and τ_2 (the glucose and various mean planes are all viewed edge-on).

The tilt angle (τ_2) is defined as the angle between the mean plane through O4, C4, C1 and O4′ atoms and the O4 mean plane. The tilt angle, τ_2, is schematically illustrated in Figure 1.8 with the glucose residue and appropriate mean planes all viewed edge-on. In theory, if the glucose residues were completely undistorted from ideal conformation then the two definitions of the tilt angle would produce identical values. In practice, however, the tilt angles obtained from these two definitions differ from one another because the formation of the macrocycle somewhat distorts the conformation around the glycosidic linkages. The tilt angle (τ_2) has been traditionally reported for a large number of crystallographic investigations of CD structures.

Each glucose unit is not orthogonal to the mean O4 plane, but is inclined with the O6 sides towards the inside or outside of the macrocycle. A positive tilt angle denotes that

the glucose unit is inclined with the O6 side towards the inside of the macrocyclic cavity (Figure 1.8) while a negative tilt angle denotes that the glucose unit is inclined with the O6 side towards the outside of the macrocyclic cavity. For α-, β- and γ-CD, the tilt angles are mostly positive and the result is that the O6 end is truncated for these CDs.

Guest Inclusion

The hydrophobic cavity of the CD has the ability to include guest molecules with polarity lower than water, the only requirement being that the guest molecule must be of appropriate shape and size to fit into the cavity, even if only partially. The pyranose conformation is affected by the interaction of included guest molecules, although it is difficult to detect significant changes in bond distances, angles and torsion angles. No covalent bonds are formed or broken during the formation of a guest-cyclodextrin complex and in aqueous solution the complexes readily dissociate. Initially, it was thought that the main driving force for complexation was the replacement of the high enthalpy water molecules, located in the CD cavity, by a suitable guest (Figure 1.9).[42,43] The exchange process was therefore primarily determined by enthalpy and entropy changes with van der Waals forces and hydrophobic interactions regarded as secondary. However, Liu *et al.*[44] claimed that the exclusion of cavity-bound water and the release of conformational strain are not the only factors to be considered. In other words, the enthalpy and entropy changes during water exclusion from the cavity are not good criteria for the determination of a driving force due to the enthalpy-entropy compensation.[44] Liu *et al.* also claimed that the primary forces of inclusion are therefore the van der Waals and hydrophobic interactions along with hydrogen bonding and steric effects.[36, 45-53a]

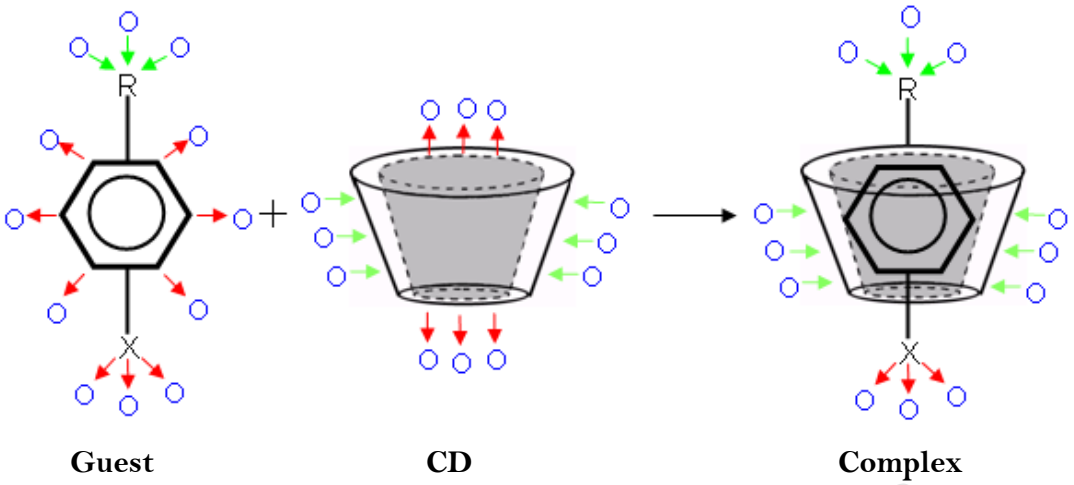

O - Water
Red arrows - repulsive interactions
Green arrows - attractive interactions

Figure 1.9 Guest inclusion by cyclodextrins and expulsion of water from the CD cavity.

Orientation of Guest in CD Cavity

Size and Shape

The primary factor determining the orientation and fit of a guest molecule in the cyclodextrin cavity is that the guest must be able to fit into the cavity, even if it is only partially included. The physical dimensions and cavity volumes of α-, β- and γ-CD are presented in Table 1.1. CDs are somewhat flexible hosts which can adapt to the topologies of the guests embedded in their cavities. The macrocyclic host adjusts its geometry to the topology of the guest during complex formation in a process that can best be envisaged to occur via an induced-fit type mechanism.

Dipole Moment Alignment

Large values of the dipole moments have been calculated for α-, β- and γ-CD using the X-ray structures of the three CDs. The relative strengths are in the order α-CD < β-CD < γ-CD, which is expected as the number of glucosyl residues in the macrocycle increases. The dipole moments are of the order of 10-20 Debye and are directed with the positive end of the dipole at the primary hydroxyl end and the negative end at the

secondary hydroxyl rim. In the inclusion complexes of CDs with aromatic molecules, the guest dipole moment has been noted to adopt an anti-parallel direction to that of the CD.

The overall electric field of CDs is expressed strongly within the cavity of the macrocyle and the dipole moment of a CD is therefore thought to strongly influence the orientation of polar guest compounds in the CD cavity.

The direction of the cyclodextrin dipole moment can be expressed as the tilting angle, ω, between the dipole moment vector and the axis of the cavity. If ω is sufficiently smaller than 90° then the dipole moment is directed from the secondary to the primary hydroxyl side, and this is the case for all CDs that have been studied thus far. The direction of the guest dipole moment can be expressed as Ω, the angle between the vector of the CD dipole moment and the vector of the guest dipole moment (Figure 1.10). When these two vectors are anti-parallel the angle Ω is 180°.[53b]

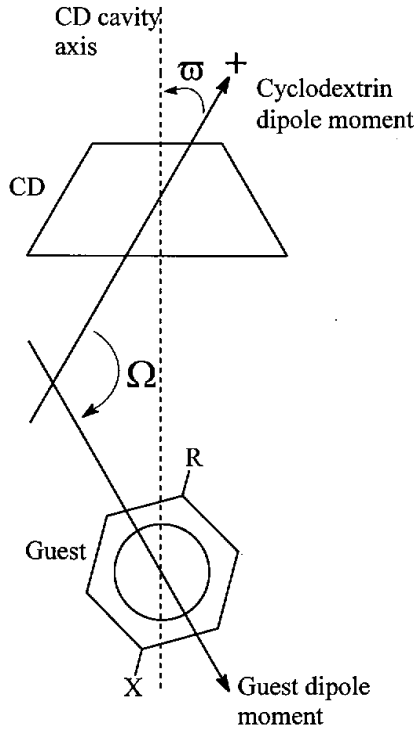

Figure 1.10 The relationship between the cyclodextrin and guest dipole moments.

Derivatised Cyclodextrins

With native cyclodextrins having low solubilities, especially in the case of β-CD, methylation of β-CD at the C2-OH, C3-OH and C6-OH hydroxyl positions successfully enlarges the hydrophobic surface area of the entire cyclodextrin. An additional 2 Å is added to the height of the cyclodextrin with a simultaneous solubility enhancement in water. The overall effect is that the topology of inclusion is altered for these modified cyclodextrins.[38] This allows the accommodation of larger guests in the cavity as well as in the interstitial space between CD molecules. Heptakis(2,6-di-*O*-methyl)-β-cyclodextrin (DIMEB) and heptakis(2,3,6-tri-*O*-methyl)-β-cyclodextrin (TRIMEB) are two β-CD derivatives which are modified at the C2-OH, C6-OH and C2-OH, C3-OH and C6-OH hydroxyl positions, respectively. As none of the O3-H hydroxyl groups is modified in DIMEB, it therefore retains the O2•••H-O3′ hydrogen bonds. The average O2•••O3′ distances are similar to those of β-CD.[54] This results in DIMEB and β-CD having similar conformations. The molecule of TRIMEB has none of the O2•••O3′ interactions that occur in DIMEB and β-CD. The conformation of TRIMEB differs from that of β-CD as it has only the C6-H•••O5 hydrogen bonds between adjacent methylglucose units which stabilise its structure.[55]

Crystal Forms of Parent and Modified Cyclodextrins

Crystal Forms of α-, β- and γ-cyclodextrin

For α-CD, there are three hydrated forms which all crystallise in the orthorhombic crystal system in the space group $P2_12_12_1$. The three forms have 6, 7.57 and 11 water molecules per molecule of α-CD. Included in the α-CD search, an unhydrated form was also identified crystallising in space group $P2_12_12_1$.[40] The search of the Cambridge Structural Database (CSD)[40] produced 18 β-cyclodextrin structures including repeat determinations. All of these are hydrated forms of β-cyclodextrin with the level of hydration ranging from 1 to 12.26 water molecules per molecule of cyclodextrin. There are 10 different hydrated forms with 1, 9, 9.35, 10.41, 11, 11.19, 11.56, 11.89, 12 and 12.26 water molecules. All 18 forms are monoclinic, crystallising in the space group $P2_1$. γ-CD presented three crystal forms having different levels of hydration: 11, 14 and 17 water molecules.[40] These three forms crystallise in the space group $P2_1$.

Crystal Forms of DIMEB

There are 11 structures of the DIMEB parent recorded on the CSD, ten of which are hydrated forms while the remaining structure is anhydrous. Of the reported hydrated forms (8) the level of hydration ranges between 1.1 and 15 water molecules per cyclodextrin molecule. Within the set of hydrates, five of these have unreported hydration values. The atomic coordinates for only five of the structures were provided in the CSD. These included three different hydrates and the single anhydrous form.[40] All the DIMEB parent compounds crystallise in the space group $P2_12_12_1$ except for one form with two water molecules per cyclodextrin which crystallises in the space group $P2_1$.

Crystal Forms of TRIMEB

TRIMEB has three reported forms listed on the CSD, an anhydrate, a monohydrate and a trihydrate. From the calculated PXRD traces, unit cell parameters and the packing arrangements, the anhydrous form is the dehydrated form of the trihydrate.[40]

Crystal Forms of TRIMEG

There are three different structures of octakis(2,3,6-tri-*O*-methyl)-γ-cyclodextrin (TRIMEG) all of which are hydrated with 2, 4.8 and 4.5 H_2O molecules per molecule of CD. Two of the structures crystallise in the orthorhombic crystal system in the space group $P2_12_12_1$ while the third is monoclinic crystallising in the space group $P2_1$.[40]

Crystal Forms of Peracetylated Cyclodextrins

Hexakis(2,3,6-tri-*O*-acetyl)-α-cyclodextrin (TriAcACD), heptakis(2,3,6-tri-*O*-acetyl)-β-cyclodextrin (TriAcBCD) and octakis(2,3,6-tri-*O*-acetyl)-γ-cyclodextrin (TriAcGCD) were investigated and characterised by Bettinetti *et al.*[56] Thermal analysis (DSC and TGA), PXRD and FTIR were employed in the characterisation. From their studies it was concluded that recrystallisation of the peracetylated CDs from various solvent systems produced solvates, while hydrates and amorphous forms were obtained from spray drying or microwave-drying. However, the crystal structure of TriAcGCD containing mixed solvents was determined by Caira *et al.*,[57] the mixtures including isopropanol/water and ethanol/water.[40]

Cyclodextrin Complex Packing Arrangements in the Solid State

Single crystal X-ray analysis is a very powerful technique for studying CDs and their complexes in the solid state. The technique provides information regarding structural aspects of CDs and included guests and the nature of their interactions. Several reviews present comprehensive discussions of these structural aspects as determined by crystallographic studies.[58] These structures may be classified according to their unit cell parameters and packing arrangements. The consequence of detailing packing arrangements stems from the fact that complexes with similar packing arrangements have similar PXRD patterns. PXRD is an important screening technique used in the initial characterisation of presumed complexes.

β-CD Complexes

β-CD inclusion complexes can regularly arrange themselves in either cage type or channel type structures.[59] Small guest molecules are usually associated with cage structures. These guests are easily enclosed by the CD cavity. Channel structures are favoured for larger guests. Cage structures are usually monomeric arrangements while the channel type structures are typically dimeric.

Cage Type Monomeric

Cage type structures are usually arranged in such a way that the cavity is blocked off by adjacent molecules leaving no contact between guests. There are four cage type monomeric structures (Figure 1.11): herringbone (**HB**), layer (**LY**), brickwork (**BW**) and zigzag (**ZZ**). For β-CD complexes, herringbone, layer and brickwork structures usually crystallise in the space group $P2_1$, while the zigzag type crystallises in the space group $P2_12_12_1$.[40]

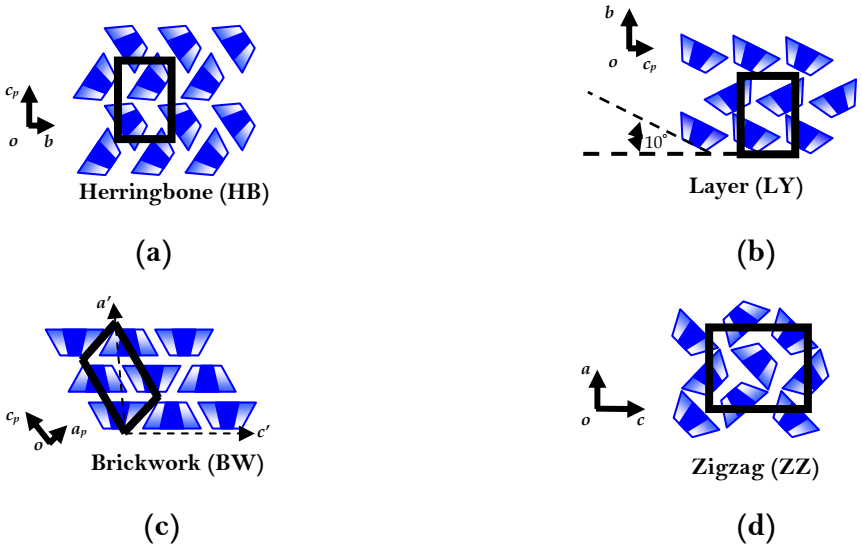

Figure 1.11 (a) Herringbone packing arrangement for monomeric β-CD complexes. (b) Layer packing arrangement with layer propagation along the b-axis. (c) Brickwork packing showing the alternating 'primary rim up' – 'primary rim down' of successive CD molecules in the direction of c′. (d) Zigzag arrangement of the β-cyclodextrin monomers along the c-direction.

Channel Type Monomeric (Figure 1.12) and Channel Type Dimeric (Figure 1.13)

The helical channel type (**HC**) structure crystallises in the hexagonal space group $P6_1$. It is an unusual arrangement with an isolated cavity.[40] β-CD is able to form hydrogen bonded dimers in order to accommodate larger or multiple guests. These dimeric units are held together by several O-H•••O hydrogen bonds. Similar to the monomeric unit, the dimeric unit is able to assemble into a number of three-dimensional motifs. Mavridis *et al.*[60] identified four modifications; however, more categories have since been added.[58,61] The four modifications are: channel (**CH**), intermediate (**IM**), screw channel (**SC**) and chessboard (**CB**). The space groups associated with these modifications are as follows: P1 and C2 with channel type, P1 with intermediate, $P2_1$ with screw channel and $C222_1$ with chessboard.

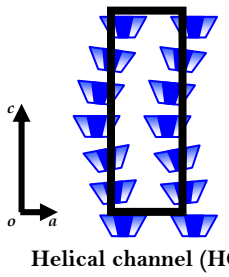

Figure 1.12 The helical channel arrangement of β-CD monomers.

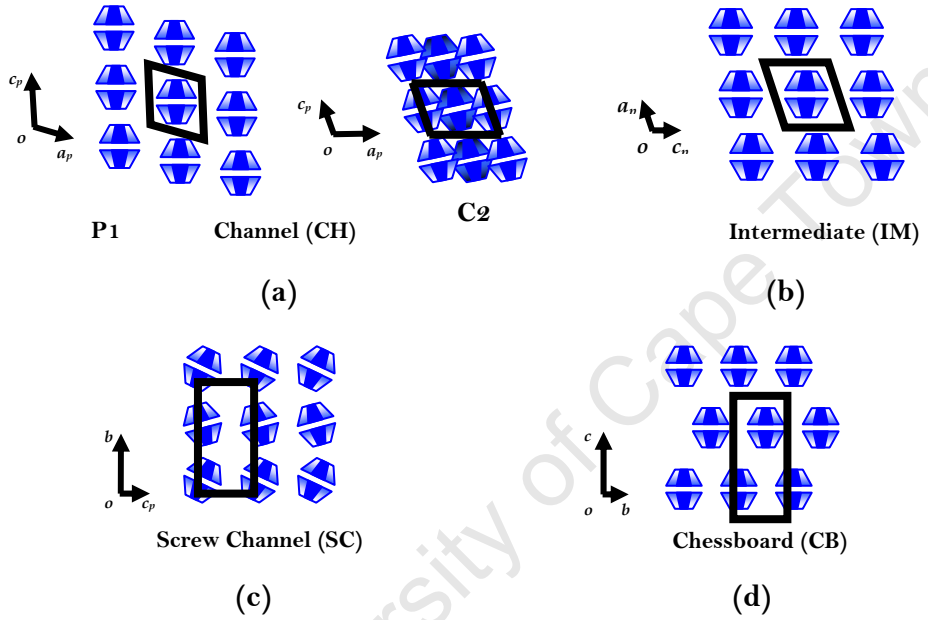

Figure 1.13 (a) Channel packing arrangement for P1 (left) and C2 (right) forms. (b) The intermediate arrangement for β-CD dimers. (c) Dimeric layers of the screw channel arrangement. (d) Chessboard packing motif.

Packing Arrangements of DIMEB Complexes

DIMEB and its complexes generally crystallise in the space groups $P2_1$ and $P2_12_12_1$. The packing arrangements vary from channel type head-to-tail, to modified brick type and modified herringbone motifs. The guest may be located in the cyclodextrin cavity or in the interstitial spaces.[40]

Packing Arrangements of TRIMEB Complexes

TRIMEB and its inclusion complexes favour the space group $P2_12_12_1$ with the molecules in a screw channel type structure,[40] although structures with space group $P2_1$ have been identified.[62,63] The molecules are arranged in a head-to-tail manner.

The Hydrogen Bonded Network of CD Structures

Different hydrogen bonding interactions that may occur between CDs, included guests and the water molecules of crystallisation in the cyclodextrin inclusion complex are as follows:

1. Cyclodextrin to cyclodextrin hydrogen bonds (CD-CD)
2. Cyclodextrin to water hydrogen bonds (CD-W)
3. Water to water hydrogen bonds (W-W)
4. Guest to cyclodextrin hydrogen bonds (CD-G)
5. Guest to water hydrogen bonds (G-W)
6. Guest to guest hydrogen bonds (G-G)

The β-CD molecule almost always contains a ring of intramolecular O2•••O3 hydrogen bonds which gives the macromolecular structure a rigid, cyclic shape. These consist of seven O2(n)•••O3(n-1) intra-CD bonds. Neutron diffraction studies have shown that this type of hydrogen bonding is of the flip-flop nature in β- and γ-cyclodextrin with both O2(n)-H•••O3(n-1) and O2(n)•••H-O3(n-1) hydrogen bonds being observed. The mean O2(n)•••O3(n-1) distance is 2.88 Å for β-CD.

Isostructurality

Two or more crystalline phases are said to be isostructural if they have similar unit cell dimensions, the same space group (this includes structures which are related by a metric transformation) and common moieties having nearly identical atomic co-ordinates.[64] Practically, isostructurality of two phases is recognized when their X-ray diffraction patterns match, implying similarity of unit cell dimensions. The closer the registration of X-ray reflections both in terms of their angular positions and relative intensities, the greater the degree of isostructurality.

When large monocrystals of CD complexes suitable for X-ray analysis cannot be consistently identified or their poor quality prevents structure determination, isostructurality is employed to determine the structures of such CD complexes.[58,65] Since microcrystalline precipitates are more readily obtained in attempts to prepare CD inclusion complexes, PXRD, by itself, is employed as a means of complex identification and characterisation.[58,65]

A CD inclusion complex is generally a ternary system comprising host CD, guest and water molecules. For CD inclusion complexes, isostructurality is basically confined to the host CD (i.e. for example when two complexes of the same host are considered). The outcome of the above prerequisites is nearly identical packing arrangements and superimposable PXRD traces. Thus, PXRD is an important tool in determining isostructurality in the absence of single crystal X-ray data.

Effects of CDs on Important Drug Properties in Formulation

Effect on Drug Solubility and Dissolution

CDs play a vital role in the formulation of poorly water-soluble drugs by improving apparent drug solubility and/or dissolution through inclusion complexation or solid dispersion. The CDs act as hydrophilic carriers for drugs with inadequate molecular characteristics for complexation, or as tablet dissolution enhancers for drugs with a high dose, with which use of a drug/CD complex is difficult, for example, paracetamol.[66]

Methylated CDs are known to be the most powerful solubilisers. With the reduction of drug crystallinity on complexation, CDs contribute to the increased apparent drug solubility and dissolution rate.[67,68] Furthermore, CDs, as a result of their ability to form inclusion complexes in dissolution medium, can enhance drug dissolution even when there is no complexation in the solid state.[69] β-CD is well known to be a good solubiliser for several drugs but it is not as effective as the methylated derivative DIMEB.[70] CDs can also act as release enhancers, for example: β-CD enhanced the release of theophylline from hydoxypropyl methylcellulose (HPMC) matrix by increasing the apparent solubility and dissolution rate of the drug.[71,72]

Effect on Drug Bioavailability

CDs improve the bioavailability of poorly soluble drugs by enhancing the drug solubility, dissolution, and/or drug permeability. CDs increase the permeability of hydrophobic drugs by making the drug available at the surface of the biological barrier, e.g. skin, mucosa, or the eye cornea, from where it partitions into the membrane without disrupting the lipid layers of the barrier (Figure 1.14). Here it is imperative to use just sufficient CD to solubilise the drug in the aqueous vehicle since excess may decrease the drug availability.[73,74,75] At low concentrations of randomly methylated β-CD (RAMEB), when hydrocortisone was in suspension, increasing the CD concentration increased the drug flux. At higher CD concentrations, when the drug was in solution, increasing the CD concentration decreased the flux.[76] It was found that addition of polymers can further enhance the drug permeability from aqueous CD solutions.

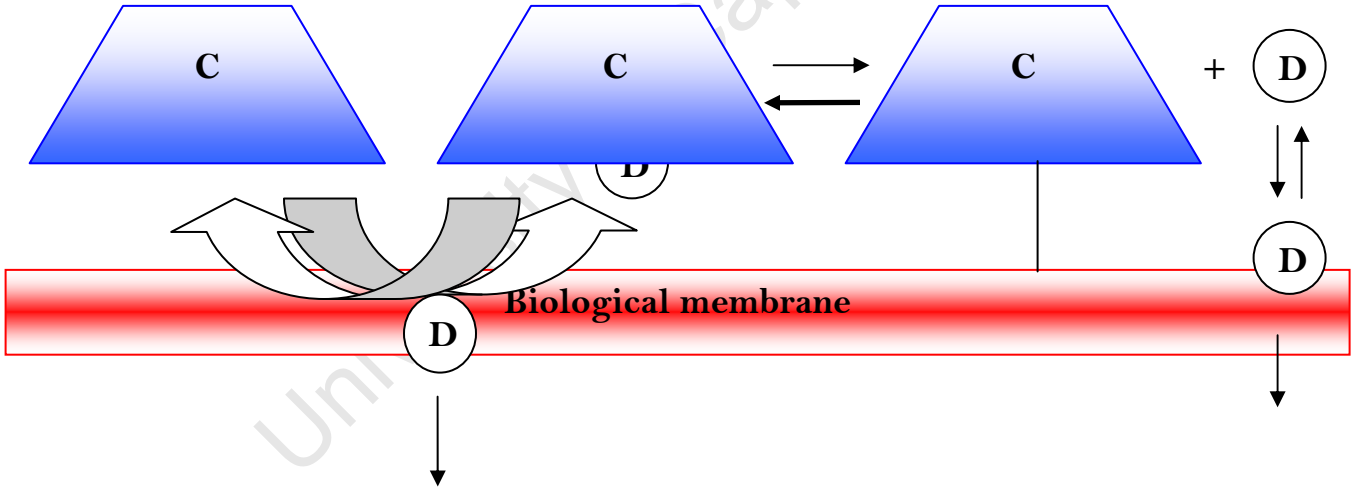

Figure 1.14 Mode of penetration enhancement by CDs (adapted from reference 77).

Effect on Drug Safety

CDs have been used to improve irritations caused by drugs.[77] The enhanced drug effectiveness and potency caused by CD-increased drug solubility, may reduce drug toxicity by making the drug effective at lower doses. β-CD improved the antiviral action of ganciclovir on human cytomegalovirus clinical strains and the resultant increase in the potency reduced the drug toxicity.[78] The toxicities associated with crystallisation of poorly water-soluble drugs in parenteral formulations can often be reduced by formation of soluble drug:CD complexes.

Effect on Drug Stability

CDs can enhance the stability of several labile drugs against dehydration, hydrolysis, oxidation, and photodecomposition and thereby increase the shelf life of drugs.[79] CD-induced enhancement of drug stability may be a result of inhibition of drug interaction with vehicles and/or inhibition of drug bioconversion at the absorption site.[80] By providing a molecular shield, CD complexation encapsulates labile drug molecules at the molecular level and thus insulates them against various degradation processes.

The stabilising effect of CDs depends on the nature and effect of the included functional group on the drug stability and the nature of the vehicle. Since the hydrolysis of drugs encapsulated in CDs is slower than that of free drugs,[81] the stability of the drug/CD complex, plays a major role in determining the extent of protection.[82-85] Very low concentrations of hydroxypropyl β-CD (HPBCD) (1% or lower), due to formation of a more physically unstable complex, did not protect taxol as effectively as higher CD concentrations.[86]

CD Applications in Drug Delivery

Oral Drug Delivery

Applications of CDs in oral drug delivery include improvement of drug bioavailability due to increased drug solubility, improvement of rate of dissolution, and stability of the drug at the absorption site e.g. the gastrointestinal tract (GIT) drug-induced irritation, and taste masking. CD complexation was found to decrease local drug irritation and also modify the time of drug release during GI transit. An itraconazole oral preparation

containing 40% (w/v) of HPBCD (with reduced drug irritation) has been commercialised in the United States and Europe.[82]

CDs enhance the mucosal drug permeability by increasing the free drug availability at the absorptive surface.[87,88] CD complexation can present improved and uniform absorption of low-soluble drugs with poor and unpredictable absorption and also enhance the drug activity on oral administration.[89-91]

The relative safety, efficacy in terms of complexation, cost, and acceptance in pharmacopeias, are some important factors to be considered in selecting a CD for drug complexation. HPBCDs were shown to have a better oral safety profile than β-CD and other parent CDs, but only limited data are available on the oral safety of the methylated CDs. However, for oral administration all CDs can be considered practically non-toxic due to lack of CD absorption through the GIT. Hence, the relative safety profile of CDs is a concern when drug doses used in complexes exceed the LD50 (i.e. dose that kills 50% of the sample population) of CDs.[79] β-CD is the most cost-effective compound of all CDs, whereas HPBCD is more expensive. The monograph of β-CD is already incorporated in various pharmacopeias and national formularies (NF).[79] Hence, β-CD can be considered most favourable for oral use when it is effective for drug complexation. Modified CDs like HPBCD and DIMEB may be used when they are more effective and when their peculiar property is required in formulation.[92,93]

Parenteral Drug Delivery

Amorphous HPBCD has been studied extensively for parenteral use on account of its high aqueous solubility and minimal toxicity. HPBCD allows parenteral administration of various drugs with no significant toxicity problems. As mentioned earlier, an itraconazole parenteral injection containing HPBCD (40% w/v) has been commercialised in the United States and Europe.[82,94] Applications of CDs in parenteral delivery are solubilisation of drugs, reduction of drug irritation at the site of administration, and stabilisation of drugs in the aqueous environment. Formation of a stable, water-soluble dexamethasone complex with sugar branched β-CDs suggested the potential of these CDs as excellent carriers in steroidal injectable formulations.[95] Aqueous phenytoin parenteral formulations containing HPBCD exhibited reduced drug

tissue irritation and precipitating tendency because their pH values were significantly closer to the physiological value (7.4).[96]

Ocular Delivery

Applications of CDs in aqueous eye drop preparations include solubilisation and chemical stabilisation of drugs, reduction of ocular drug irritation, and enhancement of ocular drug permeability. Vehicles used in ophthalmic preparations should be non-irritating to the ocular surface to prevent fast washout of the instilled drug by reflex tearing and blinking. Hydrophilic CDs, such as HPBCD, have shown to be non-toxic to the eye and are well tolerated in aqueous eye drop formulations. An example is the decreased ocular irritation of a lipophilic pilocarpine prodrug by HPBCDs.[79]

HPBCD also enhanced the ocular permeability of dexamethasone acetate and inhibited the conversion of the salt to a less permeable dexamethasone.[79] Since only the free drug can permeate biological membranes, ophthalmic delivery of drugs can be limited by the dissociation of drug/CD complexes in the precorneal area due to the limited dilution in this area. The dissociation of drug/CD complexes depends more on the binding of drugs to precorneal proteins, absorption by corneal tissue, and displacement of drugs from CD complexes by precorneal fluid components.

Nasal Drug Delivery

CDs are useful adjuvants in nasal drug delivery. They enhance nasal drug absorption by increasing aqueous drug solubility and by enhancing nasal drug permeability. However, large interspecies differences were found in CD-enhanced nasal drug absorption. The safety and non-toxicity of CDs in nasal drug formulations have been demonstrated by the clinical data, with CDs showing no adverse effects. Merkus et al.[97] demonstrated that CDs can be safely used to improve nasal bioavailability of drugs, especially peptides. DIMEB improved the nasal bioavailability of estradiol in rats and rabbits.

Rectal Drug Delivery

Applications of CDs in rectal delivery include enhancing drug absorption from a suppository base, increasing drug stability in the base or at the absorption site, providing sustained drug release, and alleviating drug-induced irritation.[80,98]

Drug release from the suppository base is important in rectal absorption because of the high viscosity of rectal fluids. The effect of CDs on rectal drug absorption can be influenced by the partition coefficient of the drug and its CD complex, magnitude of the complex stability constant, and nature of the suppository base (oleaginous or hydrophilic). Hydrophilic CDs (especially methylated and hydroxypropyl CDs) enhance the absorption of lipophilic drugs by improving the drug release from oleaginous vehicles and by increasing the drug dissolution rate in rectal fluids. Formation of hydrophilic CD complexes was found to inhibit the reverse diffusion of drugs into oleaginous vehicles by reducing the drug/vehicle interaction. Rectal absorptions of flurbiprofen and biphenylacetic acid were enhanced by DIMEB and HPBCD, respectively.[77]

Controlled Drug Delivery

CDs, due to their ability to complex drugs and act as functional carrier materials in pharmaceutical formulations, can potentially deliver efficient and precise required amounts of drugs to targetted sites for a necessary period of time. β-CD derivatives are classified as hydrophilic, hydrophobic, and ionisable derivatives. The hydrophilic derivatives improve the aqueous solubility and dissolution rate of poorly soluble drugs, while the hydrophobic derivatives retard the dissolution rate of water-soluble drugs from vehicles. Hence hydrophilic and hydrophobic CD derivatives are used in immediate and prolonged release type formulations, respectively. The ionisable CD derivatives, on the other hand, improve inclusion capacity, modify drug dissolution rate, and alleviate drug irritation.

Colon-Specific Drug Delivery

CDs are hardly hydrolysed and only slightly absorbed in the stomach and small intestine but are absorbed in the large intestine after fermentation into small saccharides by colonic microbial flora. The hydrolysing property of CDs makes them useful for colon drug targetting. Biphenyl acetic acid (BPAA) prodrugs for colon-specific delivery were developed by conjugation of the drug onto one of the primary hydroxyl groups of α-, β-, and γ-CDs[97] through an ester or amide linkage. In the case of ester prodrugs, the maltose and triose conjugates released the free drug after initial

hydrolysis of the susceptibile ester linkage, but in the case of amide prodrugs, the conjugates remained as such providing delayed release due to the resistance of the amide bond to hydrolysis. The CD-based prodrug approach was used for colon-specific and delayed drug delivery. For example, when tested in rats with carageenan-induced inflammation, the absorption of BPAA from γ-CD prodrugs was found to be from caecum and colon in contrast to that from the highly soluble β-CD complex, which was mainly from the small intestine.[99]

Peptide and Protein Delivery

Problems related to the practical use of therapeutic peptides and proteins are their chemical and enzymatic instability, poor absorption through biological membranes, rapid plasma clearance, unusual dose response curves, and immunogenicity. CDs, because of their bioadaptability in pharmaceutical use and ability to interact with cellular membranes, can act as potential carriers for the delivery of proteins, peptides, and oligonucleotide drugs.[100]

β-CD improved insulin loading of alginate microspheres prepared by an emulsion-based process. The process proved to be important in the development of an oral insulin drug delivery system as the absorption of insulin from optimised microspheres was found to take place from the GI region.[101]

Gene and Oligonucleotide Delivery

The toxicity and immunogenicity associated with viral vectors led to the development of nonviral vectors for gene delivery. Besides the plasmid or virus-based vector systems, "naked" nucleotide derivatives have also been investigated for possible use as therapeutic agents through several routes of administration. Gene delivery technologists are now testing CD molecules in the hope of finding an optimal carrier for the delivery of therapeutic nucleic acids. However, the limitations of CDs, such as CD-associated toxicity (e.g. DIMEB) must be considered before their clinical use.[102]

Dermal and Transdermal Delivery

CDs have been used to optimise local and systemic dermal drug delivery. Applications of CDs in transdermal drug delivery include enhancement of drug release and/or

permeation, drug stabilisation in formulation or at the absorptive site, elimination of drug-induced local irritation, sustaining of drug release from vehicle, and modification of drug bioconversion in the viable skin. Parent CDs (α-, β-, and γ-CDs) and various chemically modified CD derivatives with extended physicochemical properties and inclusion capacity have been used in transdermal drug delivery.[80]

CDs enhance drug delivery by increasing the drug availability at the barrier surface, where the free drug partitions from the CD cavity into the lipophilic barrier. The free drug fraction at the barrier surface depends on the drug dissolution rate, relative magnitude of the stability constants of the CD complexes with the drug and the competing agent at the absorption site, and the drug absorption rate constant. In ointments, just as in suppositories, a drug in the CD complex may be displaced by ointment components, depending on the magnitude of the stability constant of the drug/CD complex. Hence, for optimum drug release, the vehicle or the CD complex chosen should be such that the complex barely dissociates but still maintains a high drug thermodynamic activity in the vehicle.[103] The order of prednisolone release rate from a hydrophilic ointment was drug alone < γ-CD complex < β-CD complex < DIMEB complex, which was reflective of the order of the complex stability constants.[80] For absorption, the CD complex must dissociate to release free drug (the actual absorbable species) and the dissociation of the CD complex depends on the magnitude of the complex stability constant. If the complex stability constant is too high, the complex may not release the free drug at the absorption site and thus may decrease or inhibit drug absorption.[103]

CDs have also been used to reduce drug degradation in topical preparations. β-CD maintained the stability of tixocortol 17-butyrate, 21-propionate in vaseline and oil/water emulsion bases even after 30 days.[80] Complexation with CDs suggested a sensible means to enhance the physicochemical properties of drugs for transdermal delivery. β-CD and HPBCDs increased the skin permeability of dexamethasone and also improved its stability in skin by protecting it against skin metabolism.[104]

Brain Drug Delivery or Brain Targetting

The concept of Bodor's chemical delivery system (CDS) (e.g. covalent coupling of drugs to 1-methyl-1,4-dihydronicotinic acid through an enzymatically labile linkage, which

increases drug lipophilicity) was applied for targetting drugs such as steroids, antitumor agents, and calcium channel antagonists to the brain.[105] However, presence of the lipophilic moiety makes prodrugs of CDSs poorly water-soluble. HPBCD, due to its ability to solubilise drugs and also to enhance the chemical stability of dihydronicotinic acid in aqueous solution solved the solubility problems of the CDS.[105] Formulation development of CDSs is based on the need for appropriate dosage form, stability, solubility, and dissolution characteristics. Brewster and Loftsson[106] discussed the use of chemically modified, especially water-soluble, CD derivatives such as HPBCD in the formulation development of CDSs. HPBCD contributed to the development and preclinical testing of several CDSs by providing a stable and water-soluble dosage form suitable for parenteral administration. Use of CDs in the formulation of CDSs can be confirmed by the significantly improved solubility, stability, and pharmacological activity of CDSs of thyrotropin-releasing hormone analogues on complexation with HPBCD.[105]

CD Applications in the Design of Novel Delivery Systems

Liposomes

In drug delivery, the concept of entrapping CD-drug complexes into liposomes combines the advantages of both CDs (such as increasing the solubility of drugs) and liposomes (such as targetting of drugs) into a single system and thus avoids the problems associated with each system.[107] Liposomes entrap hydrophilic drugs in the aqueous phase and hydrophobic drugs in the lipid bilayers and retain drugs *en route* to their destination. The fact that some lipophilic drugs may interfere with bilayer formation and stability limits the range and amount of valuable drugs that can be associated with liposomes. By forming water-soluble complexes, CDs would allow insoluble drugs to accommodate in the aqueous phase of vesicles and thus potentially increase drug-to-lipid mass ratio levels, enlarge the range of insoluble drugs amenable for encapsulation (i.e. membrane-destabilising agents), allow drug targetting, and reduce drug toxicity. Problems associated with intravenous administration of CD complexes such as their rapid removal into urine and toxicity to kidneys, especially after chronic use, can be avoided by their entrapment in liposomes.[108,109]

Microspheres

In the presence of a high percentage of highly soluble hydrophilic excipients, complexation may not improve the drug dissolution rate from microspheres. Nifedipine release from chitosan microspheres was impeded on complexation with HPBCD in spite of the enhanced drug-loading efficiency. Since CD molecules rarely diffuse out of the microspheres, even with a low stability constant, the complex must first release the free drug that can permeate out of the microspheres. Therefore the observed slow nifedipine release from the microspheres was reported to be due to lesser drug availability from the complex and also due to formation of hydrophilic chitosan/CD matrix layer around the lipophilic drug that further decreases the drug matrix permeability.[110] Sustained hydrocortisone release with no enhancement of its dissolution rate was observed from chitosan microspheres containing its HPBCD complex. The sustained hydrocortisone release was reported to be due to formation of a layer adjacent to the interface by the slowly-dissolving drug during the dissolution process that makes the microsphere surface increasingly hydrophobic.[111]

Microcapsules

β-CD microcapsules, because of their ability to retard the release of water-soluble drugs through semipermeable membranes, can act as release modulators to provide efficiently controlled release of drugs. Terephthaloyl chloride (TC) crosslinked β-CD microcapsules were found to complex *p*-nitrophenol rapidly and the amount complexed increased as the size of the microcapsules decreased.[112] TC crosslinked β-CD microcapsules retarded the diffusion of propranolol hydrochloride through dialysis membrane.[112] Double microcapsules, prepared by encapsulating methylene blue with different amounts of β-CD microcapsules inside a crosslinked human serum albumin (HSA), showed decreasing release rate of methylene blue with increasing amount of β-CD microcapsules.[112] Dissociation of methylene blue complex with β-CD microcapsules was found to serve as an additional mechanism in controlling the release kinetics of HSA double microcapsules. In the case of HSA microcapsules with parent β-CD, the hydrating property of the CD, by promoting the diffusion of water into the microcapsules, caused an increased release rate of methylene blue compared with those without the CD. However, in the case of HSA double microcapsules (i.e. with β-CD

microcapsules), the hydrophobic groups introduced during crosslinking suppressed the CD hydration and provided controlled release without enhancing the diffusion of water that can impair the complexation of methylene blue.[112]

Nanoparticles

Nanoparticles are stable systems suitably designed for targetted drug delivery and to enhance the efficacy and bioavailability of poorly soluble drugs. However, the safety and efficacy of nanoparticles are limited by their very low drug loading and limited entrapment efficiency that may lead to excessive administration of polymeric material.[113,114] Two applications of CDs have been found very promising in the design of nanoparticles: one is increasing the loading capacity of nanoparticles and the other is spontaneous formation of either nanocapsules or nanospheres by nanoprecipitation of amphiphilic CD diesters. Both of these proved to be useful due to the great interest in nanoparticles in oral and parenteral drug administration. CDs increased the loading capacity of poly(isobutylcyanoacrylate) nanoparticles. The increased loading capacity was reported to be a result of increased drug concentration in the polymerisation medium on addition of the drug:CD complex and increased number of hydrophobic sites in the nanosphere structure on association of large amounts of CDs to the nanoparticles.[109] HPBCD increased saquinavir loading into poly(alkylcyanoacrylate) nanoparticles by providing a soluble drug reservoir in polymerisation medium that feeds the nanoparticle-formation process. A dynamic equilibrium was observed between the complex, the dissociated species, and the forming polymeric particle.[109,115,116] It was indicated that during nanoparticle formation the free drug becomes progressively incorporated into the polymer network, driven by the drug partition coefficient between the polymer and polymerisation medium.

Thus, the most noteworthy uses of CDs in the pharmaceutical industry include:

- Increasing aqueous solubility, dissolution rates, release rates and bioavailability of various water-insoluble drugs
- Improving chemical stability of unstable drugs by providing increased protection from photodegradation, hydrolysis, decomposition, oxidation, racemisation and isomerisation

- Suppressing volatile and unpleasant odours or tastes associated with the drug
- Avoiding incompatibility problems with other drugs or excipients in a formulation
- Reducing local irritance and haemolysis caused by a drug.

In conclusion, cyclodextrin complexes of pharmaceuticals have significant consequences with regard to their physical performance and worldwide about thirty different pharmaceutical products containing CDs have reached the market thus far.[117,118] The enhanced physical properties of such complexes can be costly initially but in the long run patient benefit can prevail over these expenses. The supramolecular modification of drugs covers a wide range of activities of which polymorphism and cyclodextrin inclusion have already added much value to the discussion. An additional, yet innovative approach to modifying drugs is by co-crystallisation strategies. An overview of co-crystallisation and its potential application in the pharmaceutical industry follows.

1.3 PHARMACEUTICAL CO-CRYSTALS

Introduction

Crystalline material obtains its major physical properties from its molecular arrangement within the solid, and altering the placement and/or interactions between these molecules can have a direct impact on the properties of the particular solid.[119,120] Solid-state chemists employ a variety of different strategies when attempting to modify the chemical and physical solid-state properties of active pharmaceutical ingredients (APIs), namely, the formation of salts, polymorphs, solvates, and co-crystals, as illustrated in Figure 1.15.[119]

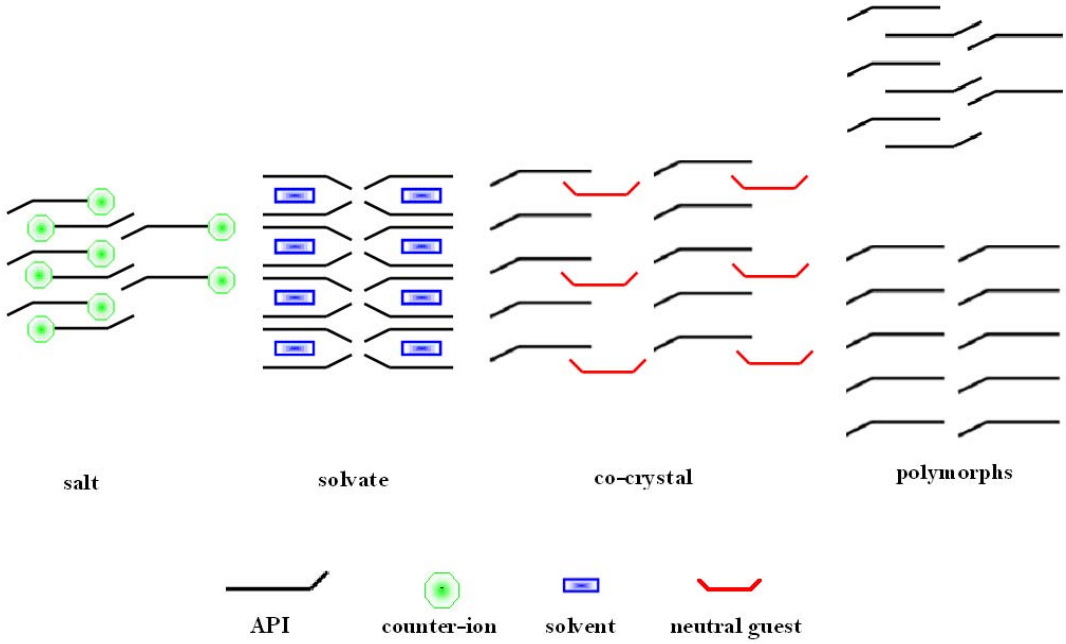

Figure 1.15 Physical state properties of APIs (adapted from reference 119).

These days many of the medicines on the market are administered as salts since salt formation is one of the principal solid-state approaches used to alter the physical properties of APIs.[119] The API must, however, include a suitable (basic or acidic) ionisable site, which can be a major drawback with this approach. Co-crystals present a different pathway, where any API regardless of acidic, basic, or ionisable groups, could possibly be co-crystallised.[119] This feature helps complement existing methods by re-introducing molecules that had limited pharmaceutical profiles based on their non-

ionisable functional groups. Additionally, the number of potential non-toxic co-crystal formers (or co-formers) that can be incorporated into a co-crystalline reaction is very large.[121]

A co-crystal is a multicomponent assembly of compounds held together by freely reversible, noncovalent interactions. It is believed to be the consequence of a molecular recognition event between different molecular species[122,123] and further clarification of the definition is that co-crystals are "made from reactants that are solids at ambient temperature".[124]

Crystal Engineering and Design of Pharmaceutical Co-crystals

The most frequently studied functional groups in crystal engineering are carboxylic acid moieties. They present an essential building block in the formation of intermolecular interactions. In supramolecular chemistry a more appropriate term given to this building block is a 'supramolecular synthon'. The carboxylic acid group exists in most prescription drugs and its complementary hydrogen bond donor and acceptor sites make supramolecular homosynthon I favourable (Figure 1.16). However, supramolecular heterosynthon II is favoured over I and supramolecular heterosynthon IV is favoured over supramolecular homosynthons I and III. Supramolecular heterosynthons are energetically more favoured and their formation is the most consistent and robust route to designing co-crystals.[121,124,125]

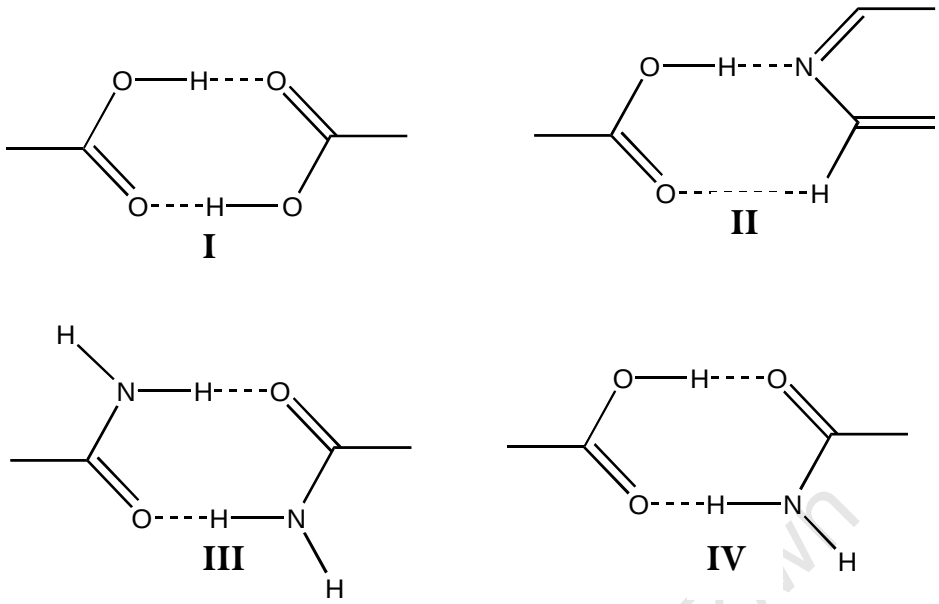

Figure 1.16 Examples of supramolecular homosynthons and heterosynthons.

Generally, for superior co-crystallisation research, theme functional group compatibility (supramolecular synthons), as illustrated in Figure 1.16, serve as an established primary step. The API is evaluated according to number and arrangement of hydrogen bond donors and acceptors,[124] salt forming ability (where difference between conjugate acid and conjugate base is at least ≥ 3 pK_a units, 'rule of three'),[124] conformational flexibility, and solubility requirements.[125-128] APIs that are rigid, highly symmetrical, have strong non-bonded interactions, and have low molecular weight are more likely to co-crystallise with additional components (co-formers or counter-molecules). Suitable co-formers are frequently selected based on hydrogen bonding rules,[126] probable molecular recognition events,[121] and toxicological profiles. Prediction of a co-crystallisation reaction is not yet possible,[128] and thus reactions must be carried out experimentally under varied conditions with different techniques to produce co-crystals.[119]

Co-crystal Characterisation

A number of different characterisation techniques can be used to help distinguish between co-crystals and salts, and it should be noted that in some cases differentiation between the two may be somewhat difficult. Single crystal X-ray diffraction is the preferred characterisation technique; however, suitable X-ray quality crystals cannot always be produced.[119] Thus, various solid-state, spectroscopic techniques such as

Raman, infrared, and solid-state NMR spectroscopy are used when attempting to characterise potentially new co-crystalline materials,[129,130] especially when the locations of hydrogen atoms are indistinct.

Infrared spectroscopy can also be a very powerful tool in detecting co-crystal formation, especially when a carboxylic acid is used as a co-former and/or when a neutral O–H•••N hydrogen bond is formed between an acid and a base. Distinct differences, within the IR spectra, can be observed between a neutral carboxylic acid moiety and a carboxylate anion.[122,124] A neutral carboxylic group (-COOH) displays a strong C=O stretching band around 1700 cm^{-1} and a weaker C–O stretch around 1200 cm^{-1}, while a carboxylate anion ($-COO^-$) displays both asymmetric CO_2 stretch (1650-1540 cm^{-1}) and symmetric CO_2 stretch (1450-1360 cm^{-1}). If a neutral intermolecular O–H•••N hydrogen bond were to form between the components, then two broad stretches around 2450 and 1950 cm^{-1} would be observed.[124] Observations about the state of the carboxylic moiety (neutral or ionic) can also be confirmed through measuring the C–O and C=O bond distances from single-crystal X-ray data. A typical C=O bond distance is around 1.2 Å, while the C–O bond distance is around 1.3 Å; however, if deprotonation has occurred (as in $-COO^-$) then the resonance stabilised C–O bond distances will be practically identical.[119]

Preparation of Co-crystals

Briefly, co-crystals are usually synthesised by slow evaporation from a solution that contains stoichiometric amounts of the components, by sublimation, growth from melt, slurries, neat grinding and solvent drop-grinding.[123] A detailed understanding of the supramolecular chemistry of the functional groups present in a given molecule is a prerequisite for designing a co-crystal since it facilitates selection of appropriate co-crystal formers. With multiple functional groups, the hierarchy of possible supramolecular synthons is not easily addressed.[124] Furthermore, the role of the solvent in nucleation of crystals and/or co-crystals can be critical in obtaining a particular co-crystal from solution.[124] A more detailed description of the preparative methods for co-crystallisation and analysis of co-crystals is presented in Chapter 2.

Relevance of Pharmaceutical Co-crystals

Co-crystallisation will profoundly affect physical properties such as solubility, stability, dissolution rate, and bioavailability of the API. Co-crystallisation proposes several opportunities without making or breaking covalent bonds by modifying chemical and physical properties of APIs.[125] Co-crystals in the context of the pharmaceutical industry are not limited to form and formulation; they may also be used to isolate or purify an API during processing and the co-former could be discarded prior to formulation. Additionally co-crystallisation with homochiral co-crystal formers might be used to separate enantiomers as well.[125] A detailed discussion of the physicochemical properties such as melting point, stability, solubility, dissolution, bioavailability, scale-up, polymorphism, intellectual property and lifecycle management of co-crystals follows, with special emphasis on the pharmaceutical industry.

Physicochemical Properties of Co-crystals

Melting Point

To determine the melting point of a compound is standard practice as a means of characterisation or purity assessment. In the pharmaceutical sciences, the melting point is also important due to its relationship with aqueous solubility and vapour pressure.[131] The melting point, in fact, has been directly correlated with the Logarithm of solubility.[132] Being able to establish the melting point of a particular API before it is synthesised would be very beneficial in order to modify its aqueous solubility. However, correlations relating chemical structure directly to melting point data remain vague.[133] Given the number of factors contributing to the melting point of a crystalline solid, including the molecular arrangement within the crystal, molecular symmetry, intermolecular interactions, and conformational degrees of freedom for a molecule, one clearly observes the difficulties in attempting to draw comparisons from molecular structure to crystalline lattice energy to melting point. When observing multi-component systems such as co-crystals, the situation becomes more complex because each component has its own characteristic properties and those can influence the environment (and intermolecular interactions) around its neighbours.[132]

The API AMG517 (an analgesic) co-crystallises with 10 co-formers and the melting points of the resulting co-crystals were compared.[134] Each of the co-crystals displayed a melting point that fell between the melting point of AMG517 and that of the co-former. A plot generated using the melting points of the co-crystals and co-formers displayed a direct proportionality between the two (r=0.7849). Hence, the variability of the melting point of the co-crystal can be attributed to the variability of the co-former's melting point. These data thus showed that within the set of AMG517 co-crystals the melting point can be altered according to which co-former is chosen; for example, if a higher melting co-crystal is desired, then a higher melting co-former should be selected.

High melting points even though desirable at times, may result in poor solubility characteristics. Alternatively, low melting points can hinder processing, drying, and stability characteristics.

Stability

Stability is a key factor studied during the development of a new chemical entity. Several types of stability need to be considered depending on the structure and characteristics of the molecule. Chemical and physical stability data are generally obtained under accelerated stability conditions to determine developability and shelf life.[135] Water uptake is included from a handling and packaging point of view. The amount of water present can also lead to form changes or even degradation and so the effect of water uptake should be investigated early in the process.[136] Thermal stress studies are also incorporated, and extra work may be expected for hydrates or thermally labile materials. In the case of co-crystals and salts, solution stability may be a factor due to dissociation of the material, resulting in precipitation of the less soluble parent compound or a less soluble form (such as a hydrate in aqueous media).[137]

Relative Humidity Stress

Relative humidity (RH) variation is a vital concern when developing any drug compound.[136,138] X-ray powder diffraction (PXRD) data collected on a solid at the end of a moisture balance experiment provides information on the final form, but not necessarily on any form conversions that may have transpired during the experiment.

Moisture uptake throughout the course of the experiment may justify longer exposure at a specific relative humidity using a relative humidity chamber and subsequent analysis of the sample after equilibration.

An example for water sorption/desorption data was found for co-crystals where a 1:1 indomethacin/saccharin co-crystal showed about <0.05% water uptake at 95% RH.[139] No solid-state transformation was suggested, although PXRD data of the sample after the moisture balance experiment were not reported. Hence, relative humidity may not be a major concern for this co-crystal; however, longer exposure to these relative humidities may produce more significant effects.

Thermal Stress

High temperature stress is a common condition used to determine chemical and physical stability based on accelerated stability conditions.[135] Paracetamol co-crystals of 4,4'-bipyridine, 1,4-dioxane, *N*-methylmorpholine, morpholine, *N*,*N*-dimethylpiperazine, and piperazine were analysed by DSC.[140] The paracetamol/4,4'-bipyridine sample was the only co-crystal that did not lose the co-former upon heating and by coincidence exhibited a melting endotherm corresponding to the monoclinic form of paracetamol. Heating studies provide information on elevated temperature transitions and can provide support regarding possible long-term stability problems and guidance on drying steps.

Chemical Stability

Chemical stability is generally studied to minimise any chemical degradation that may occur during the developmental stages of a new compound and during formulation. The comparison of a co-crystal with the parent API can provide important information for development. A 1:1 carbamazepine:saccharin co-crystal was compared with carbamazepine (Form III) in a chemical stability study using temperature (5, 40, and 60 °C at ambient humidity) and elevated RH conditions (25 °C/60% RH and 40 °C/75% RH) over two months.[141] Degradation was not observed for either material at the elevated temperatures; however, both materials showed similar degradation patterns under the second set of conditions. Hence, it was proved that the co-crystal was just as stable as the marketed carbamazepine form under the set conditions.[119]

Solution Stability

The definition of solution stability is the ability of the co-crystal components to stay in solution and not readily crystallise. A range of vehicles including water, simulated gastric fluid (SGF), simulated intestinal fluid (SIF), formulation vehicles, and buffered solutions may be employed. Solubility or dissolution experiments may be included to obtain a more complete picture of the behaviour of the co-crystal and the solid form remaining at the end of the experiment. Because dissociation of a co-crystal can occur, solution stability is a key consideration for development. In the study of caffeine co-crystals,[142] the 2:1 caffeine/oxalic acid co-crystal was found to be stable at all relative humidities up to 98% RH for 7 weeks. The material was then slurried in water at ambient temperature for two days,[142] and no change in physical form was observed, demonstrating the stability of the material.

Solubility

Increasing the solubility of a poorly soluble compound is beyond a doubt one of the main motives for studying co-crystals. There are a number of considerations when discussing solubility data of which the first is equilibrium versus kinetic solubility measurements. Kinetic solubility values are approximate values usually based on one measurement at one time point. For equilibrium solubility, a number of time points and measurements are recorded to ensure that the solution has reached equilibrium, as evidenced by a plateau in the concentration data. This is called powder dissolution.[129] Powder dissolution rates can also be dependent on particle size. Another consideration is form changes during the experiment. When form changes occur, the solubility data obtained may not be relevant to the starting compound in the experiment. Form changes can be suggested by solubility data collected at various time points by a precipitous drop in concentration indicating crystallisation of a less soluble form (Figure 1.16).[119] Suggested form changes can be confirmed by analysis of the solid form remaining at the end of the experiment.

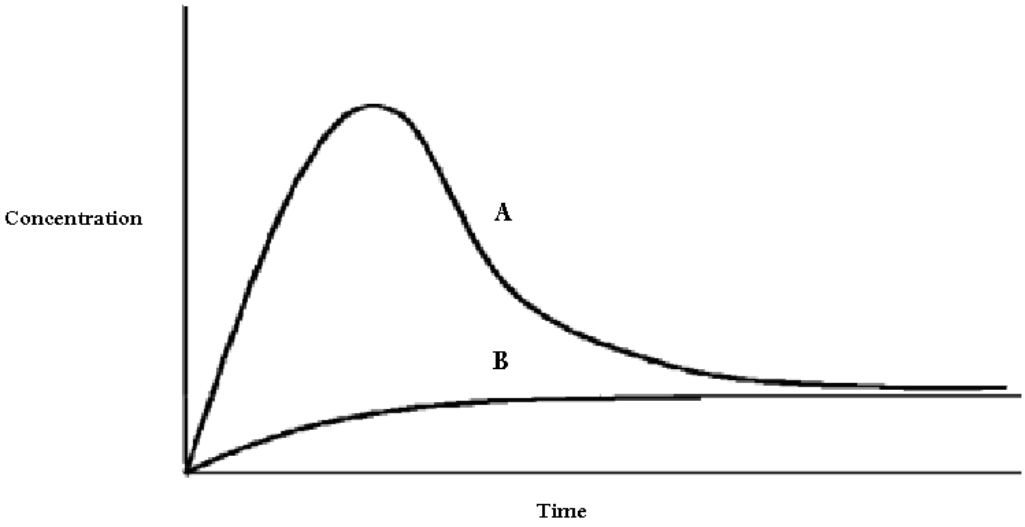

Figure 1.16 Schematic of a solubility curve due to a form change and precipitation of a less stable form (curve A); at equilibrium, the curve will level out to the solubility of the less soluble form. Curve B represents the less soluble form.

Intrinsic Dissolution

Intrinsic dissolution measures the rate of dissolution without the effect of particle size. A compressed disc or pellet is used and solution concentration is measured over time to determine the dissolution rate. The disc remains intact during the experiment, so compression pressures may be critical for poorly compressible powders.[119] No form change should occur during compression of the disc. PXRD data can be obtained on the initial disc and the remaining disc after completion of the experiment to determine any major form changes that may affect the dissolution data. Data for the glutaric acid co-crystal of 2-[4-(4-chloro-2-fluorophenoxy)phenyl]pyrimidine-4-carboxamide[143a] were collected in water over 90 min and showed that the co-crystal dissolution was about 18 times faster than that of the parent compound. PXRD of the solid left behind showed mainly the glutaric acid co-crystal, with minor peaks for the parent material, indicating that the results were not distorted by any form changes during the dissolution test.

Bioavailability

Bioavailability is a measure of the rate and extent of the active drug that reaches systemic circulation.[143b] The bioavailability of APIs in animals such as rodents, rabbits,

dogs, pigs, and primates is an important parameter to consider when preparing new forms of a compound. During early drug development, small studies (4-6 animals) to determine pharmacokinetic data are undertaken. The same animals are generally used for all forms/formulations, with a washout period of about a week. This gives a direct comparison within the same animals for all the materials in the study.[119]

Both the parent material and the co-crystal will give a direct assessment of bioavailability improvements due to the co-crystal. The amount of drug in the blood is measured periodically after oral administration of the original form and after administration of the co-crystal.[119] It is important to note that the materials used in the study need to be formulated in the same way if a direct comparison is desired. Most dosing is done orally and formulation possibilities include powder in a capsule, powder and excipient in a capsule, or liquid formulations (solutions or suspensions). It is important to differentiate between solutions and suspensions since dissolution of the solid in a solution could significantly enhance bioavailability. Absolute bioavailability includes not only the co-crystal formulation, but an IV formulation as well to determine maximum exposure based on the IV data and a comparison with the oral formulation.[119]

In a bioequivalence study, a 1:1 AMG 517/sorbic acid co-crystal[134,144] was compared to the parent free base administered in a rat model. A significant increase in bioavailability was observed for the co-crystal. It was found that a 30 mg/kg dose of the co-crystal resulted in comparable exposure to a 500 mg/kg dose of the free base.

Scale-up

For pharmaceutical co-crystals to move from small scale screening to large scale high co-crystal purity and yields, adequate scaling-up processes must be employed. With slow evaporation and grinding being the two most common techniques for co-crystal production, limitations with regard to scaling up are inevitable.[145]

A carbamazepine/saccharin co-crystal was produced on a 30 kg scale through solution crystallisation.[141] The components were dissolved in a mixture of ethanol and methanol (~3:1) and refluxed at 70 °C for 1 h. The temperature was then lowered, and the precipitate was filtered, dried, and characterised as the 1:1 co-crystal of carbamazepine and saccharin. Notably, no seeding was required under the reaction conditions selected, to produce the desired co-crystalline form in high purity.

A carbamazepine/nicotinamide co-crystal scale-up study outlined three criteria to be examined during the crystallisation methodology: (a) to determine an appropriate solvent system; (b) to identify the pathway, through multicomponent solid-liquid phase equilibrium diagrams, to produce the desired form; (c) to determine a mechanism to induce nucleation and control the desaturation kinetics of the process. Through a seeding strategy in ethanol, the co-crystal was successfully produced on a 1 L scale in ethanol with yields in excess of 90%.

Ternary phase diagrams should also be considered when scaling up co-crystals from solution because information about the relationship between equilibria of the solid phases and solvent choices is then accessible. The solubilities of the individual components must be determined and mapped since the phase region where the most thermodynamically stable co-crystal is located will be altered based on whether or not the components possess similar solubilities in a given solvent.[119] Thus, evaluation and optimisation of scaleable co-crystals is essential if the pharmaceutical industry sees a viable future for such products.

Co-crystal Polymorphism

Since polymorphic compounds can possess very different physical and chemical properties, polymorphic co-crystals can possess varying physicochemical properties between forms. For example, a conformational polymorphic pair of 1:1 co-crystals was observed when a chloroform solution of caffeine and glutaric acid was allowed to slowly evaporate.[146] Crystals of two different morphologies, rods (Form I) and blocks (Form II), crystallised concomitantly. As revealed by X-ray studies, differences arose in the torsion angles involving the methylene carbons on the acid component. Each of the forms could be produced individually through mechanical grinding. In the absence of solvent or when a fairly nonpolar solvent was used, Form I was produced; however, when a more polar solvent was employed, Form II resulted. Form II was found to be more stable with respect to humidity, as Form I displayed partial conversion to Form II after 1 day at 43% RH, with full conversion to Form II after 1 day at 75% RH. This example clearly shows the differences in stability that polymorphic co-crystalline forms can possess.

Intellectual Property (IP) and Lifecycle Management

Finally, patents are a key element of drug development, especially when covering solid forms. Pharmaceutical patents include composition of matter (molecular structure, solid form, or formulation), method of use (medical indication), and manufacturing processes.[119] The three criteria: novelty, utility, and non-obviousness, must be met for an invention to qualify for patent coverage. To date, there are no known co-crystal products on the market.

Co-crystals can also play a role in lifecycle management.[119] Lifecycle management can involve drug product improvements along with new solid forms. Early in the development process, chemical structures are patented and additional IP protection can be obtained by patenting different solid forms throughout development. If an approved drug product contains a new patented solid form, especially where the solid form offers a commercial advantage over the original form, the solid form patent might provide meaningful IP protection after the expiration of the original patent. However, a solid form that was not found by the innovator, but was found and patented by a competitor, could significantly alter this strategy. Co-crystal screens for potential blockbuster drugs could end up being very large in order to protect, not only the co-crystals found, but also any polymorphs, hydrates, solvates, or other solid forms of the individual co-crystals.[119]

1.4 MOTIVATION AND OBJECTIVES OF THE STUDY

Two pharmacologically active steroids, 2-methoxyestradiol (2ME) and 2-methoxyestradiol-*bis*-sulfamate (2MES), as well as the antiretroviral, nevirapine (NV), were investigated in this study (Figure 1.17).

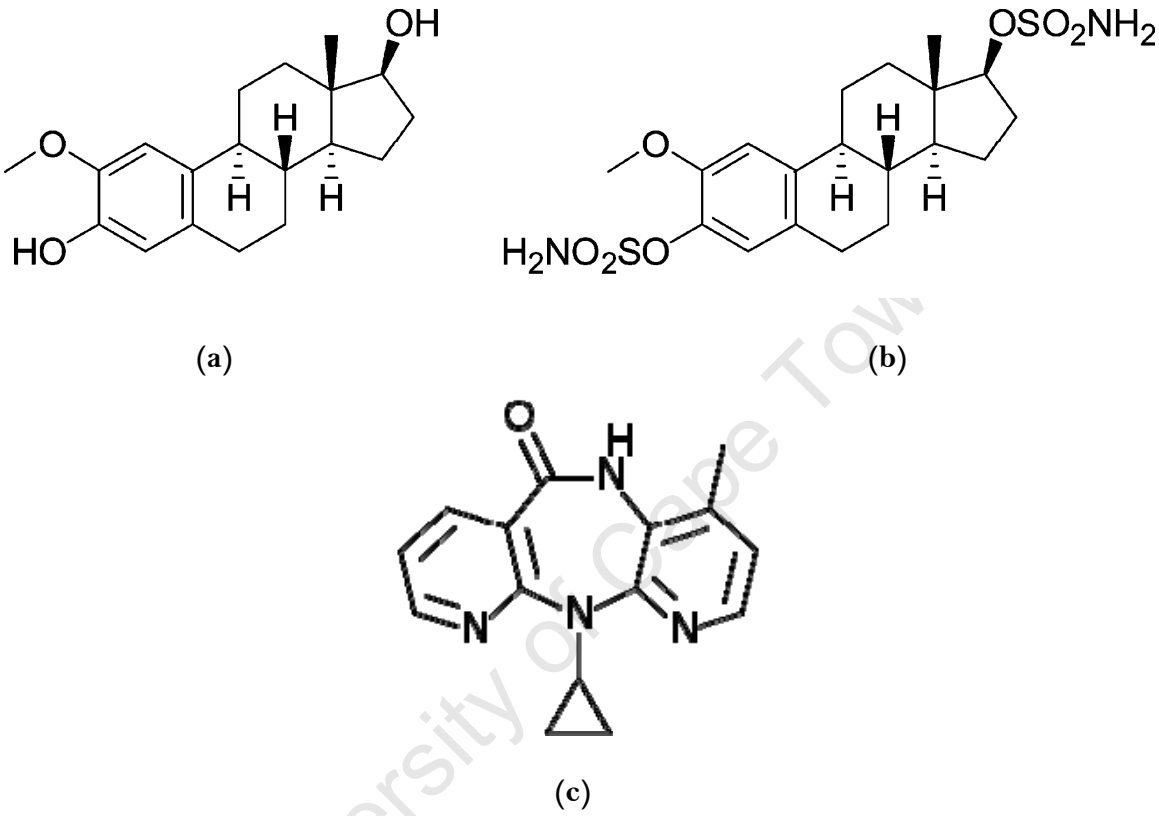

(a) (b)

(c)

Figure 1.17 Pharmacologically active molecules used in this study: (a) 2-methoxyestradiol, (b) 2-methoxyestradiol-*bis*-sulfamate and (c) nevirapine.

2-Methoxyestradiol (2ME) belongs to the family of drugs called angiogenesis inhibitors and is derived from estrogen, although it binds poorly to known estrogen receptors. The chemical name for 2ME is (17β)-2-methoxyestra-1,3,5(10)-triene-3,17-diol. Estradiol, the major endogenous estrogen, metabolises to 2ME via enzymes in vascular cells and furthermore circulates at measurable levels in humans.[147-9] 2ME prevents the formation of new blood vessels that tumours need in order to grow (angiogenesis) and has undergone Phase 1 clinical trials against breast cancers.[147-9] Preclinical models suggest that 2ME could also be effective against inflammatory diseases such as rheumatoid arthritis while also displaying vasodilator activity.[148]

Several studies have been conducted showing 2ME to be a microtubule-inhibitor and effective against prostate cancer in rodents.[148] 2ME is available as a capsule (Panzem®) formulation and NanoCrystal® dispersion (NCD) formulation. In the Phase II trial of the NCD formulation it was found that 2ME was well tolerated and had better bioavailability than the capsule formulation.[148] However, anti-tumour activity was modest, with therapeutic benefit exceeding one year in selected subjects (dose 1000 mg 4 times a day).[148] Studies have indicated that 2ME also inhibits the proliferation of vascular smooth muscle and inhibits injury-induced neointima formation *in vivo*.[149] It has vasculoprotective effects in rat models of drug-induced hypertension and pulmonary hypertension and reduces the oxidation of low-density lipoprotein *in vitro* which raised questions about the anti-atherosclerotic effects of 2ME.[149]

Investigation of its anti-atherosclerotic effects[149] led to the conclusion that 2ME reduces atherosclerotic lesion formation *in vivo* and this finding led to several implications:
1) 2ME may partially mediate the anti-atherosclerotic effect of estradiol in mouse models;
2) the anti-atherogenic activity of an estradiol metabolite lacking estrogen receptor activating capacity may argue that clinical trials on cardiovascular effects of hormone replacement therapy should use estradiol rather than other estrogens; and
3) 2ME may also hold promise for cardiovascular disease prevention.[149]

Furthermore, it was discovered that sulfamoylation significantly enhances the anti-cancer activity of estrogen derivatives, which led to the synthesis of 2MES,[149,150] a sulfamoylated derivative of 2ME and consequently, inclusion of this compound in this study.

2-Methoxyestradiol-3,17-*O,O-bis*-sulfamate (2MES) is a sulfamoylated derivative of 2ME with enhanced activity and improved pharmacokinetic properties and a promising candidate for early clinical trials.[151] After a single oral administration (10 mg/kg) of 2MES, significant concentrations of this compound were still detectable at 24 h.[150] In contrast, no 2ME or metabolites of 2ME were detected in plasma at any time after a 10 mg/kg oral dose. Thus, the bioavailability of 2ME is very low, whereas for 2MES it was 85 %.[151] No significant metabolites of 2MES were detected in plasma after oral or

intravenous dosing, showing that 2MES is resistant to metabolism.[150] In a tumour efficacy model, oral administration of 2MES at 20 mg/kg/day for 28 days almost completely inhibited tumour growth. Inhibition of tumour growth was maintained for a further 28 days after the cessation of dosing, and at this dose 2ME did not inhibit tumour growth.[150] Display of such significant pharmacological potential of 2ME and the advanced activity of its derivative, 2MES, were bound to provoke the interest of the formulating chemist.

Neither 2ME nor 2MES is recorded in the CSD,[40] hence single crystal X-ray structural elucidation was considered essential for the commencement of the study. Polymorphic behaviour in steroids is quite common (about 66% of steroids show polymorphic behaviour), hence elucidating other forms of both 2ME and 2MES could be of much commercial interest since any modification of the crystal structures could alter physicochemical properties as well as biological activity considerably. 2ME is sparingly soluble in aqueous media at pH 1 to 8 with an experimental value of 0.0048 g/L (25 °C) across the pH ranges. The solubility of 2MES was not in evidence in the literature and for comparative reasons one of the first objectives was to determine its solubility relative to that of 2ME.

With 2ME currently in clinical trials as a treatment for different cancers and with trials being carried out relating to an oral version of 2ME to treat primary tumours, the oral version of 2ME seems to be poorly suited to entering the bloodstream and reaching the actual tumour site.[151] This stated, it is the physicochemical property of solubility that represents the limiting factor for the oral administration of 2ME (0.0048g/L water at pH 7 and 25°C). Hence, the formation of complexes of selected cyclodextrins (CDs) with 2ME may extend the applications of 2ME. CDs are able to enhance the stability, aqueous solubility, dissolution and ultimately, the bioavailability of drugs.[152] To date, there is no record of any attempts to complex 2ME with CDs. However, many attempts were made to complex other steroidal molecules with CDs. Thus far, the structure of only one steroidal cyclodextrin inclusion complex, that containing rocuronium bromide as guest,[143a] has been elucidated using single crystal X-ray analysis.[40] Significant solubility improvement of 2ME by CD inclusion would be of great interest to

researchers. Thus, investigation of the interaction between 2ME and a wide variety of CDs was considered a worthy topic for research.

Nevirapine, condemned as "the drug from hell" by AIDS dissidents while heralded as a "godsend" by many health professionals, is used to eliminate the deadly HIV virus.[153] HIV is an acronym for the Human Immunodeficiency Virus, a retrovirus that causes AIDS (acquired immunodeficiency syndrome) by infecting helper T cells of the immune system. HIV uses the enzyme reverse transcriptase to incorporate its own genetic material into host cells, which then allows it to reproduce freely. Nevirapine, a member of the dipyridodiazepinone class of anti-HIV drugs with the systematic name 11-cyclopropyl-5,11-dihydro-4-methyl-6H-dipyrido[3,2-b:2′,3′-e][1,4]diazepin-6-one (Figure 1.17), manufactured by Boehringer Ingelheim, one of a class of drugs known as non-nucleoside reverse transcriptase inhibitors (NNRTIs),[154] prevents this enzyme from functioning. This results in a reduced amount of virus in the body and an increase in the CD4 cell (T cell) count, improving the host's immune function, and thereby reducing the risk of new and opportunistic infections, and death.

In 2002, nevirapine was at the centre of a court case and a major political debacle where South African health professionals and AIDS activists were jointly lobbying their government, protesting in the streets and finally taking the matter to court.[153] The court case arose due to government not providing adequate access to the HIV treatment programme thereby contravening the 'right to health' and access to modern medicine. The people of South Africa won the case and government was forced to provide treatment to all with HIV and AIDS.

Nevirapine has been widely used in adults as one of a combination of drugs to treat established HIV infection. It has a special role in the prevention of mother-to-child transmission of HIV, as it is effective when given alone as a single dose to the mother at the beginning of labour and as one dose administered to the baby within 72 hours of birth.[155] Nevirapine given to HIV-positive pregnant women rapidly crosses the placenta into the foetus with its effects lasting through the first week of life. The timing of its delivery to the mother during labour is important as up to two-thirds of infants born

with HIV are infected in the birth canal.[155] Thus, nevirapine as a 'risk' or 'necessity' is every medical practitioner's nightmare and this applies to numerous other APIs in the pharmaceutical industry.

Clinical trials have confirmed the efficacy of nevirapine in preventing mother-to-child transmission of HIV. No trials are available comparing nevirapine with placebo. The Ugandan HIVNET 012 study involving 626 women showed that nevirapine was able to reduce mother-to-child transmission by 47 %, with only 8.1 % of infants exposed to nevirapine acquiring HIV at birth.[156] Almost all the babies were breast-fed, resulting in ongoing exposure to HIV. Despite this, the benefits of nevirapine were maintained with a 42 % reduction in transmission at the age of 12 months.[156]

In the South African Intrapartum Nevirapine Trial (SAINT), 1306 mother/infant pairs were randomised to either nevirapine during labour and post-delivery, or multiple doses of AZT/3TC during labour and for one week after delivery to mother and baby. In both treatment arms, about 40 % of infants were breast-fed. Eight weeks after birth, there was no significant difference observed between the rate of HIV infection or death across the two treatment arms, with a rate of 14.3 % in the simpler nevirapine arm and 12.5 % in the more involved and expensive dual therapy arm.[157] For pregnant women already receiving highly active antiretroviral therapy, there appeared to be no additional advantage of adding nevirapine to an existing regimen.[157]

Nevirapine was approved by the FDA in 1996 for use in combination with nucleoside analogues in adults with HIV infection. Approval was based on studies showing that the combination of nevirapine with zidovudine plus didanosine was more effective in increasing CD4 T-lymphocyte counts and decreasing HIV viral load than a regimen of zidovudine plus didanosine alone. Approval for pediatric use was granted in 1998. The FDA has granted generic versions of nevirapine "tentative approval" status for purchase and use only as part of the President's Emergency Plan for AIDS Relief (PEPFAR) in resource-limited countries. Nevirapine is available in tablets and oral suspension. The adult dose is 200 mg daily for 14 days, then 200 mg twice daily; nevirapine should not be initiated in women with CD4 >250 cells/μL or men with CD4 >400 cells/μL, unless the benefit clearly outweighs the risk. The paediatric dose (age 15 days to adolescence)

is 150 mg/m^2 daily for the first 14 days, then 150 mg/m^2 twice daily. The maximum total daily dose is 400 mg.

For the purpose of this study, our interest in this drug stems from its unique chemical structure, which differs significantly from other commercially available NNRTIs.[158] Specifically, from a crystal engineering viewpoint, the presence of the amide function CO–NH in the nevirapine molecule presents a unique candidate for co-crystallisation experimentation as reviewed earlier in the chapter.

For the co-crystallisation experiments, the following 12 compounds were chosen for this study as suitable co-formers with nevirapine viz. saccharin, nicotinamide, isonicotinamide, succinic acid, tartaric acid (racemic, D and L), citric acid, oxalic acid, stearic acid, L-aspartic acid and maleic acid. These potential co-formers were chosen based on the presence of their carboxylic acid moieties and/or because they appear on the GRAS (generally regarded as safe) list. Nevirapine, as noted by its structure, was uniquely identified for successful attempts at co-crystallisation. It should be noted that during co-crystallisation experimentation, several nevirapine solvates were identified and shared with the University of North-West for publication purposes (see page *iv*).

Objectives

The primary objectives of the study described in this thesis were:

1. The preparation of 2-methoxyestradiol and 2-methoxyestradiol-*bis*-sulfamate polymorphs using several methods discussed in chapter 2. The characterisation of these products by TGA, DSC, HSM and PXRD.
2. The preparation of 2-methoxyestradiol cyclodextrin inclusion complexes using methods discussed in chapter 2. The characterisation of these products by TGA, DSC, HSM and PXRD.
3. The attempted preparation of a limited series of nevirapine co-crystals as 'proof of concept' using methods discussed in chapter 2 and their characterisation by TGA, DSC, HSM and PXRD.
4. The investigation of the detailed solid-state features of the polymorphs, cyclodextrin inclusion complexes and co-crystals using single crystal X-ray diffraction.

5. Furthermore, measurement of the solubilities and/or dissolution profiles of the various targetted products was considered an important objective to assess the possible pharmaceutically-relevant consequences of supramolecular modification.

1.5 REFERENCES

1. Bernstein J., *Polymorphism in Molecular Crystals – IUCr Monographs on Crystallography*, Oxford: Clerendon Press, **2002**, 14.
2. Guillory J.K., *In: Polymorphism in Pharmaceutical Solids, Brittain H.G. (Ed.)*, New York: Marcel Dekker, Inc., **1999**, 5, 183-226.
3. Aulton M.E. (Ed.), *Pharmaceutics: The Science of Dosage Form Design*, Spain: Churchill Livingstone Press, Second Edition, **2002**, pp. 8, 26, 142-149.
4. Mitscherlich E., *Ann. Chim. Phys.*, **1822**, 19, 350.
5. Lima-de-Faria J. (Ed.), *In: Historical Atlas of Crystallography*, Dordrecht, The Netherlands: Kluwer Academic Publishers, **1990**, 68-69.
6. Lehmann O., PhD Thesis, *Die Krystallanalyse oder die Chemische Analyse durch Beobachtung der Krystallbildung mit Hülfe des Mikroskops*, Wilhelm Englemann, Leipzig, **1891**.
7. Amici G.B., *Ann. Chim. Phys.*, **1844,** 3, 114-120.
8. Ostwald W.F.Z., *Phys. Chem.*, **1897**, 22, 289-330.
9. Tammann G., *The States of Aggregation (Trans. R. F. Mehl)*, London: Constable Company Ltd., **1926**, 116-157.
10. Caira M.R., *In: Topics in Current Chemistry*, Berlin, Heidelberg: Springer-Verlag, **1998**, 198, 164-208.
11. Burger A., Ramberger R., *Mikrochim. Acta*, **1979**, II, 259-272.
12. Yu L., *J. Pharm. Sci.*, **1995**, 84, 996-974.
13. Volmer M., *Kinetic der Phasenbildung*, Stankopf, Leibzig, **1939**.
14. Corradini P., *Chem. Ind. (Milan)*, **1973**, 55, 122-129.
15. Etter M.C., Macdonald J.C., Bernstein, J., *Acta Crystallogr.*, **1990**, B46, 256-262.
16. Bernstein J., Davis R.E., Shimoni L., Chang N-L., *Angew. Chem., Int. Ed. Engl.*, **1995**, 34, 1555-1574.
17. Romans R.G., Scott D.A., Fisher A.m., *Ind. Eng. Chem.*, **1940**, 32, 908-910.
18. Weissbuch I., Popovitz-Biro R., Lahav M., Leiserowitz L., *Acta Crystallogr.*, **1995**, B51, 115-148.
19. Ngooi T-K., McGolrick J.D., Antczak C., Tindall J.L.A., Preparation of Form 1 Ranitidine Hydrochloride, US patent 5,338,871., **1994**.
20. Maryanoff C.A., *CA*, **1995**, 122, 240, 076k.

21. Ibragimov B.T., Talipov S.A., *J. Incl. Phenom. Mol. Recognit. Chem*, **1994**, 17, 325.
22. Caira M.R., *Polymorphism*, *Encyclopedia of Supramolecular Chemistry*, (Vol 1), Atwood J.L., Steed J.W. (Eds), New York: Marcel Dekker, Inc., **2004**.
23. Yu L., Reutzel-Edens S.M., Mitchell C.A., *Org. Process Res. Dev.*, **2000**, 4, 396-402.
24. Caira M.R., de Vries E.J., *Chem. Comm.*, **2003**, 16, 2058-2059.
25. Okada M., Kamachi M., Harada A., *Macromolecules*, **1999**, *32*, 7202–7207.
26. Szejtli J., In: *Topics in Inclusion Science – Cyclodextrin Technology*, Davies J.E.D. (Ed.), Dordrecht, The Netherlands: Kluwer Academic Publishers, **1988**.
27. Villiers A., *Compt. Rend.*, **1891**, 112, 536.
28. Schardinger F., Z. *Untersuch. Nahr. U. Genussm.*, **1903**, 6, 865.
29. Schardinger F., *Wien. Klin. Wochschr.*, **1904**, 17, 207.
30. Schardinger F., *Zentralbl. Bakteriol. Parasintenkd.*, **1905**, 14, 772.
31. Schardinger F., *Zentralbl. Bakteriol. Parasintenkd.*, Infektionskrankh. Hyg. Abt. 2 Naturwiss: Mikrobiol. Landwirtsch. Technol. Umweltschutzes, **1911**, 29, 188.
32. Freudenberg K., Blomquist G., Ewald L., Soff K., *Ber. Dtsch. Chem. Ges.*, **1936**, 69, 1258.
33. French D., *Adv. Carbohydrate Chem.*, **1957**, 12, 189.
34. Cramer F., *Einschlussverbindungen (Inclusion Compounds)*, Springer-Verlag, Berlin, **1954.**
35. WHO, Toxicological Evaluation of Certain Food Additives and Contaminants, *The Forty-first meeting of the Joint FAO/WHO Expert Committee on Food Additives*, WHO, Geneva, **1993**, WHO Food Additives Series 32, pp. 173-193.
36. Saenger W., *Angew. Chem. Int. Ed. Engl.*, **1980**, 19, 344-361.
37. Breslow R., Dong S.D., *Chem. Rev.*, **1998**, 98, 1997-2012.
38. Saenger W., Jacob J., Gessler K., Steiner T., Hoffman D., Sanbe H., Koizumi K., Smith S. M., Takaha T., *Chem. Rev.*, **1998**, 98, 1787-1802.
39. Sabadini E., Cosgrove T., Do Carmo Egidio F., *Carbohydr. Res.*, **2006**, 341, 270-274.
40. Cambridge Structural Database and Cambridge Structural Database System, Version 5.30, November **2009**, Cambridge Crystallographic Data Center, University Chemical Laboratory, Cambridge, England.

41. a. Lipkowitz K.B., Green K., Yang J., *Chirality*, **1992**, 4, 205.
b. Lichtenthaler F.W., Immel S., *Liebigs Ann.*, **1996**, 27.
c. Harata K., *In Inclusion Compounds*, Attwood J.L., Davies J.E., MacNicol D.D. (Eds.), London: Oxford University Press, **1984**, Vol. 5, Ch. 9.
42. Frömming K.-H., Szejtli J., Topics in Inclusion Science - *Cyclodextrins in Pharmacy*, Dordrecht, The Netherlands: Kluwer Academic Publishers, **1993**, Vol. 5, Ch.1.
43. Szejtli J., *Chem. Rev.*, **1998**, 98, 1743-1753.
44. Liu L., Guo Q-X., *J. Incl. Phenom. Macrocycl. Chem.*, **2002**, 42, 1-14.
45. Bender M.L., Komiyama M., *Cyclodextrin Chemistry*, Berlin: Springer-Verlag, **1978**.
46. Hallen D., Schoen A., Shehatta I., Wadsoe I., *J. Chem. Soc. Faraday Trans.*, **1992**, 88, 2859-2863.
47. Rekharsky M.V., Mayhew M.P., Goldberg R.N., Ross P.D., Yamashoji Y., Inoue Y.A., *J. Phys. Chem. B.*, **1997**, 101, 87-100.
48. Matsui Y., Mochida K., *Bull. Chem. Soc. Jpn.*, **1979**, 52, 2808-2814.
49. Barone G., Castronuovo G., Del Vecchio P., Elia V., Muscetta M., *J. Chem. Soc. Faraday Trans. 1*, **1986**, 82, 2089-2101.
50. Fujiwara H., Arakawa H., Murata S., Sasaki Y., *Bull. Chem. Soc. Jpn.*, **1987**, 60, 3891-3894.
51. Sanemasa I., Osajima T., Deguchi T., *Bull. Chem. Soc. Jpn.*, **1990**, 63, 2814-2819.
52. Harrison J.C., Eftink M.R., *Biopolymers*, **1982**, 21, 1153-1166.
53. a.Tabushi I., Kiyosuke Y., Sugimoto T., Yamamura K., *J. Am. Chem. Soc.*, **1978**, 100, 916-919.
b. Sakurai M., Kitagawa H., Hoshi Y.I., Chûjô R., *Carbohydr. Res.*, **1990**, 198, 181.
54. Harata K., *Seimei Kogaku Kogyo Gijutsu Kenkyushu Kenkyu Hokoku*, **1993**, 1, 1-24.
55. Harata K., In *Comprehensive Supramolecular Chemistry, Cyclodextrins*, Atwood J.L., Davies J.E.D., MacNicol D.D., Vogtle F., (Eds.), Pergamon, Oxford, **1996**, Vol. 3, Ch. 9.
56. Bettinetti G., Sorrenti M., Catenacci L., Ferrari F., Rossi S., *J. Pharm. Biomed. Anal.*, **2006**, 41, 1205-1211.

57. Caira M.R., Bettinetti G., Catenacci L., Cruickshank D., Davies K., *Chem. Comm.*, **2007**, 1221-1223.

58. Caira M. R., *Rev. Roum. Chim.*, **2001**, 46, 371-386.

59. Frömming K.-H., Szejtli J., Topics in Inclusion Science - *Cyclodextrins in Pharmacy*, Dordrecht, The Netherlands: Kluwer Academic Publishers, **1993**, Vol. 5, Ch. 4.

60. Mentzafos D., Mavridis I.M., Le Bas G., Tsoucaris G., *Acta Crystallogr.*, **1991**, B47, 746-757.

61. Lubhelwana S., MSc Dissertation, *Crystal Isostructurality and X-ray Diffraction Studies of Cyclodextrin Inclusion Compounds*, University of Cape Town, South Africa, **2005**.

62. Caira M.R., Bourne S.A., Vilakazi S.L., Reddy L., *Supramol. Chem.*, **2004**, 16, 279-285.

63. Caira M.R., Hunter R., Bourne S.A. and Smith V.J., *Supramol. Chem.*, **2004**, 16, 395-403.

64. Kálmán A., Párkányi L., *In Advances in Molecular Structure Research*, JAI Press Inc., **1997**, 189-226.

65. Smith V.J., Rougier N.M., de Rossi R.H., Caira M.R., Buján E.I., Fernández M.A., Bourne S.A., *Carbohydr. Res.*, **2009**, 344, 2388-2393.

66. Tasic L.M., Jovanovic M.D., Djuric Z.R., *J. Pharm. Pharmacol.*, **1992**, 44, 52-55.

67. Londhe V., Nagarsenker M., *Indian J. Pharm. Sci.*, **1999**, 1, 237-240.

68. Bettinetti G., Gazzaniga A., Mura P., Giordano F., Setti M., *Drug Dev. Ind. Pharm.*, **1992**,18, 39-53.

69. Becket G., Schep L.J., Tan M.Y., *Int. J. Pharm.*, **1999,** 179, 65-71.

70. Ueda H., Ou D., Endo T., Nagase H., Tomono K., Nagai T., *Drug Dev. Ind. Pharm.*, **1998**, 24, 863-867.

71. Sangalli M.E., Zema L., Moroni A., Foppoli A., Giordano F., Gazzaniga A., *Biomaterials.*, **2001**, 22, 2647-2651.

72. Pina M.E., Veiga F., *Drug Dev. Ind. Pharm.*, **2000**, 26, 1125-1128.

73. Higuchi T., Connors K.A., *Adv. Anal. Chem. Instr.*, **1965**, 4, 212-217.

74. Loftsson T., Stefánsson E., *Drug Dev. Ind. Pharm.*, **1997**, 23,473-481.

75. Van Dorne H., *Eur. J. Pharm. Biopharm.*, **1993**, 39, 133-139.

76. Loftsson T., Másson M., Stefánsson E., *Cyclodextrins as Permeation Enhancers*, 17th Pharmaceutical Technology Conference and Exhibition, Dublin, Ireland, March 24-26, **1997**.
77. Rajewski R.A., Stella V.J., *J. Pharm. Sci.*, **1996**, 85, 1142-1168.
78. Nicolazzi C., Venard V., Le Faou A., Finance C., *Antiviral Res.*, **2002,** 54, 121-127.
79. Loftsson T., Brewster M., *J. Pharm. Sci.*, **1996**, 85, 1017-1025.
80. Matsuda H., Arima H., *Adv. Drug Deliv. Rev.*, **1999,** 36, 81-99.
81. Li J., Guo Y., Zografi G., *J. Pharm. Sci.*, **2002**, 91, 229-243.
82. Nagase Y., Hirata M., Wada K., Arima H., Hirayama F., Irie T., Kikuchi M., Uekama K., *Int. J. Pharm.*, **2001,** 229, 163-172.
83. Kang J., Kumar V., Yang D., Chowdhury P.R., Hohl R.J., *J. Pharm. Sci.*, **2002,** 15, 163-170.
84. Ma D.Q., Rajewski R.A., Velde D.V., Stella V.J., *J. Pharm. Sci.*, **2000**, 89, 275-287.
85. Dwivedi A.K., Kulkarni D., Khanna M., Singh S., *Ind. J. Pharm. Sci.* **1999**, 61, 175-177.
86. Szente P.A., Tong P.P., Thomas C.D., United States Patent, Patent no: 6,284,746B1, Date of Patent: Sep. 4, **2001.**
87. Zuo Z., Kwon G., Stevenson B., Diakur J., Wiebe L.I., *J. Pharm. Sci.*, **2000**, 3, 220-227.
88. Yoo S.D., Yoon B.M., Lee H.S., Lee K.C., *J. Pharm. Sci.*, **1999,** 88, 1119-1121.
89. Choi H.G., Lee B.J., Han J.H., Lee M.K., Park K.M., Yong C.S., Rhee J.D., Kim Y.B., Kim C.K., *Drug Dev. Ind. Pharm.*, **2001,** 27, 857-862.
90. Veiga F., Fernandes C., Teixeira F., *Int. J. Pharm.*, **2000,** 202, 165-171.
91. Fathy M., Sheha M., *Pharmazie*, **2000**, 55, 513-517.
92. Okimoto K., Ohike A., Ibuki R., Aoki O., Ohnishi N., Irie T., Uekama K., Rajewski R.A., Stella V.J., *Pharm. Res.*, **1999,** 16, 549-554.
93. Okimoto K., Miyake M., Ohnishi N., Rajewski R.A., Stella V.J., Irie T., Uekama K., *Pharm. Res.*, **1998**,15, 1562-1568.
94. Stevens D.A., *Pharmacotherapy*, **1999**, 9, 603-611.

95. Shinoda T., Kagatani S., Maeda A., Konno Y., Hashimoto H., Hara K., Fujita K., Sonobe T., *Drug Dev. Ind. Pharm.*, **1999**, 25, 1185-1192.

96. Blanchard J., Ugwu S.O., Bhardwaj R., Dorr T., *Pharm. Dev. Technol.*, **2000,** 7, 249-255.

97. Cramer F., Saenger W., Satz H.C., *J. Am. Chem. Soc.*, **1967,** 89, 14-20.

98. Merkus F.W., Verhoef J.C., Marttin E., Romeijn S.G., van der Kuy P.H.M., Hermens W.A.J.J., Schipper N.G.M., *Adv. Drug Deliv. Rev.* **1999**, 36, 41-57.

99. Minami K., Hirayama F., Uekama K., *J. Pharm. Sci.*, **1998**, 87, 715-720.

100. Irie T., Uekama K., *Adv. Drug Deliv. Rev.*, **1999,** 36, 101-123.

101. Dass C.R., *J. Pharm. Pharmacol.*, **2002**, 54, 3-27.

102. Uekama K., Hirayama F., Irie T., *Chem. Rev.*, **1998**, 98, 2045-2076.

103. Lopez R.F., Collett J.H., Bently M.V., *Int. J. Pharm.*, **2000**, 200, 127-132.

104. Doliwa A., Santoyo S., Ygartua P., *Drug Dev. Ind. Pharm.*, **2001**, 27, 751-758.

105. Wu W.M., Wu J., Bodor N., *Pharmazie*, **2002,** 57, 130-134.

106. Brewster M.E., Loftsson T., *Pharmazie*, **2002**, 57, 94-101.

107. McCormack B., Gregoriadis G., *J. Drug Target.*, **1994**, 2, 449-454.

108. McCormack B., Gregoriadis G., *Int. J. Pharm.*, **1998,** 162, 59-69.

109. Duchêne D., Ponchel G., Wouessidjewe D., *Adv. Drug Del. Rev.*, **1999,** 36, 29-40.

110. Filipovic-Grcic J., Laan M.B., Skalko N., Jalsenjak I., *Int. J. Pharm.*, **1996**,135, 183-190.

111. Filipovic-Grcic J., Voinovich D., Moneghini M., Becirevic-Lacan M., Magarotto L., Jalsenjak I., *Eur. J. Pharm. Sci.*, **2000**, 9, 373-379.

112. Pariot N., Levy F.E., Andry M.C., Levy M.C., *Int. J. Pharm.*, **2002**, 232, 175-181.

113. Memisoglu E., Bochot A., Sen M., Duchêne D., Hıncal A.A., *Int. J. Pharm.*, **2003**, 25, 143-153.

114. Monza da Silveira A., Ponchel G., Puisieux F., Duchêne D., *Pharm. Res.*, **1998**, 15, 1051-1055.

115. Boudad H., Legrand P., Lebas G., Cheron M., Duchêne D., Ponchel G.,

Int. J. Pharm., **2001**, 218, 113-124.

116. Loftsson T., Duchêne D., *Int. J. Pharm.*, **2007**, 329, 1-11.

117. Loftsson T., Jarho P., Másson M., Järvinen T., *Expert Opin. Drug Deliv.*, **2005**, 2, 335-351.

118. Brewster M.E., Loftsson T**.,** *Adv. Drug Deliv. Rev.*, **2007**, 59, 645-666.

119. Schultheiss N., Newman A., C*ryst. Growth Des.*, **2009**, 9, 2950-2967.

120. Dunitz J.D., *Cryst. Eng. Comm.*, **2003**, 4, 506.

121. Desiraju G.R., *Cryst. Eng. Comm.*, **2003**, 5, 466-467.

122. Aakeröy C.B., Salmon D.J., *Cryst. Eng. Comm.*, **2005**, 7, 439-448.

123. Vishweshwar P., McMahon J.A., Bis J.A., Zawarotko M.J., *J. Pharm. Sci.*, **2006**, 95, 3.

124. Aakeröy C.B., Salmon D.J., *Cryst. Eng. Comm.* **2005**, 7, 439-448.

a. Kartum G., Vogel W., Andrussov K., *Chem. Comm.*, **2005**, 2820-2822.

c. Childs S.L., Stahly G.P., Park A., *Mol. Pharmaceutics*, **2007**, 4, 323-338.

125. **a.** Chiarella R.A., Davey R.J., Petterson M.L., *Cryst. Growth Des.* **2007**, 7, 1223-1226.

b. Childs S.L., Rodríguez-Hornedo N., Reddy L.S., Jayasankar A., Maheshwari C., McCausland L., Shipplett R., Stahly B.C., *Cryst. Eng. Comm.* **2008**, 10, 856-864.

c. Chadwick K., Davey R., Sadiq G., Cross W., Pritchard R., *Cryst. Eng. Comm.*, **2009**, 11, 412-414.

d. ter Horst J.H., Deij M.A., Cains P.W., *Cryst. Growth Des.*, **2009**, 9, 1531-1537.

126. **a.** Etter M.C., *J. Chem. Phys.* **1991**, 95, 4601-4610.

b. Etter M.C.,*Chem. Res.*, **1990**, 23, 120-126.

127. **a.** Allen F.H., *Acta Crystallogr., Sect. B*, **2002**, 58, 380-388.

b. Bruno I.J., Cole J.C., Edgington P.R., Kessler M.K., Macrae C.F., McCabe P., Pearson J., Taylor R., *Acta Crystallogr., Sect. B*, **2002**, 58, 389-397.

c. Fábián L., *Cryst. Growth Des.*, **2009**, 9, 1436-1443.

128. Issa N., Karamertzanis P.G., Welch G.W.A., Price S.L., *Cryst. Growth Des.*, **2009**, 9, 442-453.

129. Newman A.W., Childs S.L., Cowans B.A., *Salt Cocrystal Form Selection*, In *Preclinical Development Handbook*, Hoboken: John Wiley and Sons, **2008**, 455-481.

130. Li Z.J., Abramov Y., Bordner J., Leonard J., Medek A., Trask A.V., *J. Am. Chem. Soc.*, **2006**, 128, 8199-8210.

131. Abramowitz R., Yalkowsky S.H., *Pharm. Res.*, **1990,** 7, 942-947.

132. Jain N., Yalkowsky S.H., *J. Pharm. Res.*, **2001**, 90, 234-252.

133. a. Katritzky A.R., Jain R., Lomaka A., Petrukhin R., Maran U., Karelson M., *Cryst. Growth Des.*, **2001**, 1, 261-265.
b. Dunitz J.D., Gavezzotti A., *Angew. Chem., Int. Ed.* **2005**, 44, 1766-1787.

134. Stanton M.K., Bak A., *Cryst. Growth Des.*, **2008**, 8, 3856-3862.

135. International Conference on Harmonization (ICH) Q1A, *Stability testing of new drug substances and products*, Accessed 23 September **2009**. http://www.ich.org/LOB/media/MEDIA419.pdf.

136. Reutzel-Edens S.M., Newman A.W., *The Physical Characterization of Hygroscopicity in Pharmaceutical Solids*, *In* Polymorphism, Hilfiker R. (Ed.), Weinheim: Wiley-VCH, **2006**, 235-258.

137. Brittain H.G., *J. Pharm. Sci.*, **2008**, 97, 3611-3636.

138. Newman A.W., Reutzel-Edens S.M., Zografi G., *J. Pharm. Sci.*, **2008**, 97, 1047-1059.

139. Basavoju S., Bostrom D., Velaga S.P., *Pharm. Res.*, **2008**, 25, 530-541.

140. Oswald I.D.H., Allan D.R., McGregor P.A., Motherwell W.D.S., Parsons S., Pulham C.R., *Acta Crystallogr., Sect. B*, **2002**, 58, 1057-1066.

141. Hickey M.B., Peterson M.L., Scoppettuolo L.A., Morisette S.L., Vetter A., Guzman H., Remenar J.F., Zhang Z., Tawa M.D., Haley S., Zaworotko M.J., Almarsson O., *Eur. J. Pharm. Biopharm.*, **2007**, 67, 112-119.

142. Trask A.V., Motherwell W.D.S., Jones W., *Cryst. Growth Des.*, **2005**, 5, 1013-1021.

143. a. McNamara D., Childs S.L., Giordano J., Iarriccio A., Cassidy J., Shet M.S., Mannion R., O'Donnell E., Park A., *Pharm. Res.*, **2006**, 23, 1888-1897.

b. Bermajo M., Gonzalez-Alvarez I., *How and Where Dugs are Absorbed? In Preclinical Development Handbook*, Hoboken: John Wiley and Sons, **2008**, 249-280.

144. Bak A., Gore A., Yanez E., Stanton M., Tufekcic S., Sysed R., Akrami A., Rose M., Surapaneni S., Bostick T., King A., Neervannan S., Ostovic D., Koparka R. A., *J. Pharm. Sci.*, **2008**, 97, 3942-3956.

145. Sheikh A.Y., Abd Rahim S., Hammond R.B., Roberts K.J., *Cryst. Eng. Comm.* **2009**, 11, 501-509.

146. Jones W., Motherwell W.D., Trask A.V., *Chem. Commun.*, **2004**, 890-891.

147. Matei D., Schilder J., Sutton G., Perkins S., Quon C., Sidor C., Gynaecol. Oncol., **2009**, 115, 90-96.

148. The Medical News, *Panzem (2-methoxyestradiol) Drug a Possible Candidate for Breast Cancer Treatment*, November, **2007**, retrieved 20 December **2007**. http//www.news-medical.net/news/2007/11/02/32073.aspx?page=2,

149. Ireson C.R., Chander S.K., Purohi A., Perera S., Newman S.P., Parish D., Leese M.P., Smith A.C., Potter B.V.L., Reed M.J., *Br. J. Cancer*, **2004**, 90, 932-937.

150. Wood L., Leese M.P., Mouzakiti A., Purohit A., Potter B.V.L., Reed M.J., Packam G., *Apoptosis*, **2004**, 9, 321-332.

151. Bourghardt J., Bergström G., Krettek A., Sjöberg S., Borén J., Tivesten Å., *Endocrinology*, **2007,** 148, 4128-4132.

152. Stella V.J., Rajewski R.A., *Pharm. Res.*, **1997**, 14, 556-567.

153. Saloojee H., *Save our Babies Nevirapine - Godsend or a Drug from Hell?*, *Science in Africa - Africa's First On-Line Science Magazine*, **2002**, retrieved 25 December **2007**.

154. Perdersen O.S., Pedersen E.B., *Antiviral Chem. Chemother.*, **1999**, 10, 285-314.

155. Brocklehurst P., Volmink J., *Antiretrovirals for Reducing the Risk of Mother-to-child Transmission of HIV Infection (Cochrane Review)*. Cochrane, Database, Syst. Rev., **2002**, CD003510.

156. Owor M., *The One-year Safety and Efficacy Data of the HIVNET 012 Trial 2001*, XIII International AIDS Conference, Durban, South Africa, 9-14 July **2000**.

157. Moodley D., *The SAINT Trial: Nevirapine (NVP) Versus Zidovudine (ZDV) + Lamivudine (3TC) in Prevention of Peripartum Transmission 2001*, XIII International AIDS Conference, Durban, South Africa, 9-14 July **2000**.

158. Caira M.R., Stieger N., Liebenberg W., De Villiers M.M., Samsodien H., *Cryst. Growth Des.*, **1997**, 8, 17-23.

Chapter 2

EXPERIMENTAL MATERIALS and METHODS

Chapter 2 *presents the experimental methodology of the study. It describes all materials and methods used to prepare polymorphs, cyclodextrin inclusion complexes and co-crystals. Furthermore, the chapter provides an overview of methods (both laboratory and computational) employed to identify and analyse polymorphs, cyclodextrin inclusion complexes and co-crystals.*

2.1 COMPOUNDS STUDIED

Guest Compounds

2-Methoxyestradiol (2ME) was a gift from Shimoda-Biotech (Port Elizabeth, South Africa) and 2-Methoxyestradiol-*bis*-sulfamate (2MES) was synthesized by Dr Gareth Arnott (University of Cape Town). Nevirapine (anhydrous) was originally purchased from Cipla (Mumbai, India, batch number 1001003). However, for the purposes of this study we received it as a gift from North-West University (Potchefstroom, South Africa). All three compounds were used as received.

Host Cyclodextrin Compounds

Alpha-cyclodextrin (α-CD), beta-cyclodextrin (β-CD), gamma-cyclodextrin (γ-CD), hexakis(2,3,6-tri-*O*-methyl)-α-CD (TRIMEA), hydroxypropyl-β-CD (HPBCD), randomly methylated β-cyclodextrin (RAMEB), heptakis-(2,6-di-*O*-methyl)-β-CD (DIMEB), heptakis(2,3,6-tri-*O*-methyl)-β-CD (TRIMEB), heptakis(2,3,6-tri-*O*-acetyl)-β-CD (TriAcBCD), heptakis (2,3,6-tri-*O*-ethyl)-β-CD (TriEtBCD) and octakis(2,3,6-tri-*O*-acetyl)-γ-CD (TriAcGCD) were obtained from Cyclolab (Budapest, Hungary) and were used as received.

Co-crystal Former Compounds

Saccharin, nicotinamide, isonicotinamide, stearic acid, L-aspartic acid, oxalic acid and maleic acid were obtained from Sigma-Aldrich Chemie Gmbh (Steinheim, Germany). Succinic acid and D-tartaric acid were obtained from B.D.H. Laboratory Chemicals Division (Poole, England). Citric acid, racemic and L-tartaric acid were obtained

from SAARCHEM (Pty) Ltd (Krugersdorp, Gauteng, South Africa). All compounds were used as received.

2.2 PROCEDURES FOLLOWED TO GROW POLYMORPHS

To obtain polymorphic forms of a compound the following methods were employed, as suggested by Guillory:[1]

Sublimation: a direct change of state from solid to gas[1] and back to solid.

Method I - A small quantity (10-20 mg) of the compound was placed in a petri dish that was covered with a watch glass. The petri dish was heated gently on a hot plate and the watch glass was observed to determine if crystals were growing on it.[1]

Method II- The vacuum sublimation method employed a horizontal vacuum sublimation apparatus. The latter is a piece of laboratory glassware consisting of a cylindrical, flat-bottomed flask for the sample and a water-cooled finger-type condenser. The condenser has an outer short skirt with an outer joint to fit over the neck of the flask. Above the joint there is a side-hose connector for attachment to the vacuum source. The solid was placed in the flask which was then heated under vacuum. Under this reduced pressure the solid volatilised and condensed as a purified compound on the cooled finger-type condenser surface, leaving the non-volatile residue impurities behind. Once heating had ceased and the vacuum was released, the sublimed compound was collected from the cooled surface.

Crystallisation from a Single Solvent

A known mass of the compound was dissolved in a known volume of solvent. Heating temperatures were set below the melting point of the ingredient with the lowest melt and 10 °C below the boiling point of the solvent. The solvent was added dropwise into the vial fitted with a magnetic stirrer while on a hot plate until the powders were completely dissolved. Solutions of the material being crystallised were filtered via a 0.45 µm syringe filter to remove most nuclei and transferred to a clean vial and then closed with Parafilm® containing a few holes. The solution was then left undisturbed for a reasonable period of time to allow for evaporation to occur.

Evaporation from a Binary Mixture of Solvents

Multi-component solvent evaporation methods depend on the difference in the solubility of the solute in various solvents. Here, a second solvent in which the solute is sparingly soluble was added to a saturated solution of the compound in a 'good' solvent. Often a solvent system was selected in which the solute was more soluble in the component with the higher vapor pressure. As the solution evaporated, the volume of the solution was reduced and, because the solvents evaporated at different rates, the composition of the solvent mixture changed.

Vapour Diffusion

A solution of the solute in a 'good' solvent was placed in a small, open container that was stored in a desiccator containing a small amount of a miscible, volatile non-solvent. The desiccator was then tightly closed. As solvent equilibrium was reached, the non-solvent diffused through the vapor phase into the solution, and saturation or supersaturation was achieved. The solubility of the compound in a precipitant used in a two-solvent crystallisation method such as vapour diffusion should be as low as possible (much less than 1 mg/ml), and the precipitant (the solvent in which the compound is poorly soluble) should be miscible with the solvent and the saturated solution.

Thermal Treatment

When using differential scanning calorimetry as an analysis technique, one can observe an endothermic peak corresponding to a phase transition, followed by a second endothermic peak corresponding to melting. Sometimes there is an exothermic peak between the two endotherms, representing a crystallisation step. These endothermic and/or exothermic peaks are associated with a series of thermal events, such as guest release, phase transformation, recrystallisation, melting and decomposition. Thus, the onset temperatures and enthalpy changes (area under the peak $\propto \Delta H$) of these thermal events can be determined and new polymorphs may be isolated.

Crystallisation from the Melt

The cooling of melts of polymorphic substances often yields the least stable modification, which subsequently rearranges into the stable modification in stages. Since the metastable form will have the lower melting point, it follows that supercooling is necessary to crystallise it from the melt. After melting, the system was supercooled below the melting point of the metastable form, while at the same time the crystallisation of the more stable form or forms was achieved. Quench-cooling a melt resulted in formation of an amorphous solid that on subsequent heating underwent a glass transition followed by crystallisation.

Thermal Desolvation of Crystalline Solvates

The term "desolvated solvates" has been applied to compounds that were originally crystallised as solvates but from which the solvent has been removed (generally by vaporisation induced by heat or vacuum). Often, these "desolvated solvates" retain the crystal structure of the original solvate form and exhibit relatively small changes in lattice parameters. For this reason, these types have been referred to as pseudopolymorphic solvates. However, in instances where the solvent serves to stabilise the crystal structure, the process of desolvation may produce a change in lattice parameters, resulting in the formation of either a new crystal form or an amorphous form. These solvates have been referred to as polymorphic solvates. Byrn[2] had characterised the desolvation of polymorphic solvates as occurring in four steps:
(a) molecular loosening, (b) breaking of the host-solvent hydrogen bonds (or other associations), (c) solid solution formation, and (d) separation of the product phase. The process of desolvating pseudopolymorphic solvates is simpler, involving only the two steps of: (a) molecular loosening and (b) breaking of host-solvent hydrogen bonds or associations.

Grinding

Polymorphic transformations can be achieved with both manual grinding (mortar and pestle) and mechanical grinding. Polymorphic transformations in the solid state require three steps: (a) molecular loosening (nucleation by separation from the lattice), (b) solid solution formation, and (c) separation of the product (crystallisation of the new phase).

Depending on the material and the conditions employed, grinding can result in conversion to an amorphous substance and with the exercise of care, different polymorphic forms could be obtained.[2]

Solvent-drop Grinding

Polymorphic transformation may also be initiated by adding small amounts of a suitable solvent to either manually or mechanically ground mixtures. As a further modification, each mixture was placed at various relative humidity (RH) conditions which in turn could facilitate polymorphic transformation. Samples were checked on a weekly basis using PXRD to see whether any changes had occurred.

Dicarboxylic Acids as Templates in Solution

The use of templates in solution may also facilitate polymorphic transformation of the compound. A known amount of the template is placed in a suitable solvent and stirred for a half hour at ~50 °C. The solution should be supersaturated before the addition of the compound which is stirred again for a few hours. The solution is then filtered and the solvent is allowed to slowly evaporate at ambient temperatures. Terephthalic acid was used in this study with basic solvents (alcohols).

Methods Used to Obtain Hydrated Forms of a Compound

Pharmaceutical solids may come into contact with water during processing steps such as crystallisation, lyophilisation, wet granulation, aqueous film-coating, or spray-drying. Moreover, they may be exposed to water during storage in an atmosphere containing water vapour, or in a dosage form consisting of materials that contain water (e.g. excipients) and are capable of transferring it to other ingredients. Water may be adsorbed onto the solid surface and/or may be absorbed in the bulk solid structure. When water is incorporated into the crystal of the compound in stoichiometric proportions, the molecular adduct or adducts formed are referred to as hydrates.[3] Hydrates can be prepared by re-crystallisation from water or from mixed aqueous solvents. They could also result, in some instances, from exposure of crystal solvates to an atmosphere containing water vapour. Finally, hydrates may also be obtained by

exposure to high relative humidity conditions. For example, dexmedetomidine hydrochloride exposed to 100 % relative humidity converted to a monohydrate.[4]

Methods Used to Obtain Solvated Forms of a Compound

When organic solvents are employed in the purification of new drug substances by re-crystallisation, it is often observed that the isolated crystals include solvent molecules, either entrapped within voids in the crystal or interacting via hydrogen bonding or van der Waals forces with molecules constituting the crystal. A crystal with large empty channels or cavities is not stable because of packing demands. The size and chemical environment of the cavity or channel determine what kind of solvent molecule can be included in the structure and what kind of interaction occurs between solvent and host structure. Depending on the nature of molecular packing arrangements, it may happen that the inclusion of solvent is necessary to build a stable crystal structure. The techniques used to obtain solvates were generally similar to the methods used to obtain polymorphs, i.e. crystallisation from a single solvent, from mixed solvents, or by vapour diffusion. Sometimes, it is also possible to exchange one solvent within the crystal structure for another.

Methods Used to Obtain Amorphous Forms of a Compound

Solids can exist in crystalline or amorphous form. Crystalline materials have defined structures, stoichiometric compositions, and melting points and are characterised by their chemical, thermal, electrical, optical, and mechanical properties.[5] By contrast, amorphous materials have no long-range order, so their structure can be viewed as being similar to that of a frozen liquid but without the thermal fluctuations observed in the liquid phase. While crystalline solids offer the advantages of chemical and thermodynamic stability, amorphous solids are occasionally preferred because they undergo dissolution at a faster rate. Rapid dissolution is desirable in the case of solids, which must be dissolved prior to parenteral administration. Faster dissolution is also important for poorly soluble compounds administered orally, since there is often a correlation between dissolution rate and bioavailability. In fact, there are instances in which only the amorphous form has adequate bioavailability. Several methods employed in attempts to produce amorphs are described below.

Solidification of the Melt

Amorphous solids are often created by rapidly cooling a liquid so that crystallisation nuclei can neither be created nor grow sufficiently, whereupon the liquid then remains in the fluid state well below the normal freezing point. Here the rate of cooling is high relative to the rate of crystallisation, whereupon the liquid state can persist well below the normal freezing point. As cooling continues there is a rise in the rate of increase in viscosity of the supercooled liquid per unit drop in temperature. The initially mobile fluid turns into a syrup, then into a visco-elastic state, and finally into a brittle glass. A glass is, therefore, a supercooled liquid, characterised by an extremely high viscosity. Mechanically, if not structurally, glasses can be regarded as solids.

Reduction of Particle Size

Reduction of particle size of crystalline materials to the microcrystalline level can yield a material incapable of exhibiting an X-ray powder diffraction pattern. The milling disrupts the crystal structure and imparts excess free energy and entropy associated with amorphous substances. Particle size reduction can be achieved using a variety of methods. Sometimes it is helpful to carry out the particle size reduction at reduced temperatures, such as 4 °C or at liquid nitrogen temperature, -196 °C. In other instances, grinding with an excipient was employed as a means of obtaining amorphous materials. Cyclodextrins were used for this purpose.

Removal of Solvent From a Solvate or Hydrate

Solids can sometimes be rendered amorphous by the simple method of allowing solvent molecules of crystallisation to evaporate at modest temperatures. If the solvent merely occupies channels in the crystal structure, the structure often remains intact on heating, and may improve certain properties such as flowability and uniformity of particle size,[6] but when the solvent is strongly bonded to molecules of the host, the structure will frequently collapse when the solvent is removed and one obtains an amorphous powder.

All of the above methods were employed to try to isolate new forms of both 2ME and 2MES. Full details of the preparation of individual polymorphs and solvates actually found in this study are given in the appropriate chapter.

2.3 PROCEDURES FOR PREPARING CYCLODEXTRIN COMPLEXES

To obtain cyclodextrin complexes of a compound the following methods were employed:

Complex Preparation by Co-precipitation

The complex was prepared by stirring an aqueous solution of CD (warm or cold) with the guest molecule using a fixed host:guest ratio. The calculated amounts of host and guest molecules were agitated intensely at a set temperature to achieve the common saturated solution of both the host and guest. The CD inclusion complex was crystallised from this homogenous solution upon slow evaporation, slow cooling, freezing or elevating the temperature.

Complex Preparation by Kneading

The cyclodextrin was placed in a mortar with a few drops of water and ground to a paste. An equimolar amount of the guest was added slowly with simultaneous kneading. The process required between 45 min to one hour. During this time the paste was kept moist by the dropwise addition of water. Here less water was used than in the co-precipitation method; however, excess water was removed from the paste-like product by drying in an air stream.[7,8]

Full details of the preparation of individual complexes are given in the appropriate chapter.

2.4 PROCEDURES USED TO PREPARE CO-CRYSTALS

To obtain co-crystals the following methods were employed:[9]

Slow Evaporation

Stoichiometric amounts of the components (co-crystal formers) were dissolved in a known volume of solvent system (either single solvent or binary mixture). All temperatures were kept below the melting point of the lowest melting component and 10 °C below the estimated boiling point of the solvent system. Samples were dissolved separately in the respective solvent systems, stirred with a magnetic stirrer while on a hot plate until the powders were completely dissolved. The two solutions were then mixed together in the vial with the lesser amount of solvent, stirred, extracted via syringe and filtered from the syringe through a 0.45 µm micro-filter into a clean vial. The vial was closed with Parafilm® and perforated to allow the solvent to evaporate.

Sublimation

A small quantity (10-20 mg) of the respective co-crystal formers in stoichiometric amounts was placed in a petri dish that was covered with a watch glass. The petri dish was heated gently on a hot plate and the watch glass was observed to determine if co-crystals were growing on it.[1]

Grinding

Co-crystal formation can be achieved with both manual grinding (mortar and pestle) and mechanical grinding of a physical mixture of the co-crystal formers. Depending on the material and the conditions employed, grinding can result in the formation of a co-crystal.

Solvent-drop Grinding

Addition of a small amount of suitable solvent to the ground mixture to accelerate co-crystallisation appears to be a particularly promising preparation method. Trask et al.[10] reported that grinding of cyclohexane-1,3-*cis*-5-*cis*-tricarboxylic acid and 4,4′-bipyridine in the dry state does not afford a co-crystal whereas grinding the two components with few a drops of MeOH facilitates complete conversion within minutes. Solvent-drop

grinding avoids excessive use of crystallisation solvent and hence it can be regarded as a "green" process. Solvent-drop grinding could also prove useful for polymorph control[9] and selective polymorph transformation.[10]

Full details of the preparation of individual co-crystals are given in the appropriate chapter.

2.5 PROCEDURE USED TO DETERMINE SOLUBILITY PROFILE OF A COMPOUND

The solubility profile of a compound can be determined both experimentally and theoretically. Theoretically, the simplest equation to date is a modification of the general solubility equation which uses the melting point (MP) of the compound and the octanol-water partition coefficient (K_{ow}).[11]

The equation $\log S_{solid} = 0.5 - 0.01(MP - 25) - \log K_{ow}$ is used to calculate the theoretical aqueous solubility of an organic compound.[11]

However, experimentally, the following procedure was used: a saturated solution was obtained either by stirring excess powdered solute with solvent for several hours at the required temperature until equilibrium had been attained, or by warming the solvent with an excess of the solute and allowing the mixture to cool to the required temperature. It was essential that some undissolved solid should be present at the completion of this stage in order to ensure that the solution was saturated.[12]

The following requirements were observed in all solubility determinations:

1. The solute and the solvent must be pure.
2. A saturated solution must be obtained before any solution is removed for analysis.
3. The method of separating a sample of saturated solution from undissolved solute must be satisfactory.
4. The method of analysing the solution must be reliable.
5. Temperature must be adequately controlled.

A sample of the saturated solution was obtained for analysis by separating it from the undissolved solid. Filtration was used, but precautions were taken to ensure that it was carried out at the temperature of the solubility determination, in order to prevent any change in the equilibrium between dissolved and undissolved solute.[12] The filtration process could have been simplified by the introduction of membrane filters that could be used in conjunction with conventional syringes fitted with suitable inline adapters. However, this was not employed in the present study.

Full details of the determination of the solubility of individual compounds are given in the appropriate chapters.

2.6 PROCEDURE USED TO DETERMINE DISSOLUTION PROFILE OF A COMPOUND

Dissolution studies were conducted using the rotating basket method as described in the BP 2005.[13] Gelatin capsules containing 5-10 mg of the formulation were made. Tests were carried out in the Vankel VK 700 (220 V) dissolution apparatus and with the Vankel VK 650 A Heater/Circulator Benchsaver® series used to regulate temperature at 37 °C. 900 ml flasks filled with distilled water were used and a stirring speed of 100 rpm was applied. The capsules were enclosed in stainless steel baskets to prevent floating. A 3 h run was conducted and at pre-specified times (15 minute intervals) 5 ml samples were withdrawn and filtered for analysis, with 5 ml of the distilled water being replaced to maintain a constant volume. The assay was by UV spectrophotometry at an appropriate wavelength for the active ingredient.

The powders placed in the capsules were kneaded prior to encapsulation for ~5 minutes to obtain uniform and predictable dissolution of the drug. The particle size range of the powders was between 65 and 200 μm. Powders were not sieved prior to encapsulation due to high costs and limited resources of ingredients.

2.7 ANALYTICAL METHODS USED IN THIS STUDY

Hot Stage Microscopy (HSM)

A Linkam TP92 temperature control unit linked to a Linkam TH MS600 hot stage was used to heat crystals at a controlled rate. Visual characterisation was rendered by a real-time Sony Digital Hyper HAD colour video camera fitted to a Nikon SMZ-10 stereoscopic microscope. Images that were recorded were analysed by the Soft Imaging system, analySIS.[14] HSM used under these conditions proved quite useful, allowing one to distinguish new solid phases such as polymorphs, cyclodextrin complexes and co-crystals. HSM complements TGA and DSC analysis by visually recording the thermal events during the heating and cooling process. For example, guest loss is usually indicated by the appearance of bubbles when the sample is immersed in an inert medium (e.g. silicone oil), and polymorphic transition is typically shown by colour or opacity changes in crystals.

Thermogravimetric Analysis (TGA)

Thermogravimetry (TG) measures the mass loss of a sample as a function of time or temperature. It is used to establish the stoichiometry of inclusion compounds and to study the decomposition of desolvated materials.

TG analyses for all compounds were performed on a Mettler Toledo TGA/SDTA851e instrument under N_2 gas purging at a flow rate of 30 mL/min. The Mettler TG instrument was calibrated using indium (mp = 156.6 °C) and aluminium (mp = 660.3 °C) in an automated process in which temperature calibration, tau lag calibration and sensor calibration were performed simultaneously. The cystals were rapidly dried on a filter paper to remove surface solvent. The weighed samples were placed in an open porcelain pan. The programmed TG analyses were carried out over a temperature range 30 °C to 400 °C at the predetermined linear heating rate of 10 K/min. This technique was primarily used to determine the stoichiometry of the compounds from the percentage weight loss. The samples were continuously purged by a stream of dry nitrogen gas at a flow rate of 30 mL/min.

Differential Scanning Calorimetry (DSC)

DSC measurements were performed using a Perkin-Elmer PC-7 series thermal analysis system at a scanning rate of 10 K/min under N_2 gas purge with a flow rate of 30 mL/min. The temperature range over which the traces were recorded was 30 – 400 °C. Sample masses were in the range 2-5 mg. Samples were removed from mother liquor, dried on filter paper and crushed to an appropriate particle size and sealed in a crimped, vented aluminium pan. A sealed and empty pan was used as a reference. The DSC analyser was calibrated by measuring the onset temperatures of the melting of indium (156.6 °C) and zinc (419.5 °C) while the heat flow was calibrated from the enthalpy of melting of indium (28.62 J/g). Endothermic and exothermic peaks appearing in the DSC traces were analysed in terms of their onset temperatures, temperature range of the peak (determined from the first derivative of the trace) and the enthalpy of the peak (measured in J/g). The various endothermic and exothermic peaks observed in the DSC trace were interpreted in conjunction with HSM and TGA to be associated with solvent loss, phase changes in the sample and decomposition. The decomposition of cyclodextrin inclusion complexes is a complicated and multi-stage process and is characterised by a number of thermal events observed with DSC.

UV Spectrophotometry (UV)

UV spectra were recorded on a BECKMAN DU® 640 series UV/visible spectrophotometer over a wavelength range of 190– 450 nm at a scanning rate of 1200 nm/min. All samples were dissolved in distilled water. The samples were placed in 2 mm quartz cuvettes and the concentrations were suitably adjusted such that all absorbance readings were measurable between zero and one absorbance unit. Calibration curves for the various drugs were constructed using readings taken at the λ_{max} value of the appropriate drug. The aborbance of a solution of an inclusion complex with an accurately known concentration was determined. The percentage weight of the drug in the inclusion complex could then be determined. Together with the percentage weight of water in the inclusion complex, obtained from TGA, the stoichiometry of the inclusion complex was eventually expressed in terms of the cyclodextrin : drug : water ratio. Assays for the solubility tests and dissolution tests were performed using UV spectrophotometry at an appropriate wavelength for the active ingredient.

FTIR Spectroscopy (FTIR)

IR spectra were obtained using a Perkin-Elmer 100 FTIR instrument fitted with UATR and controlled with Spectrum ® software for sample analysis. Samples were run as crystalline or amorphous powders over the range 400-4000 cm^{-1} (unless otherwise stated). Percentage transmittance was recorded against frequency. For the CD complexes obtained by kneading, shifts in certain characteristic bands of the appropriate drug molecule were indicative of interaction between CD and drug.

Crystal Structure Determination

In each case single crystals, typically between 0.2 and 0.5 mm in all dimensions, of good quality were selected for their ability to extinguish plane-polarised light uniformly. Crystals were mounted on a nylon loop and coated with paratone N oil to prevent the loss of included solvent and to provide a rigid mount during low temperature data-collection. The nylon loop was mounted on a goniometer head.

Two single crystal X-ray diffractometers were employed in this study: a Nonius Kappa CCD (Charge Coupled Device) Single Crystal X-ray Diffractometer and a Bruker KAPPA APEX II DUO diffractometer.

Data-collection

Crystal intensity data were collected on a Nonius Kappa CCD (Charge Coupled Device) Single Crystal X-ray Diffractometer, using graphite-monochromated MoKα radiation (λ = 0.71069 Å) generated by a Nonius FR590 generator operated at 50 kV and 30 mA. Unit cell determinations were carried out both at ambient temperature (294 ± 2 K) as well as low temperature (113 ± 2 K). This check was performed to ensure there were no significant changes in the unit cell dimensions that might indicate phase transformations induced by cooling. All full intensity data-sets were measured at 113 ± 2 K. The low temperatures were maintained by cooling the crystals with a constant stream of N_2 gas at a flow rate of 20 ml/min with the aid of a Cryostream cooler (Oxford Cryosystems, UK). Data were corrected for Lorentz-polarisation effects; unit cell refinement and data-reduction were performed using the programs DENZO and SCALEPACK.[15] All data were subjected to absorption correction using the multi-scan method (program SADABS[16]).

The Bruker KAPPA APEX II DUO diffractometer used graphite-monochromated Mo-Kα radiation (λ = 0.71069 Å). The unit cells of the crystals were determined at low temperature (100 ± 2 K) after their removal from mother liquor. The data collections were carried out in the above temperature range using Cryostream coolers (Oxford Cryosystems, UK). Data reduction was performed using the program SAINT.[17]

For both instruments the space group determinations were carried out by examining the systematic absences and matching the observed conditions to a known space group.[18] These assignments were confirmed by running the data through the program XPREP.[19] SHELXS-97[20] input files were generated with XPREP.

Structure Solution and Refinement

The structures presented in this thesis were solved using different structure solution programs and a variety of methods depending on the size of the structure, quality of the data and nature of the problem. SHELXS-97[20] was used to solve smaller structures, such as those of the polymorphs and co-crystal compounds. This program was, however, not adequate for the CD complexes due to the poor diffraction that crystals of these compounds exhibit, as well as the complexity of their larger structures. CD structures were solved by isomorphous replacement in cases where isostructural complexes existed, using the published coordinates of the respective cyclodextrin non-hydrogen atoms. An alternative to this method was to use SHELXD,[20] a program specifically designed for solving larger structures *ab initio*. All structures were refined on F^2 using full-matrix least-squares in the program SHELXL-97.[20] Both SHELXS-97[20] and SHELXL-97[20] were accessed via the X-SEED[21] interface. More detail on SHELXD[20] and SHELXL-97[20] follows below.

SHELXD

SHELXD[20] is used for the *ab initio* solution of structures from native data when a solution is not likely with SHELXS-97.[20] SHELXD is based on the dual-space strategy first introduced in the program *Shake and Bake*.[22-26] The dual-space approach alternates between real and reciprocal space. In reciprocal space, phases are expanded in SHELXD from the 40 % most reliable using the *tangent formula* devised by Karle and

Hauptman in 1956.[27,28] The real space cycles are required to impose the strong constraint that it is expected to find N sites with approximately equal scattering power. SHELXD makes extensive use of the Patterson function to provide better than random starting phases for the dual-space recycling. It is only limited by the requirement of atomic resolution 1.2 Å.

SHELXH-97[20]

Refinement in SHELXH-97 for larger structures involves minimisation of the function $\sum w\left(F_o^2 - F_c^2\right)^2$ using the full-matrix least-squares technique. The agreement between the observed (F_o) and calculated (F_c) structure factors is expressed by the residual index R_1, where R_1 is low for a satisfactory model and where

$$R_1 = \left(\sum \| F_o | - | F_c \|\right) / \sum | F_o | .$$

Refinement against F^2 tends to magnify the deviations of the Goodness-of-Fit, S (defined later), from unity compared with refinement against F and therefore these values are not directly comparable to structures refined against F.

The weighting scheme (w) in $wR_2 = \left[\left(\sum w\left(F_o^2 - F_c^2\right)^2\right) / \left(\sum w\left(F_o^2\right)^2\right)\right]^{1/2}$ and the parameters a and b were refined for each structure using the following expressions:

$w = 1/\left[\sigma^2\left(F_o^2\right) + (aP)^2 + bP\right]$ and $P = \left[\max\left(0, F_o^2\right) + 2F_c^2\right]/3$. The terms a and b are chosen in the above weighting scheme to yield constant distributions of $\left[w\left(F_o^2 - F_c^2\right)^2\right]$ with sinθ and $\left(F_o/F_{max}\right)^{1/2}$. S (Goodness-of-Fit) is defined by the expression

$S = \left[\sum \left(w\left(F_o^2 - F_c^2\right)^2\right) / (n-p)\right]^{1/2}$, where n is the number of reflections and p is the total number of parameters refined. For a well-behaved structure S should be close to unity, and the over-determination ratio should be of the order $n/p \approx 10$.

Additional Resources

The Cambridge Structural Database (CSD)[29] was used to obtain coordinate data for the fragments used to solve the structures reported in this thesis. Molecular parameters and geometrical data with their associated e.s.d.s and non-bonding distances were calculated using the program PLATON.[30] WinGX[31] was used as an interface for PLATON. Molecular diagrams were created with POV-Ray for Windows.[32] Molecular packing, stereo and CPK diagrams were produced using the program Weblab ViewerPro Version 3.5.[33] Diagrams showing anisotropic thermal ellipsoids were drawn with the aid of Ortep-3 for Windows.[34] LAYER was used for the graphic display of intensity data as simulated precession photographs.[35] Table 2.1 lists the final crystallographic data files pertinent to the compounds studies. They are stored on a CD-rom appended to the thesis.

Table 2.1. File types found in Appendix.

File extensions/formats	Contents
.HKL	Reflection data
.RES	SHELX co-ordinate data
.CIF	Crystallographic information file
.FCF	Structure factor tables
.LIS	Platon output
.XL	SHELX output file
.SUP	Tabulated supplementary data

X-ray Powder Diffraction (PXRD)

PXRD was used to determine characteristic 'fingerprint' traces of crystalline materials. This technique can uniquely identify materials thus allowing for the identification of new species of polymorphs, cyclodextrin complexes and co-crystals. This technique is especially useful in the absence of good quality crystals for single crystal structure determination. Polymorphism can be detected due to different packing arrangements that polymorphs exhibit. CD complexes also usually have very different PXRD traces from those of the parent CDs due to their different packing arrangements. Complexation is proven if the trace is different from that of the drug and host, as well as

a physical mixture of the latter two, or if it corresponds to that of a known complex of the particular CD, the latter indicating isotructurality.

Powder patterns of ground samples were recorded on a Philips PW1050/25 vertical goniometer with Ni-filtered CuKα radiation (λ = 1.5418 Å) produced at 40 kV and 25 mA. Samples were packed in aluminium or glass sample holders and step scans of 0.1° 2θ, with 2 s counting times, in the range 5-40° 2θ were employed. In cases where sample material was limited, PXRD patterns were recorded using a Huber Imaging Plate Guinier Camera 670. All samples were manually ground and packed into Lindemann capillaries with an internal diameter of 1 mm and a glass thickness of 0.01 mm. The capillaries were obtained from Hilgenberg, Germany. Nickel-filtered CuKα radiation (λ = 1.5418 Å), produced at 40 kV and 20 mA by a Philips PW1120/00 generator fitted with Huber long fine-focus tube PW2273/20 and a Huber Guinier Monochromator Series 611/15, were employed. For high temperature PXRD the Huber High Temperature Controller HTC 9643 unit was used with capillary rotation device 670.2. A 2θ range of 4 to 100.0° was used with step a size of 0.005° 2θ.

For each successfully determined single crystal structure LAZY PULVERIX[36] was used to generate a computed PXRD trace. These were compared with experimental traces to establish whether any phase transformations had taken place upon grinding the material in the course of preparation of samples for analysis. More importantly, when a match between the experimental PXRD trace and the computed PXRD pattern was obtained, it could be concluded that the structure of the bulk material was correctly represented by that of the crystal selected for full single crystal X-ray analysis.

2.8 REFERENCES

1. Guillory J.K., *In: Polymorphism in Pharmaceutical Solids*, Brittain H.G. (Ed.), Marcel Dekker, Inc., New York, **1999,** 183-226.
2. Byrn S.R., *Solid State Chemistry of Drugs*, New York: Pharmaceutical Academic Press, **1982**, xii, 346.
3. Khankari R.K., Grant D.J.W., *Thermochim. Acta*, **1995**, 248, 61-79.
4. Rajala R., Laine E., Örn G., *Eur. J. Pharm. Sci.*, **1994**, 1, 219-225.
5. Franks F., Kajiwara K., *J. Chem. Soc., Faraday Trans.*, **1997**, 93, 1779-1783.
6. Caira M.R., *In: Topics in Current Chemistry*, Berlin, Heidelberg: Springer-Verlag, **1998,**198, 164-208.
7. Frömming K.-H., Szejtli J., *Cyclodextrins in Pharmacy*, Netherlands: Kluwer Academic Publishers, **1994**, 84-89.
8. Szejtli J., *Topics in Inclusion Science: Cyclodextrin Technology*, Dordrecht, Netherlands: Kluwer Academic Publishers, **1988**.
9. Vishweshwar P., Jennifer A., McMahon J.A., Bis M., Zaworotko J., *J. Pharm. Sci.*, **2006,** 95, 499-516.
10. Trask A., Shan N., Motherwell S.W.D., Jones W., Feng., Tan R.B.H., Carpenter K., *Chem. Comm.*, **2005,** 880-882.
11. Ran Y., Yalkowsky S.H., *J. Chem. Inf. Comput. Sci.*, **2001**, 41, 354-357.
12. Aulton M.E. (Ed.), *Pharmaceutics: The Science of Dosage Form Design*, Spain: Churchill Livingstone, Second Edition, **2002**, 23-32.
13. British Pharmacopoeia, British Pharmacopoeia Commission Secretariat, London, UK, **2005**.
14. Soft Imaging System GmbH, *Digital Solutions for Imaging and Microscopy*, Version 3.1 for Windows (Copyright **1987-2000**).
15. Otwinowski Z., Minor W., *Processing of X-ray Diffraction Data in Oscillation Mode in Methods in Enzymology*, Carter, C.W., Sweet, R.M., (Eds.), New York: Academic Press, **1996**, Vol. 276, 307.
16. Sheldrick G.M., SADABS, University of Göttingen, Germany, **1996**.
17. SAINT, Version 7.60a, Bruker AXS Inc., WI, USA, **2006**.
18. Wilson, A.J.C. (Ed.), *International Tables for Crystallography, Vol. C: Mathematical, Physical and Chemical Tables*, Dordrecht: Kluwer Academic Publishers, **1992**, 691.

19. XPREP, *Data Preparation and Reciprocal Space Exploration*, Version 5.1, © Bruker Analytical X-ray Systems, **1997.**
20. Schneider T.R., Sheldrick, G.M., *Acta Crystallogr.*, **2002**, D58, 1772-1779.
21. Barbour L.J., *X-SEED, A Graphical Interface to SHELX*, University of Missouri, Columbia, U.S.A., **1999**.
22. Sheldrick G.M., *Direct Methods for Solving Macromolecular Structures*, Fortier S. (Ed.), Dordrecht: Kluwer Academic Publishers, **1998**, 401-411.
23. Sheldrick G.M., *Z. Kristallogr.*, **2002**, 217, 644-650.
24. Uson I., Sheldrick G.M., *Curr. Opin. Struct. Biol.* **1999**, 9, 643-648.
25. Miller R., Gallo S.M., Khalak H.G., Weeks C.M., *J. Appl. Cryst.*, **1994**, 27, 613-621.
26. Miller R., De Titta G.T., Jones R., Langs D.A., Weeks C.M., Hauptman H., *Science*, **1993**, 259, 1430-1433.
27. Karle J., *Acta Crystallogr.*, **1968**, B24, 182-186.
28. Karle J., Hauptman H., *Acta Crystallogr.*, **1956**, 9, 635-651.
29. Cambridge Structural Database and Cambridge Structural Database System, Version 5.30, **2009**, Cambridge Crystallographic Data Centre, University Chemical Laboratory, Cambridge, England.
30. Spek A.L., PLATON, *A Multipurpose Crystallographic Tool*, Version 10500 © **1980-2000**.
31. Farrugia L.J., WinGX, *J. Appl.Cryst.*, **1999**, 32, 837-838.
32. Pov-Ray for Windows, Version 3.1e.watcom.win32, The Persistence of Vision Development Team, © **1991-1999**.
33. Weblab ViewerPro Version 3.5, © by Molecular Simulations Inc., San Diego, CA. **1999.**
34. Farrugia, L.J., *J. Appl. Cryst.*, **1997**, 30, 565.
35. Barbour L.J., *J. Appl. Cryst.* **1999**, 32, 351-352.
36. Yvon K., Jeitschko W., Parthé E., *J. Appl. Cryst.*, **1977**, 10,73.

Chapter 3

CRYSTAL FORMS of 2-METHOXYESTRADIOL and its *bis*-SULFAMATE

Chapter 3 *presents the study of polymorphism of the steroids 2-methoxyestradiol (2ME) and 2-methoxyestradiol-bis-sulfamate (2MES). The chapter firstly describes the characterisation of synthetic samples of 2ME and 2MES and secondly, illustrates the successful preparation and physicochemical characterisation of the different forms of 2ME and 2MES in the solid state. After polymorphism experimentation it was evident that there are three definitive forms of 2ME.* ***Form I*** *was recrystallised from a single solvent (diethyl ether) and matched the original starting material.* ***Form II,*** *an amorph, was identified by melt studies and* ***Form III*** *is a chloroform solvate. Only one form of 2MES (****Form I****) was obtained by recrystallisation from a single solvent (amyl alcohol) and this form matched the original starting material, a hemihydrate. Furthermore, the dissolution characteristics of* ***Form I*** *and* ***Form II*** *of 2ME and* ***Form I*** *of 2MES using the BP dissolution method are illustrated and from the results it is evident that the two steroids have significantly different dissolution profiles.*

3.1 INTRODUCTION

A **steroid** is a terpenoid lipid characterised by its sterane core and additional functional groups. The core is a carbon structure of four fused rings: three cyclohexane rings and one cyclopentane ring (Figure 3.1). The steroids vary by the functional groups attached to these rings and the oxidation state of the rings.

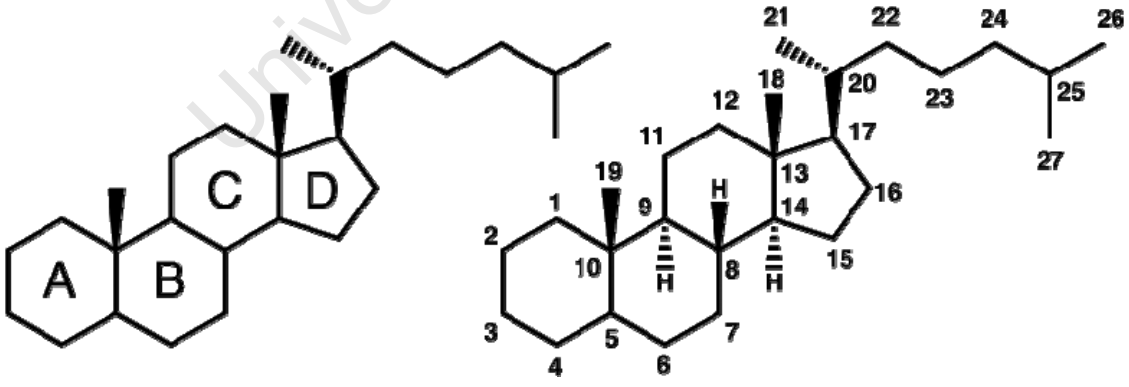

Figure 3.1 IUPAC recommended ring lettering (left) and atom numbering (right) of the steroid skeleton.[1,2]

Hundreds of distinct steroids are found in plants, animals, and fungi. All steroids are made in cells either from the sterols lanosterol (animals and fungi) or cycloartenol (plants). Both lanosterol and cycloartenol are derived from the cyclisation of the triterpene squalene.[3] Sterols are special forms of steroids, with a hydroxyl group attached to atom C-3 and a skeleton derived from cholestane,[1] with cholesterol being one of the best known sterols. Steroid classification can be based upon their taxonomy and function (Table 3.1) and chemical composition (Table 3.2).

Table 3.1 Taxonomical and Functional Classification of Steroids

Taxonomical and Functional Classification of Steroids					
Animal steroids	Insect steroids	Ecdysteroids	Ecdysterone		
	Vertebrate steroids	Steroid hormones	Sex steroids	Produce sex differences or support reproduction	Androgens, estrogens, and progestagens
			Cortico-steroids	Glucocorticoids and mineralocorticoids	Glucocorticoids regulate metabolism and immune function, mineralocorti-coids help maintain blood volume and control renal excretion of electrolytes
			Anabolic steroids	Interact with androgen receptors	Increase muscle and bone synthesis
		Cholesterol	Modulates the fluidity of cell membranes and is the principal constituent of the plaques implicated in atherosclerosis.		
Plant steroids	Phytosterols	Steroid alcohols	Phytochemicals		
	Brassino-steroids	Involved in plant processes such as cell expansion and cell elongation			
Fungus steroids	Ergosterols	Provitamin			

Table 3.2 Chemical Composition Classification of Steroids

Class	Example	Number of carbon atoms
Cholestanes	Cholesterol	27
Cholanes	Cholic acid	24
Pregnanes	Progesterone	21
Androstanes	Testosterone	19
Estranes	Estradiol	18

Gonane (or steroid nucleus) is the hypothetical parent (17-carbon tetracyclic) hydrocarbon molecule without any alkyl sidechains.[3]

2-Methoxyestradiol (2ME):

The sequential biochemical hydroxylation and methylation of the natural hormone estradiol gives rise to the endogenous mammalian metabolite 2ME (Figure 3.2a). In Chapter 1, 2ME is reviewed as a natural metabolite of estrogen inhibiting the cellular machinery involved in replicating cancer cells. In addition, 2ME prevents the growth of new blood vessels required to nourish tumours.

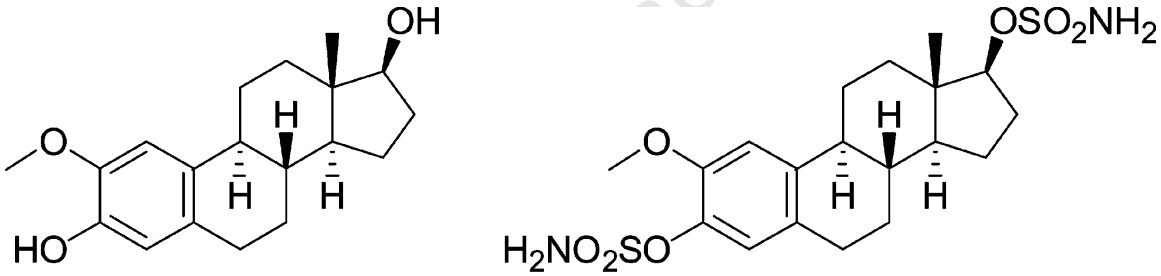

Figure 3.2 Chemical structures of (a) 2ME and (b) 2MES.

The mechanism of action of 2ME involves disruption of cellular microtubules leading to mitotic arrest and initiation of apoptosis. Preclinical studies revealed that it is orally active, inexpensive to produce and, in general effective without toxicity, hence, further studies on second-generation derivatives with superior properties, including better oral availability and different chemosensitivity profiles have been initiated.[4,5,6] Several of the new compounds synthesised involve structural modifications in ring A or ring B of 2ME. Rao et al.[7] looked at structural modifications of 2ME and found that structures in Figure 3.3 produced better biological potency than 2ME. The results also suggest that these new derivatives and 2ME share the same intracellular target, tubulin.

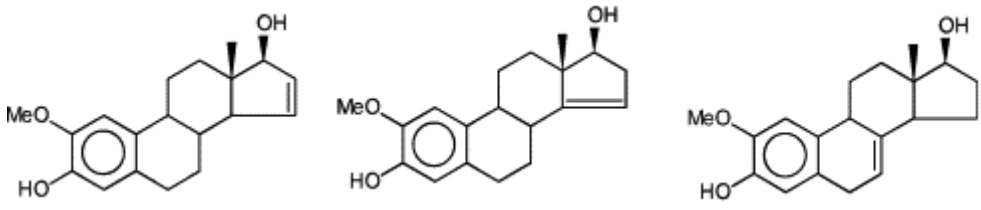

(a) **(b)** **(c)**

Figure 3.3 Structural modification of 2ME.[7]

Earlier testing of 2ME variants for inhibition of tubulin polymerisation and inhibition of endothelial cell proliferation seems to indicate that free hydroxyl groups at the 3- and 17-positions are required for potent biological activity. Furthermore, 17-hydroxy analogues are more active than 17-oxo counterparts, thus supporting the generalisation for the free 17-OH group being required for potent activity. However, an exception to this is 2-methoxyestrone-3-*O*-sulfamate which was shown by Purohit et al.[8] to be 10 times as active as 2ME against human breast cancer cells.

Other structural modifications on 2ME carried out by Cushman et al.[9,10] have focused primarily on variations at the 2- and 6-positions of the parent compound. The authors concluded that the optimum 2-substituent for cytotoxic activity appears to be an unbranched chain containing three atoms chosen from the second row of the periodic table, with activity increasing with increased electron density adjacent to the aromatic ring. The introduction of additional unsaturation in ring D for compounds a and b (Figure 3.3) gives the most interesting results and leads to a modest to dramatic increase in cytotoxicities relative to 2ME. Whether these structural modifications lead to an increased binding affinity towards tubulin or perhaps a decreased rate of metabolic inactivation remains to be investigated.[11]

Structural modification of 2ME is vast and ongoing and structure-activity relationships are fundamental in determining potency of activity of these compounds. Furthermore, any slight supramolecular modification (viz. different forms and packing arrangements) of 2ME may significantly affect physicochemical as well as structure–activity relationships of the compound.

2-Methoxyestradiol-3,17-*O,O-bis*-sulfamate (2MES):

In the search for new anti-cancer therapies with improved side-effect profiles, it has become increasingly important to also evaluate the *in vitro* cancer cell specificity of potential drugs. 2ME has decreased stability when compared to derivative molecules and attempts at improving 2ME bioavailability have been conducted, most successfully by sulfamoylation of the original molecule.[12] These sulfamoylated analogues cause increased cytotoxic and cytostatic activity, plasma half-life and bioavailability, whilst replicating the original anti-proliferative effects of 2ME.

One of the most successful sulfamoylated analogues of 2ME is 2-methoxyestradiol-bis-sulfamate (2MES).[13] The molecule was created by the addition of sulfamate groups on carbons 3 and 17 (Figure 3.2b) and was originally developed as a steroid sulfatase inhibitor. 2MES has improved oral bioavailability, high resistance to degradation and a significantly decreased IC_{50} value (concentration of drug that inhibits cell growth by 50%) when compared to 2ME.[13,14,15] It irreversibly inhibits cancer cell proliferation and tumour growth in estrogen receptor positive and negative cells as well as multiple drug resistant (MDR) cell lines.[14] The molecule is not yet commercially available and samples have to be synthesised individually. Figure 3.4 shows the typical morphological changes in 2MES-exposed cells which indicate cellular stress when compared to vehicle control samples.

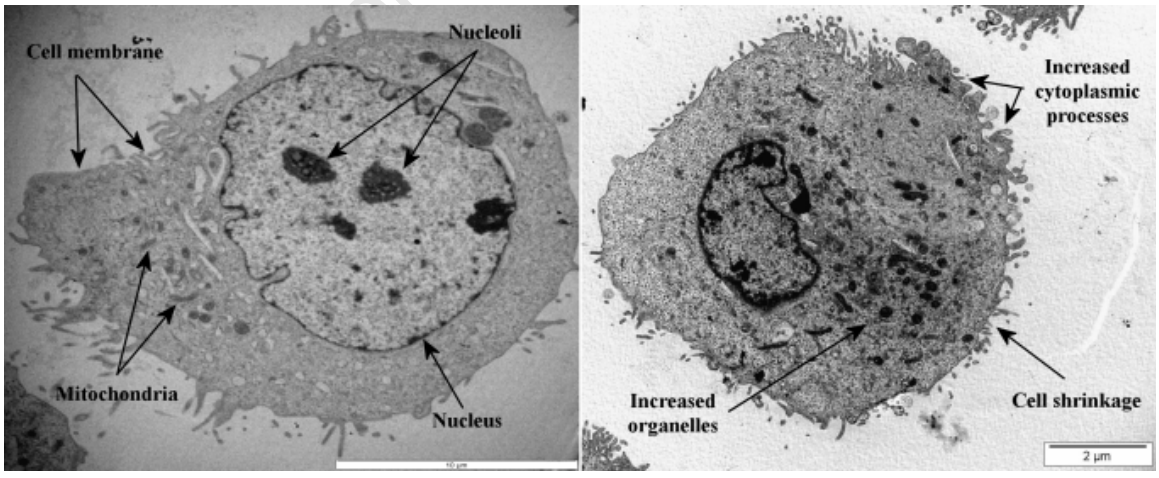

Figure 3.4 Transmission electron microscopy of cellular ultrastructure revealed slight morphological changes in 2MES-exposed cells (right) indicative of cellular stress when compared to vehicle control samples (left).[12]

A few properties of 2ME and 2MES are listed in Table 3.3. 2ME is sparingly soluble in aqueous media at pH 1 to 8 with an experimental value of 0.0048 g/L (25 °C) across the pH ranges.[16] At the commencement of this study, the solubility of 2MES was unknown and therefore one of the objectives was to determine its solubility relative to that of 2ME.

Table 3.3 Properties of 2ME and 2MES

	2ME	2MES
Molecular formula	$C_{19}H_{26}O_3$	$C_{19}H_{28}N_2O_7S_2$
Molecular weight	302.41 g/mol	460.55 g/mol
Melting point	186-187 °C	174-175 °C

Identification of Synthesised Samples of 2ME and 2MES

Microanalysis

The sample of 2ME used was a gift from Shimoda-Biotech (Port Elizabeth, South Africa). Dr Gareth Arnott (University of Cape Town) was commissioned to synthesise the 2MES using the 2ME as starting material. A 10 g batch was prepared and its structure confirmed by ^{1}H-NMR analysis. The results of C, H and C, H, N, S microanalysis for 2ME and 2MES hemihydrate respectively are listed in Table 3.4. The experimental values agree with their respective calculated values within experimental error thus showing a high degree of purity in their preparation.

Table 3.4 Microanalysis for 2ME ($C_{19}H_{26}O_3$) and 2MES ($C_{19}H_{28}N_2O_7S_2\bullet(H_2O)_{0.5}$) synthesised material

Steroid	Experimental (n=3)				Calculated			
	%C	%H	%N	%S	%C	%H	%N	%S
2ME	75.33	8.61	-	-	75.46	8.66	-	-
2MES	48.76	6.17	5.88	13.84	48.60	6.22	5.97	13.66

Henceforth, the synthesised starting materials 2ME and 2MES will be referred to as **Form I** in both instances. Many experiments using different techniques with a wide variety of recrystallisation solvents, were performed in order to isolate new forms of 2ME and 2MES. Some representative results are listed in Table 3.5 and a full listing appears in Appendix 1 on the attached CD-rom.

Table 3.5 Representative recrystallisation outcomes for 2ME and 2MES

Method 1[i]: Slow evaporation (59 solvents)			
Solvent	**Concentration (mg/ml)**	**2ME**	**2MES**
Dimethylformamide	5	Form I	No crystal
Water (deionised)	5	No crystal	Form I
Acetone	5	Form I	Form I
Methylene chloride	5	Form I	Form I
Chloroform	5	Form III	Form I
Benzene	5	Form I	No crystal

Method 2[ii]: Sublimation		
	Hot plate (watch-glass)	**Vacuum method**
2ME	Form I	Form I
2MES	Form I	Form I

Method 3[ii]: No grinding, neat grinding and solvent-drop grinding at various RH analysed every week for 7 weeks (19 solvents)			
Solvent	**Mass**	**2ME**	**2MES**
No grinding	5 mg	Form I	Form I
RH – 43%		Form I	Form I
RH – 98%		Form I	Form I
Neat grinding	5 mg	Form I	Form I
RH – 43%		Form I	Form I
RH – 98%		Form I	Form I
Dimethyl sulfoxide	5 mg/3-4 drops	Form I	Form I
RH – 43%		Form I	Form I
RH – 98%		Form I	Form I

Method 4[iii]: Solvent : water (95%:5%) mixtures (35 combinations with varying ratios)			
Solvent	**Concentration (mg/ml)**	**2ME**	**2MES**
Acetic acid (glacial)	5	No crystal	No crystal
1-Propanol	5	Form I	No crystal
Methanol	5	Form I	Form I
Acetonitrile	5	Form I	Form I
Ethyl acetate	5	Form I	No crystal

Method 5[iii]: Binary mixtures (165 combinations with varying ratios)			
1° solvent (50%)	**2° solvent (50%)**	**2ME**	**2MES**
2-propanol			
	Petroleum ether	Form I	No crystal
	Hexane	Form I	No crystal
	Carbon tetrachloride	Form I	No crystal

Method 6[iii]: Vapour diffusion			
Non-Solvent	**Solvent**	**2ME**	**2MES**
Diethyl ether	Acetone	Form I	No crystal
Diethyl ether	Isopropyl Amine	Form I	No crystal
Methanol	Diethyl ether	Form I	Form I

Method 7[iv]: Thermal methods		
	2ME	**2MES**
Crystallisation from the melt	Form II	Form I

Method 8[iii]: Dicarboxylic acid (terephthalic acid) as template in solution (11 solvents with varying ratios)			
Ratio (Drug: template)	**Solvent**	**2ME**	**2MES**
1:2	Methanol	Form I	No crystal
2:1	DMF	Form I	No crystal
2:1	Cyclohexanol	Form I	No crystal
2:1	Glycerol	Form I	No crystal

[i] Products obtained by method 1 were analysed by single crystal X-ray diffraction and HSM. Small crystals or powder masses were analysed using PXRD.

[ii] Products obtained by methods 2 and 3 were analysed by PXRD

[iii] Products obtained by methods 4, 5, 6 and 8 were analysed by HSM and single crystal X-ray diffraction

[iv] Products obtained by method 7 were analysed by HSM and DSC

NOTE: Vapour diffusion was employed to grow bigger crystals when crystals from slow evaporation were too small for diffraction purposes

3.3 2-METHOXYESTRADIOL FORMS

Sample preparation

Form I: Recrystallisation of 2ME from Diethyl Ether

A saturated solution of the raw material was prepared by adding the required amount of drug to the respective neat solvent (diethyl ether) with heating to a few degrees below the boiling point of the solvent and continuous stirring. The saturated solution was then filtered (0.45 μm) and allowed to crystallise at ~20 ºC. Crystals were kept under mother liquor prior to analysis. Large crystals of 2ME with rectangular to cubic morphology were isolated.

Form II: 2ME Amorphous

The thermal characteristics of **Form I** were measured using a differential scanning calorimetry (DSC) instrument. The sample was heated from 30 to 190 ºC at 10 K/min, cooled to 30 ºC and reheated from 30 to 250 ºC at 10 K/min. DSC measures temperature and enthalpy (heat) associated with transitions in materials. A glassy mass (2ME amorphous) was found upon cooling of the melt.

Form III: 2ME Chloroform Solvate

A saturated solution of the raw material was prepared by adding the required amount of drug to chloroform with continuous stirring at ~20 ºC (no heating was required due to the low boiling point of the solvent viz. 60-61 ºC). The saturated solution was then filtered (0.45 μm) and allowed to crystallise at ~20 ºC. Crystals were kept under mother liquor prior to analysis. Unstable, plate-like crystals were obtained.

Thermal Analyses

Hot Stage Microscopy

HSM was used to analyse the thermal behaviour of the various crystals upon heating at a constant rate of 10 K/min with photographs of **Form I, II and III** crystals presented below (Figure 3.5). The analysis was performed with the sample immersed in silicone oil to assess the presence of included solvent as would be indicated by bubble formation. The photographs of the three forms were recorded at (a) start of analysis, (b) onset of opacity, (c) the first sign of melting, (d) completion of melt and the onset of decomposition.

Form I remained relatively stable throughout the heating process with no change until 185 °C. The crystal then melted and at 200 °C, the crystal started to decompose.

Form II (amorphous phase) became opaque at 112 °C whereby transition to a crystalline form occurred. The crystalline form was identified as **Form I** since the next phase change occurred within the same melting range as **Form I** (185 °C). Decomposition of the crystal occurred at 200 °C.

Form III was identified as an unstable solvated crystal since it became opaque at 65 °C indicating loss of the chloroform solvent. The crystal collapsed and the resulting powder then melted within a similar range as that for **Form I.** Decomposition once again occurred at ~ 200 °C.

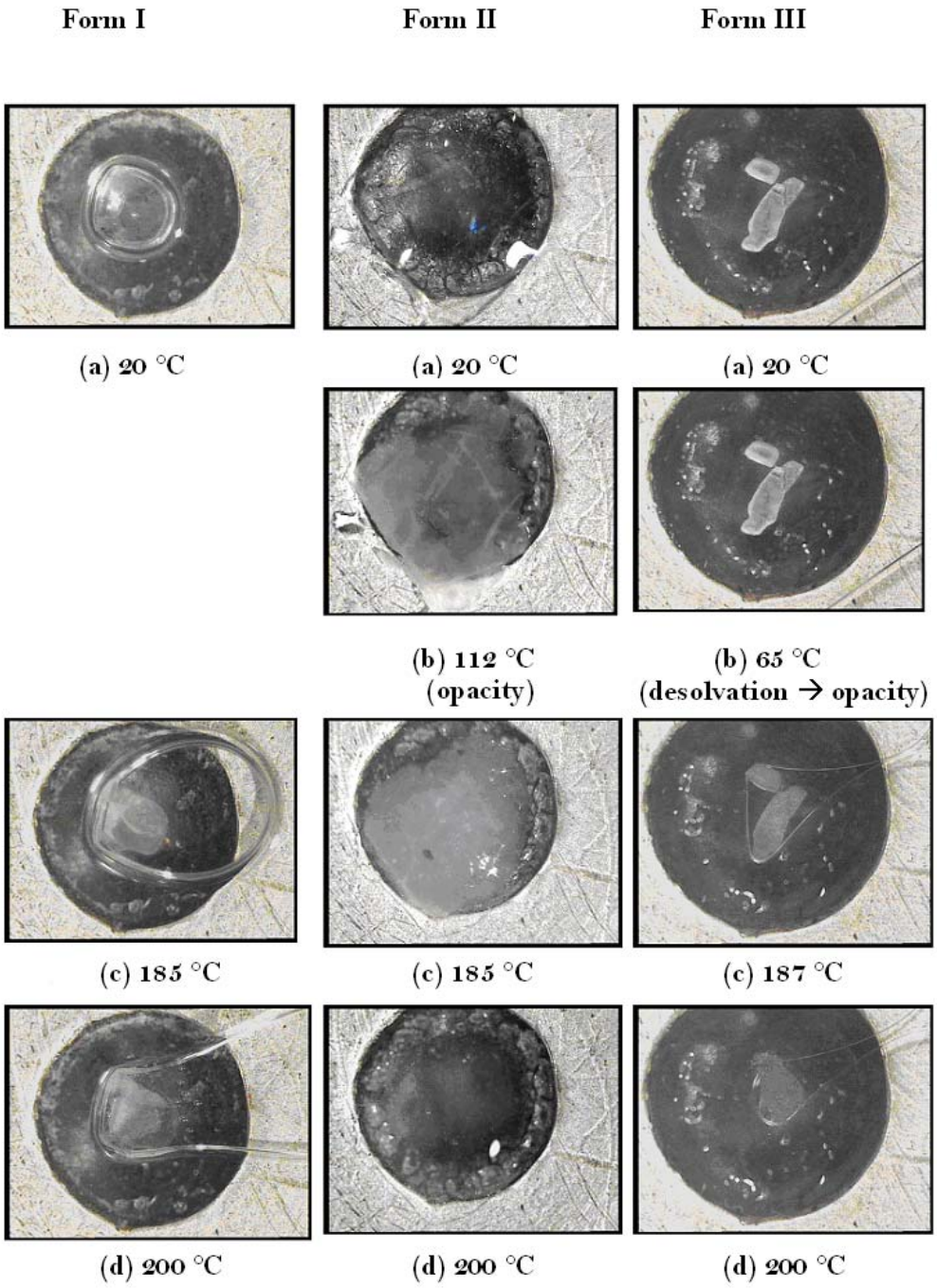

Figure 3.5 HSM photographs of Forms I, II and III of 2ME.

Differential Scanning Calorimetry and Thermogravimetric Analysis

TGA analyses for both **Form I** and **Form II** of 2ME [not shown] indicated negligible mass losses in the range 30-200 °C, thus confirming that they were not solvates. TGA and DSC analyses of **Form III** proved to be quite challenging since the solvate desolvated immediately after removal from mother liquor; however, TGA was eventually recorded (Figure 3.6) which established the stoichiometry of **Form III.** There was a 44.6 ± 0.1 % mass loss (n=2) which established the stoichiometry as 1:2 for 2ME : chloroform (theoretical mass loss = 44.12 %) .

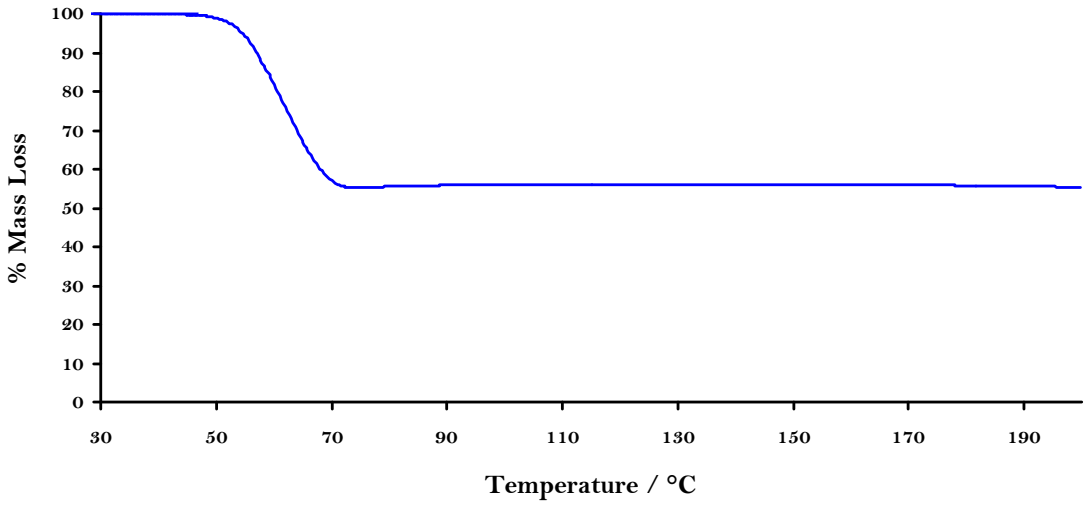

Figure 3.6 TGA trace of Form III.

DSC analysis for **Form I** was performed in the 30-210 °C temperature range and proved to correlate well with HSM findings. The DSC trace for **Form I** shown in Figure 3.7 exhibited a single endotherm (173.5-192.1 °C) representing fusion.

The DSC trace for **Form II** in Figure 3.7 (quenched melt) was as expected from the HSM analysis. Initially, the trace plateaued very closely to the baseline; then, between 92.4 and 120.1 °C we see a distinct exotherm which identifies the transition from glassy (amorphous) phase to crystalline phase (**Form I)** of 2ME. This result correlates well with the HSM analysis where the **Form II** mass opacified at this stage, indicating phase change.

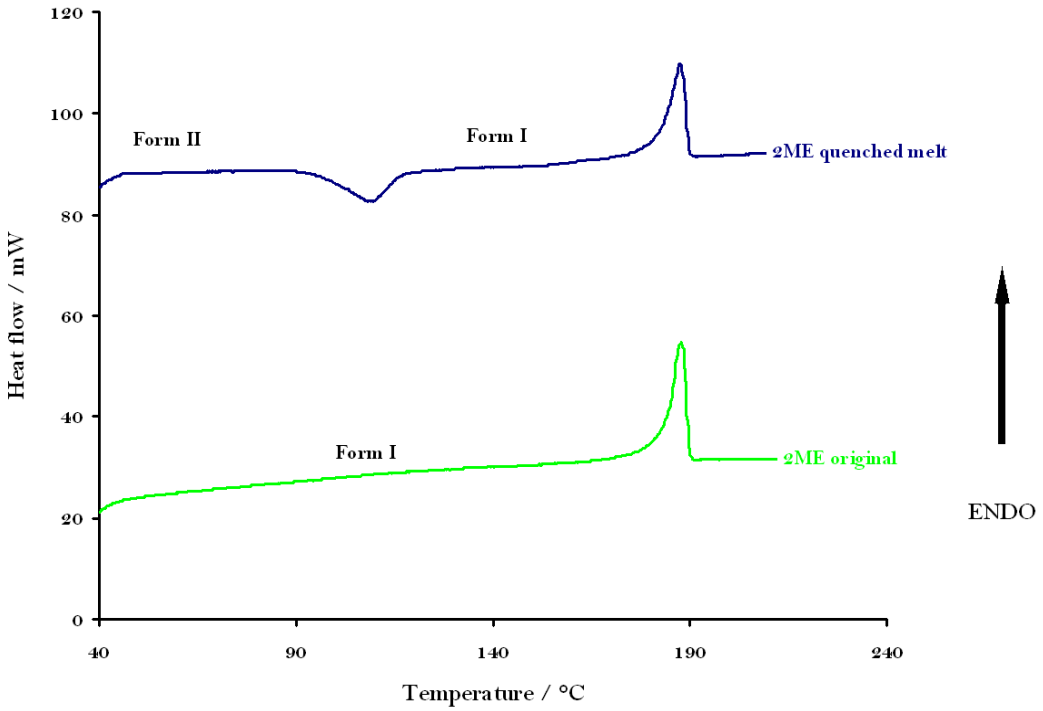

Figure 3.7 DSC traces of Form I and Form II.

Experimental PXRD Patterns

Experimental PXRD patterns of **Forms I, II** (amorphous form)**, III** (before and after desolvation) are presented in Figure 3.8. The powder patterns of **Form I, II** and **III** differ significantly showing that these can serve as references for their identification. **Form I** has four intense peaks (2θ values 15.4°, 16.1°, 17.1° and 21.7°) and four weaker peaks (10.9°, 14.2°, 21.0° and 27.9°) which matched the original 2ME material and **Form III** desolvated. The trace for **Form II** had no peaks, indicating a glassy mass as was seen in HSM at 20 °C. The material following desolvation of **Form III** displayed the same PXRD pattern as **Form I** indicating that **Form III** reverts to the most stable form established thus far. It has, however, been reported that desolvation of solvates may improve flowability and particle size[17] of the original compound.

The experimental pattern for **Form III** was quite difficult to obtain since each PXRD run produced the **Form I** pattern. We account for the transformation to **Form I** as being due to rapid solvent loss during the preparation and analysis of the sample.

Furthermore, obtaining a PXRD pattern for **Form III** proved challenging since crystals were quite large and had to be ground for sample preparation. Grinding of the sample led to rapid desolvation and transformation to **Form I**. Eventually, after careful manipulation of the **Form III** removed from the mother liquor and immersed in silicone oil (without grinding), a reproducible **Form III** PXRD pattern was achieved.

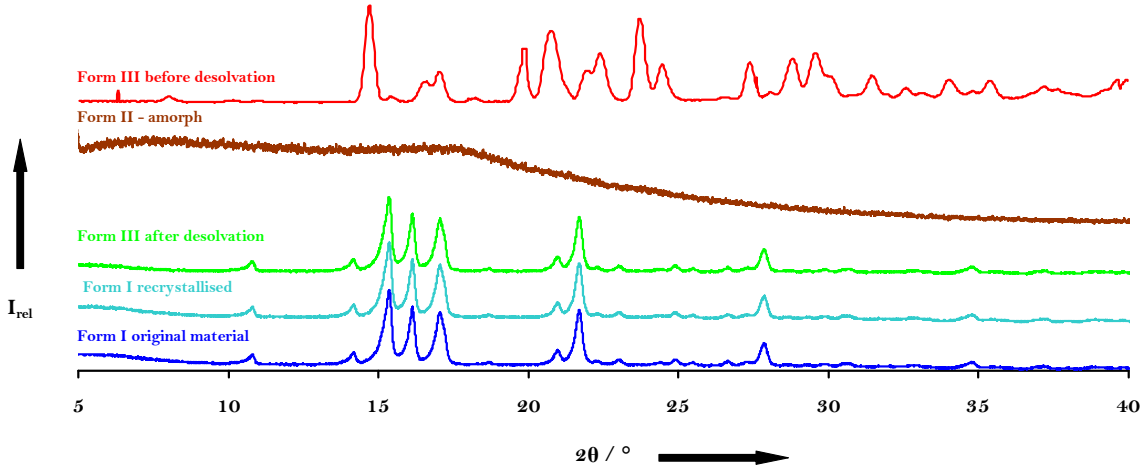

Figure 3.8 PXRD pattern of Forms I (original and recrystallised), II (amorphous), and III (before and after desolvation).

X-ray Crystallographic Analysis of Form I and Form III

Data-collection

Diffraction intensities were collected on a Nonius Kappa CCD diffractometer using graphite-monochromated MoKα radiation at low temperature (-160 °C for **Form I** and -100 °C for **Form III**). Unit cell determinations were performed at both room temperature (21 °C) and low temperatures to ensure that no phase changes were effected on cooling the crystals. The program XPREP[18] was used to determine the space groups of **Forms I** and **III**. For **Form I** Laue symmetry 2/m was confirmed for the collected intensity data, thus indicating the monoclinic system. The reflection conditions were hkl: none; h0l: none; 0k0: k=2n indicating the space groups $P2_1$ (non-centrosymmetric) and $P2_1/m$ (centrosymmetric). Since 2ME is a chiral molecule the former space group was the correct choice. The $|E^2-1|$ value of 0.838 confirmed this choice. For **Form III** Laue symmetry $\bar{1}$ was confirmed for the collected intensity data, thus indicating the triclinic system and therefore the space group P1 (non-

centrosymmetric) and P $\bar{1}$ (centrosymmetric) were implied. Since the 2ME molecule is chiral, P1 was chosen. Intensity statistics provided by XPREP[18] showed $|E^2-1| = 0.735$ indicating a non-centrosymmetric space group and the structure was successfully solved and refined in the space group P1. No disorder was observed for either structure and the final residual factors R_1 for observed data $[F_o > 4\sigma(F_o)]$ were 0.0366 and 0.0297 for **Forms I** and **III** respectively.

The unit cell determinations at room temperature and low temperature for **Form I** are presented in Table 3.6. The close similarity between the data for **Form I** at room temperature and low temperature indicates that no phase change took place on cooling the crystal. In the case of **Form III**, attempts to measure the unit cell at room temperature failed because the crystal spontaneously desolvated.

Table 3.6 Unit cell parameters for Form I

	Form I (21 °C*)	**Form I** (-160 °C)
Space group		$P2_1$
a (Å)	6.243	6.2540(2)
b (Å)	11.313	11.2919(3)
c (Å)	11.567	11.5524(4)
α (°)	90.17	90
β (°)	97.21	97.356(1)
γ (°)	89.91	90
Volume (Å^3)	810.43	809.11(4)

*For room temperature unit cell data, no *e.s.d.*s are reported since relatively few intensity frames were collected

Structure Solution and Refinement

SHELXS-97[19] was used for the structure solution of **Forms I** and **III**. The asymmetric unit of **Form I** comprised one 2ME molecule while that of **Form III** consisted of one 2ME molecule and two chloroform ($CHCl_3$) molecules. Direct methods revealed the positions of all the non-hydrogen atoms and allowed their placement. The 2ME molecules were included in the models with their correct known absolute configuration. All non-hydrogen atoms were then refined isotropically on F^2 with SHELXL-97[20] and subsequently with anisotropic thermal parameters. Hydrogen atoms were located in the

difference electron density maps and were then placed in fixed geometric positions using a riding model. They refined isotropically with thermal parameters equal to 1.2 times those of their parent atoms in the case of phenyl hydrogens and 1.5 times those of the parent atom for the methyl hydrogen atoms. The hydroxyl hydrogen atoms were assigned a common variable isotropic temperature factor and were placed using the hydrogen bond search model. For **Form I**, the absence of heavy atoms led to a Flack parameter value that did not indicate absolute structure unequivocally. The Friedel opposites were therefore merged (MERG 4 in SHELXL-97[20]). Least-squares weights were employed in the final cycles of the refinement.

Refinement data for low-temperature structure determinations of **Form I** and **Form III** are presented in Table 3.7

Table 3.7 Crystal and refinement data for Form I and Form III

Parameter	Form I	Form III
Molecular Formula	$C_{19}H_{26}O_3$	$C_{19}H_{26}O_3 \bullet 2(CHCl_3)$
Formula Weight/g mol^{-1}	302.41	541.17
Crystal System	Monoclinic	Triclinic
Space group	$P2_1$	P1
a (Å)	6.2540(2)	6.3150(2)
b (Å)	11.2919(3)	9.3352(3)
c (Å)	11.5524(4)	11.1622(5)
α (°)	90	104.386(2)
β (°)	97.356(1)	95.464(2)
γ (°)	90	107.774(2)
Volume (Å^3)	809.11(4)	596.44(4)
Z	2	1
Density$_{calc}$ / g cm^{-3}	1.241	1.507
μ (MoKα) / mm^{-1}	0.082	0.742
F(000)	328	280
Crystal size / mm^3	0.15 x 0.18 x 0.22	0.18 x 0.26 x 0.28
Temperature (K)	113(2)	173(2)
Range scanned θ / °	$1.00 \leq \theta \leq 26.02$	$3.99 \leq \theta \leq 27.88$
Index ranges	h: -7, 7 k: -13, 13 l: -14, 14	h: -7, 8 k: -12, 12 l: -14, 14
ϕ scan angle / °	1.0	1.0
ϕ scan angle range, frames	327, 327	363, 363
ω scan angle / °	1.0	1.0
ω scan angle range, frames	134, 134	562, 562
Dx / mm	30	30
Total no. of reflections collected	3106	17779
No. of unique reflections	1655	5185
No. of reflections with $I > 2\sigma(I)$	1373	4697
No. of L.S. parameters	203	278
R_{int}, R_σ	0.026, 0.049	0.035, 0.039
Flack parameter	0(1)	0.03(4)
S	1.010	1.030
R_1 [$F_o > 4\sigma(F_o)$]	0.0366	0.0297
No. of reflections omitted	3	26
wR_2 (all reflections)	0.0842	0.0721
Weighting scheme	a = 0.0487, b = 0	a = 0.0391, b = 0.1123
$(\Delta / \sigma)_{mean}$	< 0.001	< 0.001
Δρ excursions / eÅ^{-3}	0.182, -0.219	0.353, -0.438

Description of the Structures

With few exceptions, steroids generally crystallise in the monoclinic and orthorhombic crystal systems.[21] Since the naturally-occurring steroids and their synthetic derivatives contain asymmetric centres, they must crystallise in space groups which lack inversion centres and mirror planes.[21] Furthermore, the majority of steroids crystallise in the monoclinic space group $P2_1$ or the orthorhombic space group $P2_12_12_1$. Thermal-ellipsoid plots of the asymmetric units of **Form I** and **Form III** are presented in Figures 3.9 and 3.10.

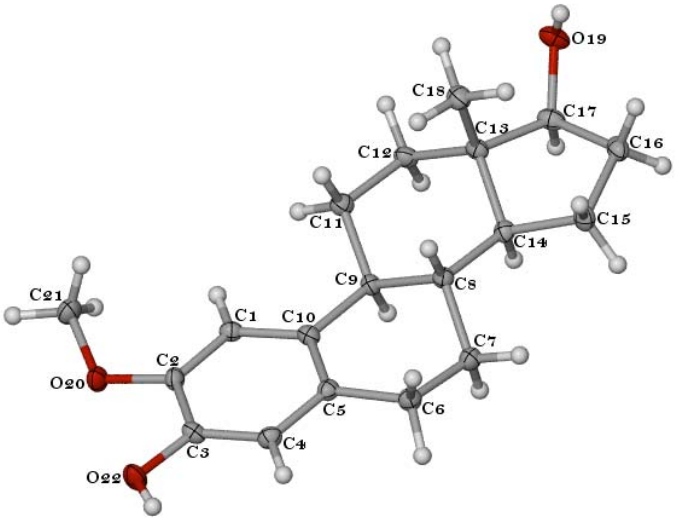

Figure 3.9 The asymmetric unit in Form I with thermal ellipsoids drawn at the 50% probability level.

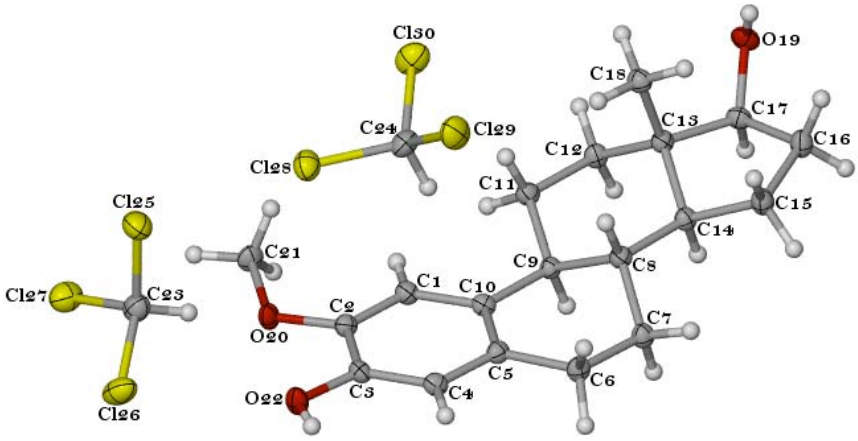

Figure 3.10 The asymmetric unit in Form III with thermal ellipsoids drawn at the 50% probability level.

Figures 3.9 and 3.10 illustrate that the 2ME molecule appears to adopt remarkably similar conformations in **Forms I** and **Form III**. A graphical overlay of the two molecules (Figure 3.11) illustrates that the two 2ME molecules are nearly perfectly superimposable. A detailed geometrical analysis of the respective molecules follows to present a more detailed comparison of their structures.

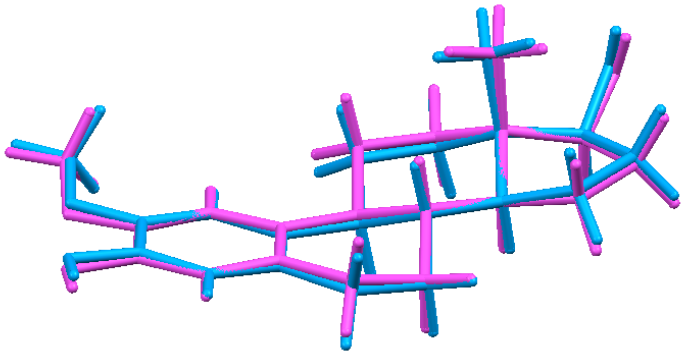

Figure 3.11 Overlay of 2ME in Forms I (blue) and Form III (pink).

Geometrical Analysis of 2ME in Form I and Form III

Table 3.8 presents selected, representative bond distances and torsion angles of the 2ME molecule in **Form I** and **Form III** for comparison as well as the distances and angles for all the strong intermolecular hydrogen bonds in both forms. In addition, the differences between corresponding molecular parameters for 2ME in **Forms I** and **III** are listed in Table 3.8. A full set of the molecular parameters is available in Appendix 4 on the CD-ROM provided.

Table 3.8 Common selected geometrical parameters for the 2ME molecule in Form I and Form III

Parameter	Form I	Form III	|Δ|
Selected bond distances (Å)			
O19-C17	1.431(3)	1.436(2)	0.005
C13-C18	1.540(3)	1.535(3)	0.005
O20-C2	1.391(3)	1.386(2)	0.005
O20-C21	1.432(3)	1.432(3)	0.000
O22-C3	1.366(3)	1.368(2)	0.002
C1-C10	1.408(3)	1.407(3)	0.001
C8-C9	1.546(3)	1.546(3)	0.000
C13-C14	1.541(3)	1.537(3)	0.004
Selected torsion angles (°)			
C21-O20-C2-C1	-20.6(3)	-12.4(3)	8.2
C9-C10-C5-C6	3.2(3)	-0.2(3)	3.0
C13-C14-C15-C16	-34.1(2)	-36.5(2)	2.4
C14-C15-C16-C17	7.7(2)	11.8(2)	4.1
C15-C16-C17-C13	21.3(2)	17.1(2)	4.2
C16-C17-C13-C14	-41.3(2)	-38.9(2)	2.4
C17-C13-C14-C15	46.7(2)	46.9(2)	0.2
D-H•••A (Å)			
O19-H19•••O20^{i}	2.810(3)	2.899(2)	0.089
O22-H22•••O19^{ii}	2.671(3)	2.669(2)	0.002
D-H•••A (°)			
O19-H19•••O20^{i}	154	154(2)	0
O22-H22•••O19^{ii}	171	177	6

Symmetry operators for both forms: (i) x,y,1+z and (ii) -1+x,y,-1+z

This geometrical comparison confirms what is illustrated in Figure 3.11, namely that the steroid molecules in both crystal forms have very similar geometrical features. Corresponding bond lengths are equal within experimental error, with torsion angles differing to some extent. The notable consistency of the steroid molecules in each form is indicative of the rigidity and stability of this conformer and therefore the following closer, detailed examination of its structure is necessary.

Overall Description of the 2ME Molecule in Form I and Form III

The basic steroid nucleus consists of three fused six-membered rings (A, B, C) (Figures 3.9 and 3.10) and one cyclopentane ring (ring D). Ring A is aromatic and rings B and C are cyclohexane rings. The standard steroid numbering and ring nomenclature are indicated (Figure 3.9). The asymmetric carbon atoms in 2ME are C8, C9, C13, C14 and C17. As regards the conformations of the respective rings in the 2ME molecule, ring A is planar (since it is aromatic), ring B adopts a half-chair conformation, ring C a chair conformation and ring D an envelope conformation with flap at C13. The A-end[21] is generally referred to as the head and the D-end[21] is generally referred to as the tail of the steroid. More specifically, the head-tail designation usually refers to C3 and C17 respectively or to substituents at these positions. Table 3.9 lists the endocyclic torsion angles in rings B, C and D that define their precise conformations.

Table 3.9 Endocyclic torsion angles (°) in rings B, C and D of Form I and Form III

Ring	Form I	Form III
Ring B		
C5-C6-C7-C8	44.1(3)	37.1(2)
C6-C7-C8-C9	-64.5(2)	-64.0(2)
C7-C8-C9-C10	52.4(2)	57.6(2)
C8-C9-C10-C5	-22.9(3)	-26.6(2)
C9-C10-C5-C6	3.2(3)	-0.2(3)
C10-C5-C6-C7	-13.6(3)	-4.7(3)
Ring C		
C8-C9-C11-C12	53.7(3)	51.3(2)
C9-C11-C12-C13	-54.8(3)	-54.8(2)
C11-C12-C13-C14	55.8(2)	58.1(2)
C12-C13-C14-C8	-59.8(3)	-61.5(2)
C13-C14-C8-C9	59.0(2)	57.5(2)
C14-C8-C9-C11	-54.5(2)	-51.1(2)
Ring D		
C13-C14-C15-C16	-34.1(2)	-36.5(2)
C14-C15-C16-C17	7.7(2)	11.8(2)
C15-C16-C17-C13	21.3(2)	17.1(2)
C16-C17-C13-C14	-41.3(2)	-38.9(2)
C17-C13-C14-C15	46.7(2)	46.9(2)

Hydrogen Bonding Motifs and Crystal Packing in Form I and Form III

The hydrogen bonding motif for **Form I** is shown in Figure 3.12a. In the structure there are two intermolecular hydrogen bonds which create a ring with graph set analysis descriptor $R_2^2(9)$, as indicated.[22] The 2ME molecules associate as non-centrosymmetric, hydrogen bonded dimers, the unique H-bonds being O19-H19•••O20 (x,y,1+z) and C16-H16A•••O22 (x,y,1+z). The cyclic H-bonded pattern contains a total of nine atoms, two of them being donors and two being acceptors, and is therefore designated as $R_2^2(9)$. These hydrogen bonds stabilise the layered intermolecular arrangement vertically. Furthermore, the H-bonds O22 - H22•••O19 (-1+x,y,-1+z) and O19-H19•••O20 (x,y,1+z) stabilise the intermolecular arrangement horizontally.

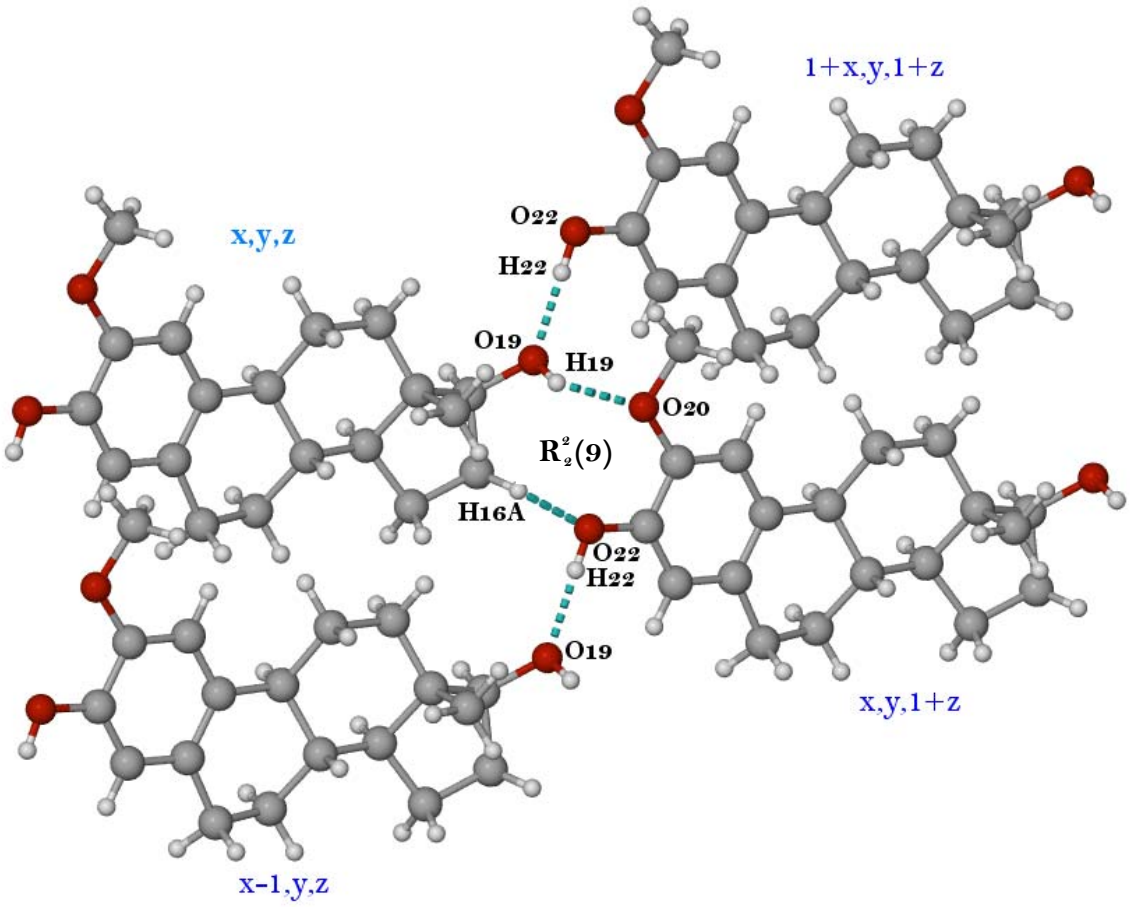

Figure 3.12 (a) Hydrogen bonding motif of Form I. Symmetry operators shown in light blue and hydrogen bonds in aqua. (Note: vertical and horizontal applies to the figure as drawn).

Figure 3.12b is a stereoview of the extended packing within a layer of 2ME molecules. The 'dimer' of Figure 3.12a is seen to propagate in a polymeric fashion producing inifinite ribbons in the vertical direction. These ribbons are linked horizontally by O-H•••O hydrogen bonds.

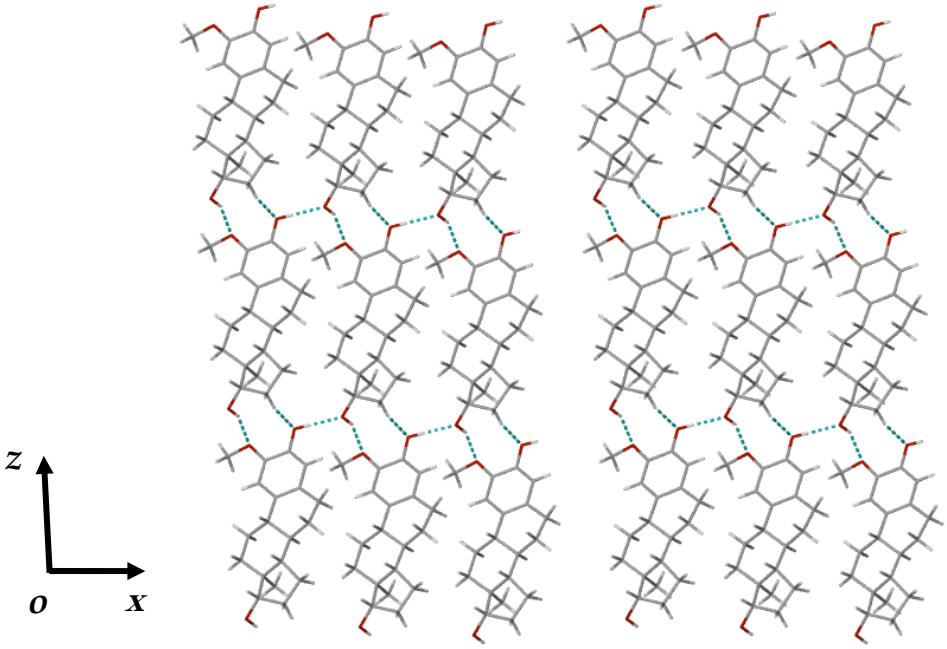

Figure 3.12 (b) Stereoview of hydrogen bonding in Form I. Hydrogen bonds in aqua.

Figure 3.13a shows the O-H•••O hydrogen bonds of **Form III** excluding the chloroform molecules for the purpose of clarity. The two intermolecular bonds seen are exactly the same as those illustrated in **Form I.** These two bonds viz. O22-H22•••O19 (-1+x,y,-1+z) and O19-H19•••O20 (x,y,1+z) contribute to the formation of continuous ribbons of 2ME molecules related by translation along the *x*-direction.

Figure 3.13b shows the hydrogen bonding motif of **Form III** inclusive of four hydrogen bonds (one of the two chloroform molecules is now included in the illustration). Two of these intermolecular hydrogen bonds (C-H•••O) give rise to the ring motif with graph set descriptor $R_1^2(5)$ shown. The 2ME molecule bonds with a chloroform molecule via the hydrogen bonds C23-H23•••O20 and C23-H23•••O22. The two bonds contain a total of five atoms, one of them being a donor and two atoms being acceptors, and the motif is hence designated as $R_1^2(5)$.

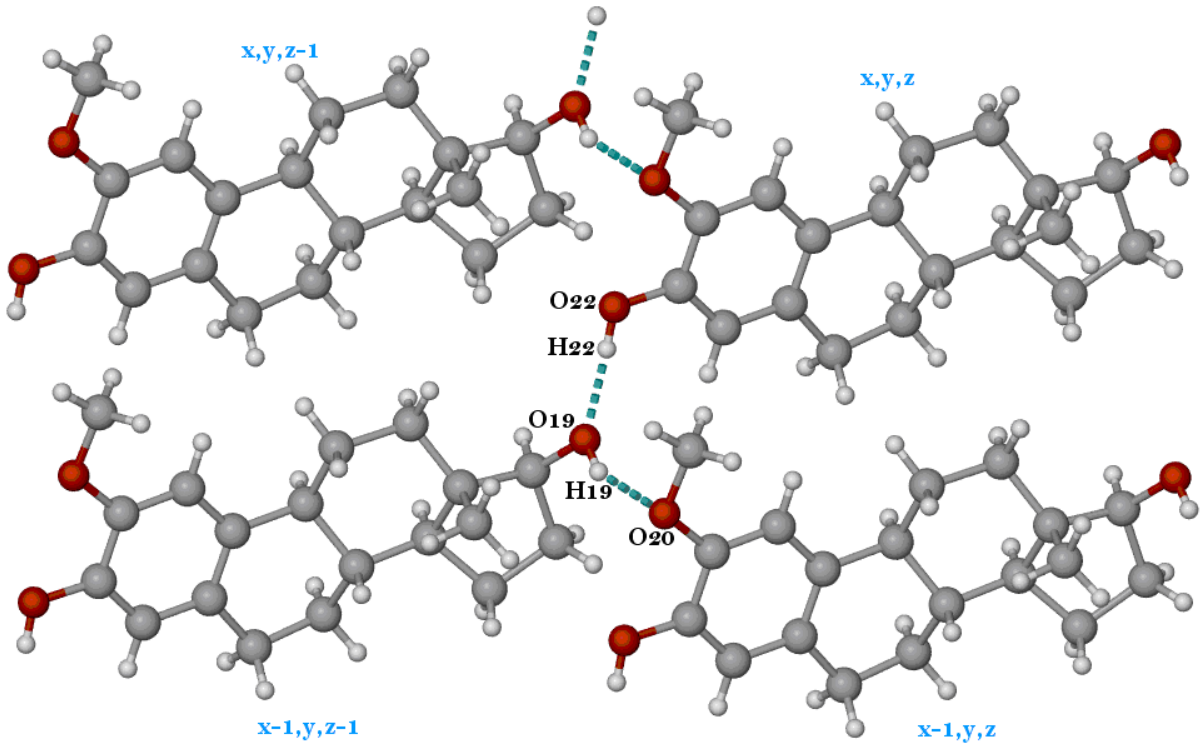

Figure 3.13 (a) Hydrogen bonding motif of Form III omitting chloroform molecules. Symmetry operators shown in light blue and hydrogen bonds in aqua.

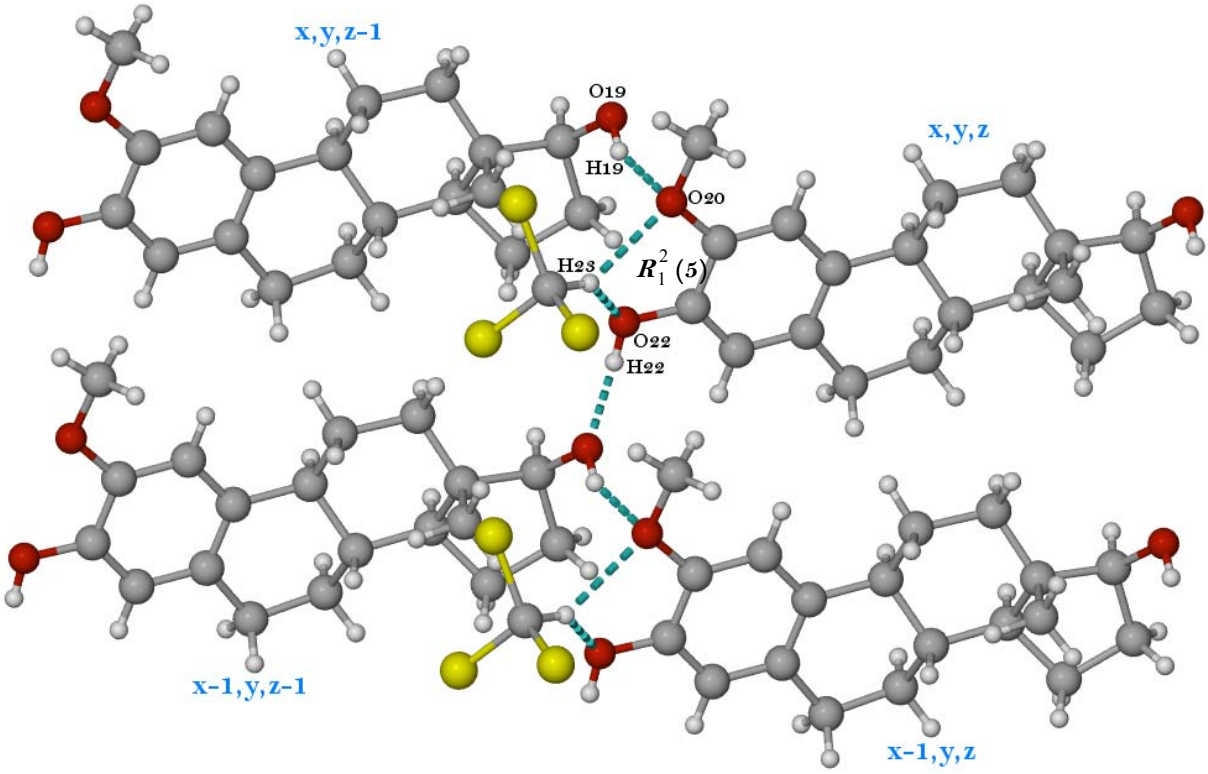

Figure 3.13 (b) Hydrogen bonding motif of Form III including one of the crystallographically independent $CHCl_3$ molecules. Symmetry operators shown in light blue and hydrogen bonds in aqua.

Figure 3.13c is a stereoview of the crystal packing in **Form III**. The hydrogen bonded 2ME molecules form a layer, upon which the $CHCl_3$ molecules are themselves layered. One of the $CHCl_3$ molecules engages in hydrogen bonding (C-H•••O) to the 2ME layer, as indicated, while the other is involved in a C-H•••π interaction with the A-ring of the 2ME molecule.

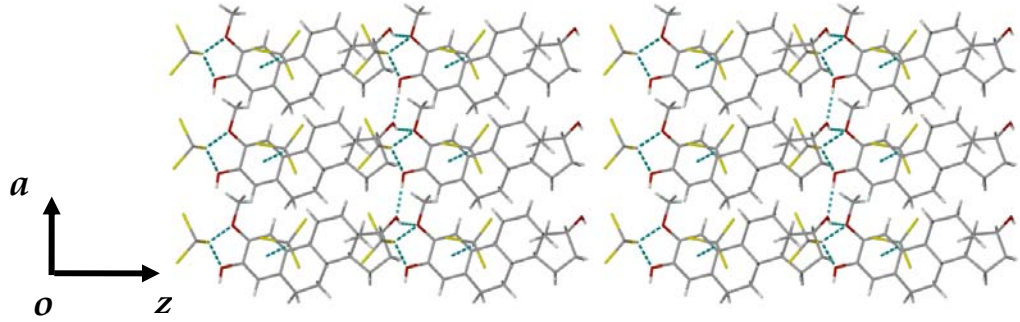

Figure 3.13 (c) Stereoview of hydrogen bonding in Form III. Hydrogen bonds shown in aqua.

Hydrogen Bonding Interactions in Form I and Form III

Table 3.10 lists all the intermolecular hydrogen bonds for both **Form I** and **Form III** as calculated by PLATON.[23] All hydrogen bonds are formed with head-to-tail (A ring to D ring) arrangement. Noticeably, **Form I** has an additional hydrogen bond between 2ME molecules. Analogous hydrogen bonds made within **Forms I** and **III** are O22-H22•••O19 (-1+x,y,-1+z) and O19-H19•••O20 (x,y,1+z). In addition, **Form I** features a C16-H16A•••O22 bond which is the second hydrogen bond to O22. In fact each of the three O-atoms in both forms engages in two hydrogen bonds. Atom H23 of one of the two $CHCl_3$ molecules in the asymmetric unit engages in bifurcated C-H•••O hydrogen bonding with O20 and O22. The second chloroform molecule engages in the C-H•••π interaction described above. These interactions are clearly shown in Figure 3.13c.

Table 3.10 Hydrogen bonding interactions for Form I and Form III

Hydrogen bond	H•••A (Å)	D•••A (Å)	D-H•••A (°)	Symmetry codes
Form I				
O19-H19•••O20	2.03	2.810(3)	154	x,y,1+z
O22-H22•••O19	1.84	2.671(3)	171	-1+x,y,-1+z
C16-H16A•••O22	2.53	3.454(3)	154	x,y,1+z
Form III				
O19 - H19•••O20	2.12(2)	2.899(2)	154(2)	x,y,1+z
O22 - H22•••O19	1.83	2.669(2)	177	-1+x,y,-1+z
C23 - H23•••O20	2.57	3.467(3)	149	
C23 - H23•••O22	2.43	3.256(3)	139	
C24 - H24•••Cg(A)	2.73	3.621(3)	148	

Chloroform molecules are located between the assemblies of the 2ME molecules as shown in Figure 3.14. No guest-guest interactions are observed within the layers. Figure 3.15 illustrates a space-filling diagram along [001], indicating that each chloroform molecule appears to be slightly hidden by 2ME molecules, by implication, presenting a very closely packed layered arrangement.

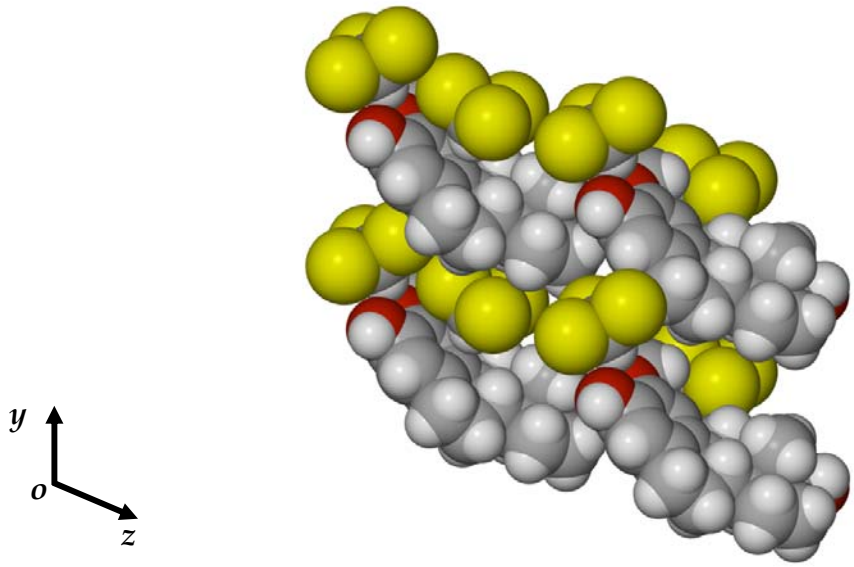

Figure 3.14 Space-filling illustration of Form III along [100].

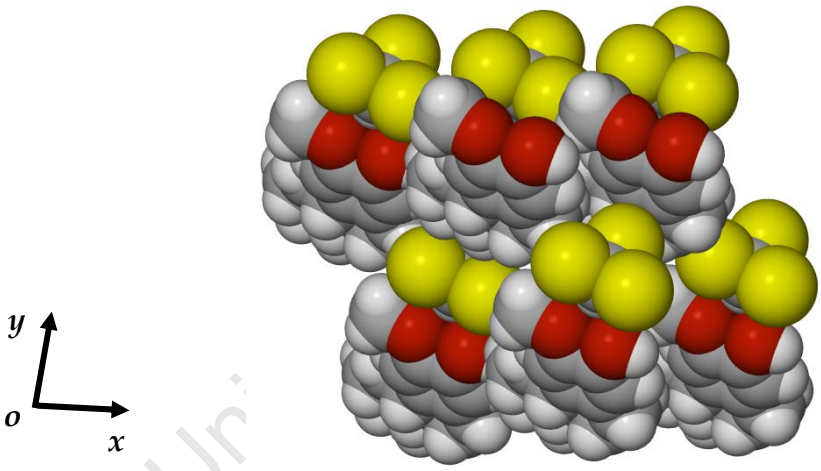

Figure 3.15 Space-filling illustration of Form III along [001].

The program SECTION[24] was used to examine the topology of guest (chloroform) inclusion in the **Form III** crystal. This program draws atoms with their van der Waals radii at desired intervals along a selected crystal axis, thus revealing features of the packing such as channels or isolated sites which may accommodate guest molecules. In Figure 3.16a and 3.16b the unit cell is sectioned at two representative values of x. Guest chloroform molecules are shown in blue and they clearly occupy layers that exist

between layers of host 2ME molecules (grey). The layers run parallel to the *xz*-plane and the $CHCl_3$ molecules occur in pairs, separated by small intervals along z. Such layers provide obvious paths for diffusion of $CHCl_3$ molecules out of crystals of **Form III** and their presence explains the rapid desolvation observed for this solvate even at room temperature.

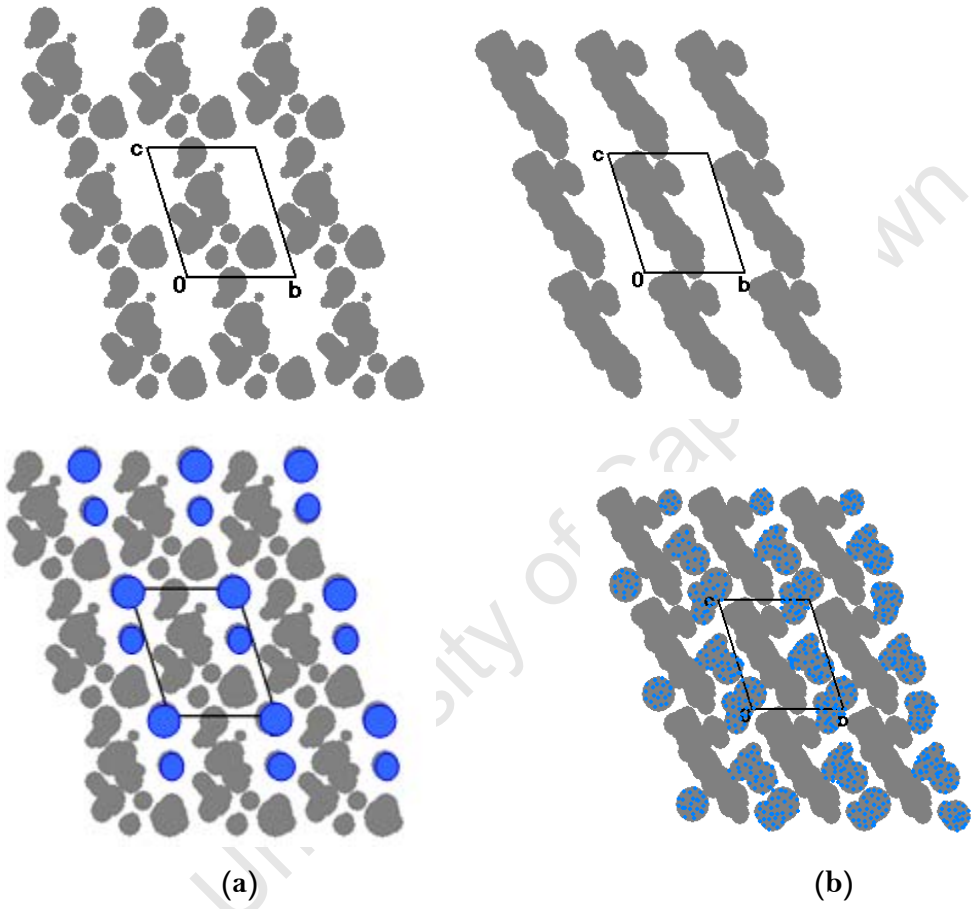

Figure 3.16 Sections through Form III illustrating guest in blue between layers of 2ME molecules represented by grey areas, viewed along [100] with the unit cell sectioned at representative levels (a) 0 Å and (b) 3.4 Å from 0,0,0. Chloroform molecules are omitted in the upper diagrams.

Calculated PXRD Patterns

Following the structural refinements, the single crystal X-ray data were used to compute simulated PXRD patterns with the program Lazy-Pulverix.[25] The peaks of the computed versus experimental patterns (Figure 3.17) for each of **Form I** and **III** matched in their respective numbers and 2θ positions. The relative intensity

distribution of the peaks of the experimental pattern is similar to that of the computed pattern in each case indicating the lack of preferred orientation in the analysed sample. The close agreement of experimental and computed patterns is also an indication of the correctness of the single X-ray crystal structural models. The slight shifts of the experimental patterns with respect to the computed patterns to lower 2θ are due to the temperature differences at which the respective traces were obtained. For each of **Form I** and **Form III**, correspondence between the experimental and calculated PXRD patterns also indicates that the bulk materials represent pure phases.

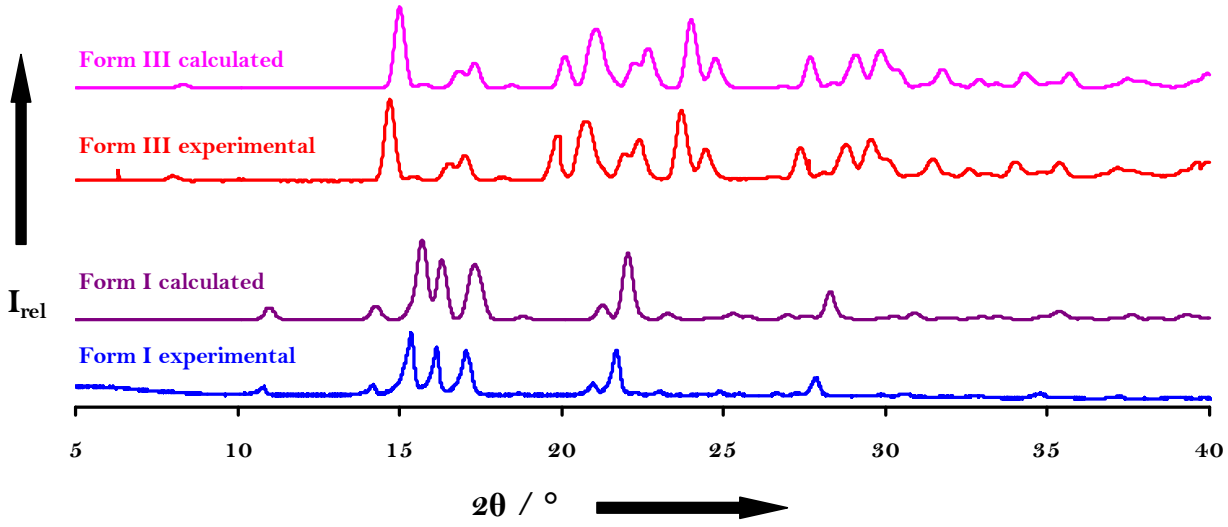

Figure 3.17 Calculated vs experimental PXRD patterns for Form I and Form III of 2ME.

3.3. 2-METHOXYESTRADIOL-*bis*-SULFAMATE HEMIHYDRATE

Characterisation of Synthesized Sample of 2MES (Form I)

Microanalysis and Thermogravimetric Analysis

The result of CHNS microanalysis for **Form I** was established before commencement of recrystallisation experiments (Table 3.4). Furthermore, initial thermogravimetric analysis (TGA) of **Form I** (not shown since analogous to Figure 3.19) presented a 2.1 ± 0.2 % (n=3) mass loss in the temperature range 30-175 ºC, which established the MES:H_2O ratio as 2:1 (theoretical mass loss = 1.92 %).

Sample Preparation

Form I: Recrystallisation of 2MES Hemihydrate

A saturated solution of the raw material was prepared by adding the required amount of drug to amyl alcohol with heating to a few degrees below the boiling point of the solvent with continuous stirring. The saturated solution was then filtered (0.45 µm) and allowed to crystallise at ~20 ºC. Crystals were kept under mother liquor prior to analysis. Large plate-like crystals of 2MES hemihydrate were harvested.

Thermal Analyses

Hot Stage Microscopy

HSM photographs of **Form I** are presented below (Figure 3.18). Thermal behaviour of **Form I** was observed upon heating at a constant rate of 10 K/min. The analysis was performed with crystals immersed in silicone oil to assess the presence of included solvent as commonly indicated by bubble formation. The photographs of **Form I** were recorded at (a) the start of the analysis, (b) the first indication of bubbling due to dehydration (range ~90 - 160 ºC, (c) the first sign of melting (~175 ºC) and (d) the onset of decomposition of the anhydrous phase (indicated by colour change of the colourless crystal to brown) and the subsequent appearance of bubbling as a result of decomposition.

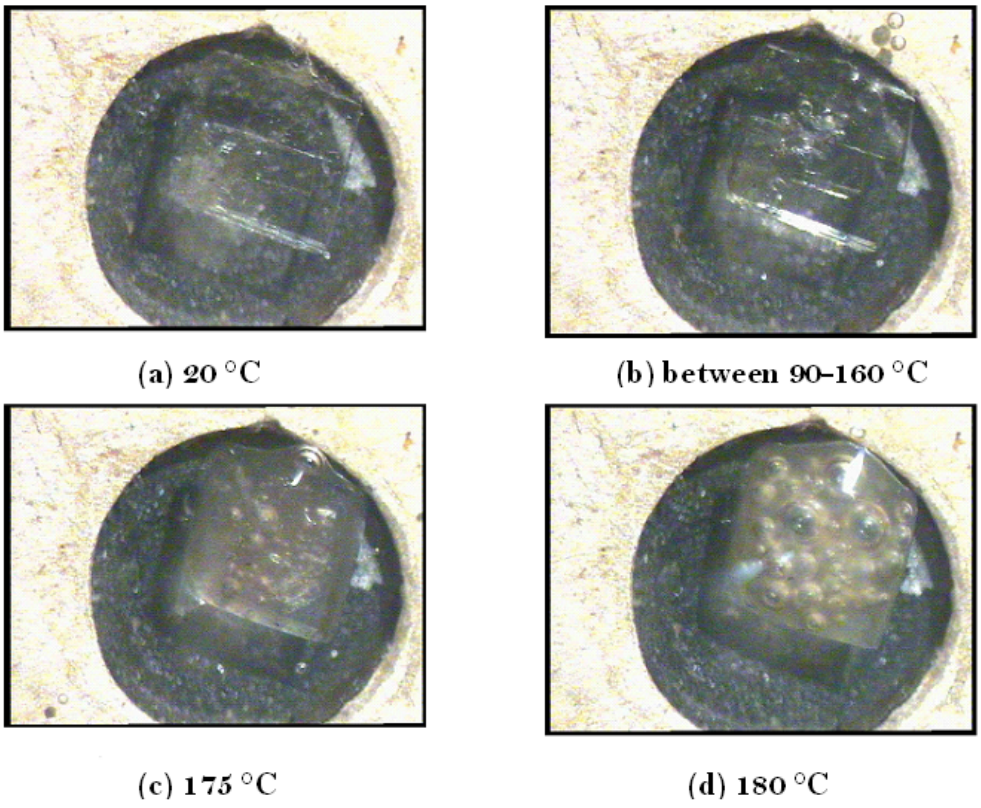

Figure 3.18 HSM photographs of Form I recorded at various temperatures.

Differential Scanning Calorimetry and Thermogravimetric Analysis

The TGA trace (Figure 3.19) for the recrystallised sample of **Form I** presented a 2.2 ± 0.2 % (n=3) mass loss (theoretical mass loss = 1.92 %) in the temperature range 30-175°C, establishing the MES:H_2O ratio as 2:1 which matched the original starting material. It is evident from Figures 3.18, 3.19 and 3.20 that the compound spontaneously degrades upon reaching the melting point. Consequently, loss of solvent is indicated from 30-175°C and thereafter the second mass loss step commences upon degradation and therefore cannot be accounted for as solvent loss. Furthermore, very significant degradation of 2MES occurs beyond 175 °C (indicated by the third step). To maintain the purity of the compound during experimentation, **Form I** had to be stored under special conditions avoiding light and maintaining a temperature of 25 °C owing to possible photodegradation. [To test the storage conditions of **Form I**, it was noted

that upon exposing 2MES to constant light for prolonged periods it started to discolour (turned brown) indicating degradation].

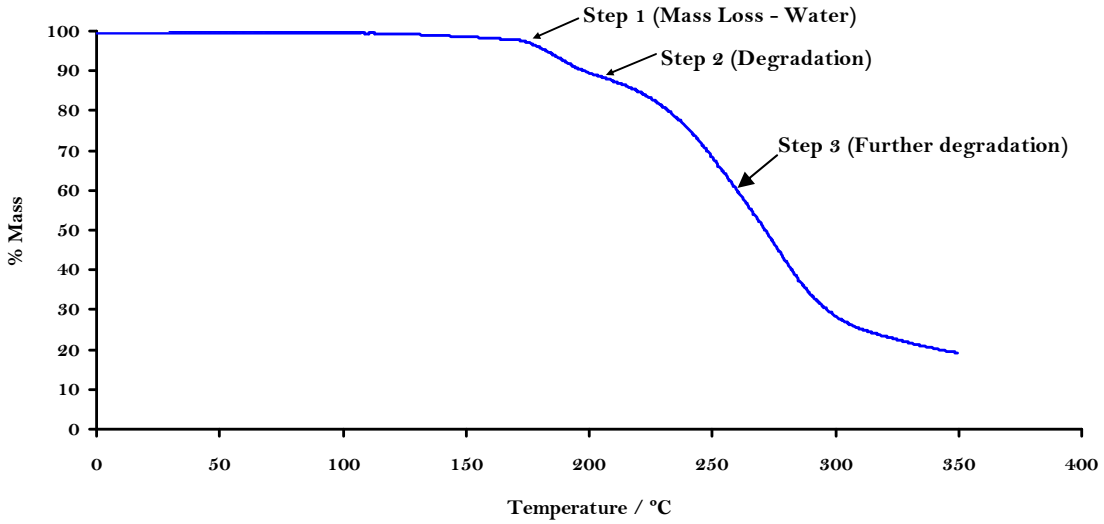

Figure 3.19 TGA trace of Form I.

The DSC trace (Figure 3.20) for **Form I** indicates an endotherm between 170 °C and 179 °C, peaking at 175 °C with immediate exothermic effect following. This correlates well with HSM analysis. **Form I** was further analysed immediately after melting had occurred by subjecting the melted sample to quenched cooling to detect whether any further polymorphic forms would arise. Degradation of **Form I** was again confirmed by the absence of an expected glass transition in the DSC trace of the quenched melt (Figure 3.20).

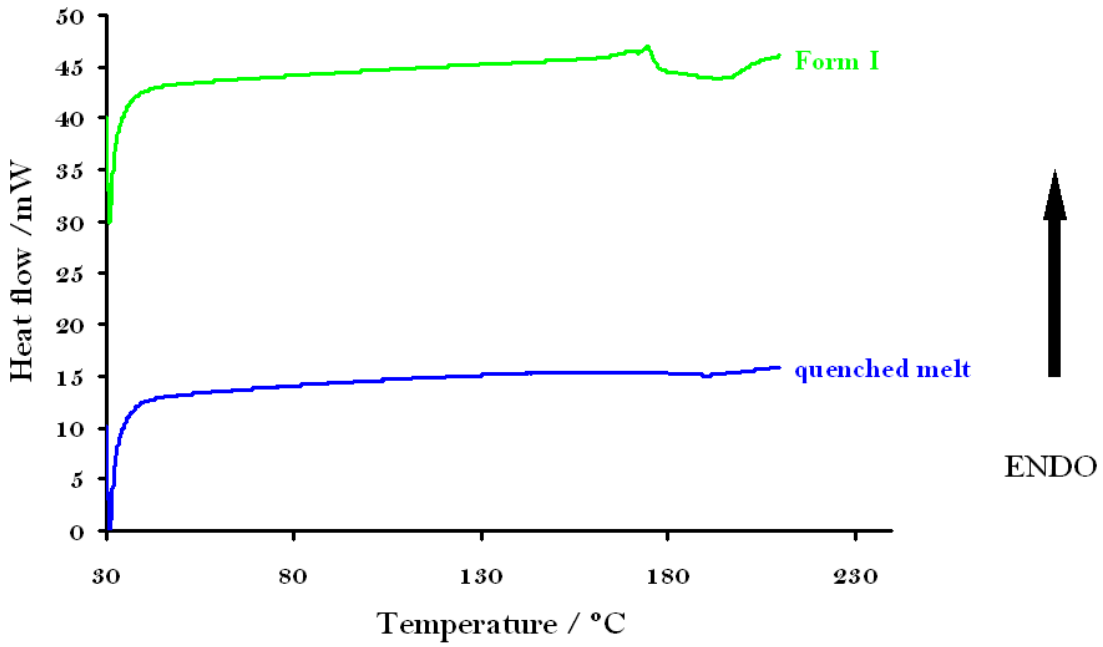

Figure 3.20 DSC trace of Form I and quenched melt.

Experimental PXRD Pattern

The PXRD patterns for **Form I** (those of both the originally synthesised material and material recrystallised from amyl alcohol) are shown in Figure 3.21. These patterns are practically indistinguishable and serve as references for this phase. The pattern is quite distinct, with five strong peaks appearing at 2θ values 7.9, 12.9, 15.9, 18.9 and 20.1°.

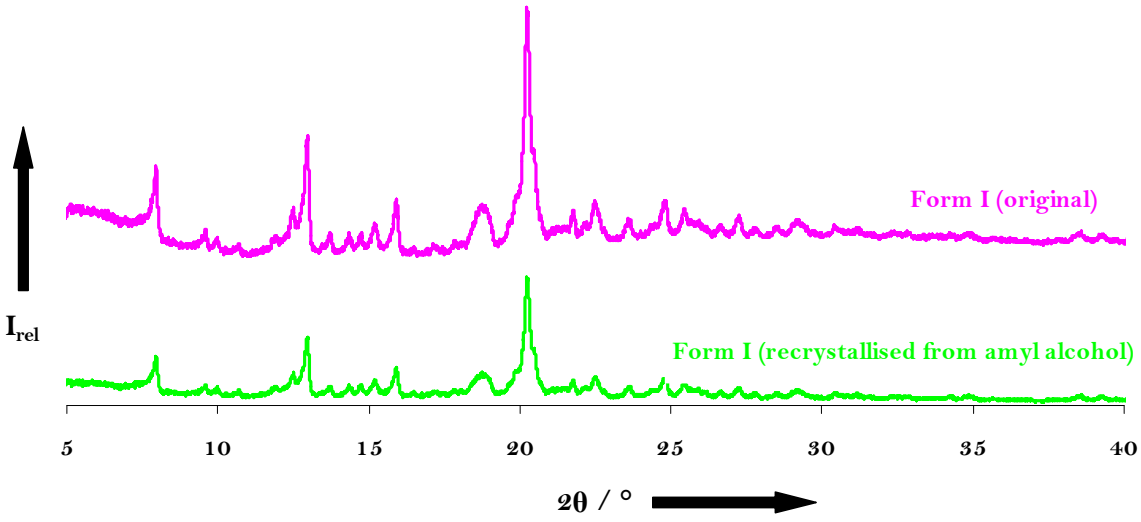

Figure 3.21 Experimental PXRD patterns of Form I.

X-ray Crystallographic Analysis of Form I of 2ME2

Data-collection

Multiple data-collections and structure refinements were performed to overcome a crystal twinning problem. Crystal twinning occurs when two separate crystals share some of the same crystal lattice points in a symmetrical manner. The result is an intergrowth of two separate crystals in a variety of specific configurations. A twin boundary or composition surface separates the two crystals. Twinning can originate in three ways: as growth twins, transformation twins and glide or deformation twins. **Form I** was classified as a growth twinned crystal which may be a contact twin or penetration twinned crystal and hence X-ray diffraction results from apparently single crystals were quite misleading. On testing several different crystals on the diffractometer, a monoclinic unit cell was persistently indicated. Full data-collection followed and a structural model was obtained in the monoclinic space group $P2_1$. However, this did not refine satisfactorily. Further careful examination of the reciprocal lattice revealed the twinning described above with either rotation, reflection, or glide deformation occurring. The relationship of the twinned crystal and its counterpart may be expressed in terms of a symmetry operation needed to bring it about, the most common type of which is formed by rotation of 180° about a zone axis, leading to pseudo-twofold symmetry. For the least troublesome crystal specimen investigated, it was found that the reciprocal lattices of the twin components were rotated by ~3° relative to one another. However, it was not possible to measure accurately the reflection intensities from the major component only, though attempts were made to do so. Eventually, a very thin lamina section was selected and this showed no indication of twinning, yielding an orthorhombic unit cell. Selection of this specimen, with one very small dimension (~0.08 mm), did however compromise the ability to correct the final intensities adequately for absorption error, as described further below.

Diffraction intensities were collected on a Bruker Apex Duo diffractometer using graphite-monochromated MoKα radiation at room temperature (21 °C) and low temperature (-160 °C). Unit cell determinations were performed at both these temperatures (Table 3.11) to ensure that no phase change occurred on cooling the crystal.

Table 3.11 Unit cell parameters for Form I

	Form I 21 °C*	**Form I** -160 °C
Space group		$P2_12_12_1$ (orthorhombic)
a (Å)	9.52	9.499(1)
b (Å)	10.62	10.585(2)
c (Å)	43.75	43.643(6)
α (°)	90	90
β (°)	90	90
γ (°)	90	90
Volume (Å^3)	4424	4388.1(1)

*For room temperature unit cell data, no *e.s.d.*s are reported since relatively few intensity frames were collected.

From Table 3.11, it is evident that no phase change occurred on cooling the crystal to -160 °C, the temperature of the final data-collection. The program XPREP[18] was used to determine the space group of **Form I**. Laue symmetry mmm was confirmed for the collected intensity data, thus indicating the orthorhombic system. The space group $P2_12_12_1$ (No. 19) was deduced from the reflection conditions h00: h=2n; 0k0: k=2n; 00l: l=2n. Inspection of the reciprocal lattice layers with LAYER[26] confirmed these reflection conditions. Intensity statistics provided by XPREP[18] yielded $|E^2-1| = 0.687$, consistent with the non-centrosymmetric space group.

Structure Solution and Refinement

The asymmetric unit of **Form I** comprised two 2MES molecules and one water molecule. SHELXS-97[19] was used for the structure solution. The E-map resulting from routine direct methods computations revealed the positions of all the non-hydrogen atoms and allowed their placement. The 2MES molecules were included in the model with their correct known absolute configuration. All non-hydrogen atoms were initially refined isotropically on F^2 with SHELXL-97[20] and subsequently anisotropically. Hydrogen atoms on the 2MES molecules were located in difference electron density maps and were placed in fixed geometric positions using a riding model. They refined isotropically with thermal parameters equal to 1.2 and 1.3 times those of their parent atoms. The hydroxyl hydrogen atoms were assigned a common variable isotropic

temperature factor and were placed using the hydrogen bond search model. Suitable positions of the hydrogen atoms on the water molecule, consistent with reasonable hydrogen bonding, were identified and these H atoms were added to the model with appropriate O-H distance restraints. The Flack parameter value did not indicate absolute structure unequivocally. The Friedel opposites were therefore merged (MERG 4 in SHELXL-97[20]). Least-squares weights were employed in the final cycles of the refinement.

Atoms O29A and C3B were refined isotropically since attempted anisotropic refinement resulted in least-squares matrix singularities. The highest residual peak not allocated had density 2.52 eÅ^{-3} which was quite significant, appearing at 0.99 Å from S27B. This peak was attributed to residual absorption error as it had no chemical significance. It was noted earlier that to avoid the problem of crystal twinning, a thin lamina of **Form I** was necessarily selected for the X-ray analysis. Although the transmission range for the specimen selected for data-collection was moderate (T_{min} =0.929, T_{max}=0.976) and the intensity data were corrected for absorption (program SADABS),[27] nonetheless the large $\Delta\rho$ peak of 2.52 eÅ^{-3} in the vicinity of atom S27B remained. This, furthermore contributed to the high final residual factor R_1 [$F_o > 4\sigma(F_o)$] of 0.1030. The deepest hole of -1.22 eÅ^{-3} appeared at 0.71 Å from S27A. Twenty-one distance restraints were applied to the model to maintain reasonable geometries while the standard deviation used for restrained bond lengths was σ = 0.005 Å for two of these and 0.01 Å for the additional 19 restraints. Crystal and refinement data for the low temperature X-ray analysis are presented in Table 3.12.

Table 3.12 Crystal and refinement data for Form I

Parameter	Form I
Molecular Formula	$C_{19}H_{28}N_2O_7S_2 \bullet (H_2O)_{0.5}$
Formula Weight/g mol^{-1}	469.56
Crystal System	Orthorhombic
Space group	$P2_12_12_1$
a (Å)	9.499(1)
b (Å)	10.585(2)
c (Å)	43.643(6)
α (°)	90
β (°)	90
γ (°)	90
Volume (Å^3)	4388.1(1)
Z	8
Density$_{calc}$ / g cm^{-3}	1.424
μ (MoKα) / mm^{-1}	0.289
F(000)	1992
Crystal size / mm^3	0.083 x 0.179 x 0.26
Temperature (K)	173(2)
Range scanned θ / °	$1.9 \leq \theta \leq 25.2$
Index ranges	h: -11, 11 k: -12, 12 l: -51, 51
ϕ scan angle / °	0.5
ω scan angle / °	0.5
Dx / mm	51
Total no. of reflections collected	29060
No. of unique reflections	4441
No. of reflections with I > 2σ(I)	4076
No. of L.S. parameters	574
R_{int}, R_σ	0.049, 0.0313
Flack parameter	0(1)
S	1.106
R_1 [F_o >4σ(F_o)]	0.1030
No. of reflections omitted	1
wR_2 (all reflections)	0.2428
Weighting scheme	a = 0.0578, b =56.446
$(\Delta / \sigma)_{mean}$	< 0.001
Δρ excursions / eÅ^{-3}	2.52, -1.22

Description of Form I

The thermal-ellipsoid plot of the asymmetric unit of **Form I** is presented in Figure 3.22.

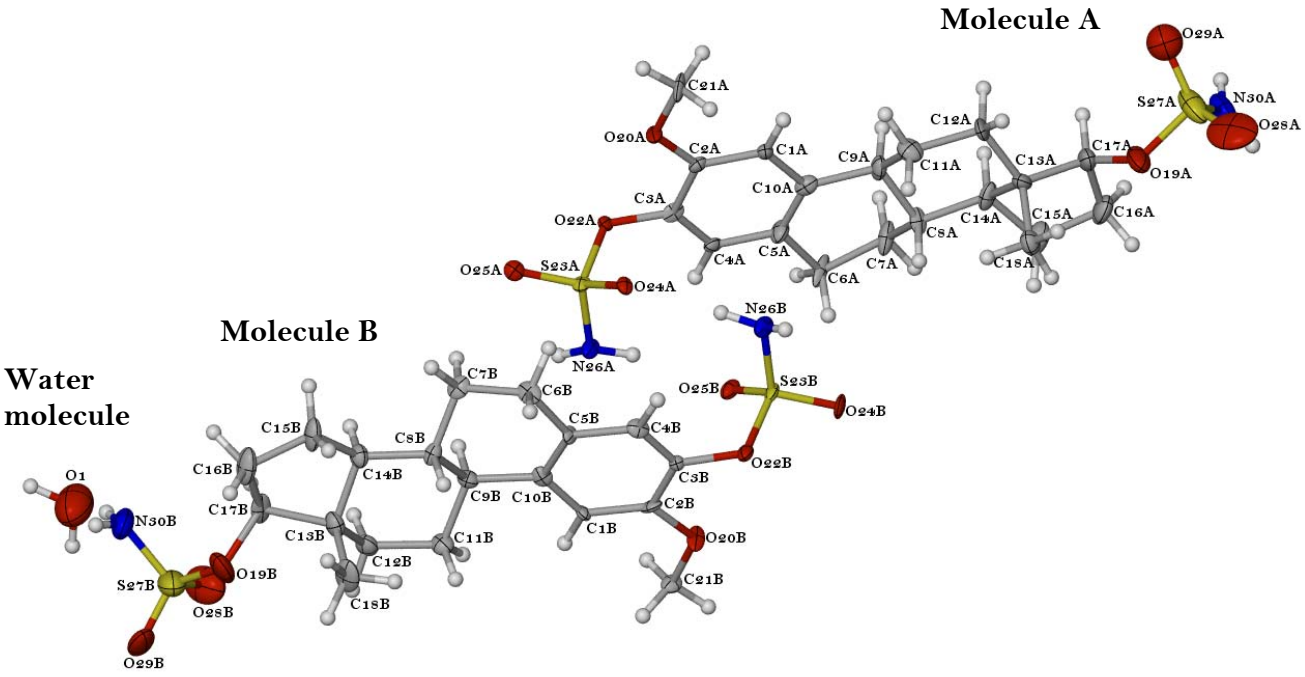

Figure 3.22 The asymmetric unit in Form I with thermal ellipsoids drawn at the 50% probability level.

In Figure 3.23, a graphical overlay of molecules A and B of the asymmetric unit in the crystal of 2MES hemihydrate is presented. This illustrates that there is a remarkable similarity between the two molecules. Figure 3.24, a graphical overlay of 2MES and 2ME **(Form I)**, illustrates that there is a remarkable similarity between the two molecules with respect to the common rigid steroid backbone, i.e. rings A, B, C and D. These figures illustrate nearly perfectly superimposable molecules. A detailed geometrical analysis of the respective molecules follows to present a more detailed comparison of their structures.

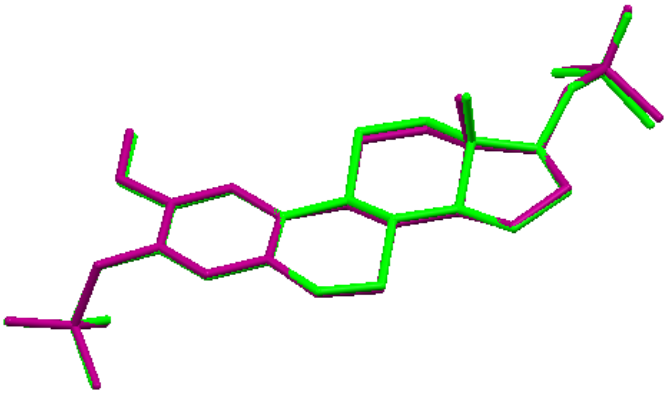

Figure 3.23 Overlay of the crystallographically independent molecules A (purple) and B (green) in the asymmetric unit of Form I of 2MES.

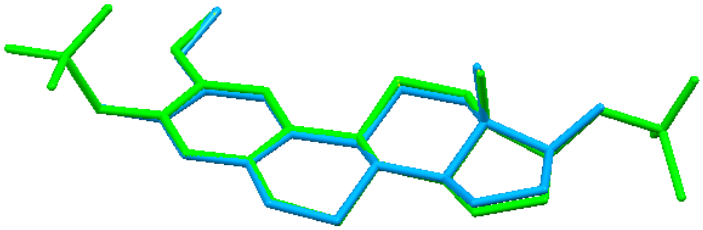

Figure 3.24 Overlay of 2MES (green – molecule B chosen arbitrarily) and 2ME (Form I) (blue).

Geometrical Analysis of 2MES in Form I

Table 3.13 presents selected, representative bond distances and torsion angles of the 2MES-A and 2MES-B molecules of **Form I** for comparison. The differences between corresponding molecular parameters are also listed in Table 3.13. A full set of the molecular parameters is available in Appendix 4 on the CD-ROM provided.

This evaluation validates what Figure 3.23 attempts to show, namely that the independent steroid molecules are geometrically almost indistinguishable. The notable consistency of the steroid molecules in each form is suggestive of the rigidity and stability of this conformer. A closer, comprehensive inspection of its structure follows.

Table 3.13 Common representative geometrical parameters for Form I (2MES-A and 2MES-B molecules)

Parameter	2MES-A	2MES-B	|Δ|
Selected bond distances (Å)			
O19-C17	1.479(2)	1.446(1)	0.033
C13-C18	1.527(2)	1.543(2)	0.016
O20-C2	1.355(1)	1.380(1)	0.025
O20-C21	1.434(1)	1.432(1)	0.002
O22-C3	1.406(1)	1.416(1)	0.010
C1-C10	1.409(1)	1.401(1)	0.008
C8-C9	1.526(2)	1.560(1)	0.034
C13-C14	1.541(2)	1.532(2)	0.009
O19-S27	1.582(1)	1.515(1)	0.067
S27-O29	1.429(1)	1.390(1)	0.102
S27-O28	1.415(9)	1.447(1)	0.032
S27-N30	1.587(1)	1.579(1)	0.008
O22-S23	1.617(7)	1.626(7)	0.009
S23-O24	1.421(7)	1.424(8)	0.003
S23-O25	1.409(8)	1.434(8)	0.025
S23-N26	1.577(9)	1.583(1)	0.006
Selected torsion angles (°)			
C21-O20-C2-C1	-2.5(1)	-0.7(1)	1.8
C9-C10-C5-C6	4.5(2)	3.0(1)	1.5
C13-C14-C15-C16	-35.4(1)	-32.8(1)	2.6
C14-C15-C16-C17	7.2(1)	5.7(1)	1.5
C15-C16-C17-C13	23.6(1)	23.2(1)	0.4
C16-C17-C13-C14	-43.8(1)	-42.1(1)	1.7
C17-C13-C14-C15	48.9(1)	44.9(1)	4.0
C17-O19-S27-O28	63.3(1)	58.0(1)	5.3
C17-O19-S27-O29	-171.9(9)	-179.0(1)	7.1
C17-O19-S27-N30	-52.5(1)	-59.4(1)	6.9
O24-S23-O22-C3	34.5(7)	-34.2(7)	0.3
O25-S23-O22-C3	163.1(7)	-162.1(6)	1.0
N26-S23-O22-C3	-81.6(7)	82.3(7)	0.7

Next, we discuss the similarity between 2ME in **Form I** and 2MES-B (arbitrarily chosen) in **Form I** as illustrated in Figure 3.24. The consistency of the rigid steroidal backbone, i.e. rings A, B, C and D, is presented in Table 3.14. The only selected torsion angle with a very significant difference was C21-O20-C2-C1 with a $|\Delta| = 19.9$ °.

Table 3.14 Common representative geometrical parameters for 2ME in Form I and 2MES-B in Form I

Parameter	2ME (Form I)	2MES-B (Form I)	$\|\Delta\|$
Selected bond distances (Å)			
O19-C17	1.431(3)	1.446(1)	0.015
C13-C18	1.540(3)	1.543(2)	0.003
O20-C2	1.391(3)	1.380(1)	0.011
O20-C21	1.432(3)	1.432(1)	0.000
O22-C3	1.366(3)	1.416(1)	0.050
C1-C10	1.408(3)	1.401(1)	0.007
C8-C9	1.546(3)	1.560(1)	0.014
C13-C14	1.541(3)	1.532(2)	0.009
Selected torsion angles (°)			
C21-O20-C2-C1	-20.6(3)	-0.7(1)	19.9
C9-C10-C5-C6	3.2(3)	3.0(1)	0.2
C13-C14-C15-C16	-34.1(2)	-32.8(1)	1.3
C14-C15-C16-C17	7.7(2)	5.7(1)	2.0
C15-C16-C17-C13	21.3(2)	23.2(1)	1.9
C16-C17-C13-C14	-41.3(2)	-42.1(1)	0.8
C17-C13-C14-C15	46.7(2)	44.9(1)	1.8

Overall Description of Form I

The molecular structures of 2MES-A and 2MES-B are chemically identical and the same remarks that applied to the parent steroid 2ME as far as ring conformations are concerned apply to the 2MES molecules. In particular, the D-ring again adopts an envelope conformation with a flap at C13. Relevant endocyclic torsion angles for 2MES-A and 2MES-B are listed in Table 3.15.

Table 3.15 Endocyclic torsion angles (°) in rings B, C and D of 2MES-A and 2MES-B in Form I

Ring	2MES-A	2MES-B
Ring B		
C5-C6-C7-C8	49.9(1)	47.2(1)
C6-C7-C8-C9	-67.3(1)	-69.1(1)
C7-C8-C9-C10	50.2(1)	54.4(1)
C8-C9-C10-C5	-19.7(1)	-22.4(1)
C9-C10-C5-C6	4.6(2)	3.0(1)
C10-C5-C6-C7	-19.6(2)	-14.7(1)
Ring C		
C8-C9-C11-C12	56.3(1)	51.3(1)
C9-C11-C12-C13	-55.7(1)	-54.0(1)
C11-C12-C13-C14	56.0(1)	57.6(1)
C12-C13-C14-C8	-60.0(1)	-61.4(1)
C13-C14-C8-C9	61.7(1)	56.1(1)
C14-C8-C9-C11	-58.5(1)	-51.0(1)
Ring D		
C13-C14-C15-C16	-35.4(1)	-32.8(1)
C14-C15-C16-C17	7.2(1)	5.7(1)
C15-C16-C17-C13	23.6(1)	23.2(1)
C16-C17-C13-C14	-43.8(1)	-42.1(1)
C17-C13-C14-C15	48.9(1)	44.9(1)

The A and D ends of the 2MES molecule have a sulfamate group attached to C3 and to C17 respectively. The sulfamate groups render the 2MES molecule more soluble in aqueous media than the parent 2ME steroid molecule. These $-SO_2NH_2$ groups are located at the equatorial positions on their respective D-rings in molecules A and B.

Hydrogen Bonding Motifs in Form I

The hydrogen bonding motif in **Form I** is illustrated in Figure 3.25. We see a dimeric H-bonded motif of the 2MES molecules in the asymmetric unit. There are two intermolecular hydrogen bonds that generate a ring which has a graph set analysis descriptor $R_2^2(8)$, as indicated.[22] The unique H-bonds are N26A-H26B•••O25B and N26B-H26D•••O24A. The cyclic H-bonded pattern contains a total of eight atoms, two of them being donors and two being acceptors, and is therefore designated as $R_2^2(8)$. A second ring (intramolecular) with graph set descriptor $S_1^1(5)$ occurs including 5 atoms with one acceptor and one donor. This bond stabilises the sulfamate conformation at the D-end of molecule A.

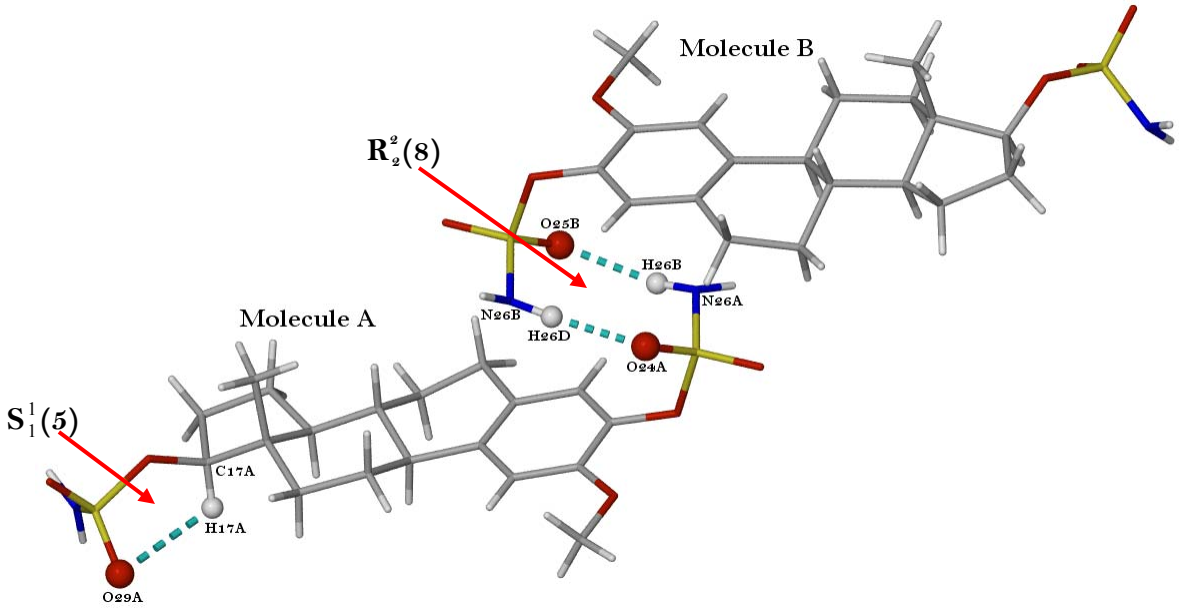

Figure 3.25 Dimeric hydrogen-bonded motif in the 2MES hemihydrate crystal.

Hydrogen Bonding Interactions in Form I

Table 3.16 lists all the hydrogen bonds for **Form I** as calculated by PLATON.[23] Of the sixteen hydrogen bonds, one is intramolecular (highlighted in bold) and 15 are intermolecular bonds.

Table 3.16 Hydrogen bonding interactions in Form I

Hydrogen bond	H•••A (Å)	D•••A (Å)	D-H•••A (°)	Symmetry codes
O1-H11•••O29B	2.07(5)	3.036(2)	168(4)	-x,-1/2+y,3/2-z
O1-H12•••O29A	2.23(7)	3.143(2)	153(8)	-1/2+x,3/2-y,2-z
N26A-H26A•••O20A	2.05(9)	2.956(1)	167(1)	-1/2+x,3/2-y,2-z
N26A-H26A•••O22A	2.55(1)	3.009(1)	111(9)	-1/2+x,3/2-y,2-z
N26A-H26B•••O25B	2.17(1)	2.980(1)	148(9)	
N26B-H26C•••O20B	2.04(7)	2.874(1)	151(1)	1/2+x,5/2-y,2-z
N26B-H26C•••O22B	2.56(1)	3.004(1)	110(9)	1/2+x,5/2-y,2-z
N26B-H26D•••O24A	2.05(1)	2.968(1)	177(1)	
N30A-H30B•••O29B	2.34(7)	3.129(1)	143(7)	-1/2-x,2-y,1/2+z
N30B-H30C•••O29A	2.23(6)	3.023(2)	143(5)	1/2-x,2-y,-1/2+z
N30B-H30D•••O1	1.83(4)	2.756(2)	170(6)	
C4B-H4B•••O24B	2.54	3.434(1)	158	1/2+x,5/2-y,2-z
C12A-H12A•••O28B	2.42	3.359(2)	158	1/2+x,3/2-y,2-z
C17A-H17A•••O29A	**2.59**	**3.013(2)**	**105**	
C21A-H21B•••O25B	2.40	3.303(1)	153	1+x,y,z
C21B-H21E•••O24A	2.42	3.320(1)	152	-1+x,y,z

Twelve host-host intermolecular hydrogen bonds exist of which eight are N-H•••O interactions and four are C-H•••O interactions. The average distance for the N-H•••O and C-H•••O interactions are 2.99 (N•••O) and 3.35 Å (C•••O) respectively while the average angles are 144 and 155°, respectively. There are three host-guest (2MES•••water) hydrogen bonds, including two O-H•••O and one N-H•••O bond. Figure 3.26 illustrates the hydrogen bond interactions for the 2MES hemihydrate which bind three 2MES molecules within the cell. Positions for hydrogen atoms on the water molecule were manually generated to account for reasonable H-bonding. The

water molecule clearly plays a pivotal role in the crystal, linking the different 2MES molecules through hydrogen bonding to their hydrophilic sulfamate groups.

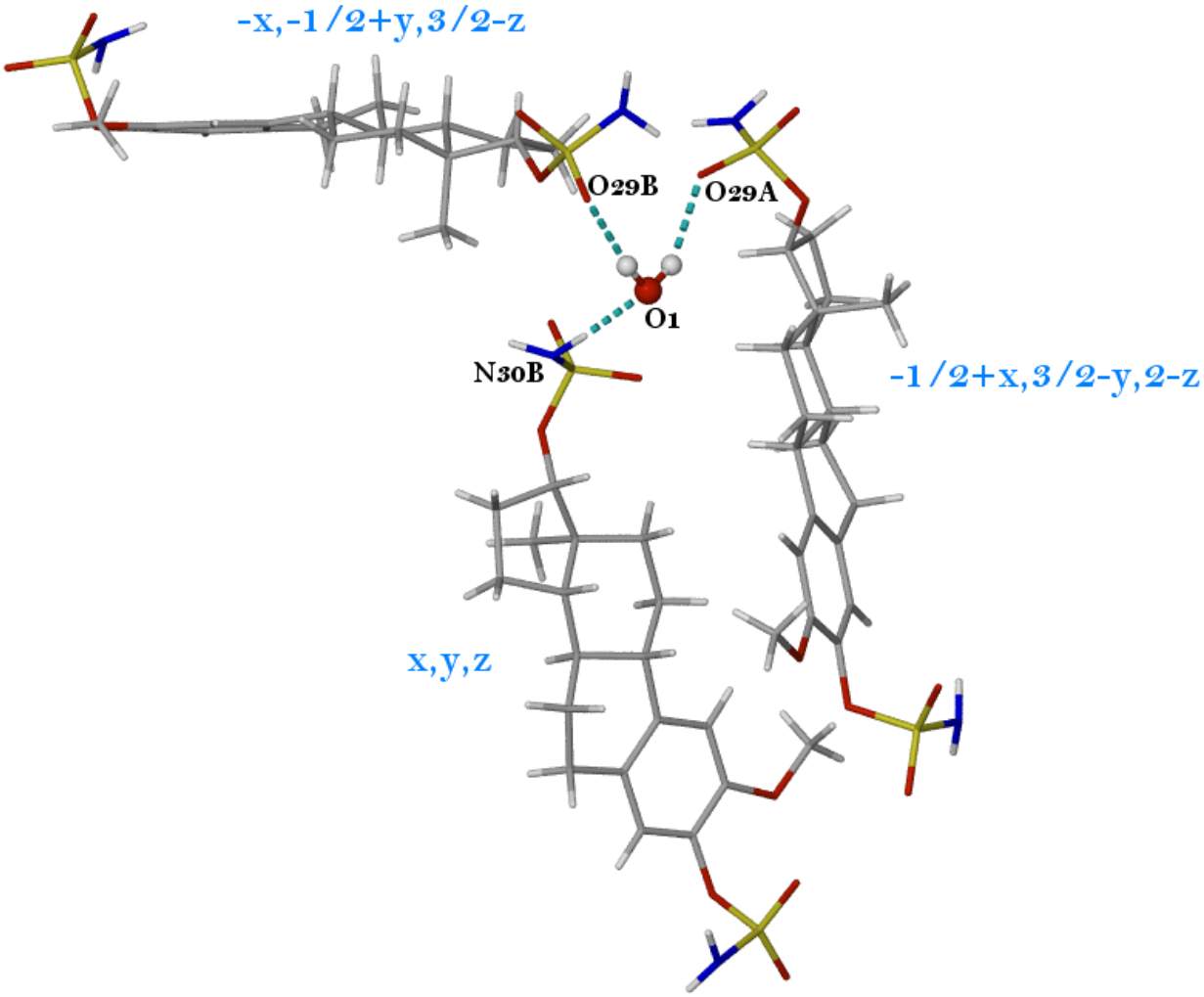

Figure 3.26 The role of the water molecule in the crystal of 2MES hemihydrate. Symmetry operators shown in light blue and hydrogen bonds in aqua.

Crystal Packing in Form I

Figure 3.27 presents crystal packing diagrams for **Form I** viewed along the crystal a- and b-axes. 2MES molecules pack head-to-head (A-ring to A-ring) and tail-to-tail (D-ring to D-ring) in a herring-bone style. An individual 2MES molecule bonds with an adjacent 2MES molecule on either end through bridging hydrogen bonds with the water molecule. Water molecules are located in isolated sites in the crystal of **Form I**, which accounts for the thermal stability of this hemihydrate.

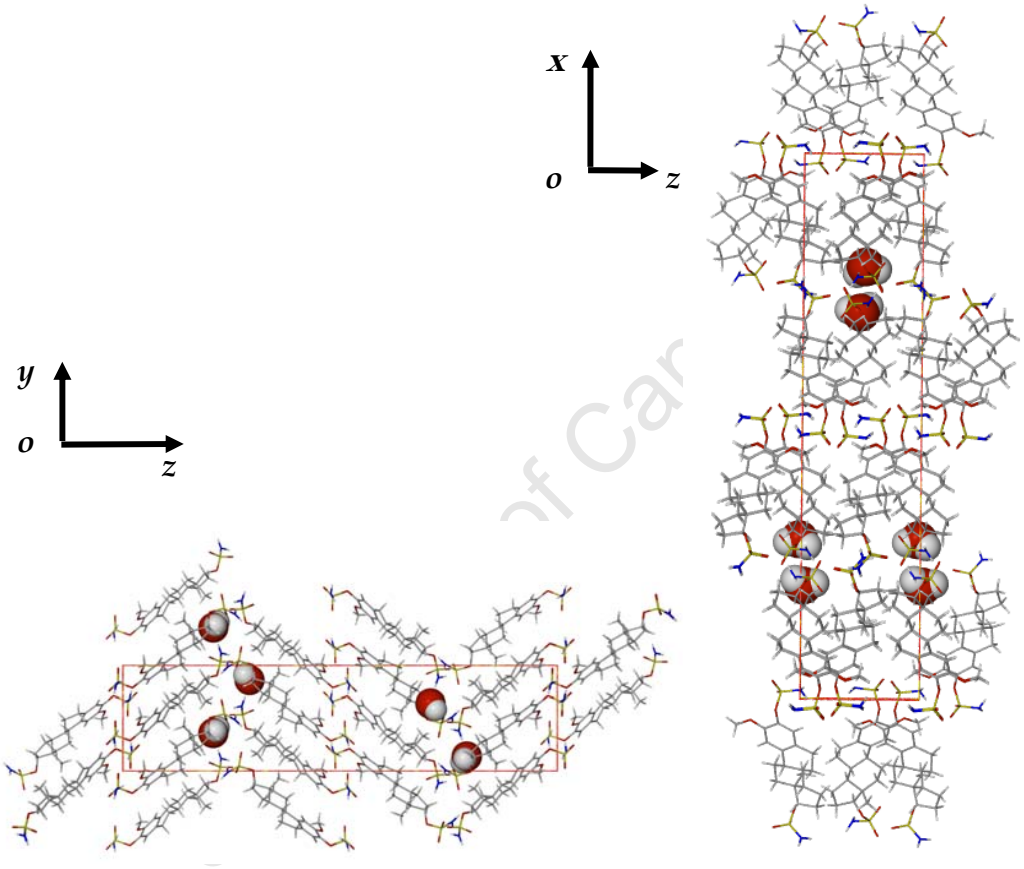

Figure 3.27 Packing in Form I of 2MES projected down [100] and [010].

Calculated PXRD Pattern

The level of agreement between the computed and experimental patterns of **Form I** (Figure 3.28) is very reasonable. This is an indication of the correctness of the single crystal structural model. As usually occurs, the calculated peak positions lie at slightly higher 2θ values than their experimental counterparts. This arises because of the

shrinkage of the unit cell of the single crystal at the low temperature of the data-collection (-160 ºC).

Variable temperature PXRD patterns were recorded for **Form I.** No indication of form change over the temperature range 21 ºC to -160 ºC was observed. The experimental pattern also suggests clear representation of 2MES hemihydrate within the bulk of the sample.

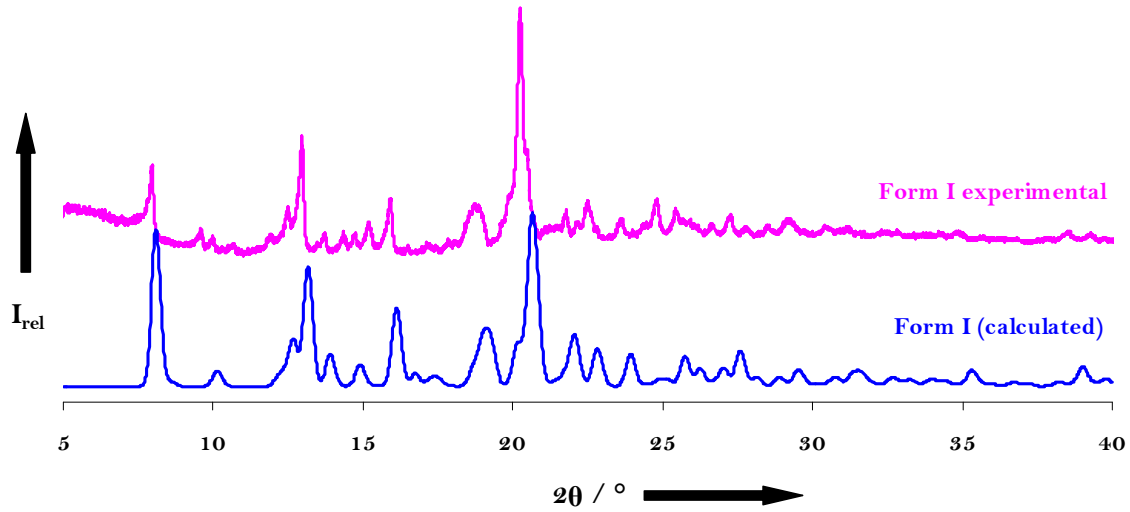

Figure 3.28 Calculated and experimental PXRD patterns for Form I of 2MES

3.4 SOLUBILITY AND DISSOLUTION OF 2ME CRYSTALLINE (FORM I), 2ME AMORPHOUS (FORM II) AND 2MES HEMIHYDRATE (FORM I)

The aqueous solubility of 2MES hemihydrate was determined experimentally using the following procedure: A saturated solution of 2MES hemihydrate was obtained by stirring excess powdered solute with solvent (distilled water) in a small glass container for 7 days at 25 °C until equilibrium was attained. Equilibrium attainment was determined by several samplings of the solubility experiment and their assay for 2MES by UV spectrophotometry since no prior information was available. This was achieved by sampling the 2MES concentration every 8 hours during the 7 days of agitation until the last three sample points were equal, indicating equilibrium. While conducting this exercise it was important not to replace the solvent removed during sampling since this

would drive the system away from equilibrium. It was essential that some undissolved solid be present at the completion of this stage in order to ensure that the solution was saturated.[28] Since 2MES hemihydrate presented a photo-labile system, protection from light was achieved by covering the glass container with an opaque material such as aluminium foil.

A sample of the saturated solution was obtained for analysis by separating it from the undissolved solid. Filtration through a 0.45 μm membrane filter was used and precautions were taken to ensure that it was carried out at the temperature of the solubility determination in order to prevent any change in the equilibrium between dissolved and undissolved solute.[28] The concentration of 2MES hemihydrate in the saturated solution was determined by UV spectrophotometry at 199 nm. A standard curve of concentration of 2MES hemihydrate versus absorbance was plotted. The concentration of 2MES hemihydrate was subsequently determined from the calibration curve $y = 0.0246x - 0.1762$ ($R^2 = 0.8848$) where y=0 and x=0.0005.

As reported earlier in Chapter 3, the solubility of 2ME in water is 0.005g/L at a pH of 7 and 25 °C. The solubility of 2MES hemihydrate was determined and it was found to have a solubility of 0.010 ± 0.002 g/L (25 °C) at pH 7 in water, hence twice the solubility of 2ME.

In vitro dissolution studies of 2ME, amorphous 2ME and 2MES hemihydrate were conducted using the rotating basket method (at 37 °C) as described in Chapter 2. The dissolution profiles for 2ME, amorphous 2ME and 2MES hemihydrate are shown in Figure 3.29. The assays were measured by UV spectrophotometry at 198 nm for 2ME and amorphous 2ME and at 199 nm for 2MES hemihydrate in distilled water. A standard curve of concentration of 2ME and 2MES in distilled water versus absorbance was plotted.

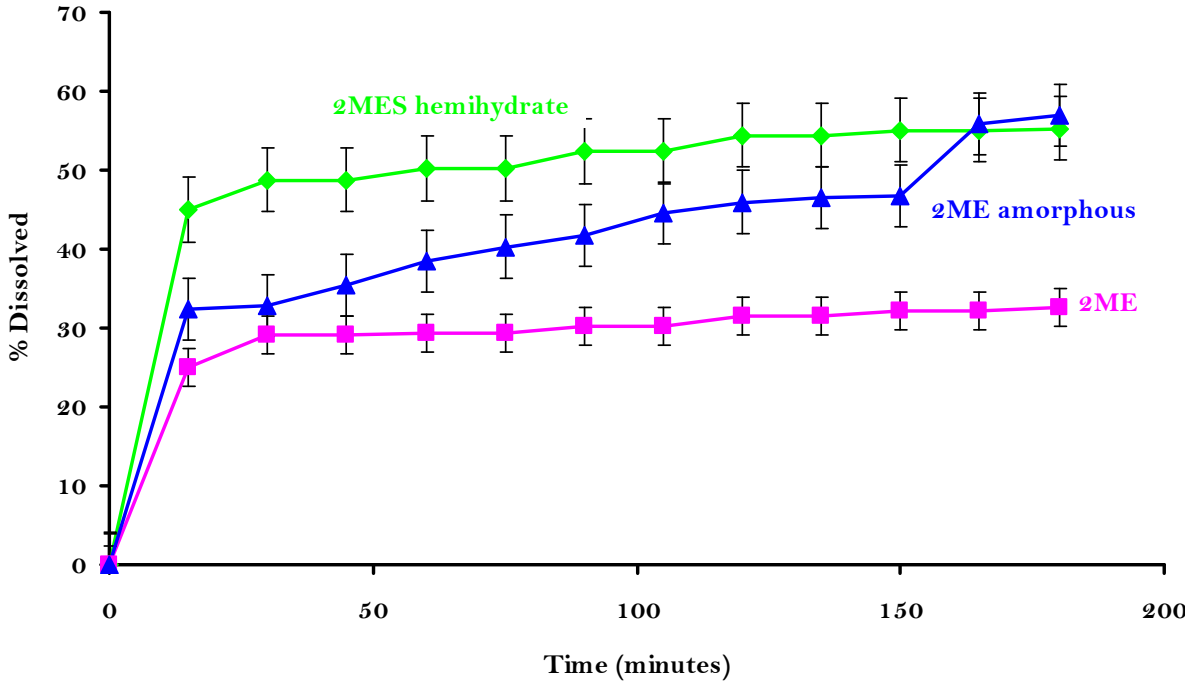

Figure 3.29 Dissolution of 2ME, amorphous 2ME and 2MES hemihydrate at 37 °C in distilled water.

The British Pharmacopoeia (BP)[29] requires that 70% dissolution must be met by *each* of the capsules tested (or by all but one of the total number of units if a retest is performed) and that the percentage is in terms of the *stated* amount. Taking account of permissible assay ranges and content uniformity, this pharmacopoeial dissolution requirement is considered to offer an acceptable degree of assurance of 'total dissolution'. The choice of a time is somewhat arbitrary, but 45 min is considered satisfactory for the majority of conventional-release (non-modified-release) products.

Figure 3.29 indicates that none of the three phases investigated passed the BP dissolution test. However, we see a significant increase in dissolution of both 2MES hemihydrate and amorphous 2ME compared to 2ME. We find that at 15 min, the percentage concentrations of 2MES hemihydrate, amorphous 2ME and 2ME are 45, 32, and 25 %, respectively. There is a further ~10 % increase in dissolution for all three profiles by 150 min. Amorphous 2ME indicated a further ~10 % increase in dissolution by the end of the 3 h run. In fact, there is a steady increase in the amorphous 2ME profile from time zero to 3 h.

The amorphous solid state possesses several advantages in comparison to the crystalline state, allowing enhanced forms of drugs to be produced. Many drugs when generated as an amorphous form will exhibit better solubility and wettability since the amorphous state is thermodynamically the form with the highest solubility. Consequently, amorphous forms will exhibit a greater solubility in a solvent than any crystalline form of the same compound. The increased solubility of amorphous actives can lead to dramatically increased intrinsic dissolution rates when compared to crystalline forms. Also, for a drug to dissolve, its surface has to be wetted by the surrounding fluid. Amorphous forms possess a chemically randomised surface which expresses equal amounts of hydrophobic and hydrophilic interactions which can lead to improved wettability expressed by a lower contact angle of the drug particle surface with a liquid. A lower contact angle represents a higher degree of hydrophilicity, with consequently faster surface wetting and faster dissolution.

To illustrate statistically the variation in dissolution profiles[30] we applied the ANOVA statistical test. The Two-Way analysis of variance (ANOVA test) was used to determine how dissolution was affected by two factors simultaneously. The percentage dissolved was the dependent variable and time was the repeated factor. Statistically significant differences ($P<0.0001$) in the dissolution rates of 2MES hemihydrate, amorphous 2ME and crystalline 2ME were observed in the analysis.

3.5 CONCLUSION

Three forms (**Form I, II,** and **III**) of 2ME and one form of 2MES (**Form I**) were isolated and characterised by thermal and X-ray diffraction methods. For 2ME, **Form II** was identified as an amorphous form and **Form III** was identified as a chloroform solvate. For 2MES, **Form I** was identified as a hemihydrate.

The melting point of 2ME **Form I**, 185 °C, was found to correspond to the previously reported melting point [186-187 °C] for 2ME.[16,31] Similarly, the melting point of **Form I** of 2MES, 175 °C, was found to correspond to the previously reported melting point [174-175 °C] for 2MES.[16]

For 2ME, **Form I** crystallises in the monoclinic space group $P2_1$ with a = 6.2540(2) Å, b = 11.2919(3) Å, c = 11.5524(4) Å, β = 97.356(1)° with two molecules per unit cell. **Form III** crystallises in the triclinic space group P1 with a = 6.3150(2) Å, b = 9.3352(3) Å, c = 11.1622(5) Å, α = 104.386(2)°, β = 95.464(2)°, γ = 107.774(2)° with one formula unit 2ME•2$CHCl_3$ per unit cell.
For 2MES, **Form I** crystallises in the orthorhombic space group $P2_12_12_1$ with a = 9.499(1) Å, b = 10.585(2) Å, c = 43.643(6) Å with eight 2MES molecules and four water molecules per unit cell.

The basic steroid structure, determined by X-ray analysis, was superimposable for 2ME **Form I, Form III** and 2MES **Form I** with minimal conformational differences existing, illustrating the rigidity of the steroid backbone.

Experimental PXRD patterns were found to be consistent with computed patterns based on single crystal X-ray diffraction data, allowing these to serve as reliable references for identification of the respective phases.

From dissolution studies conducted in aqueous medium at 37 °C, 2MES hemihydrate was determined as having twice the solubility of 2ME. The dissolution rate profiles of amorphous 2ME and 2MES hemihydrate were significantly higher than that of 2ME.

Given the generally poor solubility and dissolution rate profile of 2ME, it was considered that forming inclusion compounds between 2ME and cyclodextrins might improve these properties. An account of this approach is the subject of the following chapter.

3.6 REFERENCES

1. Moss G.P., *Pure Appl. Chem.*, **1989**, 61, 1783-1822.
2. *Britannica.com*, Facts About Gonane: Steroids, As Discussed in Steroid (Chemical Compound): Steroid Numbering System and Nomenclature, Retrieved on Feb 13, **2010**.
3. *Britannica.com*, Lanosterol Biosynthesis, Retrieved on Feb. 13, **2010**.
4. Matei D., Schilder J., Sutton G., Perkins S., Quon C., Sidor C., *Gynaecol. Oncol.*, **2009**, 115, 90-96.
5. Wood L., Leese M.P., Mouzakiti A., Purohit A., Potter B.V.L., Reed M.J., Packam G., *Apoptosis*, **2004**, 9, 321-332.
6. Ireson C.R., Chander S.K., Purohi A., Perera S., Newman S.P., Parish D., Leese M.P., Smith A.C., Potter B.V.L., Reed M.J., *Br. J. Cancer*, **2004**, 90, 932-937.
7. Rao P.N., Cessac J.W., Tinley T.L., Mooberry S.L., *Steroids*, **2002,** 67, 1079-1089.
8. Purohit A., Hejaz H.A.M., Walden L., Maccarthy-Morrogh L., Packham G., Potter B.V.L., *Int. J. Cancer*, **2000**, 85, 584-589.
9. Cushman M., He H.M., Katzenellenbogen J.A., Lin C.M., Hamel E., *J. Med. Chem.*, **1995**, 38, 2041-2049.
10. Cushman M, He H.M., Katzenellenbogen J.A., Varma R.K., Hamel E., Lin C.M., *J. Med. Chem.*, **1997**, 40, 2323-2334.
11. Rao P.N., Cessac J.W., Boyd J.W., Hanson A.D., Shah J., *Steroids*, **2008**, 73, 158-170.
12. Vorster C.J.J., Joubert A.M., *Cell. Biochem. Funct.*, **2010**, 28, 412-419.
13. Chander S., Foster P., Leese M., *Br. J. Cancer*, **2007,** 96, 1368-1376.
14. Suzuki R., Newman S., Purohit A., Leese M., Potter B., Reed M., *Biochem. Mol. Biol.*, **2003**, 84, 269-278.
15. Utsumi T., Leese M., Chander S., *Biochem. Mol. Biol.*, **2005**, 94, 219-227.
16. Sci-Finder, CAS Registry, American Chemical Society, **2010**.
17. Caira M.R., *In: Topics in Current Chemistry*, Springer-Verlag, Berlin, Heidelberg, **1998**,198, 164-208.

18. Data Preparation and Reciprocal Space Exploration, Version 5.1, (Copyright Bruker Analytical X-ray Systems, **1997**).
19. Sheldrick G.M., SHELXS-97, *Program for Crystal Structure Solution*, Institüt für Anorganische Chemie der Universität, Tammanstrasse 4, D-3400 Göttingen, Germany, **1997**.
20. Sheldrick G.M., SHELXL-97, *Program for the Refinement of Crystal Structures*, Institüt für Anorganische Chemie der Universität, Tammanstrasse 4, D-3400 Göttingen, Germany, **1997**.
21. Griffin J.F., Duax W.L., Weeks C.M., *Atlas of Steroids*, Ronald Press, New York, **1984**, Vol. 1 and 2.
22. Etter M.C., Macdonald J.C., Bernstein J., *Acta Crystallogr.*, **1990**, B46, 256-262.
23. Spek A.L., PLATON, *A Multipurpose Crystallographic Tool*, Version 10500 © **1980-2009**.
24. Barbour L.J., SECTION, *J. Appl. Crystallogr.*, **1999**, 32, 353.
25. Yvon K., Jeitschko W., Parthé E., *J. Appl. Crystallogr.*, **1977**, 10,73.
26. Barbour L.J., LAYER, *J. Appl. Crystallogr.*, **1999**, 32, 351.
27. Sheldrick G.M., SADABS, University of Göttingen, Germany, **1996.**
28. Aulton M.E. (Ed.), *Pharmaceutics: The Science of Dosage Form Design*, Second Edition, Churchill Livingstone Press, Spain, **2002**, 23-32.
29. British Pharmacopoeia, British Pharmacopoeia Commission Secretariat, London, UK, **2005**.
30. Gonjari I.D., Karmarkar A.B., Hosmani A.H., *Digest J. Nanomat. Biostruct.*, **2009**, 4, 651-661.
31. Kiuru P.S., Wähälä K., *Steroids*, **2003**, 68, 373-375.

Chapter 4

2-METHOXYESTRADIOL CYCLODEXTRIN INCLUSION COMPLEXES

Chapter 4 *highlights the results of the cyclodextrin inclusion experimentation of 2ME with selected CDs. It emphasises the successful preparation of the 2ME/CD complexes and provides a physicochemical characterisation of the complexes in the solid state. Furthermore, the chapter compares the solubility and dissolution profiles of 2ME and its derivative 2-methoxyestradiol-bis-sulfamate hemihydrate (2MES) with 2ME/CD physical mixtures and 2ME/CD complexes using the BP dissolution method. Results will indicate a markedly improved solubility and dissolution profile of 2ME when mixed and complexed with selected CDs.*

4.8 INTRODUCTION

Cyclodextrin (CD) molecules have non-polar cavities (Figure 4.1), which provide hydrophobic matrices, enabling them to form inclusion complexes with many hydrophobic guest molecules. In contrast, the outer part of the CD molecule is hydrophilic, which renders the CD soluble in water. In addition, the three-dimensional form and size of CDs provide an important physical design (namely a truncated cone with hydrophobic cavity and hydrophilic exterior) for complex formation with hydrophobic compounds or functional groups (Figure 4.2). Hence, specific CDs (α-, β- and γ-CD and their derivatives) are required for complexation of specific guest molecules with specific physical detail. The dynamic force of inclusion complex formation is the entropic effect of the displacement of water molecules from the hydrophobic environment of the CD cavity, combined with the fact that the water causes a strain on the CD ring. This strain is released following complexation, producing a more stable and lower energy state. Thus, since inclusion complexes are quite stable, they can be separated from the medium by crystallisation.[1]

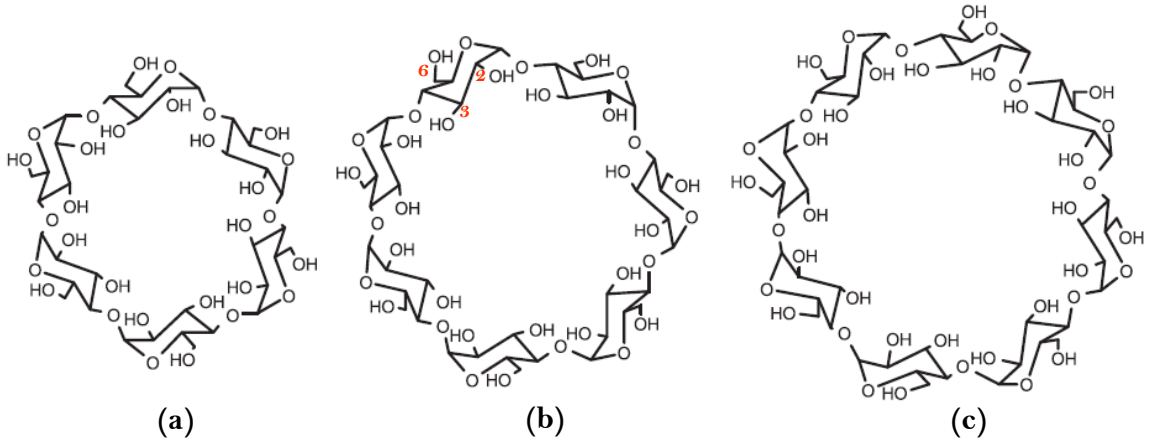

Figure 4.1 Macrocyclic ring of (a) α-CD, (b) β-CD and (c) γ-CD.

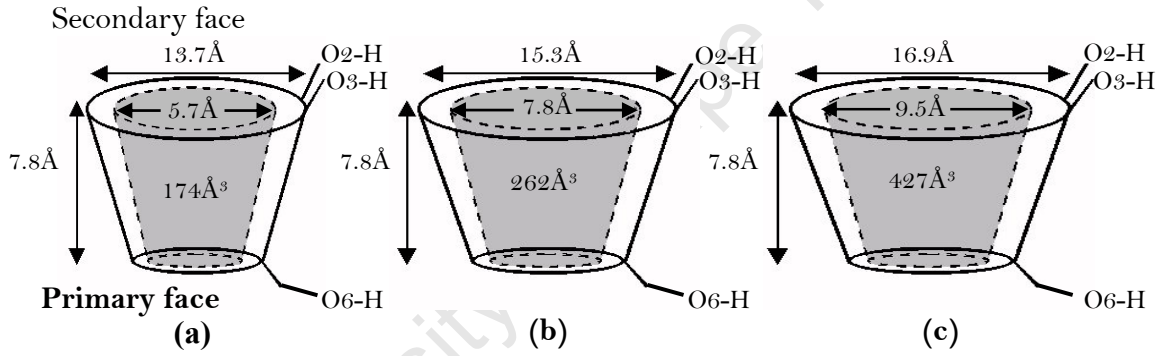

Figure 4.2 Schematic diagram illustrating physical dimensions of (a) α-CD, (b) β-CD and (c) γ-CD molecules.

Inclusion of drug molecules into CD cavities results in the improvement of the physicochemical properties of the drug. Such improvements include: increasing the stability of labile guest molecules against oxidation, visible or ultraviolet light or heat, taste modification by masking flavours or bad odours, and the controlled release of drugs and flavours. The aforementioned functions make most CDs suitable for use in pharmaceuticals, cosmetics and food.[1]

In our motivation we suggest complexing 2ME with CDs due to its limiting solubility profile (0.005 g in 1 L of water at pH 7 and 25°C). With clinical trials underway for 2ME as therapy to alleviate various cancers[2] and with other trials related to the oral

version of 2ME, supramolecular modification of the compound to enhance the solubility profile is of great significance. Hence, this study investigates the formation of complexes of selected CDs with 2ME, with the intention of improving the applications of 2ME, since CDs are able to enhance the stability, aqueous solubility, dissolution and ultimately, the bioavailability of drugs.[3]

To date, there is no obvious record of any attempts to complex 2ME with cyclodextrins. However, several attempts were made to complex other steroidal molecules with cyclodextrins. As mentioned earlier (Chapter 1) thus far the structure of a CD complex of only one steroidal compound, namely rocuronium bromide,[4] has been elucidated using single crystal X-ray analysis.

Natural Cyclodextrins and their Derivatives: The principal advantages of natural CDs as drug carriers are that they have well-defined chemical structures, providing many potential sites for chemical modification or conjugation. These modifications in turn provide CDs of differing cavity sizes, toxicity levels, pharmacological activity and water solubility.

Derivatives have been produced from the natural CDs, through chemical modification. Most of the derivatives have a different hydrophobic cavity volume from that of the parent CDs, which plays a role in accommodating larger guest molecules and thereby could enhance solubility and chemical activity of the guest drug.[1]

The following parent and derivatised CDs were investigated in this study:

α-cyclodextrin	**-**	**α-CD**
β-cyclodextrin	**-**	**β-CD**
γ-cyclodextrin	**-**	**γ-CD**
Hexakis(2,3,6-tri-*O*-methyl)-α-CD	**-**	**TRIMEA**
Randomly methylated β-CD	**-**	**RAMEB**
Hydroxypropyl-β-CD	**-**	**HPBCD**
Heptakis(2,6-di-*O*-methyl)-β-CD	**-**	**DIMEB**
Heptakis(2,3,6-tri-*O*-methyl)-β-CD	**-**	**TRIMEB**

Heptakis(*2,3,6*-tri-*O*-acetyl)-β-CD	**-**	**TRIAcBCD**
Octakis(*2,3,6*-tri-*O*-acetyl)-γ-CD	**-**	**TRIAcGCD**
Heptakis(*2,3,6*- tri-*O*-ethyl)-β-CD	**-**	**TRIEtBCD**

All the above CDs included in this study were tested for possible complex formation with 2ME and at the end of this chapter we consider dissolution studies of 2ME/CD mixtures or prepared complexes. To identify whether a mixture or complex is fit for human oral consumption we reviewed oral toxicity data. If data suggested oral toxicity for a particular CD, dissolution testing of the 2ME/CD combination was not considered.

Review of Oral Toxicity of Selected CDs

Alpha-cyclodextrin (α-CD): Owing to its small cavity volume and diameter, α-CD generally forms complexes with low molecular weight guest molecules, which have aliphatic side groups. In assessing the possible toxicity of α-CD, there was only *2-3* % absorption, following oral administration to rats.[1]

In contrast, the median lethal dose (LD_{50}) which is the oral dose at which 50% of subjects will die, was more than 10 000 mg/kg in the rat, while the LD_{50} (IV) was found to be between 500 and 750 mg/kg, which is considerably less than the former.[1] Hence, it is concluded that the oral dose of α-CD is comparatively safer than the IV dose of α-CD. However, it should be noted that α-CD is poorly metabolised by salivary and pancreatic enzymes.

Alpha-cyclodextrin Derivative:

Hexakis(2,3,6-tri-O-methyl)-α-CD (TRIMEA): It was established that the TRIMEA host may not be applicable as a drug delivery system[1] due to smaller cavity volume than α-CD.[5] Thus, dissolution studies of TRIMEA as a host were not conducted in this study. In contrast, its parent compound α-CD is of greater pharmaceutical relevance.

With respect to the solid-state structure of TRIMEA, it has two-fold rotational symmetry, with the opposite glucose residues in a like arrangement. The glucoses 1

and 4 have their C6-O6-Me groups tilted towards the cavity axis, so that they are in contact across the narrow end of the CD cavity.[5] The glucose residue 2 has its primary methoxy group directed inward. Hence, the overall shape of TRIMEA is not that of the normal CD torus, but that of a bowl or a boat. Thus, the molecular cavity is closed at the O6 end by a "lid" of primary methoxy groups and this leads to a smaller cavity volume relative to α-CD.[5]

Beta-cyclodextrin (β-CD): The advantages of using β-CD, with reference to dissolution characteristics and oral absorbability, can be considered with Phenytoin (DPH). DPH produced a higher aqueous solubility and faster dissolution when complexed with β-CD compared to DPH alone,[6] without damaging the small intestine, which in turn indicated a safe estimation for oral use.

β-CD is widely used for improving the solubility and stability of drugs, by forming complexes. Complexes are preferably formed in the presence of water since a dehydrated β-CD will result in all the water being displaced from the cavity.[6] However, β-CD does not facilitate fast dissolution of complexes due to its inherently poor water solubility at room temperature.

Beta-cyclodextrin Derivatives:

Hydroxypropyl-β-CD (HPBCD): The main advantage of HPBCD is its significantly higher solubilising power compared to β-CD. For most guest molecules, the increase is somewhere between 10- and 100-fold. The ability of CDs to stabilise the guest molecule is retained in HPBCD. Due to the substitution, binding can be altered, which can cause differences in the extent of stability obtained compared to β-CD.

HPBCD is very soluble in water and heat is not needed to increase the solubility of the CD. At very high concentrations of HPBCD (60% and more), increased temperature can be used to reduce the viscosity of the solution. Increased temperature may also be used to increase the solubility of the guest and the rate of complexation.

In the oral administration of HPBCD, teratogenicity and embryotoxicity studies have been performed at doses up to 5000 mg/kg per day in rats and 1000 mg/kg per day in rabbits. No maternal toxicity, embryotoxicity or teratogenicity was found in rats. In rabbits, no teratogenicity was observed, but slight maternal and embryotoxicity were observed at 1000 mg/kg.[7] Consequently, HPBCD is safe for oral use.

Heptakis(2,6-di-O-methyl)-β-CD (DIMEB): DIMEB is formed upon methylation of the 2 and 6 hydroxyl groups (Figure 4.1) of β-CD and is suitable for complexation due to its relatively high solubility in water and organic solvents.[8] In general, methylated CDs are exceptionally soluble in water at room temperature, even though they have a hydrophobic surface.

Water is the most frequently used solvent in which complexation experiments are conducted. The more soluble the CD is in the solvent, the more molecules become available for complexation. Furthermore, the guest (2ME in this study) must have the ability to displace any solvent molecules from the CD cavity, if the solvent forms a complex with the CD. Thus, an advantage of using water in complexation techniques is that it is easily displaced.[5] It has been found that DIMEB is capable of crystallising from hot water, without any water of hydration. However, from cold water, only poorly ordered crystals of DIMEB have been obtained.[5]

DIMEB is capable of taking on a round shape, which is effected by intramolecular O-H•••O hydrogen bonds between adjacent glucose units. In the crystalline state the CD cavity is sterically congested in inclusion complexes (somewhat closed on one end) by primary methoxy groups, which are directed towards the molecular axis. The cavity volume that remains free is then occupied by part of the C6-O6-Me rim of a neighbouring DIMEB molecule. The former may be described as 'self-inclusion.'

Self-inclusion of CD molecules or a complex between the solvent and the CD may result during complexation experiments. In establishing complex formation analytically, it is important to be able to determine that the complex is not one of self-inclusion or a solvent-CD complex, but rather that of the desired included guest molecule and the CD.

Owing to the small difference in the hydrophilic nature of the intramolecular and intermolecular spaces in DIMEB inclusion complexes, because of the presence of methyl groups, guest molecules can be found either in the cyclodextrin cavity or in the interstitial positions, with the cavity also being occupied by water molecules.[5]

Heptakis(2,3,6-tri-O-methyl)-β-CD (TRIMEB): TRIMEB is formed upon methylation of the 2, 3 and 6 hydroxyl groups (Figure 4.1) of β-CD and as with DIMEB a relatively high solubility in water and organic solvents is observed.

CDs are also useful as drug penetration enhancers. Absorption enhancement occurs by the CDs extracting lipids from cell membranes, increasing membrane fluidity and permeability. This action towards biological membranes is connected to the haemolytic and cytotoxic effect of methylated β-CDs.[9] Therefore, the methylated β-CDs, particularly DIMEB and TRIMEB are unsuitable for human consumption, due to their marked toxic effects.

In a previous study, methylated CDs were used to determine if membrane proteins exist in association with specialized microdomains called lipid rafts, by depleting cholesterol found in them.[9] Thus, cholesterol, which is also a large steroidal compound, forms complexes with CDs in aqueous solution. It has been shown that cholesterol molecules can diffuse directly from the plasma membrane into the hydrophobic core of a CD molecule, packed near the membrane surface.[9]

DIMEB and TRIMEB have a deeper cavity and are more hydrophobic than β-CD. Hence, these derivatives have a strong ability to form soluble complexes with cholesterol, in aqueous solution. Although HPBCD has a weaker ability to sequester cholesterol,[10] it is nevertheless known to form inclusion complexes with this steroid.

Randomly Methylated β-CD (RAMEB): RAMEB has been proposed to be a good carrier to deliver fatty acids to cells in a culture.[11] CD complexation of anti-inflammatory drugs in particular, offers additional advantages such as masking of taste, lowering of dose and reduction of side effects, particularly gastric irritation.
UV absorbers used in sunscreen cosmetics are usually poorly soluble in water, but their aqueous solubility can be improved by complexation with different CDs and β-CD derivatives. The phase solubility method was applied in a study of UV absorbers and different CD interactions. The molar ratio of the UV filter to CD in the solid complex was calculated from thermal analysis data. Among the CDs studied, RAMEB showed the highest complexing and solubilising power and gave rise to the product with the best dissolution profile in the study. [12]

Heptakis(2,3,6-tri-O-acetyl)-β-CD (TriAcBCD), Heptakis(2,3,6-tri-O-ethyl)-β-CD (TriEtBCD) and Octakis(2,3,6-tri-O-acetyl)-γ-CD (TriAcGCD): These CDs are less well-known derivatives and information concerning them is thus limited. Notably though, it was found that when placed in water, the aggregation of such CD molecules and the interaction of surrounding water molecules, together with the lattice energy in the solid state, may be responsible for their solubility differences when compared to parent compounds.[13,14]

Gamma-cyclodextrin (γ-CD): Studies conducted in rats and rabbits with γ-CD at doses up to 20% of the diet, did not show any teratogenic effects. Furthermore, in a 12-month study of toxicity, again rats were fed diets containing up to 20% γ-CD. Minimal changes were seen and only at the high dose, probably as a result of the presence of a large amount of an osmotically active substance in the large intestine. These changes were considered to be brief and not of toxicological significance.[8]

Following the discussion above, the following CDs were included in the dissolution tests of this study: α-, β-, γ-CD, HPBCD and RAMEB.

Since the structure of 2ME was previously described in Chapter 3, it was not considered necessary to discuss this potential guest for a second time.

4.9 OBJECTIVES OF THE STUDY

In order to enhance the solubility and dissolution of 2ME with CDs the following objectives were identified:

- To formulate complexes of 2ME with CDs and provide physicochemical characterisation of these complexes in the solid state.
- To determine the solubility of 2ME in the presence of each CD.
- To determine the dissolution profiles of mixtures of 2ME with selected, non-toxic oral CDs, if the latter were readily available and relatively inexpensive.
- To determine the dissolution profiles of the non-toxic 2ME/CD complexes formed.

Table 4.1 presents selected results of 2ME/CD complex preparation experimentation using various methods. Appendix 2 on the attached CD-rom provides the full spectrum of experiments attempted.

Table 4.1 Representative cyclodextrin inclusion complex preparation with 2ME as potential guest using various methods

Method 1[i]: Neat Grinding for 1 hour		
CD	**Ratio (H:G)**	**Result**
α-CD	1:1	Mixture
β-CD	1:1	Mixture
γ-CD	1:1	Mixture
Method 2[i]: Kneading into paste with water for 1 hour		
CD	**Ratio (H:G)**	**Result**
α-CD	1:1	Mixture
	2:1	Mixture
β-CD	1:1	Mixture
	2:1	Complex
γ-CD	1:1	Mixture
	2:1	Mixture
Method 3[ii]: Slurry method		
Exp.	**Ratio (H:G)**	**Result**
β-CD		
4°C	1:1	No complex
RT	1:1	No complex
SC	1:1	No complex
60°C	1:1	No complex
4°C	2:1	No complex
RT	2:1	No complex
SC	2:1	Complex

[i] Materials prepared using methods 1 and 2 were analysed using PXRD.

[ii] Slurries were made with water at given ratios, stirred for 24 hrs at RT and at 60 ºC for β-CD since β-CD solubility is greater at higher temperatures. Then slow evaporation (RT), rapid cooling (4 ºC), slow cooling (SC) and heating at 60 ºC were employed for crystal growth to occur; resulting crystals were analysed by single crystal X-ray diffraction and thereafter PXRD to determine bulk consistency.

4.10 COMPLEXATION BETWEEN 2ME AND β-CD, HPBCD, RAMEB, DIMEB AND TRIMEB

4.10.1 β-CD COMPLEX WITH 2ME

Preparation of BCD2ME by kneading

Complex preparation between β-CD and 2ME was achieved by kneading a 2:1 (mol/mol) host:guest mixture into a paste using water. The cyclodextrin was placed in the mortar with a few drops of water and ground to a paste. The guest was added slowly with simultaneous kneading until all of the guest was added. The process required between 45 min to one hour. During this time the paste was kept moist by the dropwise addition of water. Complexation was confirmed by powder X-ray diffraction and the resultant traces were assigned to an isostructural series.[15] This complex shall be referred to as BCD2ME.

Preparation of BCD2ME by Co-precipitation

A complex was prepared by stirring an aqueous solution of β-CD (at 60 °C) with the guest compound using a 2:1 (mol/mol) host:guest ratio. The calculated amounts of host and guest molecules were agitated intensely at an elevated temperature of 60 °C to achieve the common saturated solution of both the host and guest. The β-CD inclusion complex was crystallised from this homogenous solution upon slow cooling. Square, plate-like crystals were isolated. Subsequent analysis (see below) revealed that the complex BCD2ME obtained by kneading was identical to the crystals obtained by co-precipitation. Thus, the latter is also referred to as BCD2ME in this chapter.

Thermal Analyses

Hot Stage Microscopy

HSM was used to analyse the thermal behaviour of the complex upon heating at a constant rate of 10 K/min. HSM photographs of BCD2ME are presented below (Figure 4.3). After removal from mother liquor, the crystals of the complex displayed signs of cracking as they began to lose their water of crystallisation. The analysis was performed under silicone oil to assess the presence of included water as would be indicated by bubble formation. The photographs of the complex were recorded at (a) start of analysis, (b) the first sign of bubbling, (c) the time by which extensive crystal fragmentation had taken place, (d) the onset of decomposition of complex (indicated by colour change of a few crystals to brown) and (e) Decomposition of the entire complex with the appearance of bubbling as a result of decomposition.

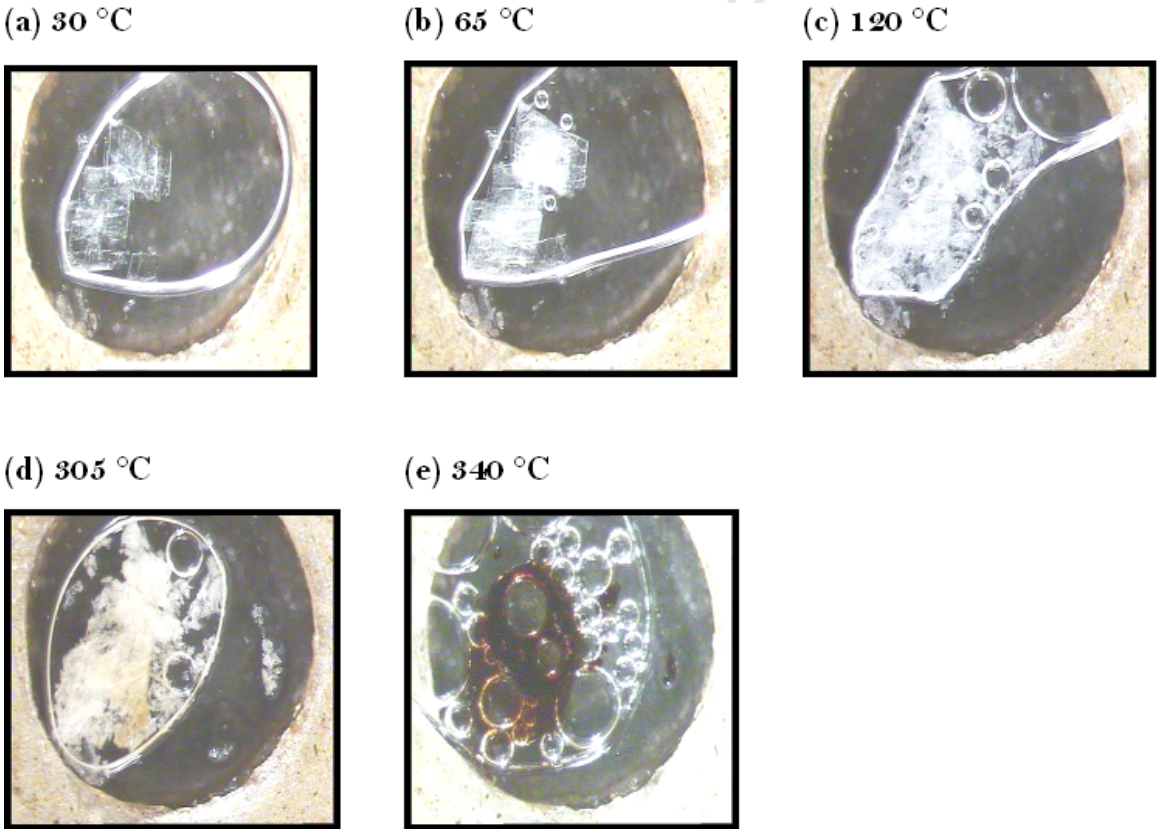

Figure 4.3 HSM photographs of BCD2ME.

Figure 4.3 indicated the first signs of release of water from the crystal appearing between 65 and 80 °C for BCD2ME and by 120 °C, extensive fragmentation of BCD2ME had occurred, a further consequence of dehydration of the crystal. Decomposition started at ~305 °C with spontaneous associated bubbling verifying extensive decomposition occurring at 340 °C .

Differential Scanning Calorimetry and Thermogravimetric Analysis

TGA and DSC traces for the BCD2ME complex are presented in Figures 4.4 and 4.5 below. TGA was used to determine water content of the BCD2ME complex which was indicated by the initial mass loss. The TGA trace for BCD2ME showed a mass loss of 8.8 ± 0.4 % (n=3) in the temperature range 30-150 °C, represented by **A** in Figure 4.4. This established the BCD2ME:H_2O molar ratio as 1:13.5 ± 0.6. The second thermal event **B** in the TGA trace represents decomposition of the complex with an onset temperature of ~309 °C.

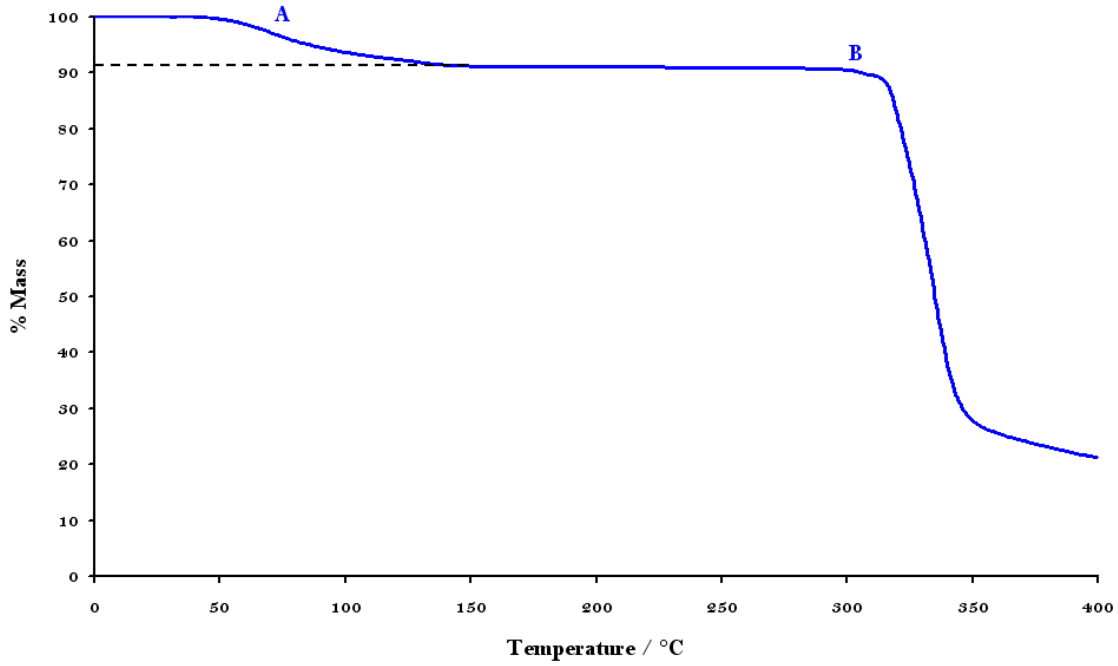

Figure 4.4 TGA trace for BCD2ME.

A summary of the observed percentage mass loss over temperature intervals between 30, 50, 100, 150 and 200°C is presented in Table 4.2.

Table 4.2 Percentage mass loss for the BCD2ME complex at various temperatures

Temperature (°C)	Sample mass(%)	Δ Mass loss (%)*
30	100	0
50	99.64	0.36
100	93.68	5.96
150	91.2	2.5
200	91.1	0.1

*Δ Mass loss (%) = [Sample mass(%) at temperatures (n-1)] – [Sample mass(%) at temperatures (n)]

In Figure 4.5 the BCD2ME complex shows endothermic events corresponding to water loss in the range 30 to 150 °C. The endotherms covered the same range over which water loss was observed from TGA (mass loss due to water loss was labelled **A** for the TGA trace). The peak of the water loss endotherm (labelled **A** in Figure 4.5) occurred at 95 °C. However this peak contained a number of shoulders occurring at 110, 140 and a further peak at ~204 °C (labelled **B**) indicating that water loss from this complex was clearly a multi-stage process. Breakdown of the host framework of the complex corresponded with decomposition of the complex molecule which begins above 290 °C (labelled **C**). The region between 290 and 350 °C showed multiple peaks further indicating the decomposition of the complex. Very large mass losses were observed in the TGA trace from 300°C onwards (labelled **B**), confirming the decomposition of the β-CD complex molecules. Disappearance of the guest (2ME) melt peak in Figure 4.5 was an added indication of complex formation.

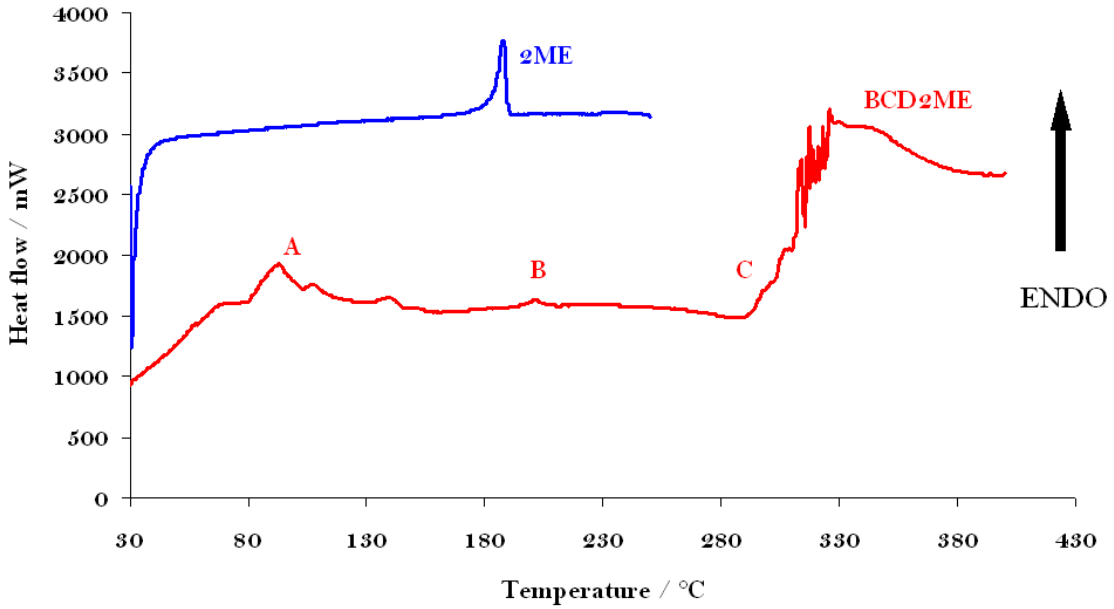

Figure 4.5 DSC trace for guest (2ME) and complex (BCD2ME).

UV Spectrophotometry

The host:guest ratios were determined by UV spectrophotometry at 198.5 nm in methanol:water (50:50 v/v) solution. The stoichiometric ratio for the BCD2ME complex was determined as 2:1.

Experimental PXRD and Isostructurality

X-ray powder diffraction may be used to establish complex formation.[15] Together with the principles of isostructurality this allows us to extract space group and unit cell information for new cyclodextrin complexes.

Firstly, we note that the experimental PXRD pattern (Figure 4.6) presents a clear indication of complexation occurring between the guest and host, with most peaks disappearing for parent compounds in the trace for the product obtained by kneading as well as in that from the co-precipitation experiment. New peaks appeared at the following 2θ values: 7.2, 9.8, 12.0 and 15.7°. Neat grinding produced only a mixture of β-CD and 2ME.

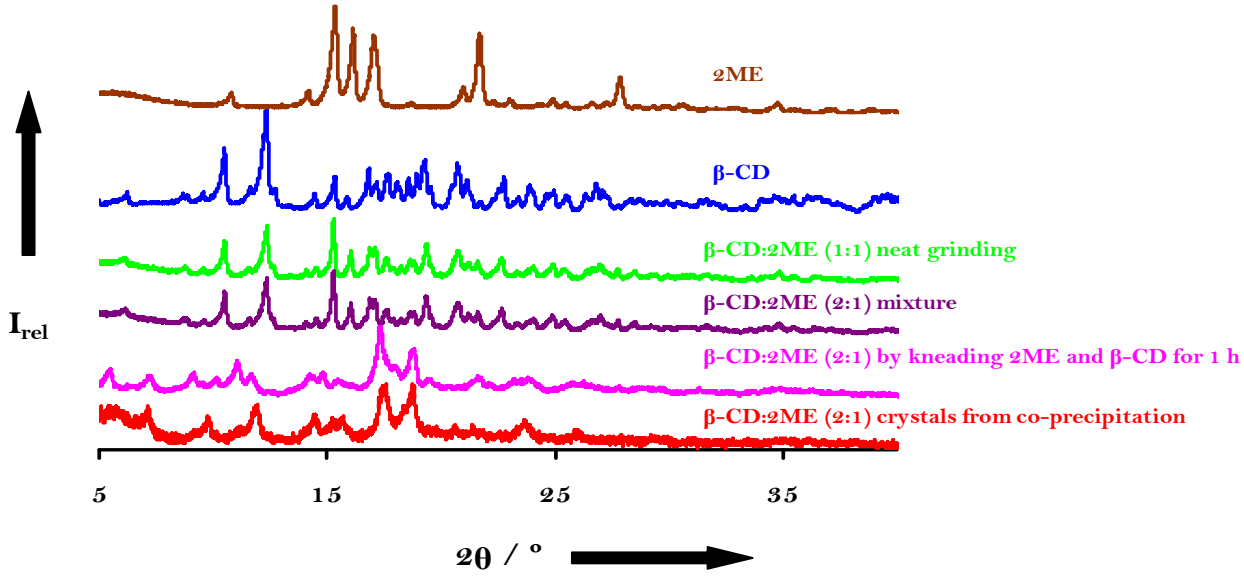

Figure 4.6 Experimental PXRD patterns of 2ME and β-CD parent compounds and various preparations thereof: neatly ground, mixture, kneaded and co-precipitated materials.

Secondly, PXRD was used as a tool to identify isostructurality between the prepared complex and known complexes. In Figure 4.7 we show that the BCD2ME complex is in fact isostructural with the known β-CD complex which contains 4-*t*-butylbenzyl alcohol as guest (CSD refcode KOFJEU).[16]

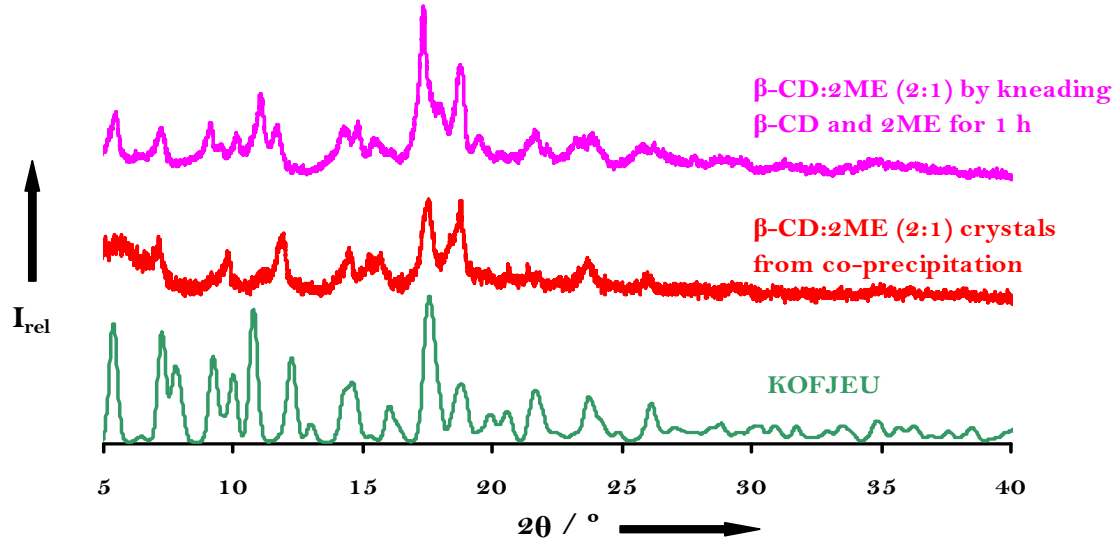

Figure 4.7 Calculated PXRD pattern of KOFJEU versus experimental patterns of BCD2ME (obtained by kneading and co-precipitation).

PXRD as used above is an efficient tool for the identification of cyclodextrin complexes but it is limited quantitatively. For example, it provides little information regarding guest orientation, crystal water content, stoichiometry and the interaction between water and the structure of the complex. In this regard single crystal X-ray diffraction is greatly superior.[15]

When the assignment of an isostructural series is undertaken, the water content, dimensions of the guest and its orientation as well as the temperature at which the data were collected affect the peak angular positions in the PXRD trace. Thus, the tolerances within which traces are deemed as indicating isostructurality are less rigid than those which are normally applied in phase identification by PXRD.[15]

Noticeably from the comparison in Figure 4.7 there is a reasonably close correspondence between the reference trace KOFJEU and the representative trace of the kneaded product as well as the co-precipitated product of 2ME with β-CD. The estimated unit cell dimensions are listed below in Table 4.3, along with the possible space group.

The unit cell parameters for the BCD2ME inclusion complex were deduced from its isostructurality with the known inclusion complex whose reference PXRD trace is presented in Figure 4.7.

Table 4.3 Possible space group and approximate unit cell parameters for the complex BCD2ME

Space group	a (Å)	b (Å)	c (Å)	α (°)	β (°)	γ (°)	Vol. (Å^3)
$C222_1$	19.2	24.4	32.8	90	90	90	15362.3

Single Crystal X-ray Crystallographic Analysis of the BCD2ME Complex

Data-collection

The unit cell parameters, crystal system and space group were determined using the Nonius Kappa CCD diffractometer. Crystals produced were not of high quality and the best crystal for single X-ray diffraction was selected and mounted using Paratone N oil and used for data-collection. Table 4.4 compares the unit cell parameters of BCD2ME with those of the known complex KOFJEU[16] to confirm the unit cell data predicted in Table 4.3.

Even though accurate unit cell dimensions were actually measured, the BCD2ME complex was undeniably isostructural with KOFJEU, as illustrated by the PXRD patterns which matched the reference trace (Figure 4.7).

Table 4.4 Unit cell parameters for BCD2ME and KOFJEU

	BCD2ME	**Known β-CD complex**
REFCODE		**KOFJEU[16]**
Spacegroup	$C222_1$	$C222_1$
a (Å)	19.376(2)	19.196(7)
b (Å)	24.053(2)	24.393(6)
c (Å)	32.412(2)	32.808(9)
α (°)	90.0	90.0
β (°)	90.0	90.0
γ (°)	90.0	90.0
Volume (Å^3)	15105.3(2)	15362.3(2)
Z	8	8

To establish whether any phase changes occurred on cooling, unit cell dimensions for BCD2ME were measured at both 21 ºC and -160 º (Table 4.5). No phase change was evident.

Table 4.5 Unit cell parameters for BCD2ME

	BCD2ME (21 °C*)	BCD2ME (-160 °C)
Space group	$C222_1$	$C222_1$
a (Å)	19.79	19.376(2)
b (Å)	24.89	24.053(2)
c (Å)	32.99	32.412(2)
α (°)	90.0	90.0
β (°)	90.0	90.0
γ (°)	90.0	90.0
Volume (Å^3)	16250	15105.3(2)
Z		8

*For room temperature unit cell data, no *e.s.d.*s are reported since relatively few intensity frames were collected

Structure Solution and Refinement

Since these were only partially successful, a very brief summary follows. The atomic co-ordinates of the β-CD molecule in the structure of KOFJEU[16] were used as a trial model for the structural elucidation of BCD2ME. Although the host molecule refined successfully, severe disorder of the guest molecule prevented its modelling and further attempts to obtain a detailed structure were abandoned in view of this outcome.

It should be noted, however, that in principle, the known host framework in the crystal could in future be used as a template for theoretical calculations in which modelling of guest orientation and placement could take place. What can be deduced from the isostructurality of BCD2ME with KOFJEU is that the former is thus also a dimeric complex i.e. the repeating motif in the crystal is a head-to-head β-CD dimer, whose structure is maintained by O-H•••O hydrogen bonds between the secondary rims of the two host molecules. The 2ME molecule is encapsulated within the host dimer.

Despite the fact that the exact nature of guest inclusion could not be established due to severe guest disorder, the BCD2ME complex was nonetheless sufficiently well characterised to pursue other aspects such as its solubility and dissolution profile, as described at the end of this chapter.

4.10.2 HPBCD AND RAMEB COMPLEXES WITH 2ME

Preparation of HPB2ME and RAM2ME

Complex preparation between HPBCD and 2ME and between RAMEB and 2ME was performed by kneading a 1:1 (mol/mol) guest:host mixture into a paste using water. In both instances the cyclodextrin was placed in the mortar with a few drops of water and ground to a paste. The guest was added slowly with simultaneous kneading until all of the guest was added. The process usually required between 45 min to one hour. During this time the paste was kept moist by the dropwise addition of water.

Experimental Powder X-ray Crystallographic Analysis of HPB2ME and RAM2ME prepared by kneading

PXRD patterns (CuKα radiation with conditions stated in Chapter 2) were obtained for all preparations and a number of characteristic 2ME peaks were observed. The 2θ range scanned was from 5 to 40° and the sample sizes were all in the range 45-50 mg.

HPBCD and RAMEB comprise mixtures of a number of isomers which have different degrees and patterns of substitution. Both CDs are therefore amorphous and their PXRD traces do not display any characteristic sharp peaks.[17] Any inclusion complex formed with RAMEB and HPBCD will likewise be an amorphous substance. However, 2ME contains a number of relatively sharp and characteristic PXRD peaks. The disappearance of these peaks in patterns of products obtained by kneading was taken as evidence for inclusion complex formation. The presence of these peaks in any of the preparations analysed signified the presence of uncomplexed drug and incomplete formation of an inclusion complex of the stoichiometry of the preparation. Figure 4.8 shows the PXRD traces of 2ME, HPBCD, a 1:1 neatly ground HPBCD:2ME trace and traces of 1:1, 2:1 and 3:2 HPBCD:2ME preparations from kneading experiments. Figure 4.9 shows the PXRD traces of 2ME, RAMEB, neatly ground 1:1 RAMEB:2ME and a 1:1 RAMEB:2ME preparation from kneading. It is evident from both figures that the characteristic peaks of 2ME are absent from the traces of the 1:1 materials that were kneaded and that the patterns resemble those of the parents HPBCD and RAMEB, thus providing evidence of inclusion complex formation. Henceforth, the preparations made

by kneading a 1:1 mixture of HPBCD:2ME and RAMEB:2ME will be referred to as HPB2ME and RAM2ME, respectively.

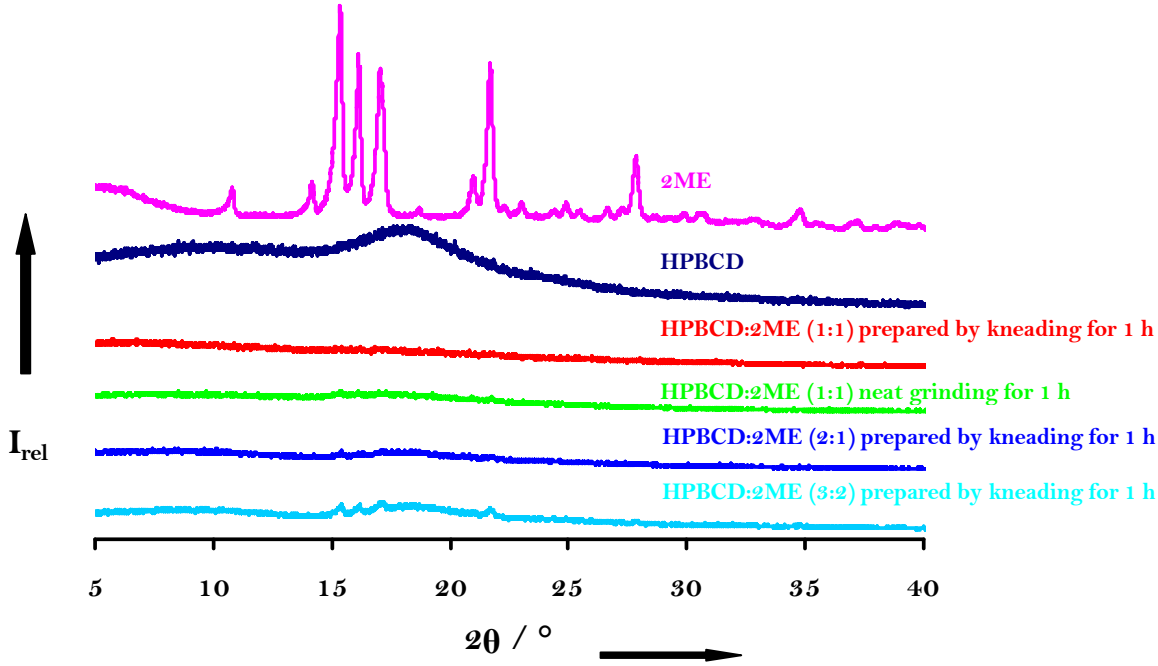

Figure 4.8 Experimental PXRD traces for 2ME, HPBCD and various preparations involving the two components.

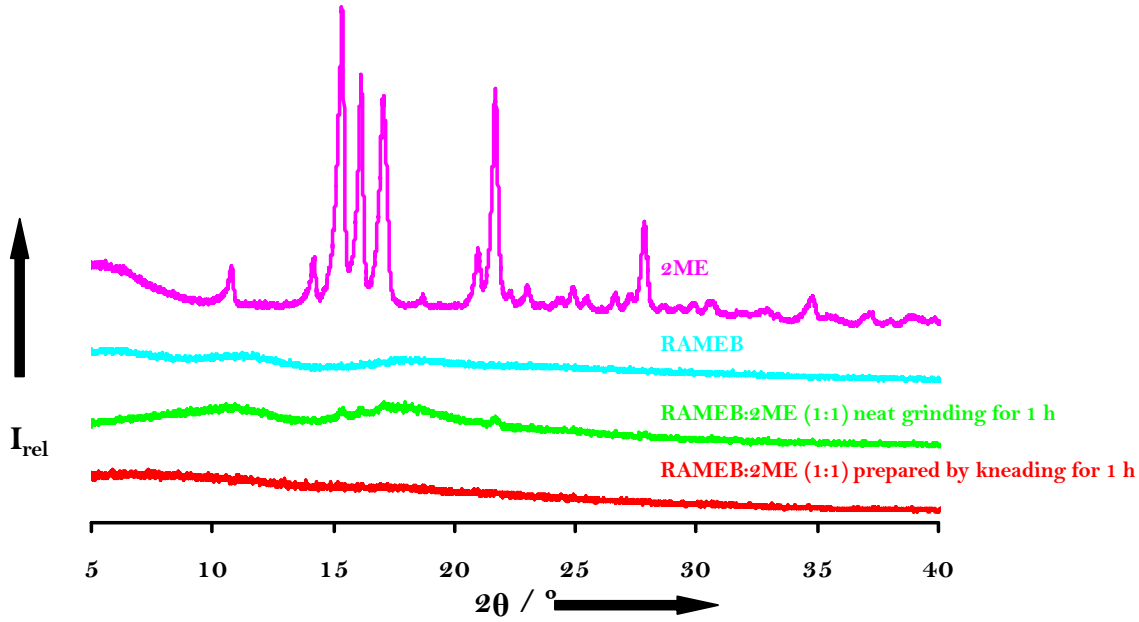

Figure 4.9 Experimental PXRD traces for 2ME, RAMEB and various preparations involving the two components.

FTIR Spectra of HPBCD and RAMEB and their Putative 2ME complexes

FTIR spectra were recorded for all preparations and various IR bands corresponding to HPBCD, RAMEB and 2ME were analysed. The IR spectra were obtained using a Perkin-Elmer 100 FTIR instrument fitted with UATR and controlled with Spectrum ® software for sample analysis. Powder samples were run over the range 400-4000 cm^{-1}. Percentage transmittance was recorded against frequency. For the CD complexes obtained by kneading, shifts in certain characteristic bands of the 2ME molecule were indicative of interaction between CD and drug.

The frequency range scanned for 2ME was between 500 and 4000 cm^{-1}. For 2ME the following υ_{max} bands were identified by Rao et al.[18]: 3424, 3202, 2905, 2863 and 1607 cm^{-1}. The experimental FTIR spectra for 2ME confirmed these υ_{max} values within experimental error. We find that for both HPB2ME (Figure 4.10) and RAM2ME (Figure 4.11) these bands are either displaced or masked by the CD from the measured value for the drug itself. Hence, we can conclude that both HPBCD and RAMEB complexed with 2ME during kneading experiments.

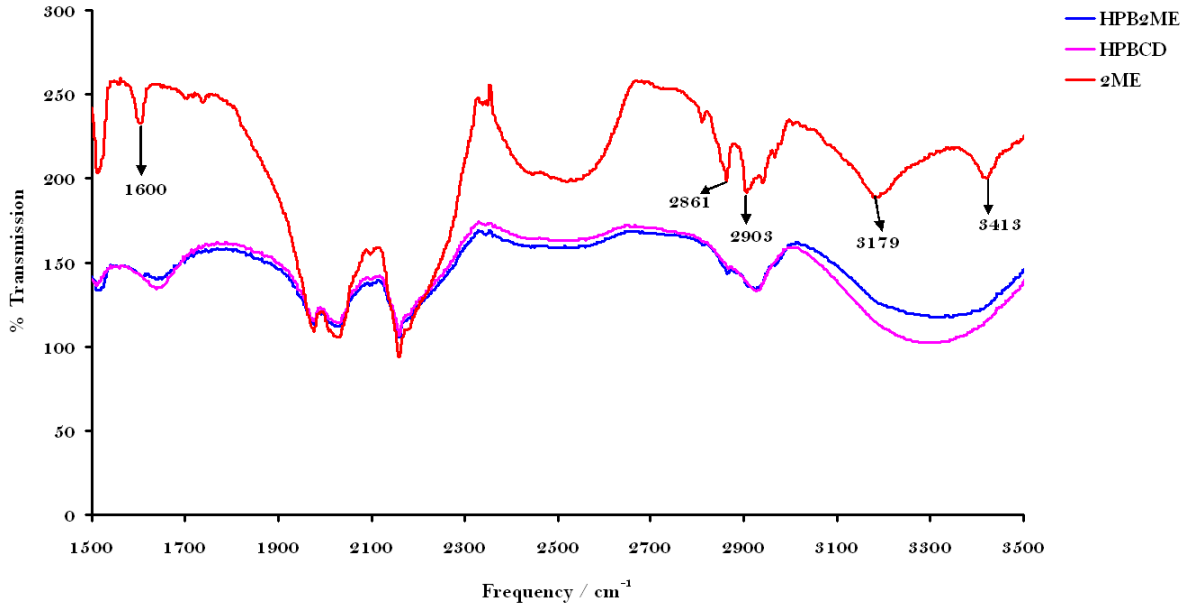

Figure 4.10 FTIR spectra of HPBCD and 2ME and that of their putative inclusion complex.

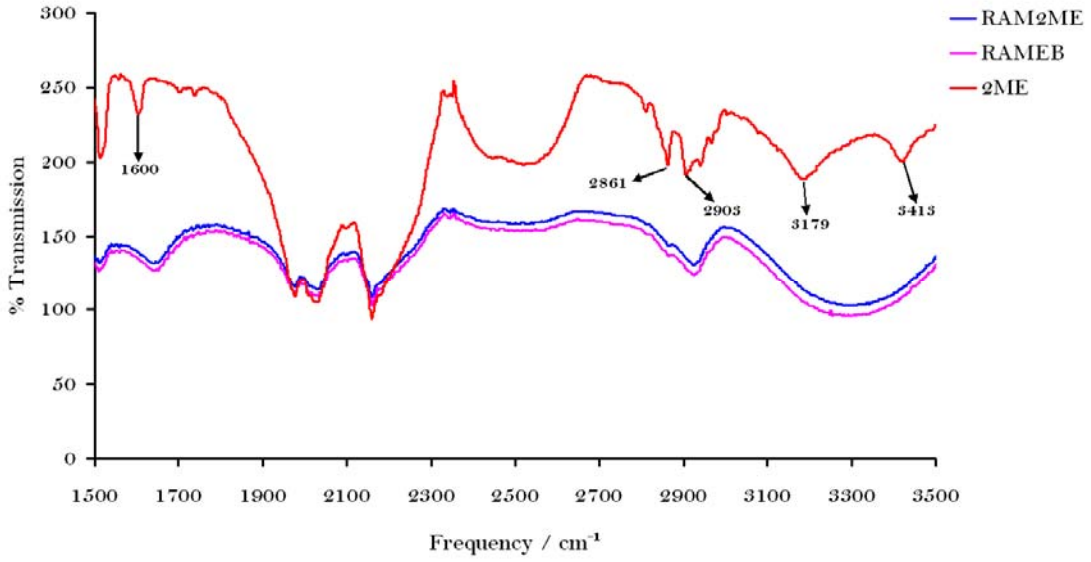

Figure 4.11 FTIR spectra of RAMEB and 2ME and that of their putative inclusion complex.

Differential Scanning Calorimetry

DSC experiments were run for all preparations and the melting endotherm for 2ME was monitored. DSC conditions were 10 K/min with temperature range 30 to 300 °C. The sample sizes were as follows: RAM2ME (1:1) 6.5 mg and HPB2ME (1:1) 7.8 mg. The disappearance of the 2ME melting endotherm was taken as further evidence for complex formation. The presence of uncomplexed, crystalline drug in a particular preparation was indicated by the presence of the melting endotherm of 2ME. All of the 2ME was complexed after manual kneading for 1 h for both HPBCD and RAMEB (1:1) preparations. Figure 4.12 shows the DSC traces of 2ME, HPBCD, 1:1 physical mixture of HPBCD and 2ME and a 1:1 preparation obtained by kneading. Figure 4.13 shows the DSC traces of 2ME, RAMEB, 1:1 physical mixture of RAMEB and 2ME and a 1:1 preparation made by kneading.

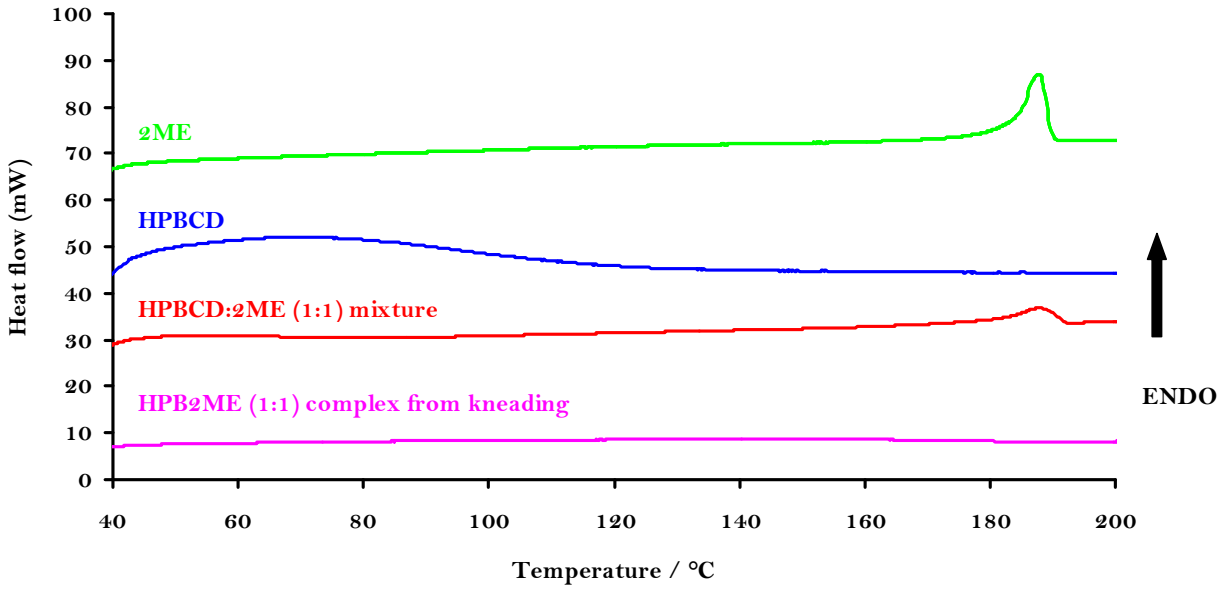

Figure 4.12 DSC of 2ME, HPBCD, HPBCD:2ME (1:1) mixture and HPB2ME (1:1) complex from kneading.

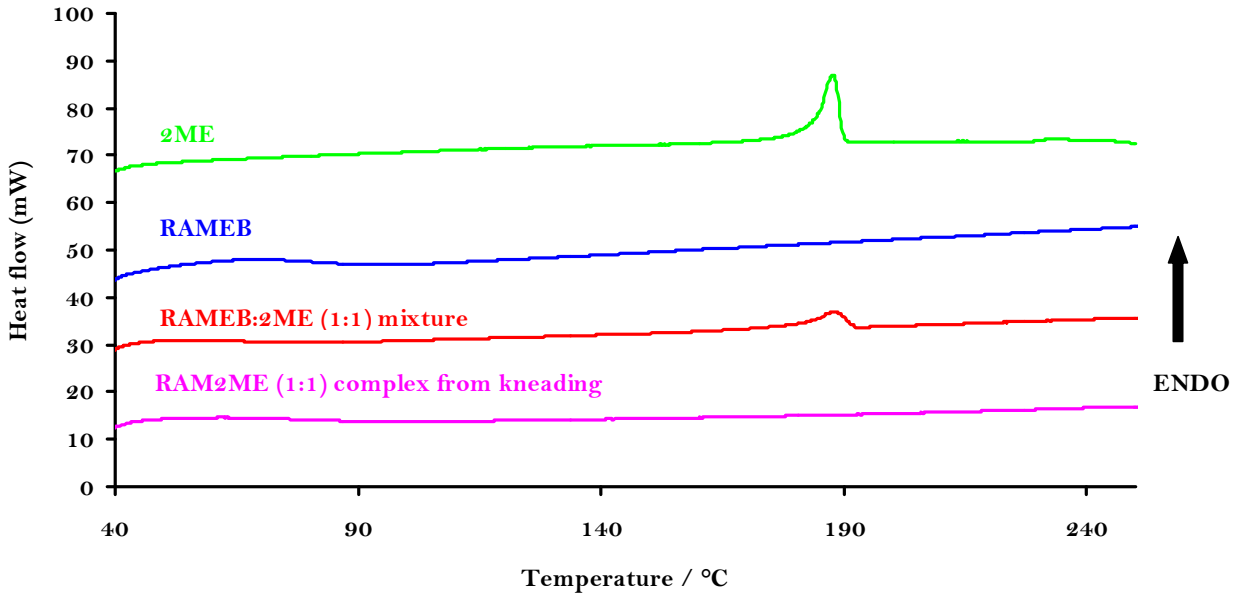

Figure 4.13 DSC of 2ME, RAMEB, RAMEB:2ME (1:1) mixture and RAM2ME (1:1) complex from kneading.

4.3.3 DIMEB COMPLEX WITH 2-METHOXYESTRADIOL

Preparation of DIB2ME

A suspension was prepared by mixing 0.033 mmol (44 mg) of the CD and 0.033 mmol (10 mg) of 2ME in 3 ml of distilled water. Since methylated CDs have an inverse temperature-solubility relationship i.e. their solubility decreases with an increase in temperature, the suspension was stirred vigorously at room temperature for 24 h. After the dissolved CD solubilised the drug and common saturation of both host and guest had been achieved, the solution was filtered (0.45 μm microfilter), and then left at 60 °C on a hot plate. Single crystals formed after several days. As shown below, the crystals are those of an inclusion complex between DIMEB and 2ME. This complex shall be referred to as DIB2ME. Large, roughly cubic-shaped crystals of DIB2ME were isolated.

Thermal Analyses

Hot Stage Microscopy

HSM was used to analyse the thermal behaviour of the complex upon heating at a constant rate of 10 K/min. After removal from the mother liquor, the crystals of the complex displayed signs of cracking as they began to lose their water of crystallisation. The crystals were promptly immersed in silicone oil on a glass slide and photographs were taken in the temperature range 30 °C to 400 °C. These HSM pictures are presented in Figure 4.14 at various stages of heating. At the start of the analysis the crystals of DIB2ME were clear and translucent and the first signs of release of water from the crystals appeared at 80 °C. At 290 °C the crystals underwent a colour change indicating the onset of decomposition. Spontaneous associated bubbling and brown discolouration verified the final decomposition at 400 °C.

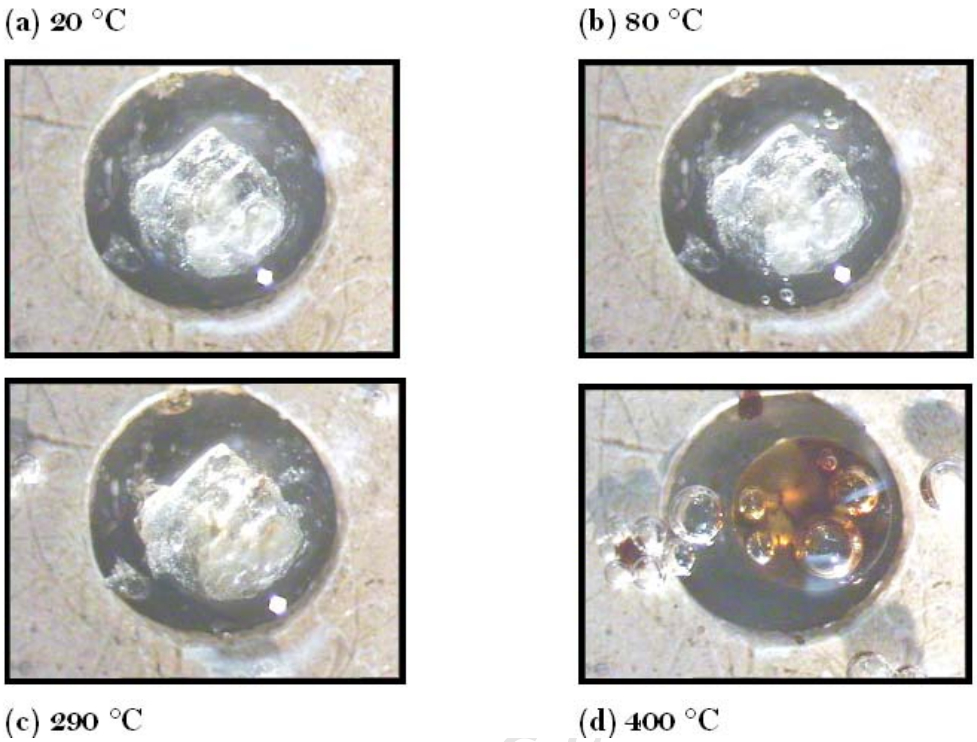

Figure 4.14 HSM photographs of DIB2ME during heating.

Thermogravimetric Analysis and Differential Scanning Calorimetry

TGA and DSC traces for the DIB2ME complex are presented in Figure 4.15 and 4.16 respectively. TGA was used to determine water content of the DIB2ME complex which is indicated by the initial mass loss. The TGA trace for the DIB2ME complex showed a mass loss of 5.3 ± 0.3 % (n=3) in the temperature range 30-300 °C, which implies 5.1 ± 0.4 H_2O molecules per complex unit.

Dehydration of the complex appeared to occur over a wide temperature range in TGA and it was not entirely clear at what temperature it ended. Estimation of the percentage mass loss due to dehydration in the TGA trace was thus based on supporting information from HSM and DSC data (see below).

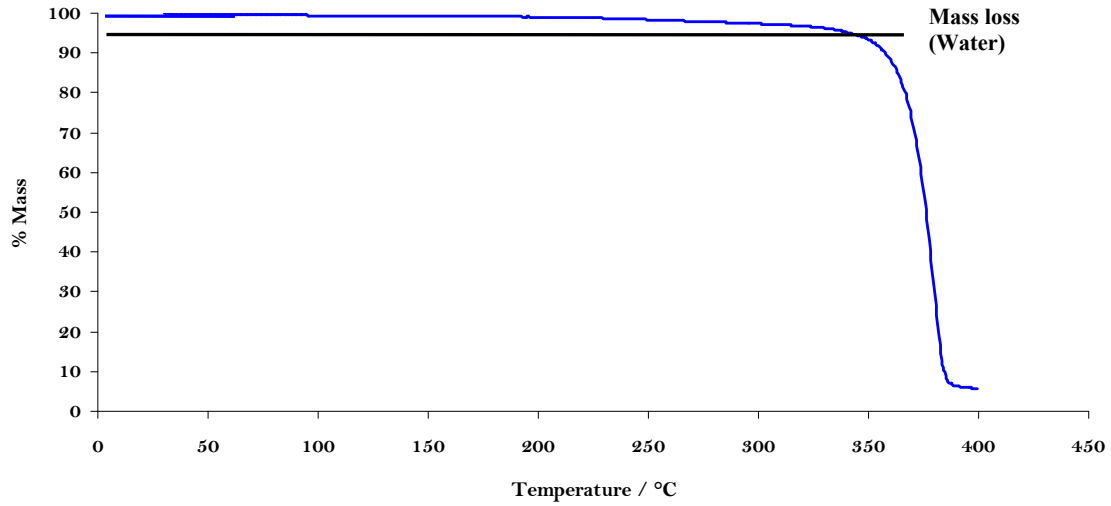

Figure 4.15 TGA trace for DIB2ME.

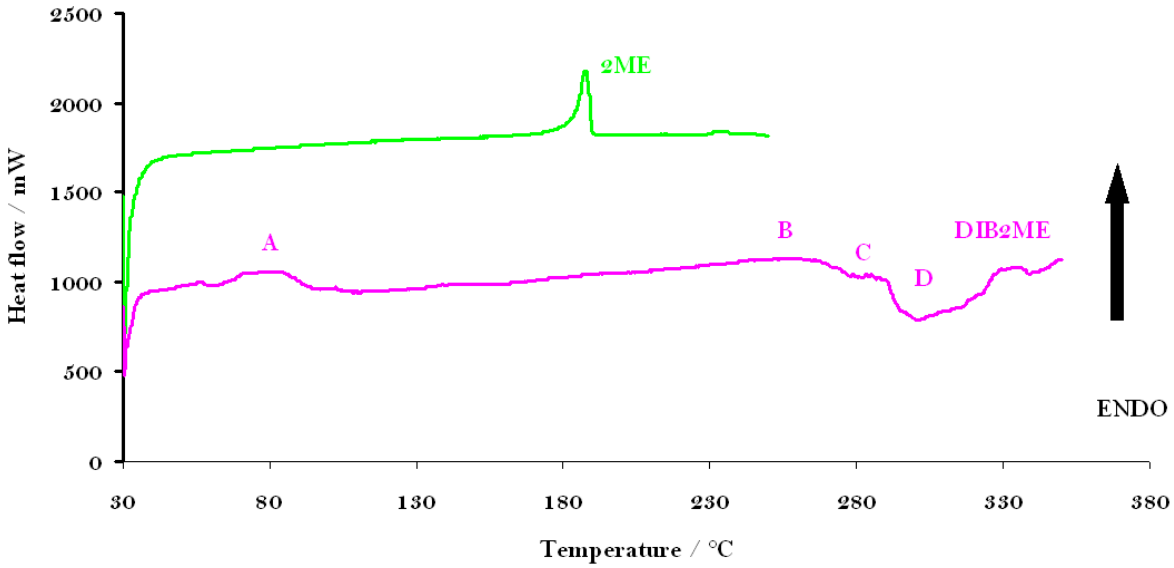

Figure 4.16 DSC trace for DIB2ME.

In Figure 4.16 the DIB2ME complex shows endothermic events corresponding to water loss in the range 30 to 300 °C. The endotherms covered the same range over which water loss was observed from TGA. The peak of the water loss endotherm (labelled A) occurred at 80 °C. However, this peak contained a number of shoulders, subsequently giving rise to a second, very small peak at 255 °C (labelled B) indicating that water loss from this complex was clearly a multi-stage process. The smaller endotherm at

287-290 °C (labelled C) indicated the onset of decomposition of the complex. The HSM analysis confirmed this visually when the crystals turned brown at these temperatures. Breakdown of the host framework of the complex corresponded with decomposition of the complex, which begins above 285 °C. The region 290-350 °C showed an exotherm, followed by a small endotherm, further indicating the decomposition of the complex. Very large mass losses were observed in the TGA trace from 320 °C onwards, confirming the decomposition of the DIMEB complex molecules. The absence of the guest peak (2ME fusion peak) in the DSC trace of DIB2ME was further evidence that the latter represented an inclusion complex.

UV Spectrophotometry

The host:guest ratio was determined by UV spectrophotometry at 198.5 nm in methanol and distilled water (50:50 v/v) for the DIB2ME complex. The stoichiometric ratio was established as 1:1.

Experimental PXRD of the DIB2ME Complex

With notable differences between the patterns of parent compounds and that of DIB2ME, PXRD analysis (Figure 4.17) indicated definite complexation of DIMEB with 2ME using the co-precipitation method. The experimental pattern does, however, show relatively low crystallinity, especially at the higher 2θ values. This may be due to excessive grinding of the sample for PXRD analysis. Neat grinding and kneading of DIMEB with 2ME essentially produced mixtures of the two compounds.

The author is aware that different polymorphs of DIMEB are known, but for simplicity only one representative DIMEB PXRD trace is indicated in Figure 4.17. The PXRD trace of DIB2ME was, however, compared with those for other polymorphs of DIMEB and found not to match any of them. As noted below, the experimental PXRD trace for DIB2ME does, in fact, correspond with that computed from the single crystal X-ray analysis.

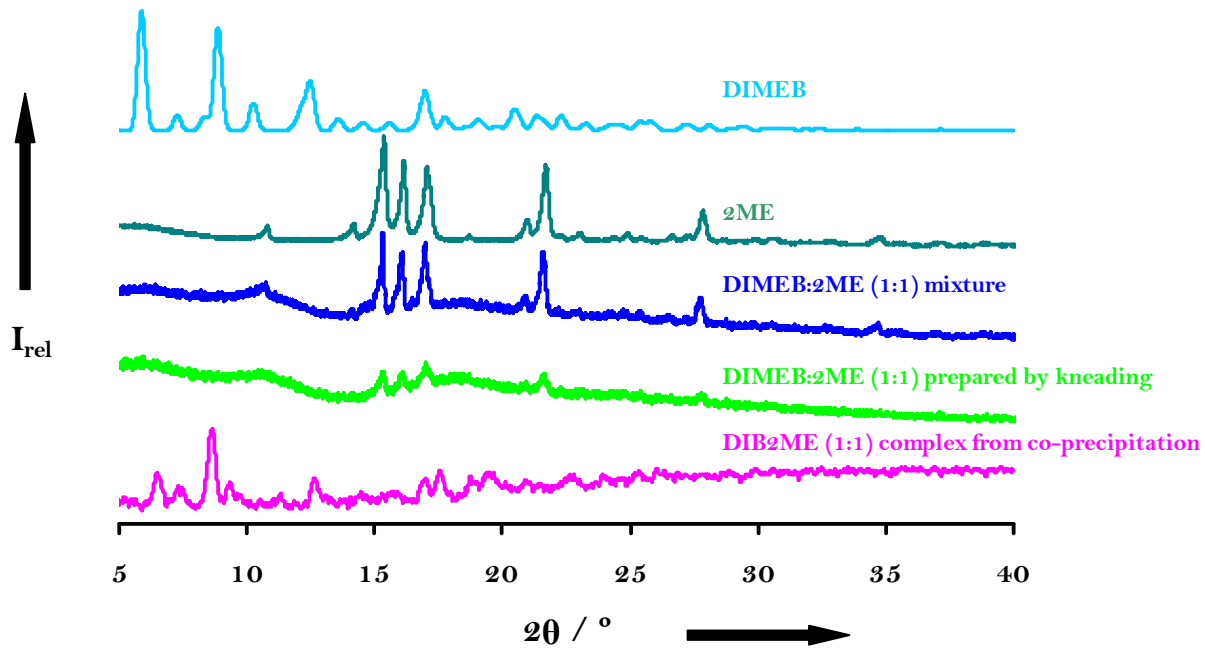

Figure 4.17 PXRD patterns of 2ME, DIMEB, 1:1 DIMEB:2ME mixture, kneaded material and DIB2ME complex obtained by co-precipitation.

Single Crystal X-ray Crystallographic Analysis of the DIB2ME Complex

Data-collection

Preliminary intensity measurements for unit cell determination were recorded on a Nonius Kappa CCD diffractometer using graphite-monochromated MoKα radiation at room temperature (21 °C) and low temperature (-160 °C). Unit cell determinations were performed at both temperatures to ensure that no phase changes were effected on cooling the crystals. A full intensity data set was subsequently collected at -160 °C. Laue symmetry 2/m was confirmed for the collected intensity data, thus indicating the monoclinic system. The space groups $P2_1$ and $P2_1/m$ were indicated by the reflection conditions hkl: none; h0l: none; 0k0: k=2n. Inspection of the reciprocal lattice layers with LAYER[19] confirmed these reflection conditions. The chiral nature of both the CD and the guest (2ME) molecule determined the space group as $P2_1$. Minor host disorder problems were encountered when solving the structure. However, a very good final residual factor R1 [$F_o > 4\sigma(F_o)$] of 0.0851 was eventually obtained. The complex did not indicate isostructurality with any known complexes.[16] The unit cell determinations at room temperature and low temperature are presented in Table 4.6.

Table 4.6 Unit cell parameters for DIB2ME

	DIB2ME (21 °C*)	DIB2ME (-160 °C)
Space group	$P2_1$	$P2_1$
a (Å)	13.789	13.5514(1)
b (Å)	24.956	24.3921(2)
c (Å)	13.952	13.7237(1)
α (°)	90	90
β (°)	97.235	97.0468(3)
γ (°)	90	90
Volume	4623.97	4502.06(6)

*For room temperature unit cell data, no *e.s.d.*s are reported since relatively few intensity frames were collected

Structure Solution and Refinement

From density considerations, the asymmetric unit was determined to consist of one complex unit. From the E-map following structure solution with SHELXD,[20] it was possible to locate most of the non-hydrogen atoms, whose refinement with SHELXH[21] followed. After the first refinement, remaining non-H atoms revealed themselves and were placed. The 2ME molecule and the CD molecule were included in the model with their correct known absolute configurations. All non-hydrogen atoms were then refined isotropically and subsequently anisotropically. Hydrogen atoms were located in the difference electron density maps and were then placed in fixed geometric positions using a riding model and were refined isotropically with thermal parameters equal to 1.2-1.3 times those of their parent atoms. The hydroxyl hydrogen atoms were assigned a common variable isotropic temperature factor and were placed using the hydrogen bond search model. The absence of heavy atoms led to a Flack parameter value that did not indicate absolute structure unequivocally. The Friedel opposites were therefore merged (MERG 4 in SHELXH[21]). Least-squares weights were employed in the final cycles of the refinement. The crystal and refinement data for the low temperature structure determination are presented in Table 4.7. The ADDSYM function in PLATON[22] indicated no extra crystallographic symmetry, reaffirming the correct choice of space group for this structure. Further refinement details, including treatment of water molecules, follow.

Table 4.7 Low temperature crystal and refinement data of DIB2ME

Parameter	DIB2ME
Molecular Formula	$(C_{57}H_{100}O_{35})\cdot(C_{19}H_{26}O_3)\cdot 5.1H_2O$
Formula Weight/g mol^{-1}	1739.67
Crystal System	Monoclinic
Space group	$P2_1$
a (Å)	13.5514(1)
b (Å)	24.3921(2)
c (Å)	13.7237(1)
α (°)	90
β (°)	97.0468(3)
γ (°)	90
Volume (Å^3)	4502.06(6)
Z	2
Density$_{calc}$ / g cm^{-3}	1.279
μ (MoKα) / mm^{-1}	0.105
F(000)	1868
Crystal size / mm^3	0.22 x 0.29 x 0.32
Temperature (K)	173
Range scanned θ / °	$1.00 \leq \theta \leq 25.35$
Index ranges	h: -16, 16 k:-29, 28 l:-16, 16
ϕ scan angle / °	1.0
ϕ scan angle range, frames	362, 362
ω scan angle / °	1.0
ω scan angle range, frames	258, 258
Dx / mm	39.30
Total no. of reflections collected	15799
No. of unique reflections	8108
No. of reflections with $I > 2\sigma(I)$	13656
No. of L.S. parameters	1077
R_{int}, R_σ	0.014, 0.023
S	1.038
R_1 ($F_o > 4\sigma(F_o)$)	0.0851
No. of reflections omitted	102
wR_2 (all reflections)	0.2540
Weighting scheme	a = 0.1810 b = 2.602
$(\Delta / \sigma)_{mean}$	< 0.001
Δρ excursions / eÅ^{-3}	0.86, -0.65

During the refinement, one of the primary methoxy groups (that on residue G6, Figure 4.18) was found to be disordered over two sites and it was modelled accordingly with the major site assigned s.o.f. x and the minor 1-x, the value of x being treated as a least-squares variable. More significantly, it was found that host residue G1 was methylated not only at the O2- and O6-positions, but also at the O3-position. In other words, the DIMEB raw material was slightly impure and the complex crystal preferentially crystallised with this contaminated isomer. Henceforth, however, we continue to refer to the inclusion complex as a 'DIMEB' complex. Ten positions were identified as possible water molecule sites. Only three (O1-O3) of the ten positions located for water molecules could be assigned full site-occupancy factors (s.o.f.s.). It was necessary to assign partial site-occupancy factors to water molecules O4-O10. The temperature factors of the disordered water molecules were fixed at 0.07 Å^2 (the mean of the U_{iso} values for O1-O3) with their partial site-occupancy factors all refining within the range 0.24584 to 0.47104. From the TG analysis 5.1 ± 0.4 (n=3) water molecules were found, while X-ray modelling resulted in 5.3 molecules, which is the same within experimental error. The s.o.f.s of the disordered water molecules are listed in Table 4.8. Seven water molecules (O4-O10) were refined isotropically while O1-O3 refined anisotropically. Water H atoms could not be located in the electron density maps. Four distance restraints were applied to the host molecule, namely C6G6-O6B (1.400 Å, σ =0.005 Å), O6B-C9B (1.400 Å, σ =0.01 Å), C6G6-O6G6 (1.400 Å, σ =0.006 Å) and O6G6-C9G6 (1.400 Å, σ =0.01 Å) to maintain reasonable geometries.

Table 4.8 Refined site-occupancies of disordered water molecules in complex DIB2ME

Atom	O4	O5	O6	O7	O8	O9	O10
s.o.f.	0.47104	0.24584	0.39197	0.30644	0.29328	0.30077	0.24883

Modelling of the 2ME Guest

All the guest hydrogen atoms were placed in idealised positions in a riding model. U_{iso} for the aromatic, methylene and methine hydrogens was 1.2 times that of the parent atom and all methyl hydrogens were given thermal parameters 1.5 times the U_{iso} of their parent atoms. The 2ME molecule presents itself at the secondary rim of the host with the D-ring of 2ME inserted into the DIMEB cavity (Figure 4.19).

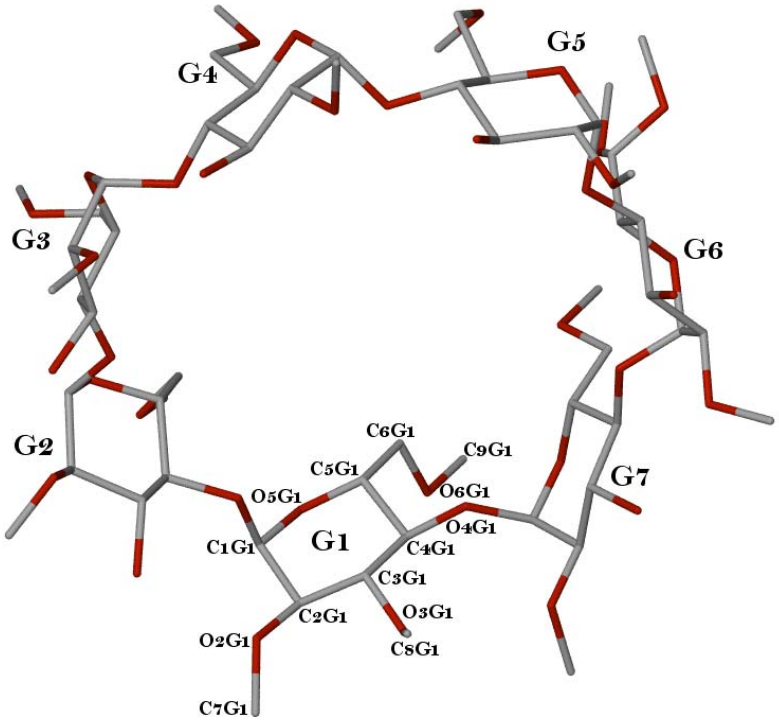

Figure 4.18 Labelling of host - DIMEB. (Note that atom O3 of G1 is methylated whereas all other residues have O2 and O6 methylation patterns).

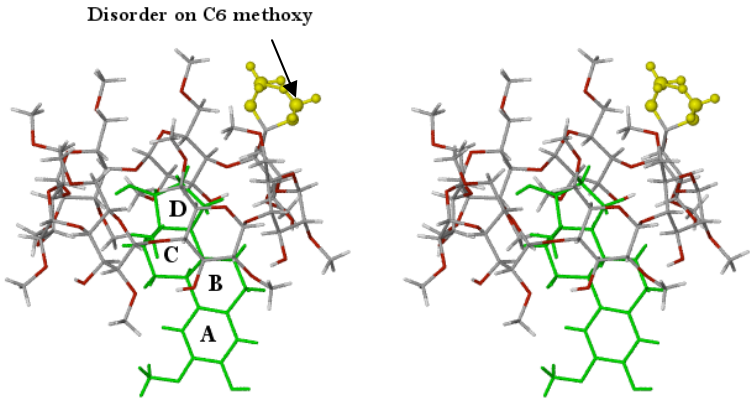

Figure 4.19 Stereoview illustrating inclusion of the 2ME molecule in the cavity of the host DIMEB molecule.

Structural Description

The glucose units of the DIMEB molecule are designated G1, G2, G3, G4, G5, G6 and G7 (Figure 4.18). The asymmetric unit of the DIB2ME complex structure (Figure 4.19) contains a single DIMEB molecule, its associated guest molecule and 5.1 water molecules.

Primary Methoxyl and Glycosidic Torsion Angles

The DIMEB molecule retains a 'round' shape, as usually observed, owing to the existence of an almost complete ring of intramolecular O3(n)-H•••O2(n-1) hydrogen bonds that link contiguous rings. These are discussed in detail later. Table 4.9 lists selected torsion angles for the glucose units. These torsion angles are defined on page 21 of Chapter 1. The primary methoxyl group of G6 is disordered over two positions (designated as 'a' and 'b') adopting the *(-)-gauche* orientation and *(+)-gauche* orientation. Four of the primary methoxyl torsion angles (ω) of DIB2ME (G1, G2, G3, G6a) correspond to the *(-)-gauche* orientation which is the preferred orientation while G4, G5, G6b and G7 have the *(+)-gauche* conformation. All the glucose residues are in the $^4C_1$-chair conformation.

Table 4.9 Principal torsion angles of DIB2ME

Glucose unit	ω(°)a	ω(°)b	Φ(°)	Ψ(°)	Θ_1(°)	Θ_2(°)
G1	-70.9(5)	-	109.6	121.4	53.8	-53.8
G2	-68.1(5)	-	108.6	127.2	50.4	-56.4
G3	-67.9(6)	-	106.6	125.9	53.3	-57.3
G4	78.9(5)	-	110.5	127.6	53.7	-54.2
G5	66.2(8)	-	107.4	127.2	52.3	-54.6
G6	-69.1(7)	+51.0	113.1	128.0	55.9	-56.9
G7	67.9(6)	-	107.9	127.5	52.3	-51.4
Mean	60.7(4)	-	109.1	126.4	53.1	-54.9

Macrocyclic Symmetry

The geometrical parameters of the O4 heptagon of the DIB2ME structure are listed in Table 4.10. These include the radii (***r***), side lengths (***l***), O4•••O4•••O4 angles (***a***), the deviation of each O4 from the mean O4 plane (***d***) and the O4•••O4•••O4•••O4 torsion

angles (***t***). These parameters are defined and illustrated in Chapter 1.The radii ***r*** for DIB2ME vary within a range of 5.02 – 5.12 Å. The lengths ***l*** for the complex vary within a range of 4.36 – 4.42 Å.

Planarity of the O4-Heptagons

The mean deviation (***d***) of the O4 atoms from the mean O4 plane of the host is 0.047 Å. In addition, the torsion angles (***t***) all lie in a range from -6.0 to +3.8˚.

Table 4.10 Geometrical parameters of the O4 polygon for DIB2ME

Glucose unit	*r*(Å)	*l*(Å)	*a*(°)	*d*(Å)*	*t*(°)
G1	5.02	4.38	126.5	0.064	3.8
G2	5.12	4.37	129.6	-0.096	2.0
G3	5.03	4.40	128.7	0.016	-5.4
G4	5.03	4.39	128.7	0.080	3.8
G5	5.07	4.36	127.4	-0.072	-1.8
G6	5.10	4.42	129.1	-0.002	3.6
G7	5.02	4.38	129.7	0.010	-6.0
Mean	5.06	4.39	128.5	0.047	3.8

*The average *e.s.d.*s for *d* and *t* are 0.003 Å and 0.6 ° respectively.

Other useful parameters which describe the overall shape of the macrocycle are the tilt angle (τ_2), intersaccharidic angle (**φ**) and the O2•••O3' distances (Table 4.11), all of which provide information about the shape of the macrocycle. For instance, τ_2 is the angle between the O4 mean plane and the mean plane through O4, C1, C4 and O4'. For DIB2ME τ_2 ranges from 8.8 to 14.3˚. All values of τ_2 are positive and the implication is that the primary rims of all the glucose residues are inclined towards the centre of the cavity. The intersaccharidic angle φ ranges from 117.6 to 118.8˚ with an average value of 118.3˚. This is in good agreement with those reported for β-CD.[16]

The parameters reported here for DIB2ME indicate that the macrocycle is highly symmetrical while the mean deviation (***d***) and torsion angle (***t***) show a nearly planar O4-heptagon.

Table 4.11 Intersaccharidic bond angles, O2(n)···O3(n-1) distances and the tilt angles for DIB2ME

CD	φ(°)	O2(n)···O3(n-1) (Å)	τ_2(°)
G1	119.5	2.810(7)	+11.0(3)
G2	117.6	2.768(7)	+14.3(2)
G3	118.1	2.80(1)	+9.7(5)
G4	117.7	2.807(6)	+13.5(4)
G5	118.7	2.873(6)	+11.9(2)
G6	118.8	2.788(9)	+12.0(3)
G7	117.6	2.879(6)	+8.8(6)

Intra- and Intermolecular Interactions

Host intramolecular interactions

The host molecule has 12 intramolecular O-H•••O hydrogen bonds which can be divided into two different types. There are six O3(n)-H•••O2(n-1) and six O3(n)-H•••O4(n-1) H-bonds. Added to the C-H•••O interactions,[23] the O-H•••O interactions further stabilise the host conformation. The mean O•••O distance for the O-H•••O interactions is 2.82 Å (range 2.76 – 2.88 Å) while the mean bond angle is 129.5˚ (range 103.0 – 169.0˚). Table 4.12 lists these hydrogen bonds.

The host molecule has 11 intramolecular C-H•••O hydrogen bonds which can be divided into five different types. There are three C7-H•••O3, three C5-H•••O4, two C4-H•••O6, two C6-H•••O5 interactions and one C9-H•••O6 interaction. Seven interactions stabilise the host conformation while four occur within a methyl glucose unit (three with C7-H•••O3 and one with C9-H•••O6). The mean C•••O distance for the C-H•••O interactions is 3.06 Å (range 2.79 – 3.48 Å) while the mean hydrogen bond angle is 120.2˚ (range 100.0 – 157.0˚).

Table 4.12 Hydrogen bonding interactions in DIB2ME (colour coded for clarity)

Hydrogen bond	H•••A (Å)	D•••A (Å)	D-H•••A (°)	Symmetry code
O19 - H19 ••• O4G2	2.42	3.186(8)	151	
O22 - H22 ••• O1	1.89	2.590(9)	140	2-x,-1/2+y,-z
O3G2 - H3G2 ••• O2G1	1.98	2.811(5)	169	
O3G2 - H3G2 ••• O4G2	2.50	2.888(4)	109	
O3G3 - H3G3 ••• O2G2	1.96	2.767(5)	160	
O3G3 - H3G3 ••• O4G3	2.51	2.848(5)	105	
O3G4 - H3G4 ••• O2G3	2.00	2.797(6)	157	
O3G4 - H3G4 ••• O4G4	2.48	2.807(5)	104	
O3G5 - H3G5 ••• O2G4	2.03	2.807(4)	153	
O3G5 - H3G5 ••• O4G5	2.50	2.833(4)	105	
O3G6 - H3G6 ••• O2G5	2.12	2.874(5)	149	
O3G6 - H3G6 ••• O4G6	2.53	2.845(4)	103	
O3G7 - H3G7 ••• O2G6	2.11	2.788(6)	138	
O3G7 - H3G7 ••• O4G7	2.53	2.831(5)	102	
C9B - H7B2 ••• O2G7	2.46	3.436(1)	176	2-x,-1/2+y,1-z
C9B - H7B3 ••• O6G5	2.41	3.290(1)	149	
C6 - H6B ••• O3G2	2.60	3.397(6)	138	2-x,-1/2+y,-z
C2G1 - H2G1 ••• O5G6	2.46	3.407(5)	158	2-x,1/2+y,1-z
C4G1 - H4G1 ••• O6G1	2.49	2.847(6)	101	
C9G1 - H7GY ••• O2G5	2.57	3.545(8)	171	2-x,1/2+y,1-z
C2G2 - H2G2 ••• O5G4	2.45	3.314(5)	144	1-x,1/2+y,-z
C4G2 - H4G2 ••• O6G2	2.48	2.837(6)	101	
C5G2 - H5G2 ••• O4G3	2.43	2.798(5)	101	
C5G2 - H5G2 ••• O19	2.42	3.275(8)	143	
C7G2 - H8G8 ••• O3G6	2.60	3.151(7)	116	
C7G2 - H8G9 ••• O3G2	2.59	3.176(6)	118	
C5G3 - H5G3 ••• O4G4	2.45	2.798(6)	100	
C7G3 - H8GC ••• O3G3	2.50	3.122(9)	121	
C1G4 - H1G4 ••• O5G2	2.52	3.328(6)	138	1-x,-1/2+y,-z
C6G4 - H6G1 ••• O5G3	2.41	3.346(6)	157	
C7G4 - H8GD ••• O6G2	2.43	3.385(2)	165	1-x,-1/2+y,-z
C6G5 - H6GY ••• O5G4	2.58	3.456(7)	148	
C7G5 - H7G4 ••• O3G2	2.58	3.227(6)	123	
C7G5 - H7G5 ••• O3G5	2.45	3.074(6)	121	2-x,-1/2+y,-z
C5G6 - H5G6 ••• O4G7	2.49	2.850(6)	101	
C4G7 - H4G7 ••• O22	2.59	3.591(6)	180	x,y,1+z
C6G7 - H6GA ••• O5G6	2.58	3.480(8)	152	
C5G2- H5G2•••O19	2.42	3.275(6)	143	

Host-Host intermolecular interactions (C-H•••O)
Host-Host intramolecular interactions (C-H•••O) and (O-H•••O)
Host-Guest intermolecular interactions (C-H•••O) and (O-H•••O)
Guest-Water interactions (O-H•••O)

Host-Host intermolecular interactions

DIB2ME has nine intermolecular hydrogen bonds which can be divided into six different C-H•••O interaction types. There are two C9-H•••O2, two C2-H•••O5, two C7-H•••O3, one C1-H•••O5, one C7-H•••O6 and one C6-H•••O5 interactions. The mean hydrogen bond distance is 3.36 Å (range 3.15 – 3.54 Å) while the mean hydrogen bond angle is 149˚ ranging from 116.0 to 176.0˚.

Host-Water interactions

DIB2ME has 14 host-water interactions. Five of the interactions are C-H•••OW (W=water) interactions with a mean bond distance of 3.26 Å (range 3.07 – 3.38 Å). The nine remaining interactions are O•••OW close contacts with a mean distance of 2.87 Å (2.75 – 3.21 Å).

Guest Inclusion

Guest Location

The guest molecule is orientated with the D-ring moiety buried within the DIMEB cavity while the A ring protrudes from the secondary rim, as shown in Figure 4.20. The guest is tilted so as to maximally occupy the DIMEB cavity. The water molecules interact with both the host and guest, serving to stabilise the complex. Figure 4.21 provides a full space-filling diagram of both guest and host in the inclusion complex viewed from both primary and secondary rims.

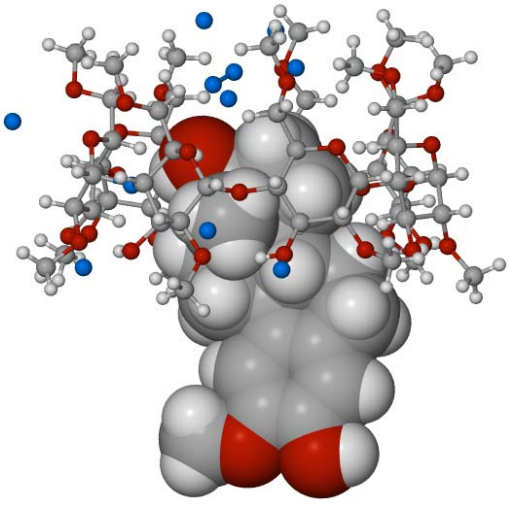

Figure 4.20 Illustration of the DIB2ME inclusion complex. Blue spheres represent water oxygen atoms.

Primary rim **Secondary rim**

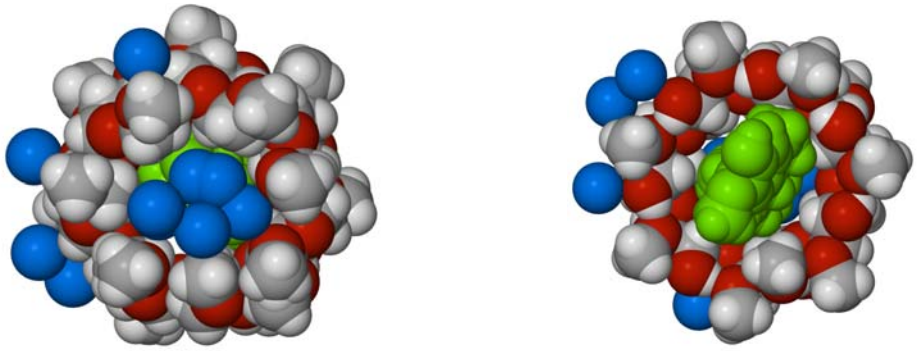

Figure 4.21 Space-filling diagrams of DIB2ME, viewed from both primary (left) and secondary (right) rims. The guest molecule is drawn in green with water oxygen atoms as blue spheres.

Guest Conformation

Table 4.13 presents selected, representative bond distances and torsion angles of the uncomplexed 2ME molecule (described in Chapter 3) and the 2ME molecule included in the DIB2ME complex for comparison. The differences between corresponding parameters were calculated and are presented in the last column of Table 4.13. This geometrical comparison confirms what is illustrated in Figure 4.22 namely that the conformations of the steroid molecules in both instances are practically identical. The notable consistency of the steroid molecules in each form is indicative of the rigidity and the stability of 2ME. One noteworthy difference is, however, the orientation of the O19-H bond, which occurs since the 2ME molecule engages in different H-bonding arrangements in the two crystal structures. Torsion angles C21-O20-C2-C1 and C21-O20-C2-C3 have a difference of ~18°, even though slight by visual inspection. Other than these differences, no significant conformational changes had been effected on the 2ME molecule when complexed with DIMEB. A full set of the molecular parameters is available in Appendix 4 on the CD-ROM provided.

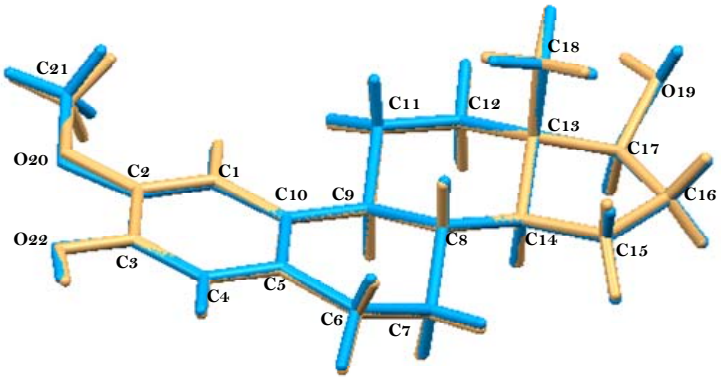

Figure 4.22 Overlay of the uncomplexed 2ME molecule (blue) and 2ME molecule encapsulated in DIB2ME (yellow).

Table 4.13 Common selected geometrical parameters for 2ME in its own crystal and in DIB2ME

Parameter	2ME	2ME of DIB2ME	|Δ|
Selected bond distances (Å)			
O19-C17	1.431(3)	1.41(1)	0.025
C13-C18	1.540(3)	1.54(1)	0.005
O20-C2	1.391(3)	1.367(7)	0.024
O20-C21	1.432(3)	1.425(8)	0.007
O22-C3	1.366(3)	1.275(6)	0.091
C1-C10	1.408(3)	1.398(7)	0.010
C8-C9	1.546(3)	1.533(7)	0.013
C13-C14	1.541(3)	1.511(7)	0.030
Selected torsion angles (°)			
C21-O20-C2-C1	-20.6(3)	2.1(1)	18.5
C21-O20-C2-C3	160.8(2)	-179.1(7)	18.2
C15-C16-C17-O19	148.8(2)	144.9(6)	3.9
C18-C13-C14-C15	-68.9(2)	-67.9(6)	1.0
C1-C2-C3-C4	-1.0(3)	-0.2(7)	0.8
C8-C9-C10-C5	-22.9(3)	-24.3(7)	1.9
C8-C14-C15-C16	-161.8(2)	-165.4(5)	3.6

Hydrogen Bonding Interactions involving the Guest Molecule

Host-guest Intermolecular Interactions

There are four host-guest hydrogen bonds in the structure of DIB2ME. Three are C-H•••O hydrogen bonds with a mean C•••O distance of 3.42 Å (range 3.28 – 3.97 Å) and a mean hydrogen bond angle of 153.7˚ (range 138.0 – 180.0˚). There is one host-guest O-H•••O interaction. There are also several host-guest close contacts. Figure 4.23 includes the most important host-guest interactions, namely the O-H•••O hydrogen bond between the hydroxyl group on ring D of the 2ME molecule and a glycosidic O4 atom, as well as a C-H•••O hydrogen bond from a host methine group to the hydroxyl oxygen atom on the D-ring of 2ME. In addition, Figure 4.23 shows the intramolecular O-H•••O hydrogen bonds that stabilise the 'round' conformation of the DIMEB molecule. Only six intramolecular O-H•••O H-bonds do so, however; since O3 of the glucose residue 1 is methylated, a seventh O-H•••O hydrogen bond does not exist.

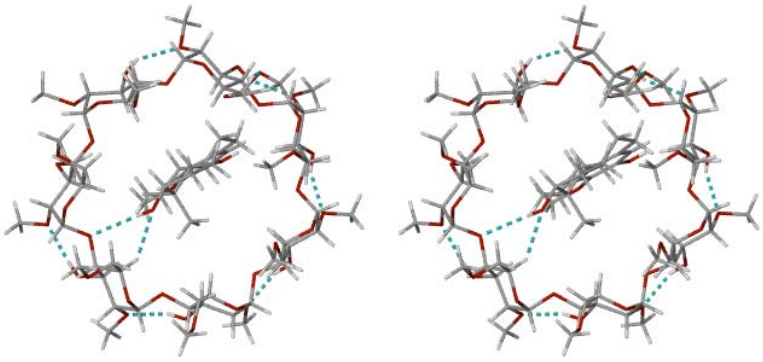

Figure 4.23 Stereoview of intermolecular and intramolecular hydrogen bonds in DIB2ME viewed from the host primary side.

Guest-Water Interactions

One hydrogen bond between the guest and included water molecules was observed, namely O22-H22•••O1 (2-x,-1/2+y,-z) (Table 4.12). There are 12 guest-water close contacts with a mean distance of 2.86 Å (range 1.88 – 3.40 Å).

Water-Water Interactions

There are four OW•••OW interactions with a mean distance of 2.88 Å (range 2.63 – 3.05 Å).

Crystal Packing

DIMEB and its complexes tend to crystallise in the space groups $P2_1$ and $P2_12_12_1$ and their packing arrangements include channel type head-to-tail, modified brick type and modified herringbone motifs. DIB2ME crystallises in the space group $P2_1$, the packing arrangement being channel-type along [-101] (Figure 4.24a).

Figure 4.24b serves as visual confirmation that the guests are isolated from neighbouring guest molecules although the protruding guest residues are in contact with methine groups of the neighbouring host molecules.

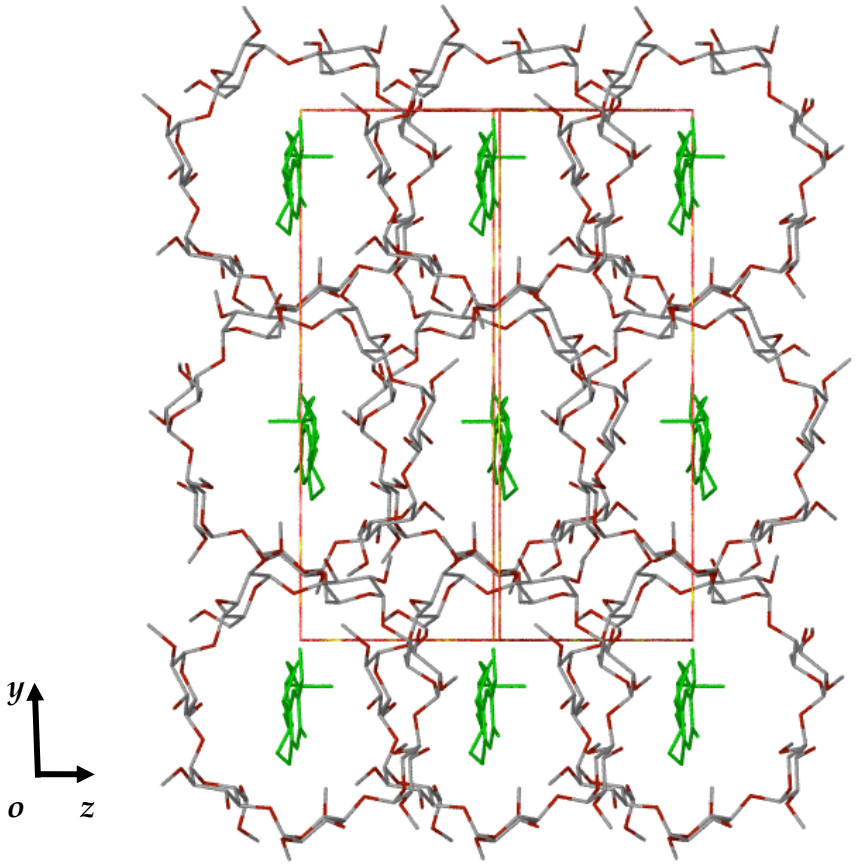

(a)

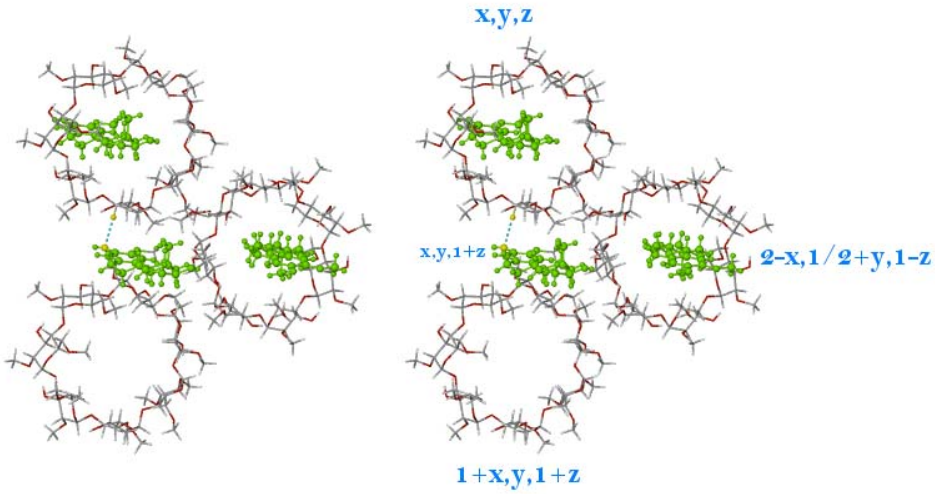

(b)

Figure 4.24 Packing diagrams of DIB2ME (a) along [-101] and (b) Stereoview of guest-host interaction C4G7-H47•••O22 (x,y,1+z) in yellow.

Experimental and Computed PXRD Traces for DIB2ME

Calculated and experimental PXRD traces for DIB2ME are shown in Figure 4.25. There is a slight shift in the peak positions to lower 2 θ for the experimental trace. This is a result of the different conditions under which the data were collected. Data for the experimental trace were collected at ambient temperature (294 K) while data for the calculated trace were collected at 113 K. The high level of agreement between the two traces does, however, confirm that the crystal selected for X-ray analysis is representative of the bulk material.

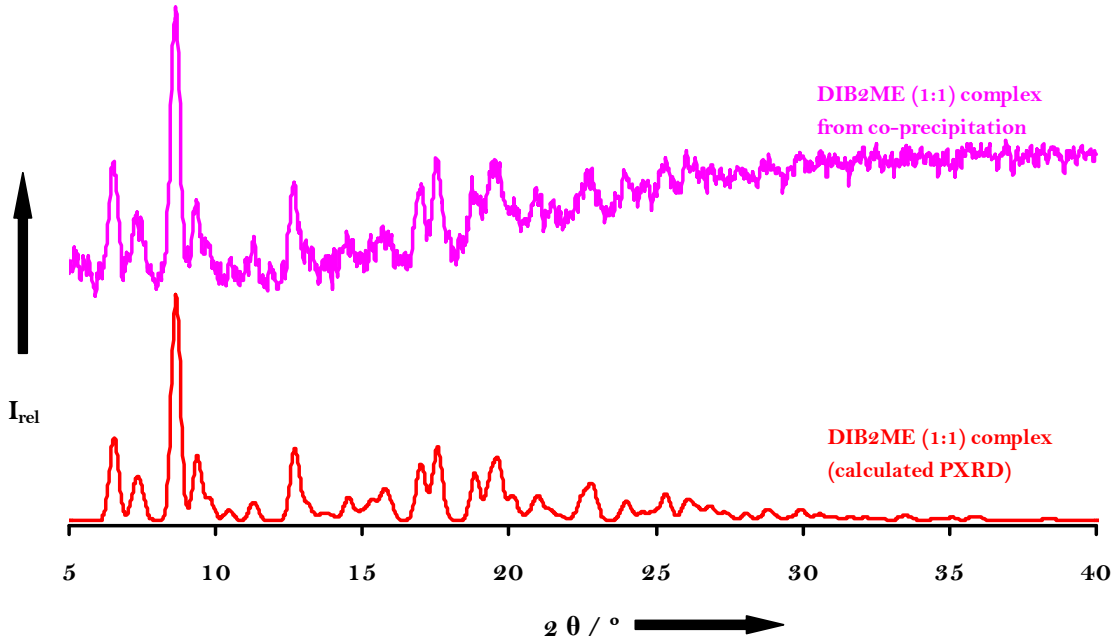

Figure 4.25 Experimental versus calculated PXRD patterns for DIB2ME.

4.3.4 TRIMEB COMPLEX WITH 2-METHOXYESTRADIOL

Preparation of TRIB2ME

A suspension was made by combining 0.033 mmol (44.27 mg) of the CD and 0.033 mmol (10 mg) of 2ME in 3 ml of distilled water. The suspension was stirred vigorously at room temperature for 24 h. We ensured that saturation of both host and guest had been achieved. The solution was then filtered (0.45 μm microfilter) and left at 60 °C on a hot plate. Single crystals formed after several days. The crystals are those of an inclusion complex between TRIMEB and 2ME. This complex shall be referred to as TRIB2ME. Large, approximately cube-shaped crystals of TRIB2ME were isolated.

Thermal Analyses

Hot Stage Microscopy

HSM was used to evaluate the thermal behaviour of the complex upon heating at a constant rate of 10 K/min. The analysis was done under silicone oil to observe bubble formation in the event of dehydration and/or decomposition. The HSM photographs of TRIB2ME complex are presented below (Figure 4.26). Crystals of the complex showed signs of fragmentation upon removal from mother liquor due to dehydration. Photographs of the complex were recorded at various stages of thermal behaviour: start of analysis, melting of crystal at 170 °C, decomposition of the complex (shown by colour change of the melt to brown) and the subsequent appearance of bubbling as a result of decomposition.

During HSM analysis it was difficult to detect release of water from the crystal since no bubbling was present before the crystal melting stage. Evidently, the amount of water present was so small as not to reveal itself through bubble formation. The crystal melted at 170 °C and decomposition commenced at ~350 °C with spontaneous associated bubbling verifying decomposition occurring between 350 and 400 °C.

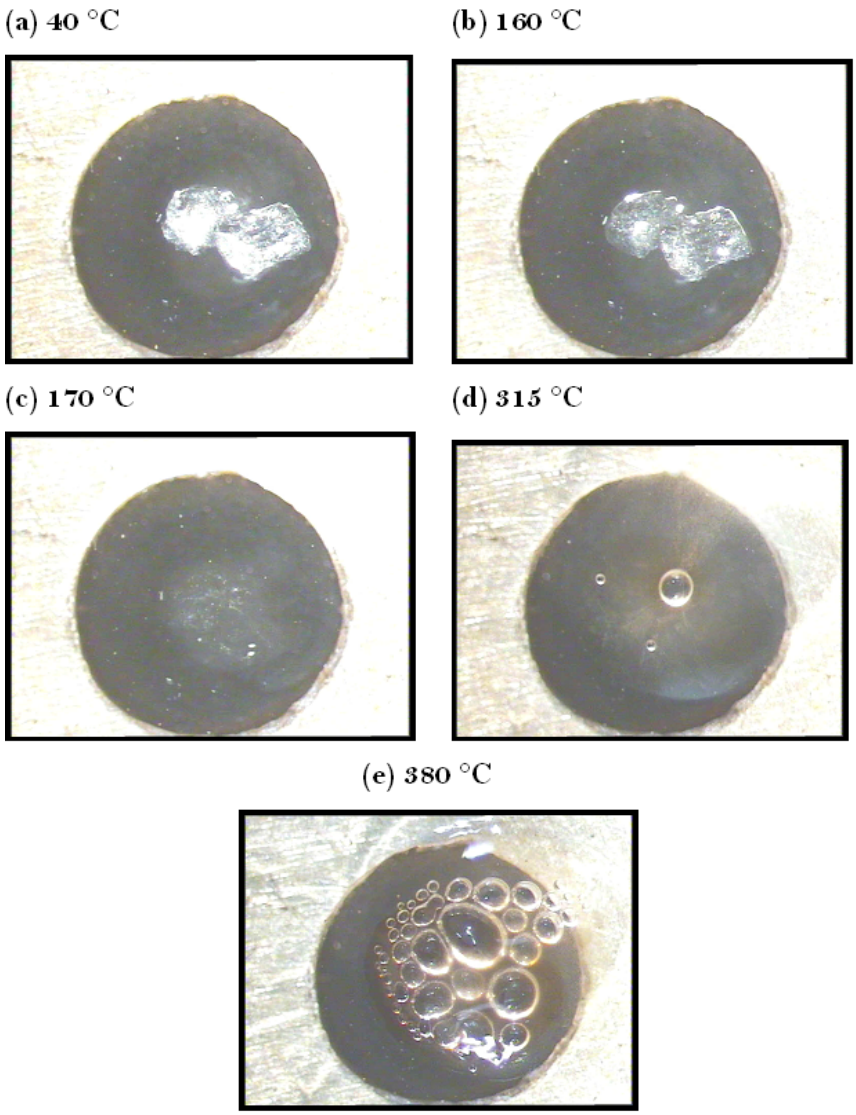

Figure 4.26 HSM photographs of TRIB2ME during heating.

Thermogravimetric Analysis and Differential Scanning Calorimetry

TGA and DSC traces for the TRIB2ME complex are presented in Figures 4.27 and 4.28 respectively. The TGA traces for the TRIB2ME complex showed a mean mass loss of 1.1 ± 0.24 % (n=3) in the temperature range 30-315 °C, which established the TRIB2ME:H_2O ratio as 1:1.07. A very small mass loss was identified which not only made it quite difficult to establish commencement of complex decomposition but also explains the absence of initial bubbling during HSM analysis. Decomposition of the crystal commenced at ~310 °C as confirmed by Figure 4.27. Figure 4.28 shows a single melt endotherm at 170 °C (onset temperature 165 °C) which correlates well with HSM.

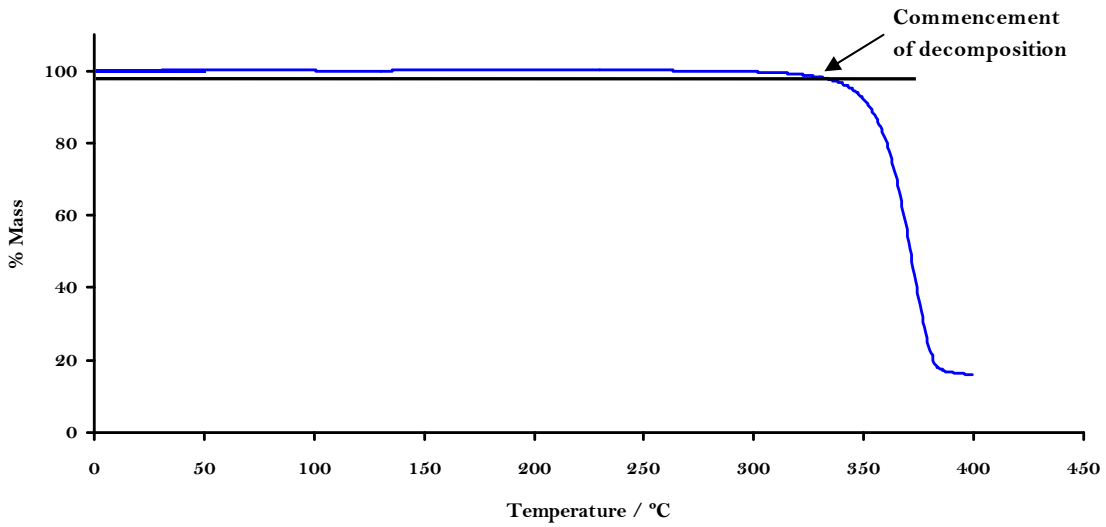

Figure 4.27 TGA trace for TRIB2ME.

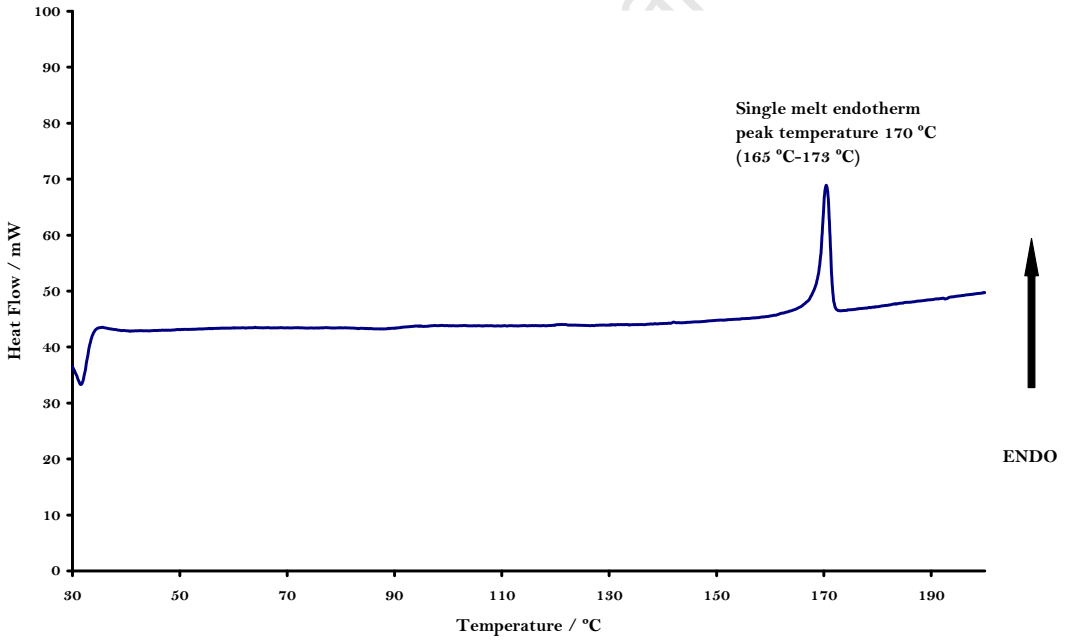

Figure 4.28 DSC trace for TRIB2ME.

UV Spectrophotometry

The host:guest ratio was determined by UV spectrophotometry at 198.5 nm in methanol and distilled water (50:50 v/v) for the TRIB2ME complex. A 1:1 host:guest stoichiometry was established.

Experimental PXRD of theTRIB2ME Complex

The PXRD patterns of TRIMEB, 2ME, a mixture of the two compounds, kneaded product and the co-precipitated TRIB2ME complex are illustrated in Figure 4.29. Both the mixture and the preparation from kneading host and guest produced an amorphous pattern for the host whereas 2ME was clearly identified. This may be due to excessive grinding of the sample for PXRD analysis. The co-precipitated material indicated definite complexation, with distinct differences upon comparison with the PXRD traces of the parent compounds. Sample preparation of the co-precipitated material required considerable trituration which led to a slightly amorphous product.

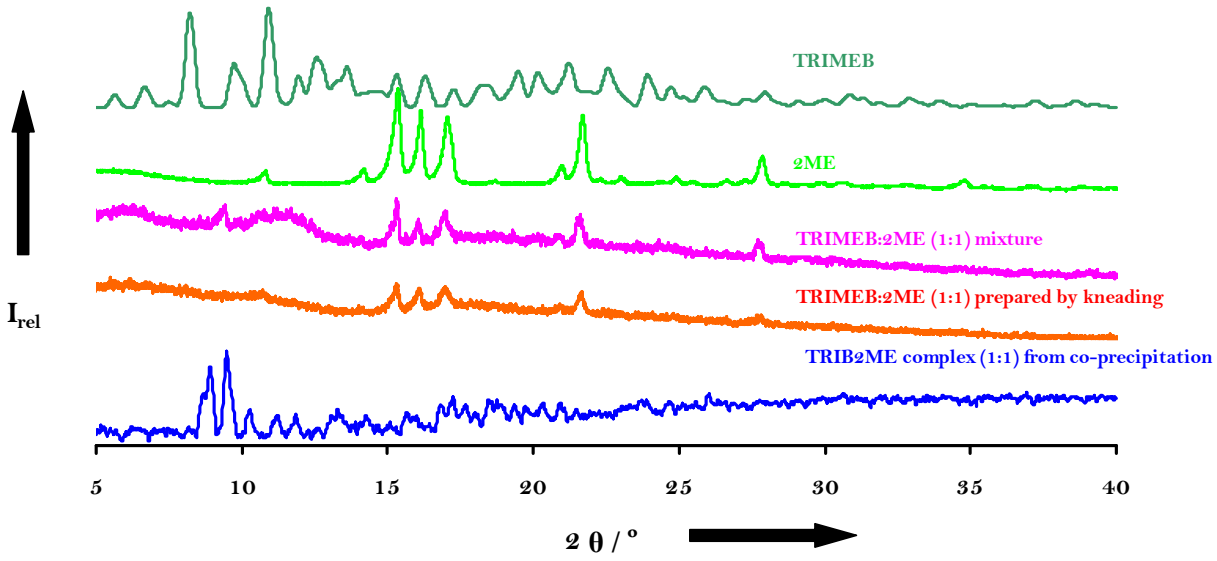

Figure 4.29 PXRD patterns of 2ME, TRIMEB, mixture, kneaded material and TRIB2ME complex obtained by co-precipitation.

Although three forms of TRIMEB are known,[16] the PXRD pattern of only one of these is included in the above figure for simplicity. The blue PXRD trace had been compared with the PXRD patterns of all three forms of TRIMEB, with no correspondence being found. As described later in this chapter, the blue trace does, in fact, match the

computed trace based on the single crystal X-ray analysis of the TRIB2ME inclusion complex.

Single Crystal X-ray Crystallographic Analysis of the TRIB2ME Complex

Data-collection

To obtain good structural resolution, intensity data-collection at low temperature was desired. The crystal was mounted on a Nonius Kappa CCD diffractometer using graphite-monochromated MoKα radiation and the unit cell determined at 21 °C. On cooling the crystal, unit cell data were determined again at -160 °C. Cell determinations were performed at both temperatures to ensure that no phase changes were effected on cooling.

Laue symmetry $\bar{1}$ was confirmed for the collected intensity data, thus indicating the triclinic system, for which the possible space groups are P1 and P $\bar{1}$. Since both host and guest molecules are chiral, P1 was chosen. This choice was confirmed by program XPREP.[24] A very good final residual factor R1 [$F_o > 4\sigma(F_o)$] of 0.0831 was obtained even though minor host disorder was encountered when solving the structure. Structure solution based on isomorphous replacement was not relevant for this complex since none of the known complexes of TRIMEB has similar unit cell parameters.[16] The unit cell determinations at room temperature and low temperature are presented in Table 4.14.

Table 4.14 Unit cell parameters for TRIB2ME

	TRIB2ME (21 °C*)	**TRIB2ME** (-160 °C)
Space group		P1
a (Å)	14.5923	14.1675(2)
b (Å)	23.9984	23.7963(3)
c (Å)	28.9756	28.2467(4)
α (°)	85.6703	85.3799(4)
β (°)	85.6492	86.3949(4)
γ (°)	73.2846	73.8357(8)
Volume	9562.5	9108.6(2)

*For room temperature unit cell data, no *e.s.d.s* are reported since relatively few intensity frames were collected

Structure Solution and Refinement

This structure presented a significant challenge owing to the unusually large size of the crystallographic asymmetric unit. From density considerations, a value of Z=4 1:1 TRIMEB:2ME complex units (plus ~4.4 H_2O molecules) were indicated as comprising the asymmetric unit. The structure was solved by direct methods using SHELXD.[20] Most of the non-hydrogen atoms were located in the E-map and the structure was developed by successive difference Fourier syntheses. Atoms were initially refined with isotropic displacement parameters. The 2ME molecules were included in the model with the correct known absolute configuration. Hydrogen atoms located in the difference electron density maps were then placed in fixed geometric positions using a riding model and were refined isotropically with thermal parameters equal to 1.2-1.3 times those of their parent atoms. Hydroxyl hydrogen atoms were placed using the hydrogen bond search model. Heavy atoms were not present, which led to a Flack parameter value that did not specify absolute structure unequivocally. The Friedel opposites were therefore merged (MERG 4 in SHELXH[21]). Least-squares weights were utilised in the final cycles of the refinement. The low-temperature crystal and refinement data for the structure determined are presented in Table 4.15. The ADDSYM function in PLATON[22] indicated no extra crystallographic symmetry, confirming the proper choice of space group for this structure and thus the crystallographic independence of the four complex units. Further refinement details are given below.

Table 4.15 Low temperature crystal and refinement data of TRIB2ME

Parameter	TRIB2ME
Molecular Formula	$(C_{63}H_{112}O_{35})\bullet(C_{19}H_{26}O_3)\bullet 1.1H_2O$
Formula Weight/g mol^{-1}	1751.86
Crystal System	Triclinic
Space group	P1
a (Å)	14.1675(2)
b (Å)	23.7963(3)
c (Å)	28.2467(4)
α (°)	85.3799(4)
β (°)	86.3949(4)
γ (°)	73.8357(8)
Volume (Å^3)	9108.6(2)
Z	4
Density$_{calc}$ / g cm^{-3}	1.278
μ (MoKα) / mm^{-1}	0.100
F(000)	3780
Crystal size / mm^3	0.18 x 0.23 x 0.26
Temperature (K)	173
Range scanned θ / °	1.00 ≤ θ ≤ 24.7
Index ranges	h: -16, 16 k:-28, 28 l:-33, 33
ϕ scan angle / °	1.0
ϕ scan angle range, frames	362, 362
ω scan angle / °	1.0
ω scan angle range, frames	258, 258
Dx / mm	40.00
Total no. of reflections collected	62716
No. of unique reflections	31829
No. of reflections with I > 2σ(I)	20492
No. of L.S. parameters	1077
R_{int}, R_σ	0.056, 0.085
S	1.023
R_1 (F_o >4σ(F_o))	0.0831
No. of reflections omitted	54
wR_2 (all reflections)	0.2353
Weighting scheme	a = 0.122 b = 12.024
(Δ / σ)$_{mean}$	< 0.001
Δρ excursions / eÅ^{-3}	0.99, -0.52

At some stage in the refinement in SHELXH,[21] a primary $-OCH_3$ group of one of the TRIMEB molecules appeared to be disordered over two positions. The disorder appeared at site C6D5 (Figure 4.30b, atoms highlighted in yellow) with the O6-CH3 residue disordered over two positions (viz. methoxy components C7D5 and C7D8). Only a single electron density peak qualifying as a water oxygen atom was found at an advanced stage of the refinement. It was included with U_{iso} ~0.16 Å^2 and its s.o.f. was allowed to refine, yielding a final value of 0.49.

To refine TRIB2ME anisotropically proved to be very challenging since the program SHELXH[21] could not accommodate the full structure with all four complex units refining in this way. The BLOC[25] technique was attempted to refine TRIB2ME anisotropically but this was abandoned because of extremely long run-times required to ensure sufficient mixing of parameters in each BLOC instruction. Hence, a more balanced approach was adopted by applying full-matrix refinement by firstly refining all four guests, then the side-chains of each glucose molecule of the host. Even after this attempt, not all the atoms refined anisotropically. However, a more balanced anisotropically refined model was achieved. Finally the water molecule O1, C6A, C6B and 9 atoms on guest D refined isotropically. With regard to the hosts, 37 atoms on host A, 37 atoms on host B, 37 atoms on host C and 43 atoms on host D were refined isotropically and the rest of the structure refined anisotropically. The one water O atom candidate which was located in the difference electron-density map, accounting for 0.49 water molecules, refined isotropically. 1.07 ± 0.23 water molecules per complex unit were found from TG analysis (n = 3). However, single crystal X-ray diffraction indicated only 0.12 (0.49/4) water molecules per complex unit. We account for the difference in waters as being due to sample manipulation for single crystal X-ray analysis since after multiple readings, TG analysis for water loss did not correlate well with the refinement data. Quantification of water content at such a low level (~1% by mass) generally presents considerable difficulty.

The complex units comprising the asymmetric unit are designated as A, B, C and D, with each glucose unit within each complex numbered 1 to 7 accordingly (Figure 4.30 a and b). Fifteen distance restraints were applied to complex D and one to complex A, B

and C each, to maintain reasonable geometries. Hence, the following DFIXs were applied: C7D1-O6D1 1.4 Å(σ = 0.008 Å); C6D1-O6D1, C6D5-O6D5, C6D5-O6D8 1.4 Å (σ = 0.001 Å); C13D-C18D, C13D-C12D 1.5 Å (σ = 0.01 Å); C13D-C17D, C13D-C14D 1.5 Å (σ = 0.001 Å); C5D5-C6D5 1.5 Å (σ = 0.005 Å); C5D5-O6D5, C6D5-C7D5, C6D5-C7D8 2.4 Å (σ = 0.005 Å); O6D5-C7D5, O6D8-C7D8 1.4 Å (σ = 0.005 Å); O4A2-H19A 2.23 Å (σ = 0.005 Å); O4B1-H19B 2.35 Å (σ = 0.005 Å); O4C2-H19C 2.08 Å (σ = 0.005 Å); O6D5-H19D 2.3 Å (σ = 0.005 Å).

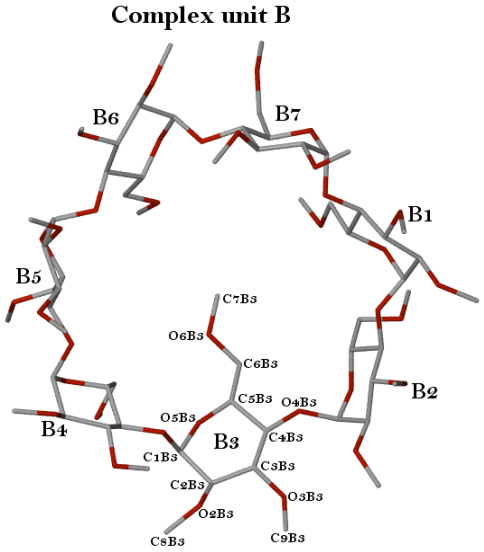

(a)

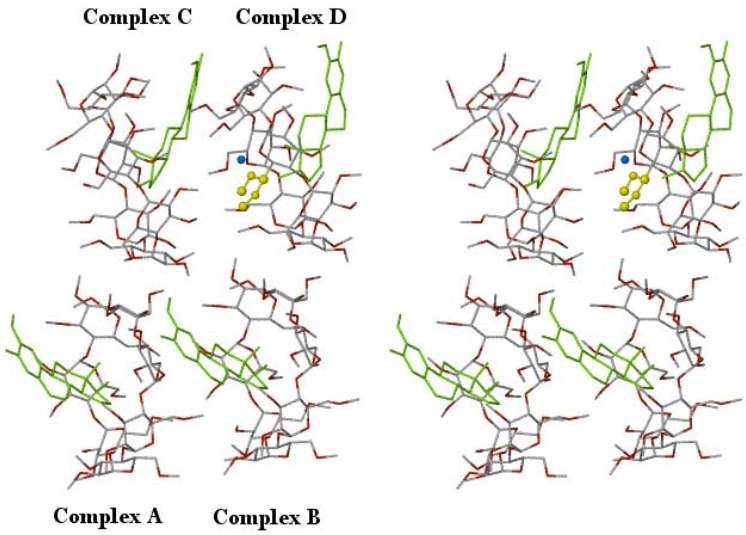

(b)

Figure 4.30 (a) Labelling of a representative host (TRIMEB) (b) Stereoview of the asymmetric unit illustrating inclusion of the 2ME molecule in the cavity of the host TRIMEB molecule.

Modelling of the 2-ME Guest

Atoms C6A, C6B, C6D, C7D, C11D, C12D, C13D, C17D, C18D, C19D and C21D were refined isotropically; all other atoms belonging to the guests were refined anisotropically. All the guest hydrogen atoms were placed in idealised positions in a riding model. U_{iso} for the aromatic hydrogens was 1.2 times those of the parent atoms and all methyl hydrogens were given thermal parameters 1.5 times the U_{iso} of their parent atoms. In all four independent complex units, the 2ME molecule was found at the secondary rim of the respective host with the D-ring of 2ME inserted into the TRIMEB cavity (Figure 4.30b).

Structural Description

The asymmetric unit of the TRIB2ME complex structure (Figure 4.30b) contains four TRIMEB molecules, four 2ME guest molecules and 0.49 water molecules. The glucose units of the TRIMEB molecule are designated A1-A7, B1-B7, C1-C7 and D1-D7 for complexes A, B, C and D, respectively (Figure 4.30a).

Primary Methoxyl and Glycosidic Torsion Angles

Selected torsion angles for the glucose units in complex unit A, B, C and D are listed in Appendix 5. For TRIB2ME, sixteen of the primary methoxyl torsion angles (ω) for glucose residues A1, A3, A5, A6, B2, B4, B5, B7 C2, C4, C6 D2, D4, D5b, D6, D7 correspond to the *(-)-gauche* orientation which is the preferred orientation while thirteen of the primary methoxyl torsion angles (for residues A2, A4, A7, B1, B3, B6, C1, C3, C5, C7, D1, D3, and D5a) have the *(+)-gauche* conformation. The primary methoxyl group of D5 is the residue that is disordered over two positions (designated as 'a' and 'b') adopting the *(-)-gauche* and *(+)-gauche* conformations. All the residues are in the $^4C_1$-chair conformation.

Macrocyclic Symmetry

Appendix 5 lists the geometrical parameters of the O4-heptagon in the four independent TRIMEB molecules in the crystal of TRIB2ME. The radii (***r***) for each complex unit within TRIB2ME vary within a range, namely 4.61 – 5.50 Å. The lengths (***l***) for the four complex units are also very similar and vary within a fairly narrow band of

4.12 – 4.56 Å. The average glycosidic oxygen angle (***a***) for the four complex units is 127.9° while the glycosidic oxygen angles of each unit fall within the range 117.8 - 139.9°.

Planarity of the O4-Heptagons

The mean deviation (***d***) of the O4 atoms from the mean O4 plane of the host is A - 0.277 Å, B - 0.289 Å, C - 0.238 Å and D 0.106 Å, with an average e.s.d. for all four complex units of 0.004 Å. The torsion angles (***t***) for all four complex units all lie in a range from -20.6 to 26.1°. Furthermore, the parameters which describe the overall shape of the macrocycle namely the tilt angle (τ_2), intersaccharidic angle (φ) and the O2•••O3' distances, are all listed in Appendix 5. For TRIB2ME, τ_2 magnitudes range from 5.2 to 50.2°, which is quite a broad range, but typical of this host.[16] For host molecules A and B, values of τ_2 are positive and the primary rims of all the glucose residues are leaning towards the centre of the cavity. For host molecules C and D, six tilt angles are positive and one is negative. The negative τ_2 magnitudes are fairly small (6.0 and 5.2° respectively). Thus for molecules A and B the macrocycle has a truncated cone like appearance (i.e. wider at the secondary rim and narrower at the primary rim). However, molecules C and D, deviate slightly from this arrangement. The intersaccharidic angle φ ranges from 113.6 to 119.6° with an average value of 116.8°. This is in good agreement with those reported for TRIMEB.[16] The parameters reported here for TRIB2ME indicate that the macrocycle is somewhat distorted.

Host Conformations

Figure 4.31 presents the TRIB2ME structure, with each complex unit of the asymmetric unit colour-coded. In Figure 4.32, we see a remarkable similarity in the host conformations of complex units A and B. However, when comparing A and B with C we see a distinct difference in overlay. Since complex D presented disorder of one host methoxy group (see brown colour of disordered atoms) coincidence of D with any of the other complex units was not possible. Nonetheless, complex unit D, if not disordered, would present a similar conformation to complex unit C. This implies that there are at least two distinct overall conformations of the TRIMEB molecule, which in turn suggests somewhat different modes of guest inclusion.

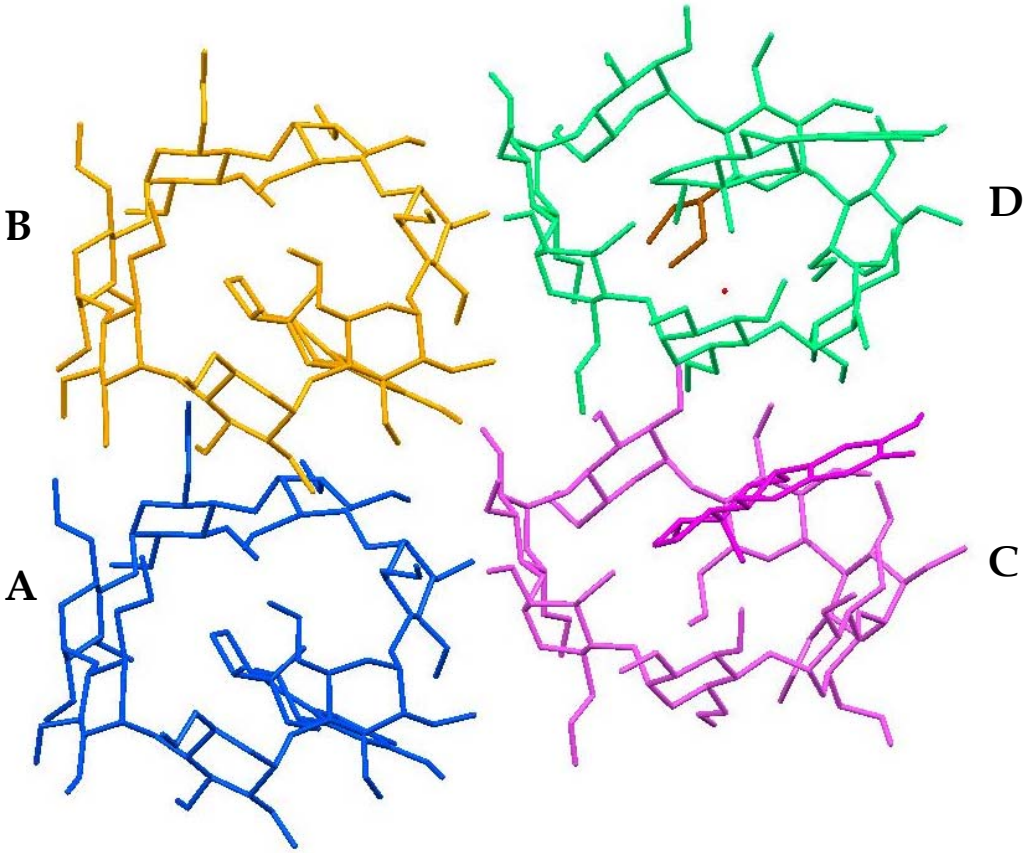

Figure 4.31 Colour coded complex units of TRIB2ME.

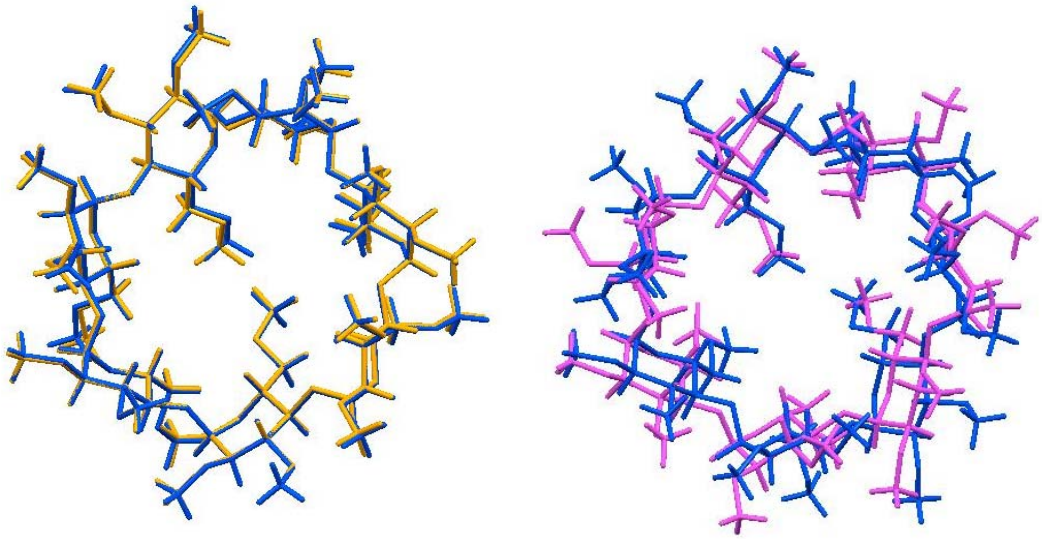

Figure 4.32 Overlay of the host molecules in complex units A and B (left) and A and C (right).

INTRA- AND INTERMOLECULAR INTERACTIONS (Appendix 4 and 5)

Host Intramolecular Interactions

The host conformations of TRIB2ME are stabilised by several analogous intramolecular C-H•••O interactions. The host molecules in TRIB2ME engage in 68 intramolecular C-H•••O hydrogen bonds (18 for host A, 15 for host B, 17 for host C and 18 for host D) which can be divided into twelve different types. There are eighteen C6-H•••O5, thirteen C5-H•••O4, eleven C9-H•••O2, eight C4-H•••O6, five C1-H•••O6, three each of C6-H•••O6, C1-H•••O3 and C8-H•••O3 and one each of C5-H•••O5, C6-H•••O4, C4-H•••O2 and C8-H•••O4 interactions. Fifty-three interactions stabilise the host conformation while fifteen occur within a methyl glucose unit (C9-H•••O2, C8-H•••O3 and C8-H•••O4). The mean bond length for the C-H•••O interactions is 3.04 Å (range 2.75 – 3.46 Å) while the mean bond angle is 118.9° (range 100.0 – 163.0°).

Host-Host Intermolecular Interactions

TRIB2ME has eleven intermolecular hydrogen bonds which can be divided into seven different C-H•••O interactions. There are three C2-H•••O5 interactions, two C8-H•••O2 and two C8-H•••O3 interactions and one each of C1-H•••O6, C4-H•••O6, C7-H•••O3 and C1-H•••O3 interactions present. The mean hydrogen bond distance is 3.46 Å (range 3.46 – 3.55 Å) while the mean hydrogen bond angle is 154.0° ranging from 134.0 to 174.0°.

GUEST INCLUSION

Guest location

In Figure 4.33 the guest molecule is partially included in the TRIMEB host with the D-ring moiety inserted in the cavity. The A, B and C rings protrude from the secondary rim. The guest is tilted to allow maximum occupation of the TRIMEB cavity and the water molecule present is hydrogen bonded to both host and guest (illustrated and discussed clearly later in text). Figure 4.34 provides a full space-filling diagram of both host and guest in the inclusion complex viewed from both primary and secondary rims.

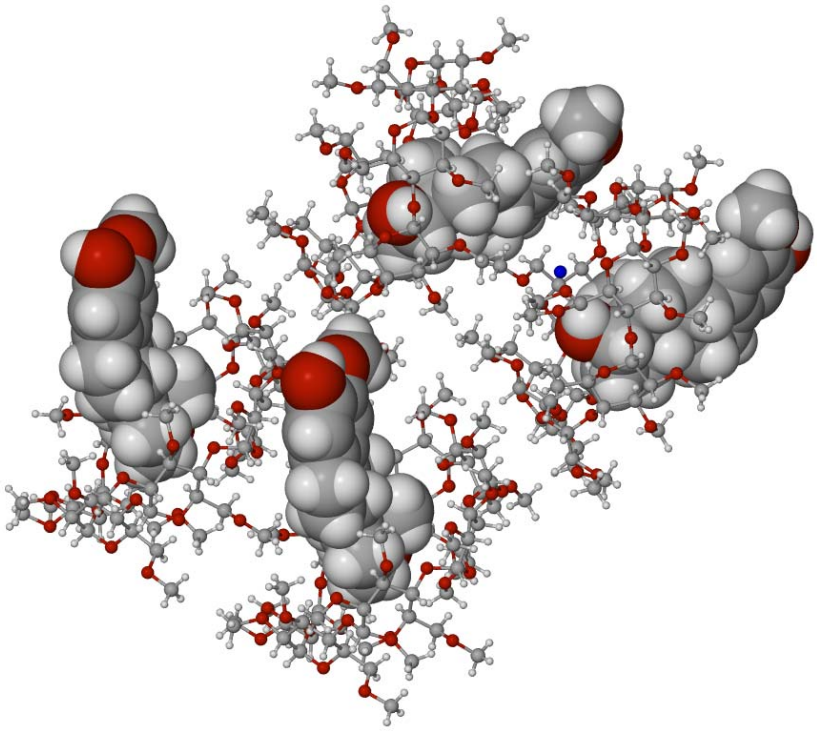

Figure 4.33 Illustration of the asymmetric unit of the TRIB2ME inclusion complex. The guest is viewed in space-filling format and the water molecule included is coloured in blue.

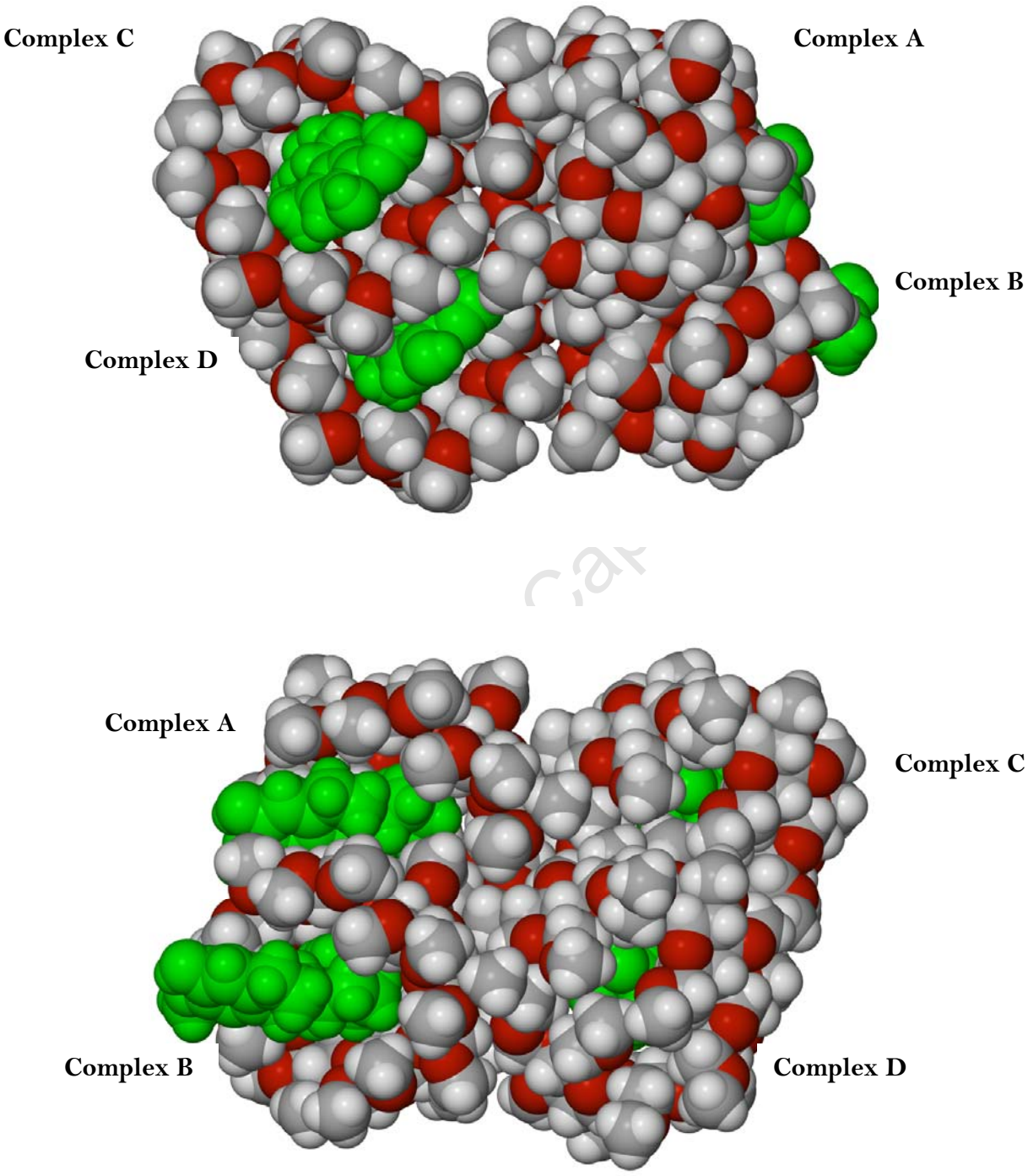

Figure 4.34 The asymmetric unit in space-filling mode: complex units A and B viewed from their primary rims (top) and complex units C and D viewed from their primary rims (bottom). Guest molecules are drawn in green.

Guest conformations

Common selected bond distances and torsion angles of 2ME (Chapter 3), 2ME in the DIB2ME complex and 2ME in the TRIB2ME complex are presented in Table 4.16 for comparison. The differences between corresponding parameters were calculated, with the mean |Δ| presented in the last column of Table 4.16. The relative conformations of the included guest were compared with the uncomplexed guest. There is explicit evidence that the steroid molecules in all instances are practically identical. The remarkable consistency of the steroid molecules in each form indicates rigidity and stability of this arrangement. No significant conformational changes had been effected on 2ME when complexed with TRIMEB. A full set of the molecular parameters is available in Appendix 4 on the CD-ROM provided.

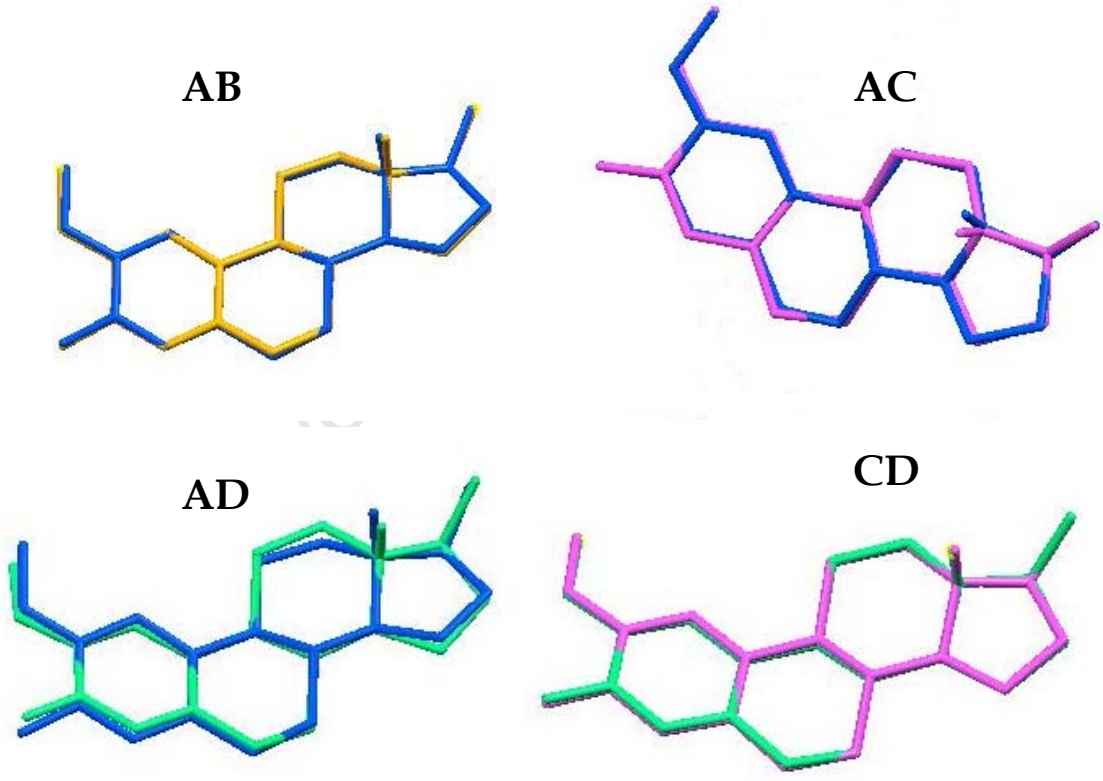

Figure 4.35 Selected overlays of the 2ME molecule encapsulated in TRIB2ME; complex unit A (blue), B (orange), C (pink) and D (green).

Table 4.16 Common selected geometrical parameters for 2ME uncomplexed, 2ME in DIB2ME complex and 2ME in TRIB2ME (complex unit A)

Parameter	2ME uncomplexed	2ME of DIB2ME complex	2ME of TRIB2ME (complex unit A)	Mean |Δ|*
Selected bond distances (Å)				
O19-C17	1.431(3)	1.41(1)	1.44 (1)	0.023
C13-C18	1.540(3)	1.54(1)	1.54(2)	0.003
O20-C2	1.391(3)	1.367(7)	1.38(1)	0.016
O20-C21	1.432(3)	1.425(8)	1.44 (1)	0.011
O22-C3	1.366(3)	1.275(6)	1.38 (1)	0.071
C1-C10	1.408(3)	1.398(7)	1.38(1)	0.021
C8-C9	1.546(3)	1.533(7)	1.56 (1)	0.021
C13-C14	1.541(3)	1.511(7)	1.54(1)	0.02
Selected torsion angles (°)				
C21-O20-C2-C1	-20.6(3)	2.1(8)	6.4(13)	12.3
C21-O20-C2-C3	160.8(2)	-179.0(5)	-176.0(8)	12.1
C15-C16-C17-O19	148.81(2)	144.9(6)	145.3(8)	2.6
C18-C13-C14-C15	-68.9(2)	-67.9(6)	-67.5(9)	0.9
C1-C2-C3-C4	-1.0(3)	-0.2(7)	2.2(14)	1.3
C8-C9-C10-C5	-22.9(3)	-24.3(7)	-44(1)	14.3
C8-C14-C15-C16	-161.8(2)	-165.4(5)	-165.2(8)	2.4

*|Δ| = |2ME-2ME of DIB2ME complex| + |2ME - 2ME of TRIB2ME (complex unit A)| + |2ME of DIB2ME complex - 2ME of TRIB2ME (complex unit A)|/3

HYDROGEN BONDING INTERACTIONS OF THE GUEST

Host-guest Intermolecular Interactions

There are ten host-guest hydrogen bonds in the structure of TRIB2ME (Table 4.17). Six are C-H•••O interactions and four are O-H•••O hydrogen bonds with mean C•••O and O•••O distances of 3.39 and 3.00 Å (ranges 3.25 – 3.53 and 2.87 – 3.18 Å) respectively and mean hydrogen bond angles of 148.5° and 155.8° (ranges 130.0 – 164.0° and 122 - 170°) respectively (Figure 4.36). There are also several host-guest close contacts.

Three of the O-H•••O hydrogen bonds (complex units A, B, C) involve the –OH group on the D-ring of 2ME as donor to a host glycosidic O4 atom (Figure 4.36). In complex D however, the –OH group on the D-ring of the guest is a donor to one of the disordered methoxy O-atoms on residue D5 while the water molecule O1 is a donor to the hydroxyl oxygen atom.

Table 4.17 Host-guest hydrogen bonding interactions for TRIB2ME

Hydrogen bond	H···A (Å)	D···A (Å)	D-H···A (°)	Symmetry codes
O19A- H19A••• O4A2	2.23	3.062(8)	169	
O19B- H19B ••• O4B1	2.35	3.184(8)	170	
O19C- H19C ••• O4C2	2.08	2.890(8)	162	
O22D-H22D ••• O5B5	2.34	2.873(1)	122	-1+x,y,-1+z
C21A- H21B ••• O6D4	2.58	3.531(1)	163	x,1+y,z
C21A- H21C ••• O3B3	2.54	3.253(1)	130	x,1+y,z
C4B -H4B ••• O5B1	2.54	3.467(1)	164	1+x,y,z
C21C - H21I ••• O6D7	2.60	3.521(1)	157	
C7C1- H7C3 ••• O19C	2.49	3.316(1)	142	
C1D5-H1D5 ••• O22D	2.53	3.308(1)	135	1+x,y,z

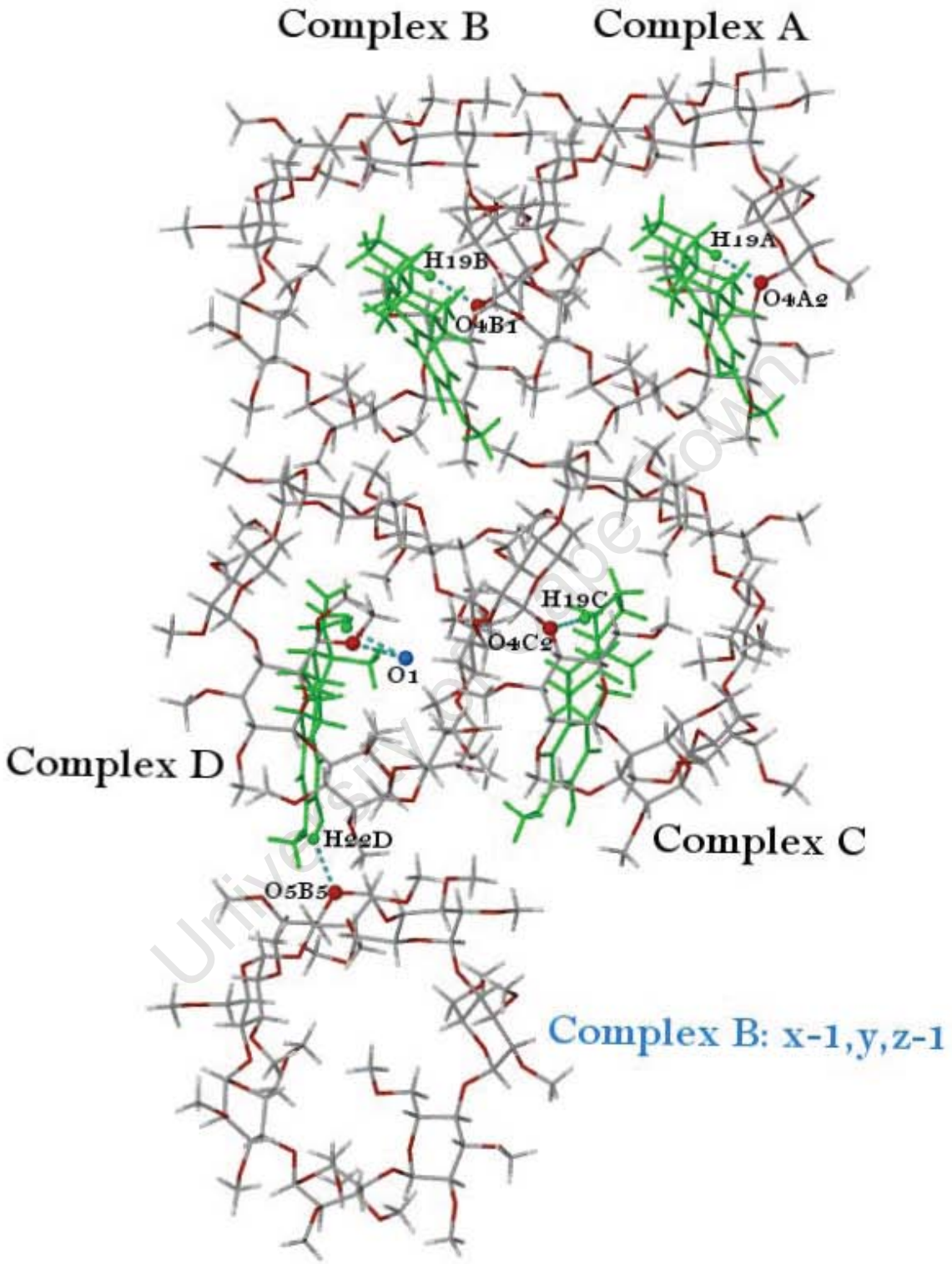

Figure 4.36 TRIB2ME showing the host-guest hydrogen bonds. Hydrogen bonds in red and symmetry operator in light blue.

Guest Intramolecular Interactions

In TRIB2ME four intramolecular hydrogen bonds were observed for the guest (Table 4.18), all four being O-H•••O hydrogen bonds with O•••O lengths in the range 2.68 - 2.72 Å (mean = 2.70 Å) and the hydrogen bond angle ranging from 110.0 to 120.0° (mean = 113.5°). The guest intramolecular interactions stabilise the guest conformation.

Table 4.18 Guest-guest hydrogen bonding interactions for TRIB2ME

Hydrogen bond	H···A (Å)	D···A (Å)	D-H···A (°)
O22B- H22B ••• O20B	2.28	2.722(1)	113
O22C- H22C ••• O20C	2.28	2.695(9)	111
O22D-H22D••• O20D	2.27	2.676(1)	110
C18D- H18J ••• O19D	2.09	2.710(3)	120

Guest-Water interactions

Since there is only one water molecule associated with the very large asymmetric unit, water interactions were minimal. The water molecule makes contact with both guest (O19D-H19D•••O1) and host (O1-H1•••O6D5) (Figure 4.37). There is only one host-water O-H•••O interaction present in TRIB2ME with a O•••O distance 2.65 Å.

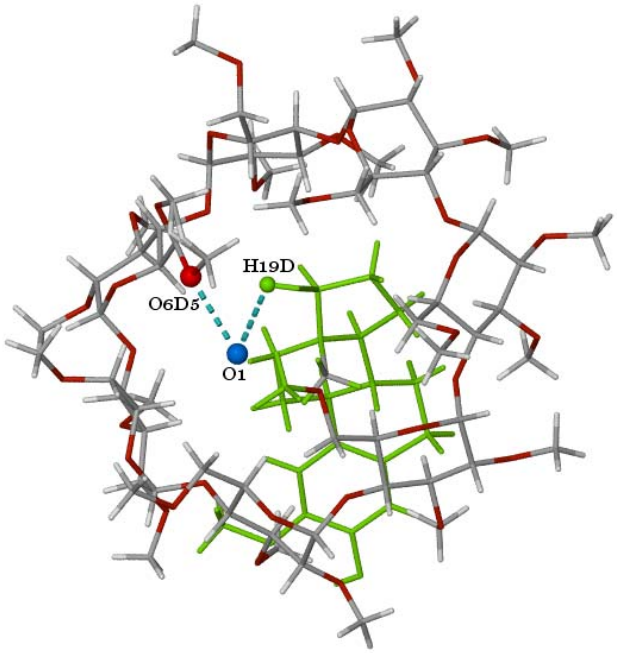

Figure 4.37 The guest-water and host-water hydrogen bonds in complex unit D of TRIB2ME.

Crystal Packing

In Figure 4.38, the cavities are aligned with continuous 'channels' down the crystal a-axis. The packing diagrams serve as visual evidence that the guests are isolated from neighbouring guest molecules while the protruding guest residues are in contact with methine groups of the neighbouring host molecules.

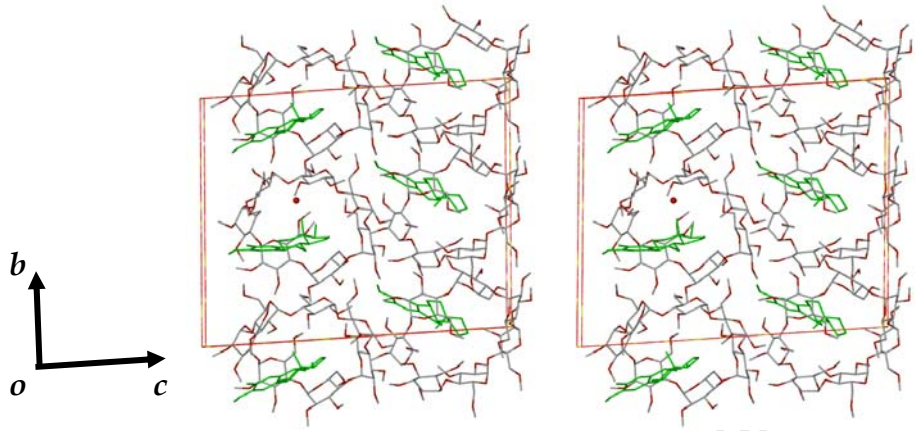

Figure 4.38 Stereoview of packing diagram of TRIB2ME along a.

Experimental and Computed PXRD Traces for TRIB2ME

The match between the experimental and calculated pattern is very convincing (Figure 4.39). Specifically, the relative intensity distributions, numbers and 2θ-values of the peaks in the patterns are in good agreement. This close agreement is an indication of the correctness of the single crystal X-ray structural model. Also, the match proves that the single crystal is representative of the bulk sample.

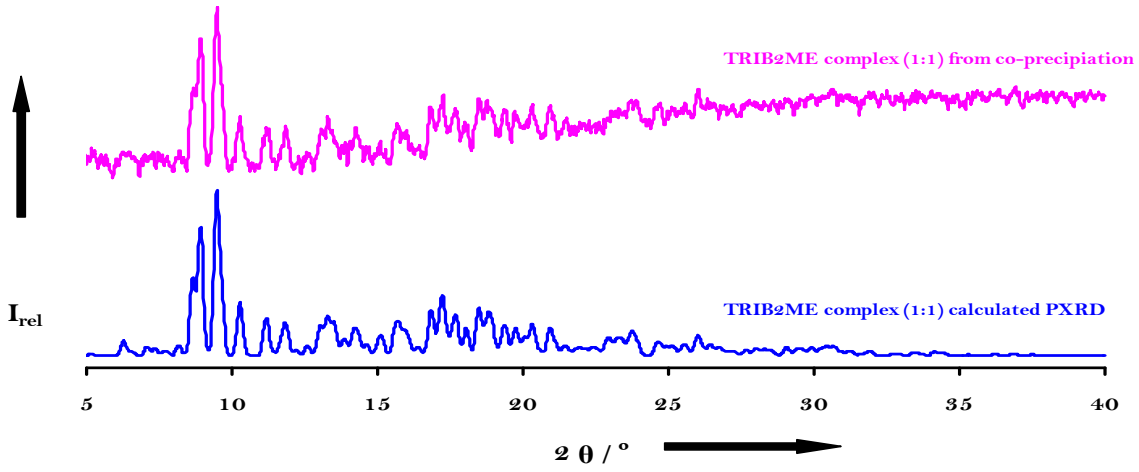

Figure 4.39 Experimental versus calculated PXRD pattern for TRIB2ME.

4.11 SOLUBILITY STUDIES

Solubility Profile of 2ME in the Presence of CDs

The aqueous solubility of 2ME in the presence of CDs was determined experimentally using the following procedure: A solution having a known arbitrary concentration of CD (typically 2%) was prepared by stirring an accurately weighed amount with solvent (distilled water) in a small glass vial till all the CD dissolved at 25 °C. For each CD, 2ME was added in small increments (about 0.0001 g at a time) until saturation occurred. A further increment was added beyond saturation to ensure turbidity (since undissolved solute was important to ensure saturation) of each sample. Samples were firstly analysed turbidimetrically and then 1 ml samples were extracted from each vial for UV analysis. It was important not to replace the solvent removed during sampling since this would drive the system away from equilibrium.

The 1 ml sample of the saturated solution was obtained for analysis by separating it from the undissolved solid. Filtration through a 0.45 μm membrane filter was used and precautions were taken to ensure that it was carried out at the temperature of the solubility determination, in order to prevent any change in the equilibrium between dissolved and undissolved solute. The concentration of 2ME in the saturated solution was determined by UV spectrophotometry at 198 nm. A standard curve of concentration of 2ME versus absorbance was plotted. The concentration of 2ME was subsequently determined from the calibration curve where absorbance was described by calibration curve $y = 0.0345x - 0.2132$ ($R^2=0.9877$), where y=0 and x=0.0005.

Solubility enhancement factors for 2ME by the three parent CDs and eight derivatised CDs were determined by dissolving the steroid in a fixed percentage concentration aqueous solution of each host compound. Relative to 2ME solubility in water (0.005g/L), the enhancement factors obtained at pH 6.8, 25ºC are recorded in Table 4.19. It is noted that the turbidimetric method of analysis could produce skewed results owing to both human error and general light scattering, hence UV analysis was employed as an alternative, possibly more accurate, technique.

Table 4.19 Solubility profile of 2ME in the presence of CD at 25°C*

2ME with	% Concentration of CD in water	2ME added g/5 ml	Enhancement factor of 2ME by UV analysis
α-CD	2% (0.1 g/5 ml)	0.001	7.5 fold
β-CD	2% (0.1 g/5 ml)	0.001	10 fold
γ-CD	2% (0.1 g/5 ml)	0.004	86 fold
RAMEB	2% (0.1 g/5 ml)	0.0035	156 fold
DIMEB	2% (0.1 g/5 ml)	0.0045	256 fold
TRIMEB	2% (0.1 g/5 ml)	0.002	23 fold
HPBCD	2% (0.1 g/5 ml)	0.003	88 fold
TRIMEA	0.5% (0.025 g/5 ml)	0.0015	4 fold
TRiAcBCD	0.001% (0.00005 g/5 ml)	0.003	8 fold
TriAcGCD	0.0025% (0.000125 g/5 ml)	0.001	2 fold
TriEtBCD	0.002% (0.0001 g/5 ml)	0.001	0.84 fold, thus no effect on solubility

* All experiments were compared to a control and repeated 3 times

From the results it was determined that all the CDs except TriEtBCD, improved the solubility of 2ME, due to one or more molecular interactions between 2ME and the particular CD. The modified CDs viz. RAMEB, HPBCD, DIMEB, TRIMEB and the natural CD, γ-CD, very significantly increased the solubility of 2ME. It was evident that DIMEB provided the greatest solubilising effect, possibly owing to its cavity size being optimal for the entrapment of the 2ME molecule. Hence, methylated CDs, with a relatively low molar substitution appear to be the most effective solubilisers. Reduction of drug crystallinity on complexation or solid dispersion with CDs also contributes to the CD increasing the apparent drug solubility and dissolution rate. Therefore, CDs, as a result of their ability to form complexes in the dissolution medium, can enhance drug dissolution, even when there is no complexation in the solid state.

β-CD and its derivative, TriAcBCD, due to their inherently poor water solubility did not improve 2ME solubility markedly. α-CD showed a modest increase in 2ME solubility; however its derivative, TRIMEA, showed a lower solubilising effect.

TriAcGCD produced limited solubility and TriEtBCD showed no improvement in the solubility of 2ME.

Ideally, studies using the phase-solubility method developed by Higuchi and Connors[26] would have provided more insight regarding the influence of a solubiliser, in this instance, the CD, on the drug being solubilised (2ME). However, due to the relatively small mass of 2ME available as a result of the high cost of its synthesis as well as the paucity of especially derivatised CDs, phase solubility studies were not feasible.

4.12 DISSOLUTION PROFILES OF 2ME WITH SELECTED CYCLODEXTRINS

Dissolution studies were conducted using the rotating basket method as described in the BP 2005.[27] Gelatin capsules containing 5-10 mg of the formulation were made. Tests were carried out in the Vankel VK 700 (220 V) dissolution apparatus and with the Vankel VK 650 A Heater/Circulator Benchsaver® series used to regulate temperature at 37 ºC. 900 ml flasks filled with distilled water were used and a stirring speed of 100 rpm was applied. The capsules were enclosed in stainless steel baskets to prevent floating. A 3 h run was conducted and at pre-specified times (15 min intervals) 5 ml samples were withdrawn and filtered for analysis, with 5 ml of the distilled water being replaced to maintain a constant volume. The assay was by UV spectrophotometry at an appropriate wavelength for the active ingredient (198 nm for 2ME).

In vitro dissolution studies were conducted using the rotating basket method as described in the British Pharmacopeia (BP) 2005.[27] The dissolution profiles for the pure drug 2ME, a derivative of 2ME called 2MES (Figure 3.2, Chapter 3), and various preparations involving 2ME with β-CD are shown in Figure 4.40, and with other selected CDs in Figures 4.41 and 4.42.

All of the capsules tested must meet the BP[27] requirements wherein 70% dissolution must be attained and the percentage must be in terms of the *stated* amount. This pharmacopoeial dissolution requirement is regarded as offering an agreeable degree of assurance of 'total dissolution'. A time of 45 min is considered satisfactory for the majority of conventional-release (non-modified-release) products. All dissolution profiles were repeated three times to establish consistency in results.

Statistical methods based on analysis of variance (ANOVA) were used to determine discrimination in dissolution profiles.[28] Anova is a statistical method for making simultaneous comparisons between two or more means. Repeated measures Two Way ANOVA was used to determine how dissolution rate was affected by two factors. The percentage dissolved was the dependent variable and time was the repeated factor.

Dissolution profiles of 2ME, 2MES and various preparations involving 2ME with β-CD.

Figure 4.40 illustrates that the dissolution rate of the BCD2ME inclusion complex was more rapid than that of the uncomplexed drug and its derivative 2MES. The complexed drug reached 100% dissolved drug after 15 min while the 2ME and 2MES samples reached 25-32% and 45-55% respectively after 15 to 180 min. The physical mixtures of 2ME: β-CD (1:1) and (1:2) initially hindered the dissolution of 2ME, possibly due to the fact that β-CD is not very soluble in water at low temperatures, which in this instance was 37°C. The 2:1 ratio further hinders dissolution due to the greater concentration of the β-CD present in each cylinder. Hence, the concentration of the CD definitely affects the dissolution profile of 2ME. After 180 min both physical mixtures reached a 32% dissolution level. The complex prepared by kneading reached 100% after 45 min, which complied with the BP standards.

Statistically significant differences in dissolution rate were observed in the Two Way ANOVA studies. This was confirmed due to the fact that the P value is <0.05 between complexed and uncomplexed material and between complexed material and physical mixtures.

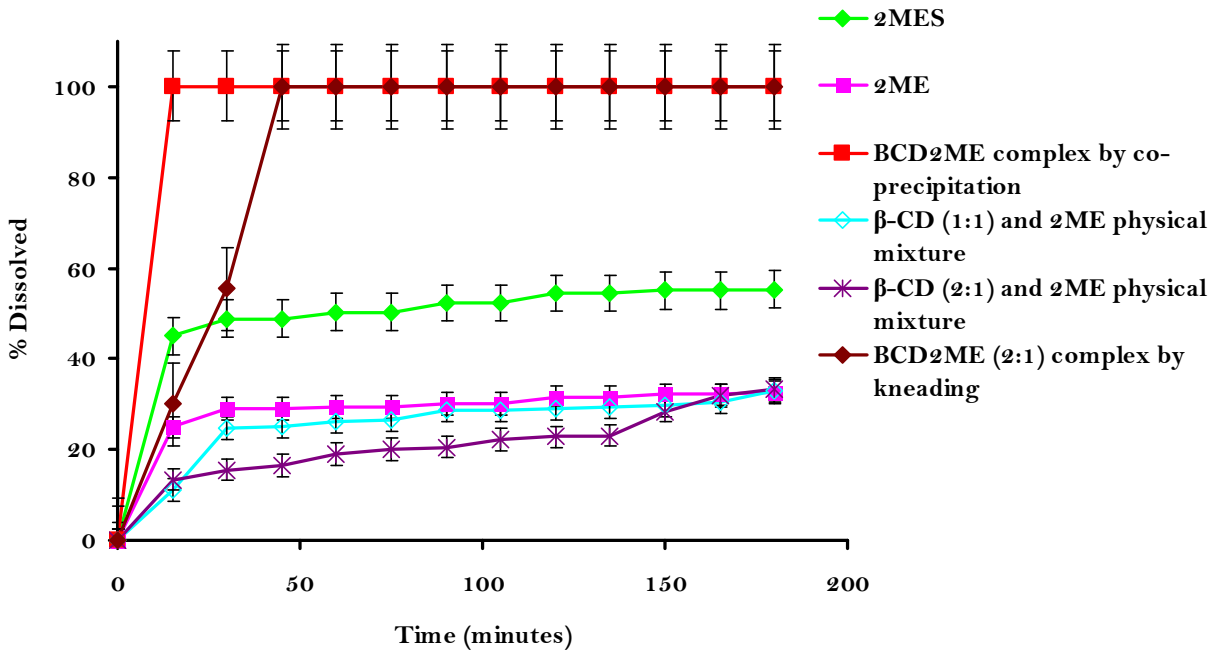

Figure 4.40 Dissolution profile of 2ME, 2MES and various preparations involving 2ME with β-CD.

Dissolution Profiles of 2ME, 2MES and Various Preparations Involving 2ME with β-CD and Other Selected CDs.

Figure 4.41 illustrates the dissolution profiles of 2ME versus 2MES versus 2ME/CD physical mixtures. The dissolution profile of 2ME improved significantly in the presence of nearly all selected CDs. The γ-CD (1:1) physical mixture produced the most rapid increase in dissolution with the first withdrawal of sample. The rate of dissolution even surpassed the dissolution profile of 2MES. RAMEB (1:1) physical mixture improved the profile of 2ME only after 45 min and α-CD (1:1) improved the profile after 75 min. HPBCD (1:1) and β-CD (1:1 and 2:1) physical mixtures initially had a poor dissolution profile compared to 2ME but later equalised the profile after the 3h run.

CDs are able to dissolve rapidly in the dissolution medium, in comparison to the pure drug, 2ME. Therefore, it can be assumed that in the early stages of the dissolution process, the CD molecules will act locally on the hydrodynamic layer surrounding the particles of the drug. The former results in a rapid increase in the amount of drug dissolved.

From the results, it was found that 30% of the pure 2ME drug went into solution within 20 min. The physical mixture of 2ME and γ-CD (1:1) showed that ~55 % of the 2ME dissolved within the same time as the former. As the time progressed, the physical mixture of 2ME and γ-CD (1:1) exhibited an increase in the percentage of 2ME dissolving, with the final percentage concentration reaching 80% within 3 h. Therefore, of all the physical mixtures studied, the γ-CD (1:1) mixture may be pharmaceutically useful in the production of controlled release preparations.

Furthermore, the physical mixture of 2ME and RAMEB (1:1) exhibited a 10% improvement in the dissolution characteristics of 2ME. At the end of the 3 h dissolution run, approximately 40% of 2ME had dissolved. In contrast, the physical mixtures of β-CD with 2ME (1:1 and 2:1) and HPBCD with 2ME (1:1), did not significantly affect the dissolution characteristics of 2ME, as the same percentage as that of the pure drug was dissolved in the dissolution medium at the end of the dissolution run.

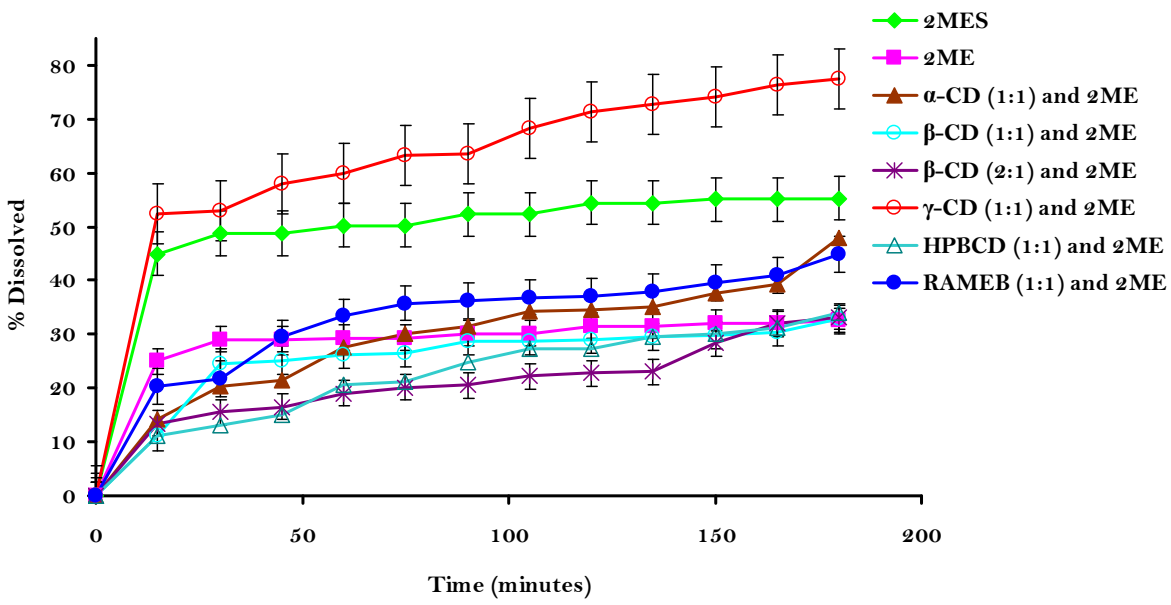

Figure 4.41 Dissolution profile of 2ME vs 2MES vs 2ME/CD physical mixtures.

In Figure 4.42 we illustrate the dissolution profile of 2ME/CD kneaded materials versus BCD2ME co-precipitated complex. It is evident from Figure 4.42 that when a drug/CD system is dispersed in a dissolution medium, a very rapid dissolution is observed. Rapid dissolution is a key characteristic behaviour of inclusion complexes. Kneading was found to be the most suitable method in the preparation of inclusion complexes for the selected parent and derivatised CDs α-, β-, γ-, RAMEB and HPBCD. Superior dissolution properties of the material prepared by kneading with γ-CD and RAMEB showed 100 % of the drug concentration being achieved within 15 min of the dissolution run (Figure 4.42). Similarly, the BCD2ME complex (2:1) prepared by co-precipitation exhibited identical behaviour to the former material prepared by kneading. In contrast, for the 2ME/β-CD (1:1) material prepared by kneading, complete dissolution was only reached at 45 minutes.

For the remaining kneaded systems containing α-CD and HPBCD, 100 % drug concentration was only attained at 105 and 90 min respectively (not clearly depicted in Figure 4.42 due to overlap of dissolution curves). Hence, the material made by kneading and the co-precipitated complex all resulted in improved dissolution properties of 2ME (compared to only 30 % of pure, uncomplexed 2ME dissolved within 20 min). From

theory,[29] it was proposed that dissolution rates of drug/CD systems depend on the diffusion and dissociation of the complex in the dissolution medium and increased wettability of the drug by inclusion complexation which, in this instance, is the possible mechanism for better dissolution of 2ME.

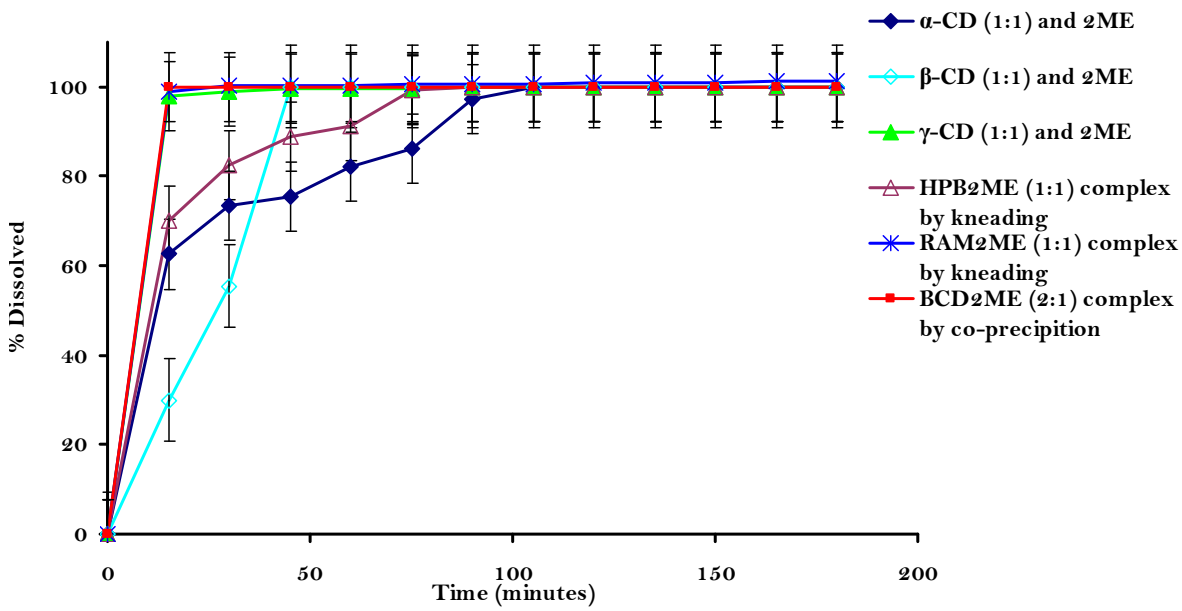

Figure 4.42 Dissolution profile of 2ME/CD kneaded material vs 2MEBCD complex. γ-CD and 2ME (lime) and RAM2ME (blue) not clearly evident in figure due to overlap with BCD2ME illustrated in red.

Statistically significant differences in dissolution rate when comparing definitive 2ME complexes with β-CD, HPBCD, RAMEB and those preparations obtained from kneading with α- and γ-CD were observed in the Two Way ANOVA studies. This was confirmed due to the fact that the P value is <0.0001. Application of Two Way ANOVA analysis indicated that the CDs had a significant influence on the initial release of drug within 15 min from the gelatin capsule ($P<0.05$). Subsequent application of one-way ANOVA, keeping the levels of 2ME fixed, also showed a statistically significant difference amongst the observed data for dissolution rate ($P<0.05$), ratifying the significant positive influence of each CD on the dissolution profiles presented.

4.13 CONCLUSION

The intention of this chapter was to give an account of the preparation and characterisation of inclusion complexes between 2ME and selected cyclodextrins. The reactions of 2ME with β-CD, RAMEB and HPBCD using the kneading method produced cyclodextrin inclusion complexes BCD2ME, RAM2ME and HPB2ME. The reaction of 2ME with β-CD, DIMEB and TRIMEB by means of co-precipitation yielded the cyclodextrin inclusion complexes BCD2ME, DIB2ME and TRIB2ME. Single crystal X-ray analysis of complex BCD2ME was partially successful; the host structure was completely determined but details of the location of the 2ME guest molecule could not be established due to its severe disorder. Instead, the structures of the DIB2ME and TRIB2ME complexes were successfully determined, no guest disorder being observed in either case.

The physicochemical characterisation of the cyclodextrin inclusion complexes in the solid state commenced via single crystal X-ray diffraction, powder X-ray diffraction (PXRD), TGA, DSC, HSM and UV spectrophotometry. Furthermore, both mixtures and complexes of 2ME with CDs were analysed with regard to solubility and their dissolution profiles. HSM, TGA and DSC provided evidence for the thermal stability of the complexes while UV spectrophotometry was used to establish the stoichiometry of the solid-state complexes. PXRD provided proof that the bulk material was the same phase as the crystals selected for single crystal X-ray diffraction.

Literature reports of single crystal X-ray analysis of cyclodextrin inclusion complexes of steroids are rare. To date, there is only one known single crystal X-ray structure elucidation of a CD/steroid complex, where the steroid rocuronium bromide is complexed with 6-perdeoxy-6-per(4-carboxyphenyl)thio-γ-cyclodextrin sodium salt.[4] The CD is a very rare one and the steroid in this instance is also atypical with significant chemical modification compared to the classical steroid molecules. It is thus important to emphasise the significance of the novel CD/2ME crystal structures reported here. We report the isolation of a total of five new cyclodextrin inclusion complexes of 2ME, including one with each of β-CD, RAMEB, HPBCD, DIMEB and TRIMEB.

The two crystal structures reported here (DIB2ME and TRIB2ME) display no guest disorder. However, in both instances we report on minor host disorder. Both structures displayed essentially the same mode of guest inclusion, with the D-ring of the guest included within the host cavity.

For BCD2ME, the principles of isostructurality were used in the identification of the complex prepared by kneading. Its PXRD pattern matched that of the complex with CSD refcode KOFJEU.[16] This enabled prediction of the space group as well as approximate unit cell dimensions of the complex in the absence of high quality single crystal X-ray data. The best crystal of BCD2ME available yielded partial solution by X-ray analysis, but the guest molecule was severely disordered, as mentioned above. Nevertheless, the BCD2ME inclusion complex was otherwise fully characterised.

Solubility studies determined that all the CDs included in the study, except TriEtBCD, improved the solubility of 2ME, due to one or more molecular interactions between 2ME and the particular CD. Dissolution studies presented markedly improved profiles for 2ME as mixtures with selected CDs, complexes prepared by kneading and the co-precipitated complex.

Finally, the objectives of this study were achieved, namely the preparation of cyclodextrin inclusion complexes of 2ME via kneading and co-precipitation methods as well as their physicochemical characterisation. Structural elucidation by X-ray diffraction of CD inclusion complexes of a classical steroid was achieved for the first time and more importantly, from an application perspective, solubility and dissolution profiles of non-toxic oral CD complexes with 2ME versus untreated 2ME and its derivative 2MES, were established.

4.14 REFERENCES

1. Del Valle M.E., *Process Biochem.*, **2004**, 39, 1033-1046.
2. The Medical News, *Panzem (2-methoxyestradiol) Drug a Possible Candidate for Breast Cancer Treatment*, November, **2007**, retrieved 20 December **2008**, http//www.news-medical.net/news/2007/11/02/32073.aspx?page=2.
3. Stella V.J., Rajewski R.A., *Pharm. Res.*, **1997**, 14, 556-567.
4. Cooper A., Nutley M., MacLean E.J., Cameron K., Fielding L., Mestres J., Palin R., *Org. Biomol. Chem.*, **2005,** 3, 1863-1871.
5. Saenger W., C*arbohydr. Res.*, **1996**, 282, 53-63.
6. Martini A., *Drug Dev. Ind. Pharm.*, **2009**, 20, 2381- 2393.
7. Coussement W., Van Cauteren H., Vandenberghe J., Vanparys P., Teuns G., Lampo A., Marsboom R., Toxicological Profile of HP-β-CD in Laboratory Animals. In: Duchêne D. (Ed.), *Minutes 5th International Symposium on Cyclodextrins, Editions de Sante:*, **1990**, 552-524.
8. Abbott P.J., *Safety Evaluation of Certain Food Additives and Contaminant. International Programme on Chemical Safety Miscellaneous Substances (IPCS)*, Fifty – Fist Meeting of the Joint FAO/WHO Expert Committee on Food Additives (JEFCA), **2000**, retrieved June **2008,** http://www.inchem.org/document/jefca/jecmono/v042je11.htm.
9. Piel G., Piette M., Barillaro V., Castagne D., Evrard B., Delattre L., *J. Incl. Phenom. Macrocycl. Chem.*, **2007**, 57, 309-311.
10. Scalia S., Villani S., Casolari A., *J. Pharm. Pharmacol.*, **1999,** 51, 1367.
11. Ulloth J.E., *Neurotoxicology*, **2007**, 28, 613-621.
12. Fenyvesi É, Otta K., Kolbe I., Novák C.S., Szejtli J., *J. Incl. Phenom. Macrocycl. Chem.*, **2004**, 48, 117-123.
13. Eastburn S.D., Bernard Y., *Biotech. Adv.*, **1994**, 12, 325-339.
14. Le Xin S., Xue Qing G., Zheng D., Mang W., *Macrocycl. Chem.*, **2010**, 87-127.
15. Caira, M.R., *Rev. Roum. Chim.*, **2001**, 46, 371-386.
16. Cambridge Structural Database and Cambridge Structural Database System, Cambridge Crystallographic Data Centre, University Chemical Laboratory, Cambridge England, Version 5.30, **2009**.

17. Dodziuk H. (Ed.), *Cyclodextrins and their complexes. Chemistry, Analytical Methods, Applications*, WILEY-VCH Verlag GmbH & Co. KGaA, Weinheim, **2006**.

18. Rao P.N., Cessac J.W., *Steroids*, **2002,** 67, 1065-1070.

19. Barbour L. J., LAYER, *J. Appl. Cryst.*, **1999**, 32, 351.

20. Sheldrick G.M., *In: Direct Methods for Solving Macromolecular Structures*, Fortier S. (Ed.), Dordrecht: Kluwer Academic Publishers, **1998**, 401-411.

21. Sheldrick G.M., SHELXH, *Program for Crystal Structure Solution*, Institüt für Anorganische Chemie der Universität, Tammanstrasse 4, D-3400 Göttingen, Germany, **1997**.

22. Spek A.L., PLATON, *A Multipurpose Crystallographic Tool*, Version 10500 © **1980-2009**.

23. Caira M.R., Griffith V.J., Nassimbeni L.R., van Oudtshoorn B., *J. Incl. Phenom. Mol. Recognit. Chem.*, **1995**, 20, 277-290.

24. Data Preparation and Reciprocal Space Exploration, Version 5.1, (Copyright Bruker Analytical X-ray Systems, **1997**)

25. Sheldrick G.M., SHELXS-97, *Program for Crystal Structure Solution*, Institüt für Anorganische Chemie der Universität, Tammanstrasse 4, D-3400 Göttingen, Germany, **1997**.

26. Higuchi T., Connors K.A., *Adv. Anal. Chem. Instr.*, **1965**, 4, 212-217.

27. British Pharmacopoeia, British Pharmacopoeia Commission Secretariat, London, UK, **2005**.

28. Gonjari I.D., Karmarkar A.B., Hosmani A. H., *Dig. J. Nanomat. Biostruc.*, **2009**, 4, 651-661.

29. Rajewski R.A., Stella V.J., *J. Pharm. Sci.*, **1996**, 85, 1142-1168.

Chapter 5

CO-CRYSTALLISATION of NEVIRAPINE with GRAS EXCIPIENTS

Chapter 5 *presents the results of the co-crystallisation experimentation of nevirapine (NV) with selected co-formers having complementary donor and/or acceptor functions. It describes the preparation of NV co-crystals and their physicochemical characterisation. The investigation of the dissolution characteristics of the NV co-crystals using the BP dissolution method as discussed in Chapter 2 is illustrated as well. From the results it is evident that the two co-crystals eventually prepared had a significant impact on the nevirapine 'as received' upon comparison of the pharmaceutically relevant physicochemical characteristics viz. melting point, solubility and dissolution profile.*

5.1 INTRODUCTION

Chapter 1 reviewed NV, a potent inhibitor of HIV-1 reverse transcriptase (Figure 5.1), as a unique candidate for co-crystallisation experimentation. The existence of the amide function CO–NH in the NV molecule indicates the possibility of alternative modes of self-association, namely via a dimer or catemer supramolecular synthon, which could lead to crystal polymorphism, whereas interaction with solvent molecules having complementary donor and acceptor functions could result in the formation of solvates. Furthermore, interaction of the NV molecule with molecules that are solid at ambient temperature and have complementary donor and acceptor functions, could result in the formation of co-crystals.

Twelve compounds were chosen for this study as potential co-formers with nevirapine viz. saccharin, nicotinamide, isonicotinamide, succinic acid, tartaric acid (racemic, as well as D and L individually), citric acid, oxalic acid, stearic acid, L-aspartic acid and maleic acid. These formers were chosen based on the presence of their carboxylic acid and/or other potentially complementary functionalities, and because they appear on the GRAS ('generally regarded as safe') list. Figure 5.1 illustrates the structures of NV and the 12 co-crystal formers selected for this study. Table 5.1 provides the melting point data, uses and solubility of NV and the 12 co-formers selected. An evaluation of both the API and co-crystal formers was carried out, including but not limited to, number and arrangement of hydrogen bond donors and acceptors, salt forming ability, conformational flexibility and solubility requirements.

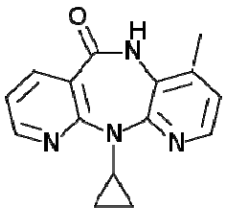

1

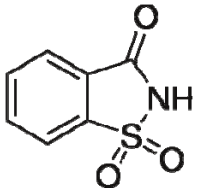

2

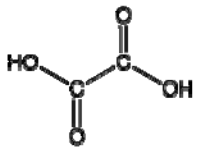

3

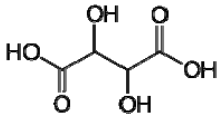

4

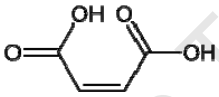

5

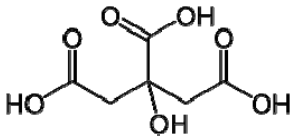

6

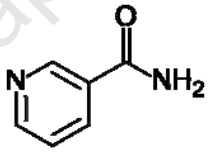

7

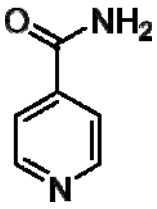

8

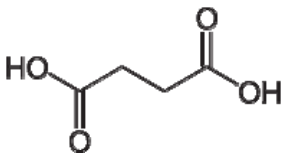

9

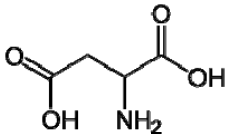

10

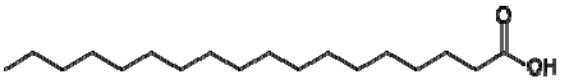

11

Figure 5.1 Structures of NV and 10 co-crystal formers included in study: (1) nevirapine (2) saccharin, (3) oxalic acid, (4) tartaric acid, (5) maleic acid, (6) citric acid, (7) nicotinamide, (8) isonicotinamide, (9) succinic acid, (10) L-aspartic acid, (11) stearic acid.

Table 5.1 Physical properties of NV and co-crystal formers

Compound	Molecular formula	Mp (°C)	Uses	Solubility in water, pH 7, 25°C
Nevirapine	$C_{15}H_{14}N_4O$	247-249	Antiretroviral agent	0.1 mg/mL, (highly soluble at pH < 3)
Saccharin	$C_7H_5NO_3S$	228.8-229.7	Artificial sweetener	1000 mg per 290 mL
Tartaric acid (Racemic mixture, *D* and *L*)	$C_4H_6O_6$	171-174 (D- and *L*-tartaric) 206 (*DL*, racemic) 146–148 (*meso*)	Antioxidant	1390 mg/mL (D- and L-) and 206 mg/mL racemic
Citric acid (as the monohydrate)	$C_6H_8O_7 \cdot H_2O$	135-152	Preservative, and adds acidic or sour taste to foods	1630 mg/mL
Stearic acid	$C_{18}H_{36}O_2$	69.6	Emollient	Sparingly soluble
Oxalic acid	$C_2H_2O_4$	101-102	Cleaning and bleaching agent	143 mg/mL
Maleic acid	$C_4H_4O_4$	131-139	Compound used for making maleate salts of bulk-drugs and prevents rancidity in oils	780 mg/mL
Nicotinamide	$C_6H_6N_2O$	129-131	Vitamin B3	1000 mg/mL
Isonicotinamide	$C_6H_6N_2O$	155-158	Co-crystal former	191.7 mg/mL
Succinic acid	$C_4H_6O_4$	185-187	Flavourant	76.9 mg/mL
L-Aspartic acid	$C_4H_7NO_4$	270-271	Amino acid	4 mg/mL

Characterisation of Nevirapine

The sample of NV used was a gift from North-West University (Potchefstroom, South Africa), originally supplied by Cipla Ltd. (batch 1001003, Mumbai, India). The University of Cape Town was commissioned to synthesise co-crystals of NV, for which this study represented the initial phase. A more extended project in this area continues within the Centre for Supramolecular Chemistry Research at the University of Cape Town for further identification of co-crystals. For the purposes of this study a 7 g batch of NV was provided and its purity confirmed by ^{1}H-NMR analysis. The result of C, H and N microanalysis for NV is listed in Table 5.2. The experimental values for NV agree with the calculated values within experimental error, thus showing a high degree of purity.

Table 5.2 Microanalysis for NV ($C_{15}H_{14}N_4O$)

Experimental (n=3)			Calculated		
%C	%H	%N	%C	%H	%N
67.48	5.52	20.85	67.65	5.30	21.04

Many experiments, using different techniques and a wide variety of recrystallisation solvents, were performed in order to isolate new co-crystals of NV. Some representative results are listed in Table 5.3 and a full listing appears in Appendix 3 on the attached CD-rom. In the table, the following abbreviations are used for simplicity: nevirapine (NV), saccharin (SC), oxalic acid (OA), tartaric acid (TTA-D, TTA-L and TTA-DL), maleic acid (MA), citric acid (CA), nicotinamide (NC), isonicotinamide (ISNC), succinic acid (SUC), L-aspartic acid (ASP) and stearic acid (STA).

Table 5.3 Selected results of attempted co-crystal preparation using various methods

Method 1[a]: Slow evaporation (192 solvent combinations with varying ratios)				
Drug	**Co-former**	**Solvent**	**Molar ratio NV:co-former**	**Result**
NV	SC	Acetonitrile	1:1	NV
		Methanol	2:1	**Co-crystal 1 (NVSC)**
		Diethyl ether	2:1	Co-crystal 1
	ISNC	n-hexane	1:1	No crystal
		n-heptane	1:1	Mixture
		THF	1:2	ISNC
	NC	Methanol	1:1	NV
		Carbon tetrachloride	1:1	NV carbon tetrachloride solvate
	SUC	Ethyl acetate	1:1	NV
		Methanol	1:1	**NV methanol solvate**
		Acetonitrile	1:1	NV hydrate
	TTA-(DL)	Diethyl ether	1:1	NV diethyl ether solvate
		Toluene	1:1	NV toluene solvate
		Amyl alcohol	1:1	**Co-crystal 2 (NVTTA)**
	CAM	Chloroform	1:1	NV
Method 2[b]: Neat grinding (manual grinding with varying ratios)				
Drug	**Co-former**	**Molar ratio NV:co-former**		**Result**
NV	SC	1:1		Mixture
		2:1		NV
Method 3[b]: Solvent-drop grinding (manual grinding with varying ratios)				
Drug	**Co-former**	**Molar ratio NV:co-former**	**Solvent**	**Result**
NV	SC	1:2	Ethanol 1 ml	Mixture
	ASP	1:2	Ethanol 1 ml	Mixture
	NC	1:2	Ethanol 1 ml	Mixture

[a]Products obtained by method 1 were analysed by HSM, single crystal X-ray diffraction and PXRD to determine bulk consistency. [b] Products obtained by methods 2 and 3 were analysed by PXRD.

NOTE: Vapor diffusion was employed when crystals from slow evaporation were too small for diffraction purposes.

5.2 PREPARATION OF NEVIRAPINE CO-CRYSTALS

For the most part, experimental methods comprised recrystallisation of solutions containing mixtures of the components (NV plus potential co-former) from a wide range of single solvents and binary solvent systems at different temperatures and solid-state co-grinding. With regard to the two co-crystals produced in this study, the following procedures were established as a means of reproducible co-crystal formation, with specific differences listed accordingly.

Preparation of NVSC and NVTTA Co-crystal

For **NVSC**, 0.076 mmol (20 mg) NV and 0.038 mmol SC (6.7 mg) were weighed and each solid was separately dissolved in minimum volumes of methanol at ~10 ºC below the b.p. of the solvent. The solution of greater volume was added to that of smaller volume and the resultant solution magnetically stirred for ~30 min, filtered (0.45 µm) and allowed to crystallise at 20 ºC.

For **NVTTA**, an analogous procedure was used. 0.038 mmol (10 mg) NV and 0.038 mmol TTA (5.7 mg) were weighed and each solid was separately dissolved in minimum volumes of solvent (amyl alcohol) at ~10 ºC below its boiling point. Again filtration and crystallisation were performed as described above.

5.3 THERMAL ANALYSES

Hot Stage Microscopy

HSM was used to analyse the thermal behaviour of the two co-crystals upon heating at a constant rate of 10 K/min. Single crystals of the two materials were immersed in silicone oil and photographs were taken in the temperature range 30 ºC to 350 ºC. These HSM pictures are presented in Figure 5.2. The analysis was done under silicone oil to assess the presence of included water or organic solvent as would be indicated by bubble formation. The photographs of **NVSC** and **NVTTA** were recorded at (a) start of analysis, (b) the first sign of melting, (c) completion of melt (d) the onset of decomposition (indicated by colour change of the crystals to brown or spontaneous bubbling). From the photographs, **NVSC** starts to melt at 223 ºC and decomposes at 315 ºC. **NVTTA** melts at 228 ºC and decomposition occurs from 240 ºC.

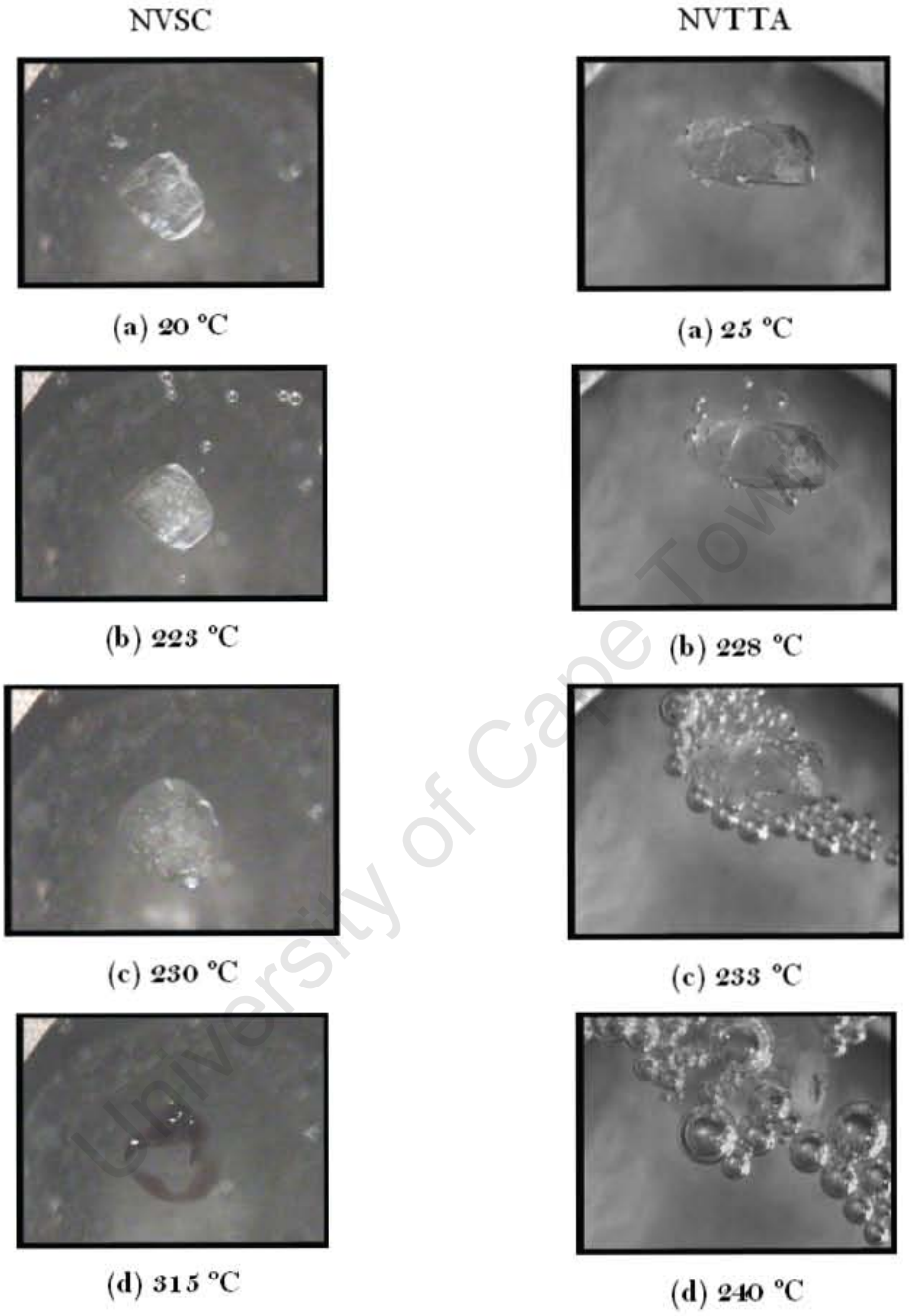

Figure 5.2 HSM photographs of NVSC and NVTTA.

Differential Scanning Calorimetry and Thermogravimetric Analysis

TGA was used to determine the possible presence of included solvent in the crystals of **NVSC** and **NVTTA**. In neither case did the TGA trace reveal significant mass loss prior to degradation at high temperatures, thus confirming that these crystals were unsolvated.

The DSC trace for **NVSC** (Figure 5.3) indicated a melting point at 223 ºC with a single endotherm [215-230 ºC]. The DSC trace for **NVTTA** (Figure 5.3) indicated a melting point at 230 ºC with an endotherm appearing between 221 and 236 ºC. In both instances the DSC data correspond well with the HSM observations. Furthermore, both of the melting points differed significantly from that of the parent API, NV (melting point 247-249 ºC) and that of the co-crystal formers SC (melting point 228-229 ºC) and TTA-DL (melting point 206 ºC). However, the melting point of **NVSC** was lower than those of either of the two parent compounds which might suggest lower stability or weaker intermolecular forces and therefore greater dissolution rate than untreated NV and SC. For **NVTTA**, the melting point appeared between those of NV and TTA-DL, possibly indicating greater stability or stronger intermolecular forces and consequently, lower dissolution rate than **NVSC**. Furthermore, the **NVTTA** melting point also suggested lower stability than NV but greater stability than TTA-DL which suggests greater dissolution rate than untreated NV.

For **NVTTA**, a second endotherm [103-114 ºC] was identified. The endotherm was extremely small and was not observed by HSM, but its origin was not pursued. Degradation of **NVSC** commenced from 315 ºC whereas for **NVTTA** degradation commenced soon after melting [240 ºC] which also corresponded well with HSM observations.

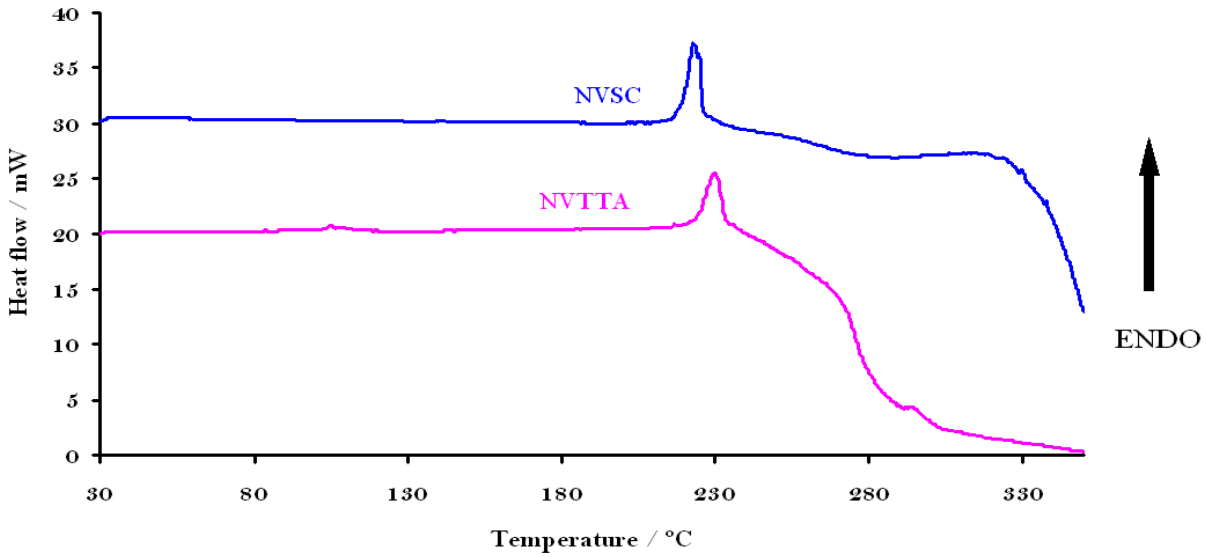

Figure 5.3 DSC of NVSC and NVTTA co-crystals.

5.4 MICROANALYSIS

The result of C, H and N microanalysis for **NVSC** and **NVTTA** is listed in Table 5.4. The experimental values for both co-crystals agree closely with the calculated values, therefore confirming their purity.

Table 5.4 Microanalysis for NVSC [2($C_{15}H_{14}N_4O$)•$C_7H_5NO_3S$] and NVTTA [$C_{15}H_{14}N_4O$•$C_4H_6O_6$]

Co-crystal	Experimental (n=3)				Calculated			
	%C	%H	%N	%S	%C	%H	%N	%S
NVSC	61.73	4.77	17.88	4.62	62.08	4.65	17.61	4.48
NVTTA	54.59	5.02	13.39	-	54.80	4.84	13.46	-

5.5 EXPERIMENTAL PXRD

First, we note in Figure 5.4 that the PXRD pattern labelled NV:SC (2:1) methanol, which is that of the material prepared according to the procedure described in 5.2 above, is significantly different from the PXRD curves of the starting components NV and SC. This is consistent with the evidence from thermal analysis that this species is a co-crystal. Secondly, we note that this PXRD pattern closely matches those for the

products obtained by the same procedure, except that solvents chloroform and acetic acid were employed instead of methanol. Other solvents that produced the same co-crystal phase include 1,4-dioxane, n-hexane, n-heptane, diethyl ether and amyl alcohol. It was of interest to note that solvent choice was not a critical parameter for the preparation of the **NVSC** co-crystal. For consistency, the **NVSC** co-crystal prepared using methanol as solvent is the one that was chosen for all subsequent analyses.

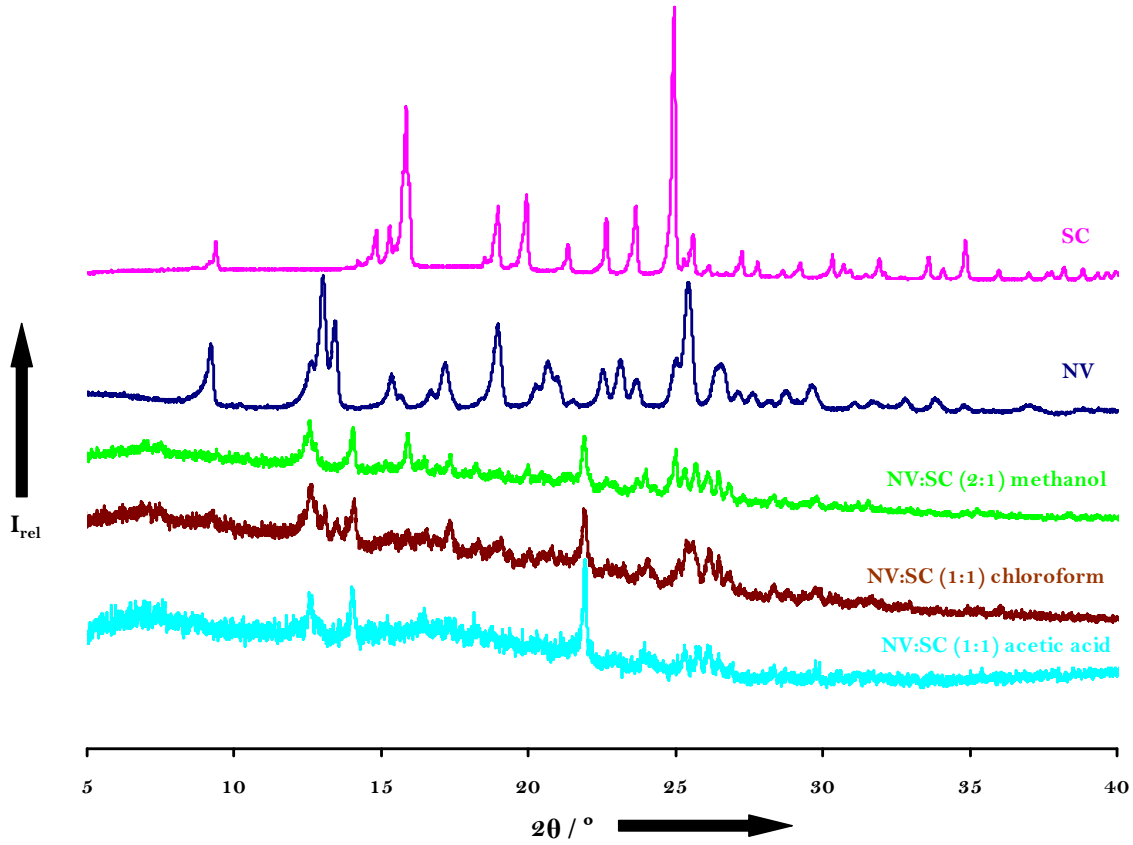

Figure 5.4 Experimental PXRD pattern of co-crystal NVSC and patterns of the individual co-crystal components NV and SC.

The PXRD pattern for the **NVTTA** co-crystal (Figure 5.5) likewise differs very significantly from those of the components NV and TTA (DL), strongly suggesting the presence of a new phase. Several other solvents were tested for co-crystal formation but no solvent other than amyl alcohol yielded **NVTTA**.

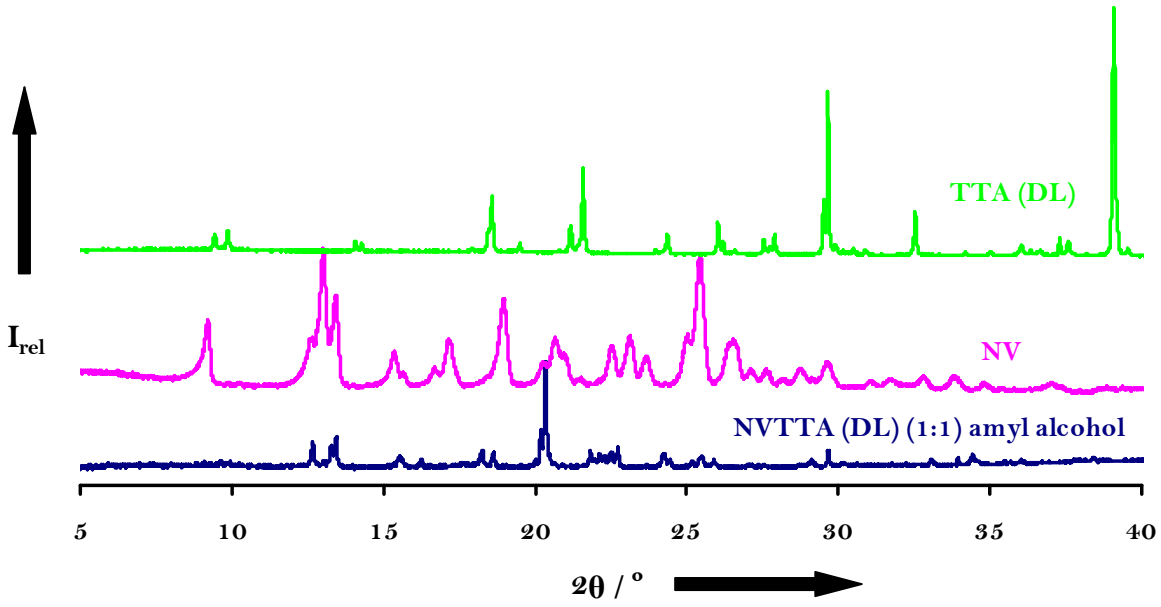

Figure 5.5 Experimental PXRD pattern of co-crystal NVTTA and patterns of the individual co-crystal components NV and TTA (DL).

5.5. X-RAY CRYSTALLOGRAPHIC ANALYSES OF NVSC AND NVTTA

Data-collection

Diffraction intensities were collected on a Nonius Kappa CCD diffractometer using graphite-monochromated MoKα radiation at low temperature (-160 ºC). Unit cell determinations were performed at both room temperature (21 ºC) and low temperature (-160 ºC) to ensure that no phase changes were effected on cooling the crystals. The program XPREP[1] was used to determine the space groups of **NVSC** and **NVTTA**.

For **NVSC,** Laue symmetry $\bar{1}$ was indicated for the collected intensity data, thus confirming the triclinic crystal system and thus implying space group P1 or P $\bar{1}$. Intensity statistics provided by XPREP[1] showed $|E^2-1| = 1.035$ for **NVSC** indicating the centrosymmetric space group P $\bar{1}$. This choice was justified by the successful solution and refinement of the structure in this space group.

Laue symmetry 2/m for **NVTTA** was confirmed for the collected intensity data, thus indicating the monoclinic crystal system. The space group $P2_1/c$ was indicated by the reflection conditions hkl: none; h0l: l=2n; 0k0: k=2n. No disorder problems were

encountered for either structure and the final R1 [$F_o > 4\sigma(F_o)$] values were 0.0468 and 0.0355 for **NVSC** and **NVTTA** respectively.

Structure Solution and Refinement

NVSC includes two NV molecules and one SC molecule in the crystal asymmetric unit (ASU) whereas **NVTTA** contains one NV and one TTA molecule in the ASU. The program SHELXS-97[2] was used for the structure solution of **NVSC** and **NVTTA.** Direct methods revealed the positions of all the non-hydrogen atoms in the respective asymmetric units and allowed their placement. All non-hydrogen atoms were refined isotropically on F^2 with SHELXL-97[3] and subsequently with anisotropic thermal parameters. Special attention was given to H-atom placement, given the co-crystal context. All hydrogen atoms were unequivocally located in difference electron density maps and were subsequently placed in fixed geometric positions using a riding model and were refined istropically. U_{iso} values for the aromatic hydrogens were 1.2 times those of the parent atoms and all methyl hydrogens were given thermal parameters 1.5 times the U_{iso} of the parent atom.

Atomic numbering schemes are shown in Figures 5.6 and 5.7. NV has one donor (N2) and three acceptors (O8, N12, N13), SC has one donor (N21) and three acceptors (O26, O27, O28). TTA has four donors (O25, , O27, O28, O29) and six acceptors (O25, O26, O27, O28, O29, O30). All of these atoms were critical during location of hydrogen atoms since, if the latter had not been unambiguously located, the possibility of salt formation would have required consideration. All components of the co-crystals were, however, found to be neutral (uncharged).

Least-squares weights were employed in the final cycles of the refinement. The unit cell determinations at room temperature (21 ºC) and low temperature (-160 ºC) are presented in Table 5.5.

Table 5.5 Unit cell parameters for NVSC and NVTTA

	NVSC (21 °C)*	NVSC (-160 °C)	NVTTA(21°C)*	NVTTA (-160 °C)
Molecular Formula	$2(C_{15}H_{14}N_4O)\bullet C_7H_5NO_3S$		$C_{15}H_{14}N_4O\bullet C_4H_6O_6$	
Space group		$P\bar{1}$		$P2_1/c$
a (Å)	9.499	9.5649(5)	9.305	9.8773(2)
b (Å)	13.699	13.8069(7)	9.416	19.2859(4)
c (Å)	13.797	13.8726(7)	19.507	9.6971(2)
α (°)	63.93	64.090(3)	91.65	90
β (°)	79.19	79.292(2)	90.74	90.665(3)
γ (°)	82.94	82.686(2)	90.31	90
Volume (Å^3)	1682.4	1616.98(2)	1853.4	1847.10(9)

*For room temperature unit cell data, no *e.s.d.*s are reported since relatively few intensity frames were collected

The unit cell data of the respective low temperature and room temperature structures of **NVSC** and **NVTTA** are in close agreement and indicated that no phase changes occurred on cooling the crystals. Crystal and refinement data for low temperature determinations are presented in Table 5.6.

Table 5.6 Crystal and refinement data for NVSC and NVTTA

Parameter	NVSC	NVTTA
Molecular Formula	$2(C_{15}H_{14}N_4O)\bullet C_7H_5NO_3S$	$C_{15}H_{14}N_4O\bullet C_4H_6O_6$
Formula Weight/g mol^{-1}	715.79	416.39
Crystal System	Triclinic	Monoclinic
Space group	$P\bar{1}$	$P2_1/c$
a (Å)	9.5649(5)	9.8773(2)
b (Å)	13.8069(7)	19.2859(4)
c (Å)	13.8726(7)	9.6971(2)
α (°)	64.090(3)	90
β (°)	79.292(2)	90.665(3)
γ (°)	82.686(2)	90
Volume (Å^3)	1616.98(2)	1847.10(9)
Z	2	4
Density$_{calc}$ / g cm^{-3}	1.470	1.497
μ (MoKα) / mm^{-1}	0.163	0.116
F(000)	748	872
Crystal size / mm^3	0.08 x 0.11 x 0.14	0.26 x 0.27 x 0.42
Temperature (K)	173	173
Range scanned θ / °	$2.99 \leq \theta \leq 26.36$	$2.06 \leq \theta \leq 26.35$
Index ranges	h: -11, 11 k:-17, 17 l:-17, 17	h: -12, 12 k:-24, 24 l:-12, 12
ϕ scan angle / °	1.0	1.0
ϕ scan angle range, frames	363, 363	254, 254
ω scan angle / °	1.0	1.0
ω scan angle range, frames	769, 769	258, 258
Dx / mm	33	36
Total no. of reflections collected	12967	12293
No. of unique reflections	6584	3753
No. of reflections with I > 2σ(I)	4445	3012
No. of L.S. parameters	471	276
R_{int}, R_σ	0.0325, 0.0480	0.030, 0.0295
S	0.868	1.030
R_1 (F_o >4σ(F_o))	0.0468	0.0355
No. of reflections omitted	15	8
wR_2 (all reflections)	0.1451	0.0876
Weighting scheme	a = 0.0957, b =0.7738	a = 0.0348, b =0.8302
(Δ / σ)$_{mean}$	< 0.001	< 0.001
Δρ excursions / eÅ^{-3}	0.249, -0.399	0.222, -0.214

Description of the Structures

NVSC crystallises in the triclinic space group P $\bar{1}$ with Z=2 co-crystal formula units (namely, two nevirapine molecules and one saccharin molecule) per unit cell. **NVTTA** crystallises in the monoclinic space group $P2_1/c$ with Z=4 1:1 co-crystal units in the unit cell.

POV-RAY[4] diagrams of the low temperature (LT) asymmetric units of **NVSC** and **NVTTA** are presented in Figures 5.6 and 5.7. The thermal ellipsoids of the LT structures indicate their reduced atomic thermal motion, which led to high precision of their structural determinations.

In Figure 5.6, a pseudo-centrosymmetric hydrogen bonded NV dimer is present with a single SC molecule and in Figure 5.7 one NV molecule is linked to a TTA molecule by hydrogen bonding. With NV, SC and TTA being strong contenders for co-crystallisation experimentation, classic supramolecular synthon formation between NV and the respective co-crystal formers was expected. We see a homosynthon formation for the API NV in **NVSC** (plus a heterosynthon between NV and SC, shown later) whereas in **NVTTA** there is a heterosynthon between the API (NV) and the co-former (TTA).

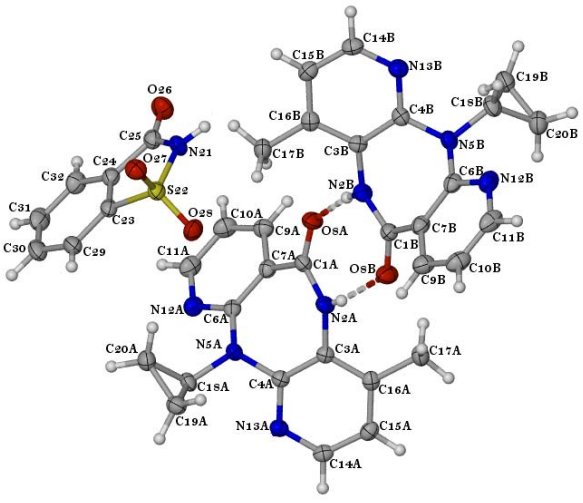

Figure 5.6 The asymmetric unit of co-crystal NVSC with atoms represented by thermal ellipsoids drawn at the 50% probability level. Principal hydrogen bonds between the two NV molecules are drawn as dashed lines.
(Note: The asymmetric unit was chosen as shown here to facilitate the drawing of the packing diagrams and does not show the H-bonding between the SC molecule and a molecule of NV. The latter is shown in Figure 5.13)

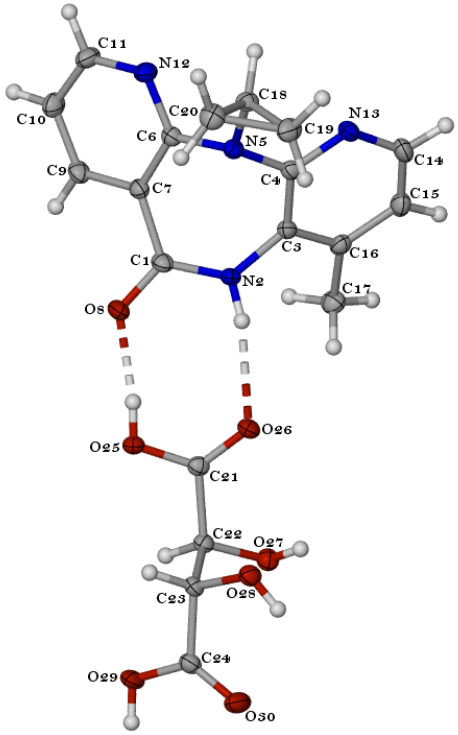

Figure 5.7 The asymmetric unit of co-crystal NVTTA with atoms represented by thermal ellipsoids drawn at the 50% probability level. Principal hydrogen bonds between the NV and TTA molecules are drawn as dashed lines.

Structural Description of Nevirapine (not co-crystallised)

Conformation of the Nevirapine Molecule (not co-crystallised)

Figure 5.8 shows the NV molecule as it occurs in a known polymorph of this API (i.e. not co-crystallised with a co-former).[5-7] The conformation shown in Figure 5.8 was compared with those in the co-crystals to establish whether there were significant differences. The molecule of NV has relatively little conformational freedom. One major possible conformational change is the rotation of the cyclopropyl residue around the N5-C18 bond. This is referred to as the 'principal torsion angle' henceforth.

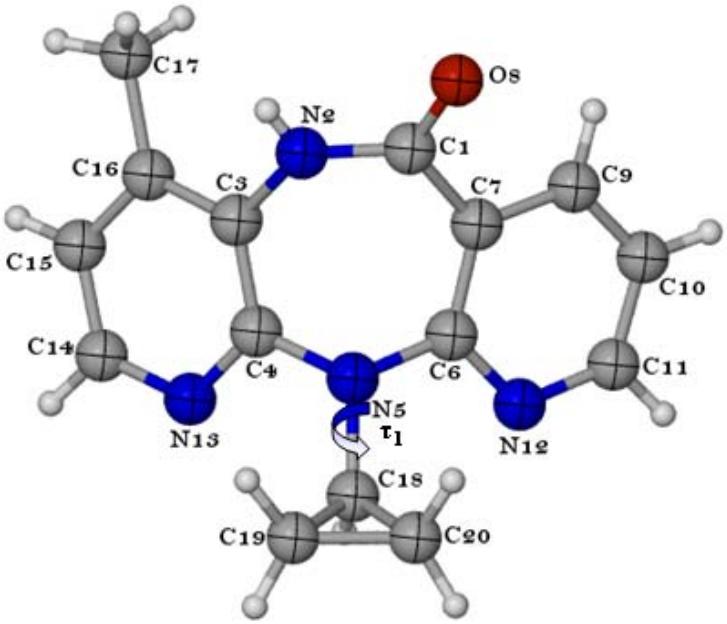

Figure 5.8 Nevirapine (not co-crystallised)[7] with atoms represented by thermal ellipsoids drawn at 50% probability level with τ_1, principal torsion angle.

Table 5.7 lists the values of the principal torsion angle τ_1 of the NV molecule in its own crystal, and for NV in co-crystals **NVSC** and **NVTTA.** The value of τ_1 for NV is significantly different from those in the two co-crystals, differing more significantly from that in co-crystal **NVTTA.**

Table 5.7 Torsion angles† for NV molecule (in its own crystal), NV in NVSC and in NVTTA.

Torsion angle (°)	NV[7]	NVSC A	NVSC B	NVTTA
τ_1(C6-N5-C18-C20)	74.1(1)	75.8(3)	76.3(3)	83.6(2)

†Since all of the structures are centrosymmetric, for each τ there are two values, one positive and the other negative, with the same magnitude. The magnitude is reported in this table.

An overlay (Figure 5.9a) of the two NV molecules (dimer) in the **NVSC** co-crystal clearly illustrates the "butterfly"[7,8] conformation of the NV molecule and the adoption of a boat conformation by the seven-membered ring. However, the NV molecule labelled A (blue) and the NV molecule labelled B (pink) in the **NVSC** co-crystal are pseudo-centrosymmetrically related. Upon overlay (Figure 5.9b) of the NV molecule in the

NVTTA co-crystal with an NV molecule in the **NVSC** co-crystal, the "butterfly" physical feature is retained. In the room-temperature structure of NV[5,6] the "butterfly angle" (that between the pyridine rings) was quoted as 121°. Figure 5.9 includes the calculated butterfly angles for **NVSC** and **NVTTA** for comparison. The values vary over several degrees, indicating some flexibility in the molecules. The butterfly shape of nevirapine is essential for the engagement of the molecule at the reverse transcriptase inhibition sites.[8] The majority of HIV-1 reverse transcriptase inhibitors that act on the binding site show a pronounced dependence for their action on major changes in molecular conformation which, in turn, are an important part of structure-activity relationship studies. The rotation of the cyclopropyl ring around the carbon-nitrogen single bond (N5-N18) primarily determines the effective conformational space of nevirapine.

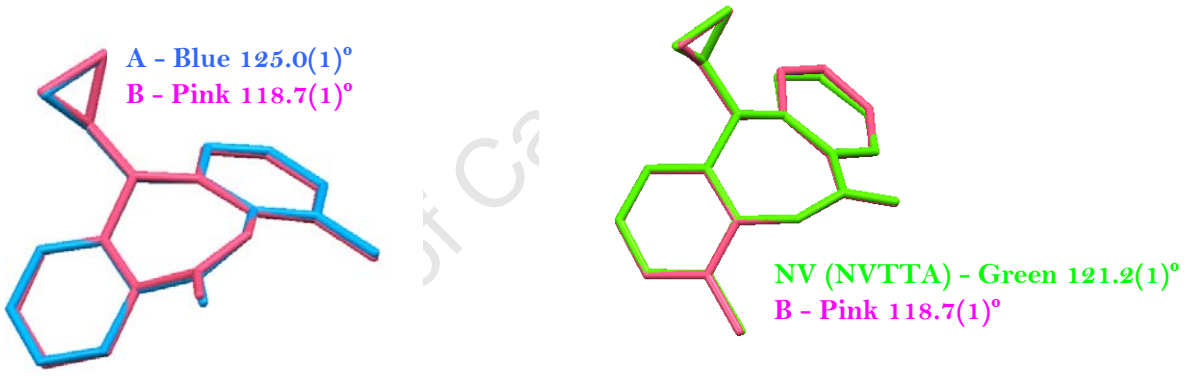

Figure 5.9 (a) Overlay of the two independent NV molecules in the NVSC co-crystal and (b) overlay of the NV molecules in NVSC (NV molecule labelled B was chosen arbitrarily) and in the NVTTA co-crystal. The individual butterfly angles are included in the figure.

Geometrical Analysis of NVSC and NVTTA

Table 5.8 presents selected, representative bond distances and torsion angles of **NVSC** and **NVTTA** for comparison as well as the distances and angles for representative strong intermolecular hydrogen bonds in both forms. The differences between corresponding molecular parameters for **NVSC** and **NVTTA** are listed in Table 5.8. A full set of the molecular parameters is available in Appendix 4 on the CD-ROM provided. This geometrical comparison confirms what is illustrated in Figure 5.9, namely that the structures of the NV molecules in **NVSC** and **NVTTA** are practically

identical. From this point of view the discussion of the co-crystals will henceforth pertain to the relationship of the NV molecule with respect to SC and TTA-DL respectively, unless stated otherwise. The remarkable consistency of the structural features of the NV molecule in both co-crystals is indicative of the stability of this arrangement and therefore closer, detailed investigation of its assembly is warranted.

Table 5.8 Selected geometrical parameters for NVSC and NVTTA

Parameter	NVSC	Parameter	NVTTA	$\|\Delta\|_{mean}$*
Selected bond distances (Å)				
O8A-C1A	1.239(3)	O8-C1	1.247(2)	0.005
O8B-C1B	1.239(3)			
N5A-C4A	1.416(3)	N5-C4	1.410(2)	0.008
N5B-C4B	1.422(3)			
C15A-C16A	1.386(3)	C15-C16	1.391(2)	0.008
C15B-C16B	1.398(3)			
Selected torsion angles (°)				
C3A-N2A-C1A-C7A	11.2(3)	C3-N2-C1-C7	-7.6(2)	3.9
C3B-N2B-C1B-C7B	-5.3(3)			
C1A-N2A-C3A-C4A	-52.0(3)	C1-N2-C3-C4	50.5(2)	1.3
C1B-N2B-C3B-C4B	50.0(3)			
N2A-C1A-C7A-C6A	39.3(3)	N2-C1-C7-C6	-37.4(2)	6.2
N2B-C1B-C7B-C6B	-45.3(3)			
C1A-C7A-C6A-N5A	-12.8(3)	C1-C7-C6-N5	4.6(2)	5.5
C1B-C7B-C6B-N5B	12.7(3)			
N2A-C3A-C4A-N5A	8.8(4)	N2-C3-C4-N5	-10.6(2)	1.2
N2B-C3B-C4B-N5B	-8.8(3)			
C7A-C6A-N5A-C4A	-54.1(3)	C7-C6-N5-C4	61.2(2)	2.7
C7B-C6B-N5B-C4B	58.2(3)			
C3A-N4A-C5A-C6A	57.5(3)	C3-N4-C5-C6	-57.9(2)	2.0
C3B-N4B-C5B-C6B	-60.5(3)			
C4A-N5A-C18A-C19A	72.8(3)	C4-N5-C18-C19	-66.9(2)	6.4
C4B-N5B-C18B-C19B	-76.5(3)			
C6A-N5A-C18A-C20A	-75.8(3)	C6-N5-C18-C20	83.6(2)	5.2
C6B-N5B-C18B-C20B	76.3(3)			
D-H•••A (Å)				
N2A-H2A•••O8B	2.975(3)	N2-H2•••O26	2.974(2)	0.045
N2B- H2B•••O8A	2.907(3)			
D-H•••A (°)				
N2A-H2A•••O8B	166	N2-H2•••O26	158	9
N2B-H2B•••O8A	171			

*$|\Delta| = (|NVA\text{-}NVB\ (NVSC)| + |NVA(NVSC)\text{-}NVTTA| + |NVB(NVSC)\text{-}NVTTA|)/3$

Overall Description of Co-crystals NVSC and NVTTA

The nevirapine molecule consists of three fused rings (Figure 5.8) with two flanking pyridine rings and a central seven-membered ring. In both **NVSC** and **NVTTA**, the seven-membered ring is angular with a boat conformation and the pyriding rings are planar. Furthermore, the NV molecule has a carbonyl oxygen atom attached to C1, a cyclopropyl ring attached to N5 and a methyl group attached to C16.

As an introduction to this section, a few points relating to the co-formers tartaric acid and saccharin follow.

The saccharin molecule in **NVSC** consists of two fused rings (Figure 5.10a) with both rings planar and a carbonyl oxygen at C25. The –NH function is the donor to a pyridine N acceptor of NV in co-crystal formation, as described further below.

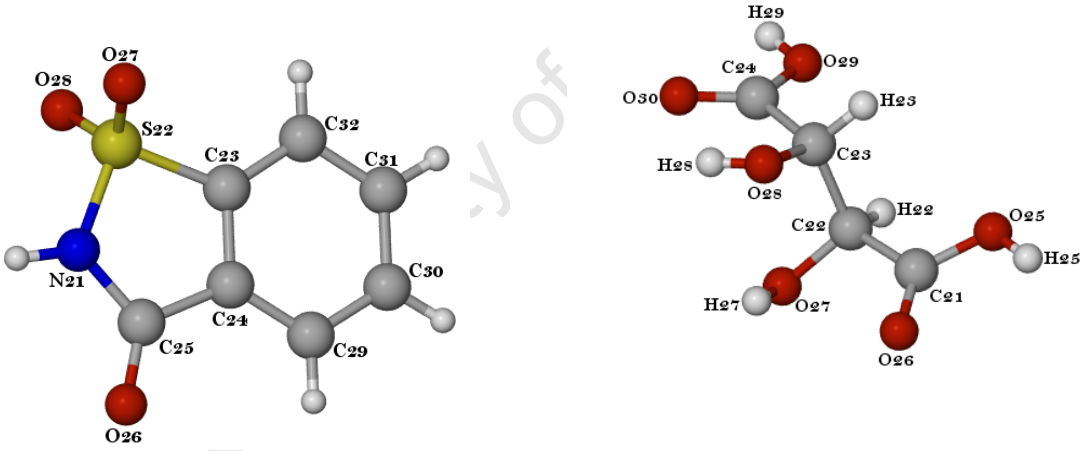

(a) (b)

Figure 5.10 (a) Structure of the saccharin molecule as found in co-crystal NVSC, (b) One of the tartaric acid molecules of the racemic pair in co-crystal NVTTA.

Naturally, tartaric acid can exist as three stereoisomers (Figure 5.11 and Table 5.9), namely the meso-compound and either one of the enantiomers, constituting a pair of diastereomers. The physical properties of the enantiomers are identical, while the

physical properties of the diastereomers are different. Also, the physical properties of the racemic mixture differ from the physical properties of either of the enantiomers.

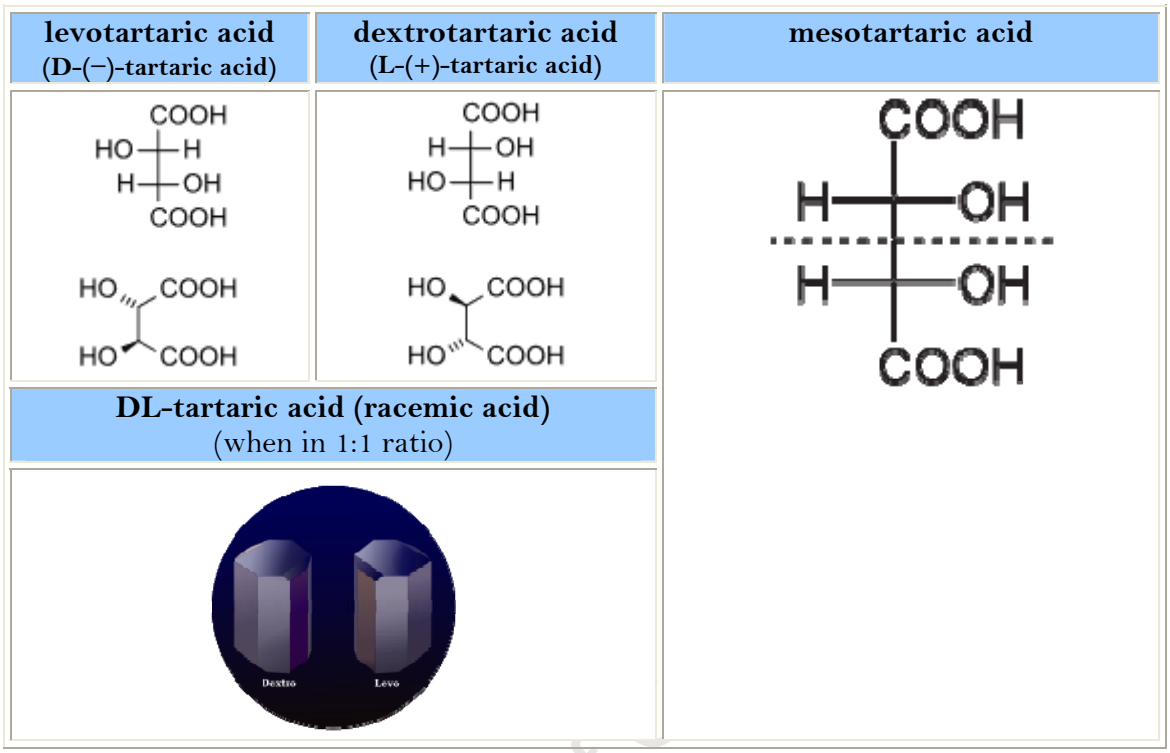

Figure 5.11 Stereoisomers of tartaric acid with tartaric acid (D and L) crystals seen through light microscope.

Table 5.9 Physical properties of stereoisomers of tartaric acid

Stereoisomers of Tartaric acid		Melting point	[α]	Solubility, g/100 g H_2O at 15°C
(2*R*,3*R*)-(+)-tartaric acid	L-	170	+11.98°	139
(2*S*,3*S*)-(−)-tartaric acid	D-	170	-11.98°	139
(2*R*,3*S*)-tartaric acid	meso	140	0°	125
(±)-tartaric acid	Racemic mixture (D,L)	206	0°	20.6

The tartaric acid molecule in **NVTTA** (Figure 5.10b) consists of two central carbons with a hydroxyl group attached to each and, at each end a carboxyl group. The carbon chain is staggered. Since the starting material for TTA was a racemic mixture, either D- or L- TTA could have been included in the co-crystal. However, the crystal of **NVTTA**

is centrosymmetric, which therefore requires the presence of an equal number of the two TTA enantiomers (Figure 5.12).

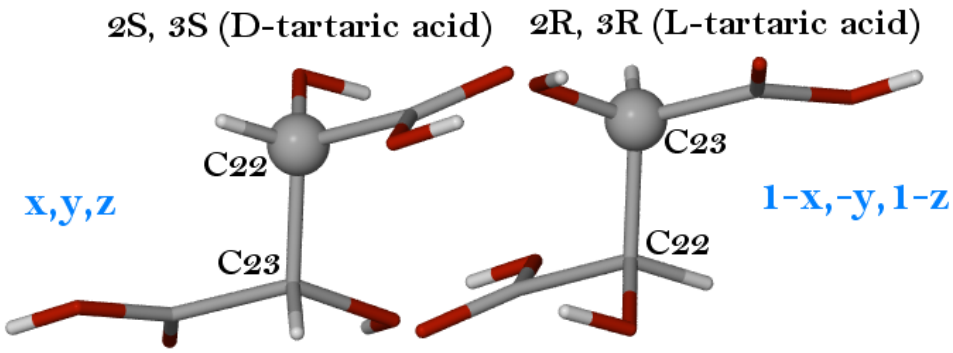

Figure 5.12 D- and L- tartaric acid molecules occurring in the NVTTA co-crystal.

Hydrogen Bonding Motifs in NVSC and NVTTA

In the **NVSC** structure (Figure 5.13) the two independent NV molecules form a pseudo-centrosymmetric dimer via two N-H•••O hydrogen bonds, giving rise to the ring motif with graph descriptor $R_2^2(8)$.[9] In addition, a molecule of SC is linked to a pyridine N atom of molecule A of NV via a hydrogen bond N-H•••N.

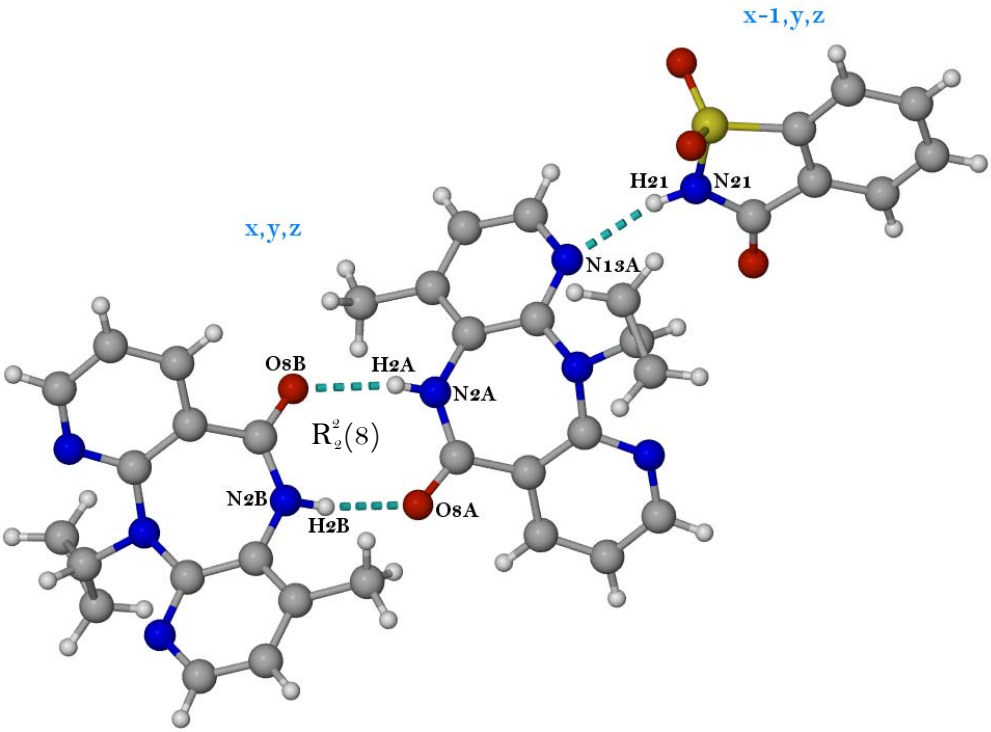

Figure 5.13 Hydrogen bonding motif in NVSC.

In the **NVTTA** structure (Figure 5.14), the primary supramolecular synthon is that between the amide group of NV and a carboxylic acid group of TTA. This synthon has a graph-set analysis descriptor $R_2^2(8)$. This API- co-former association mode is that which was contemplated originally when the author considered carboxylic acids as potential co-crystal formers with nevirapine. In examining the crystal structure further, one notes the formation of other ring motifs, one involving intramolecular stabilisation of the TTA molecule (graph-set descriptor $S_1^1(5)$) and the other, a motif $R_2^2(7)$ that is formed between two enantiomeric TTA molecules related by a centre of inversion. In addition, a hydrogen bonded ring with graph set descriptor $R_2^2(10)$ is generated between these enantiomers.

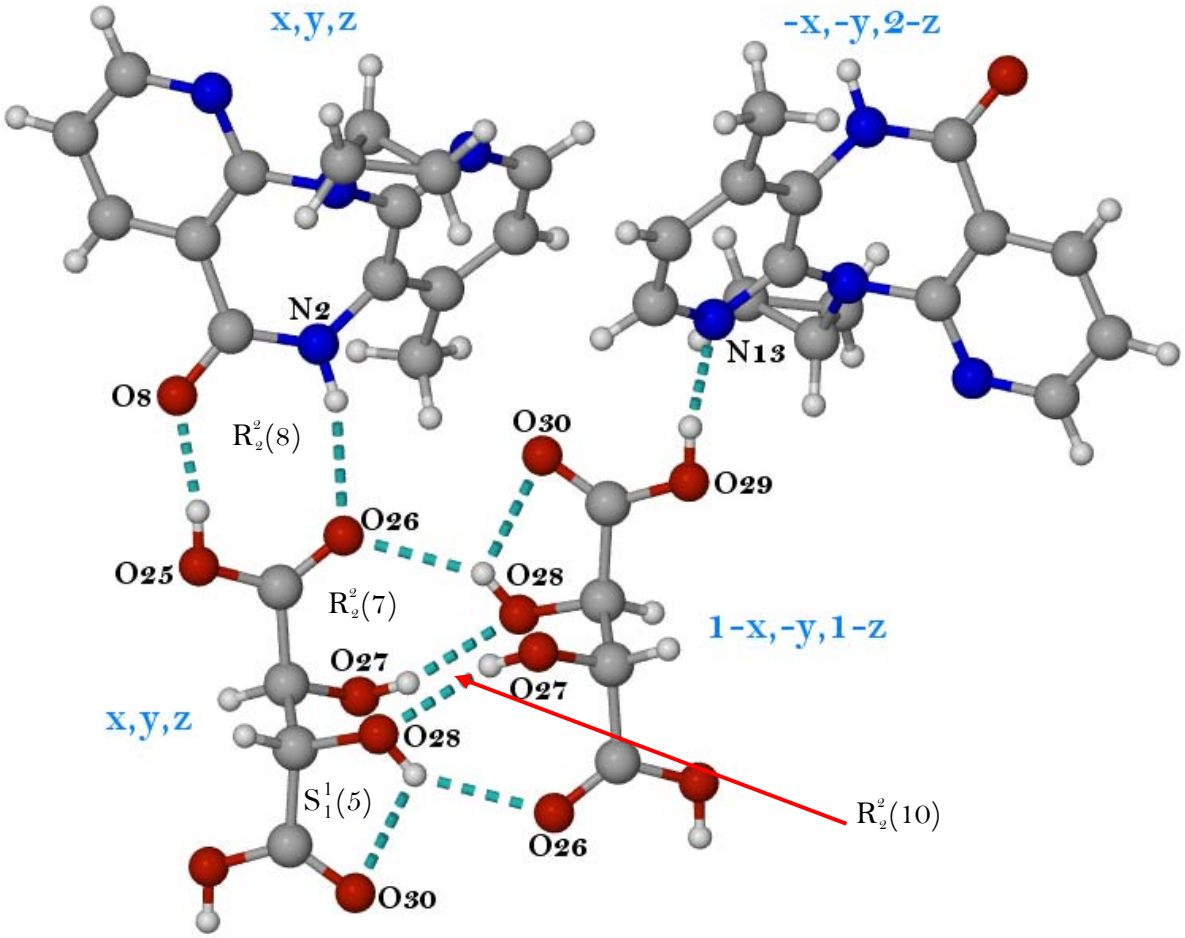

Figure 5.14 Hydrogen bonding motifs in NVTTA.

Hydrogen Bonding Interactions in NVSC and NVTTA

Table 5.10 lists all the hydrogen bonds for both **NVSC** and **NVTTA** as calculated by PLATON.[10] It is evident from Table 5.10, Figure 5.13 and Figure 5.14 that the **NVSC** co-crystal results through formation of the H-bond N21-H21•••N13A (1+x,y,z) while the **NVTTA** co-crystal forms through formation of H-bonds N2-H2•••O26 and O25-H25•••O8 and O29-H29•••NO8 (1+x,y,-1+z). The formation of the NV dimer in **NVSC** is effected via H-bonds N2A-H2A•••O8B and N2B-H2B•••O8A.

Table 5.10 Hydrogen bonding interactions in NVSC and NVTTA

Hydrogen bond	H···A (Å)	D···A (Å)	D-H···A (°)	Symmetry codes
NVSC				
N2A-H2A•••O8B	2.11	2.975(3)	166	
N2B-H2B•••O8A	2.04	2.907(3)	171	
N21-H21•••N13A	2.09	2.952(3)	167	1+x,y,z
C14A-14A•••O8A	2.47	3.361(3)	156	-1+x,y,z
C19A-19B•••O27	2.38	3.299(3)	154	-1+x,y,z
C29-H29•••O27	2.53	3.424(3)	156	1-x,1-y,2-z
C30-H30•••N13B	2.57	3.451(3)	154	-1+x,y,1+z
NVTTA				
N2-H2•••O26	2.14	2.974(2)	158	
O25-H25•••O8	1.80	2.629(2)	171	
O27-H27•••O28	2.52	2.819(2)	103	
O27-H27•••O28	2.04	2.855(2)	162	1-x,-y,1-z
O28-H28•••O30	**2.17**	**2.650(2)**	**116**	
O28-H28•••O26	2.15	2.882(2)	145	1-x,-y,1-z
O29-H29•••N13	1.79	2.609(2)	167	1+x,y,-1+z
C10-H10•••O27	2.55	3.399(2)	150	1-x,1/2+y,3/2-z
C11-H11•••O27	2.58	3.313(2)	134	-1+x,1/2-y,1/2+z
C17-H17B•••O26	2.53	3.327(2)	139	
C18-H18•••O29	2.47	3.148(2)	125	-1+x,y,1+z
C22-H22•••N12	2.53	3.435(2)	150	1+x,1/2-y,-1/2+z

Symmetry operator applies to hydrogen bonding acceptors.
Bonds in bold are intramolecular bonds.

In **NVSC**, SC is the co-crystal former and acts as the hydrogen bond donor to NV(A) H-bond N21- H21•••N13A (1+x,y,z) as indicated in Figure 5.13. It is noted that rather than behave as a co-crystal former, SC may act as a weak acid when it is co-crystallized with APIs that contain a sufficiently basic centre.[11] In this instance protonation of the API by saccharin is easily accomplished and instead of co-crystals, API saccharinates are formed.[11] For **NVSC**, a true co-crystal was indeed formed since there was no proton transfer from the SC molecule to the NV molecule. In addition to the three classical hydrogen bonds (two N-H•••O, one N-H•••N) occurring in co-crystal **NVSC**, there are three C-H•••O hydrogen bonds and one C-H•••N hydrogen bond (Table 5.10).

In co-crystal **NVTTA**, hydrogen bonding is more extensive owing to the presence of TTA, with a high hydrogen bonding capacity. Thus, a total of seven classical H-bonds (N-H•••O, O-H•••O, O-H•••N) occur and are complemented by a C-H•••N H-bond and four C-H•••O H-bonds (Table 5.10).

Crystal Packing of NVSC and NVTTA

Figures 5.15, 5.16, and 5.17 present crystal packing diagrams of **NVSC** and **NVTTA** respectively. In Figure 5.15, we view **NVSC** crystal packing along [010] which shows the SC molecules overlapping in column formation and surrounded by the NV molecules. The SC molecules, occurring in pairs across a centre of inversion, associate via intermolecular (phenyl)C-H•••O(sulfonyl) hydrogen bonding, giving rise to a ring motif $R_2^2(10)$ (not shown). As noted earlier, a pseudo-centrosymmetric dimer occurs between the crystalloraphically independent NV molecules.

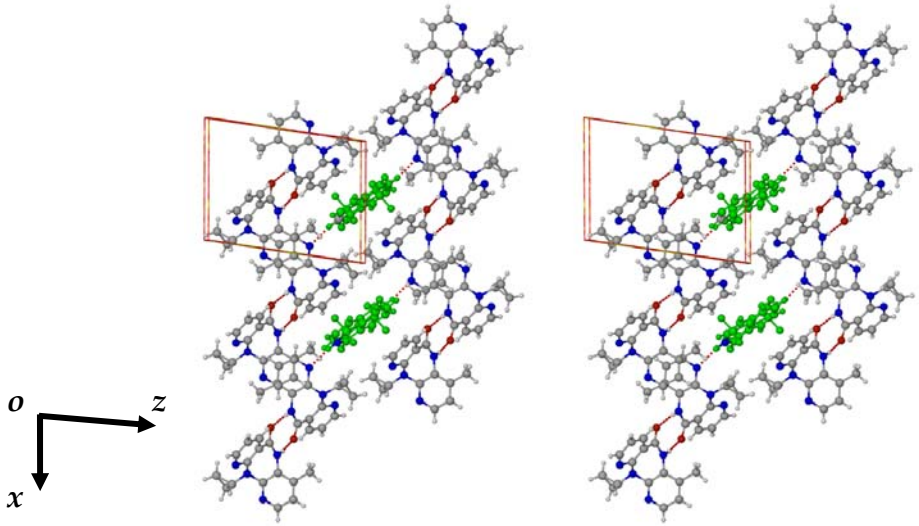

Figure 5.15 Stereoview of NVSC down b-axis (SC in green).

For **NVTTA** we view the co-crystal units down the c-axis (Figure 5.16). The TTA molecules are aligned parallel to the y-direction forming a ribbon in the centre of the cell. NV molecules are attached to this ribbon by hydrogen bonds.

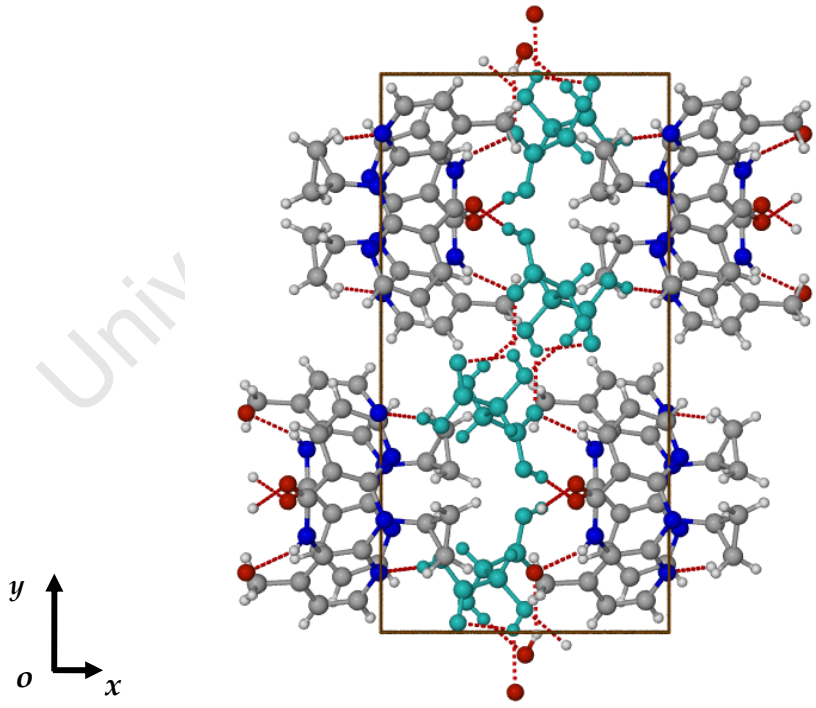

Figure 5.16 NVTTA packing diagram down the c-axis (TTA in turquoise).

In Figure 5.17, a view down the a-axis, co-crystal units are packed in a layered formation with inversion-related TTA molecules hydrogen bonding to one another, and NV molecules hydrogen bonding to TTA molecules ($R_2^2(8)$ motifs). The NVTTA co-crystal units are linked by an O-H•••N hydrogen bond.

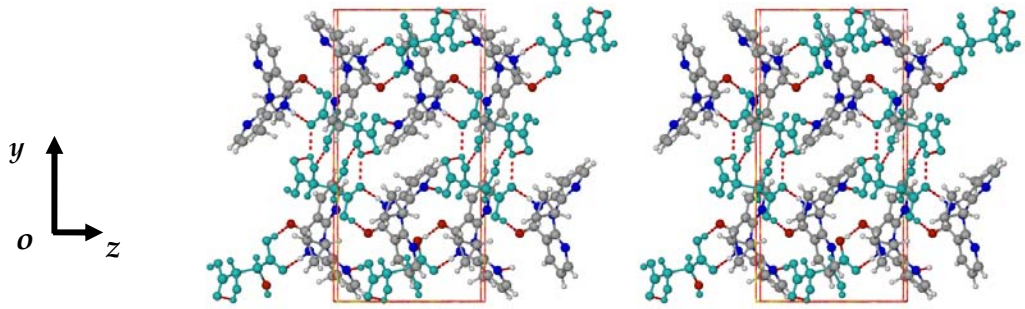

Figure 5.17 Stereoview of NVTTA packing diagram down the a-axis (TTA in turquoise).

5.7 CALCULATED PXRD

The computed and experimental patterns of **NVSC** and **NVTTA** are presented below (Figures 5.18 and 5.19). In each case, the computed pattern is based on the final, refined single crystal X-ray parameters for these phases.

In Figure 5.18, the experimental pattern presented a very close match with the computed pattern. There are two small peaks in the 5-10° range indicated in both traces. However, the experimental trace presented a high signal-to-noise ratio in this angular range. Further along the trace, distinct peaks in the regions 2θ = 12.2, 14.3, 15.9, 16.7, 17.6, 22.3, 24.5, 25.6, 27.3° are presented, which match clearly in both traces and with a much better signal-to-noise ratio. Significant intensity differences occur, indicating some preferred orientation in the sample. The slight shifts of the experimental pattern with respect to the computed pattern to lower 2θ are due to the temperature differences at which the respective traces were obtained.

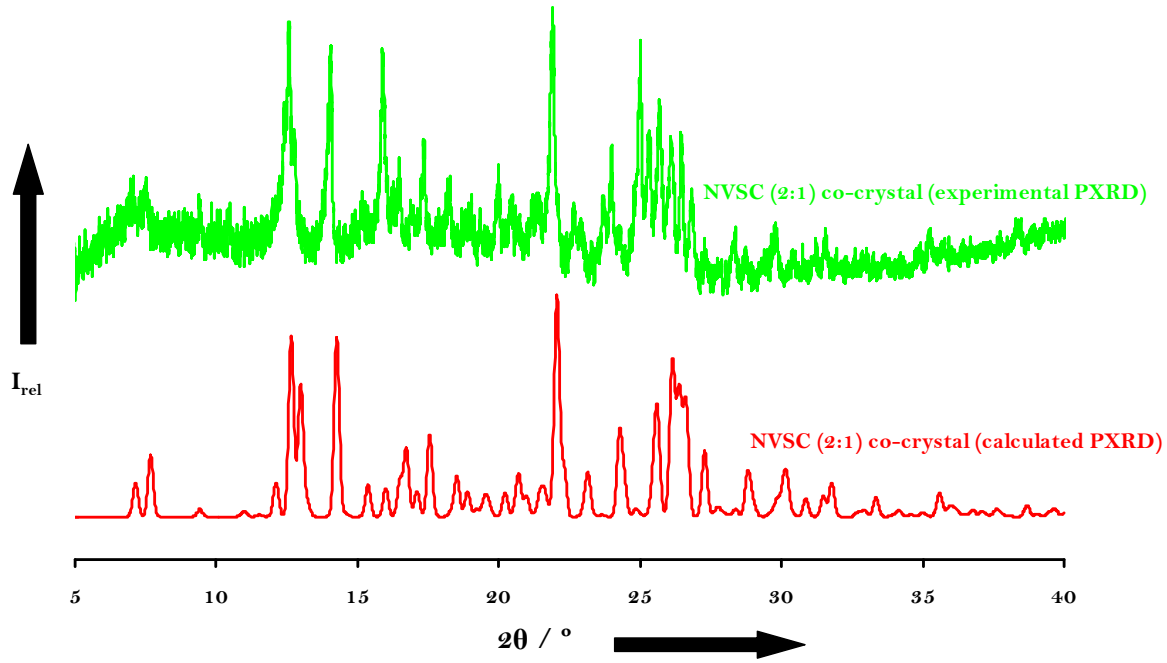

Figure 5.18 NVSC calculated versus experimental PXRD patterns.

In Figure 5.19, the experimental pattern matched the calculated pattern with slight differences at 9.2, 10.1, 27.6, 30.8, 33.7, 36.4, 38.9, 39.3° 2θ values. These peaks were of relatively low intensity in the calculated trace and practically indiscernible in the experimental trace, presumably due to residual preferred orientation. The coincidences for the stronger peaks in the traces are very convincing, even though we see slight shifts of the experimental pattern with respect to the computed pattern to lower 2θ values, again accounted for by the temperature differences at which the respective traces were obtained.

The general correspondence between the experimental and computed PXRD patterns for each of **NVSC** and **NVTTA** does, nevertheless, provide a strong assurance that the respective single crystals analysed truly represented the bulk phases.

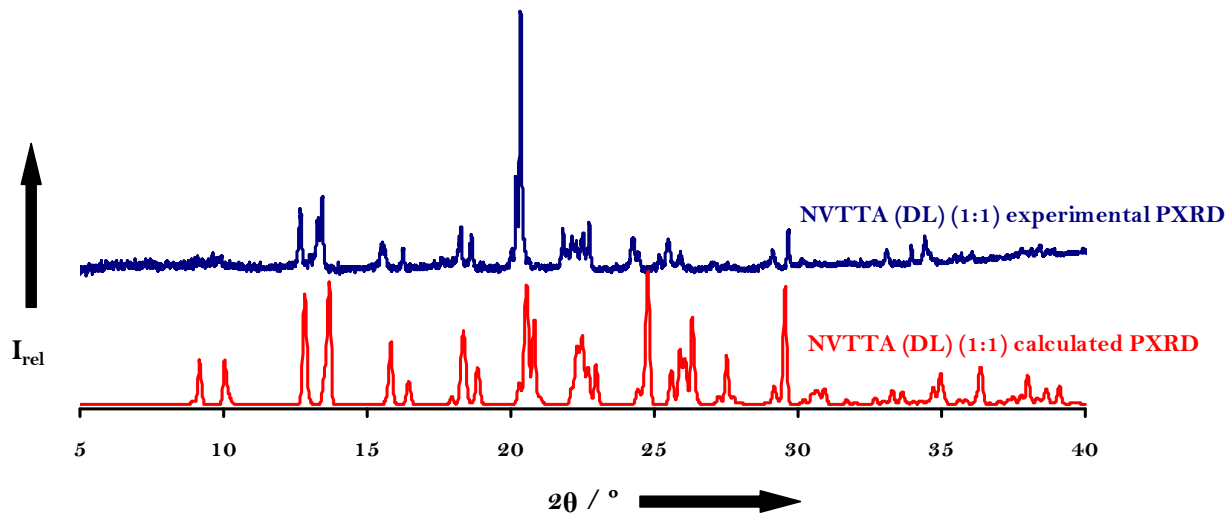

Figure 5.19 NVTTA calculated versus experimental PXRD patterns.

5.8 DISSOLUTION

In vitro dissolution studies were conducted using the rotating basket method at 37 °C as described in Chapter 2. The dissolution profiles for the pure drug NV, NV:co-crystal former physical mixture (1:1) and co-crystal are shown in Figures 5.20 and 5.21 for saccharin and DL-tartaric acid respectively. The assays were performed by UV spectrophotometry at 234 nm for NV in distilled water as the dissolution medium. A standard curve of absorbance of NV in distilled water versus concentration was plotted. Where co-crystal formers (SC and TTA-DL) were used to form physical mixtures and co-crystals, a UV-VIS scan of NV and the respective co-crystal formers was run and a standard curve of absorbance, in the presence of the respective co-crystal formers, versus concentration was plotted. The wavelength for the assay by UV remained 234 nm for NV in the presence of SC and TTA-DL, and hence 234 nm was retained for co-crystals as well.

The time for each dissolution run was 3 h. According to the BP,[12] 45 min is considered satisfactory for the majority of conventional-release (non-modified-release) products. Each of the capsules tested should yield a dissolution of 70 % and the percentage of the drug tested should be in terms of the *stated* amount. Taking account of permissible assay

ranges and content uniformity, this pharmacopoeial dissolution requirement is considered to offer an acceptable degree of assurance of 'total dissolution'.

The dissolution profile of NV clearly increases in the presence of SC and TTA-DL as a (1:1) mixture and is further increased as a co-crystal. **NVSC** reached 75 % dissolution after 45 min and 100 % dissolution after 160 min (Figure 5.20). In contrast, **NVTTA** only reached 75 % dissolution after 120 min (Figure 5.21).

Compared to NV, at 15 min, the values of % dissolved are 35, 55 and 39 %, respectively for NV, **NVSC** and **NVTTA.** After 3 h we see a significant increase in dissolution of both **NVSC** and **NVTTA**, with 69 % dissolution for NV after 3 h versus 100 % for **NVSC** and 83 % for **NVTTA**. **NVSC** reached 75 % dissolution after 45 min and 100 % dissolution after 160 min (Figure 5.20), whereas **NVTTA** reached 75 % dissolution after 120 min and only 83 % dissolution after 180 min (Figure 5.21).

Both physical mixtures **NV:SC** and **NV:TTA** demonstrate an improved dissolution profile compared to NV alone, yielding a ~10 % increase in dissolution after 3 h. However, when comparing the physical mixtures to the co-crystals, we find that the **NVSC** co-crystal profile (Figure 5.20) has a higher dissolution rate (~20 % difference compared to the physical mixture) and the **NVTTA** profile (Figure 5.21) being ~10 % higher than that of the physical mixture. Finally, we also note that the **NV:TTA** physical mixture initially hinders dissolution of NV (Figure 5.21), but subsequently (time ~90 min) NV dissolution starts to improve in the presence of TTA. The dissolution rates of the co-crystals were, in both cases, higher than those for the untreated NV and NV:co-crystal former physical mixtures (1:1).

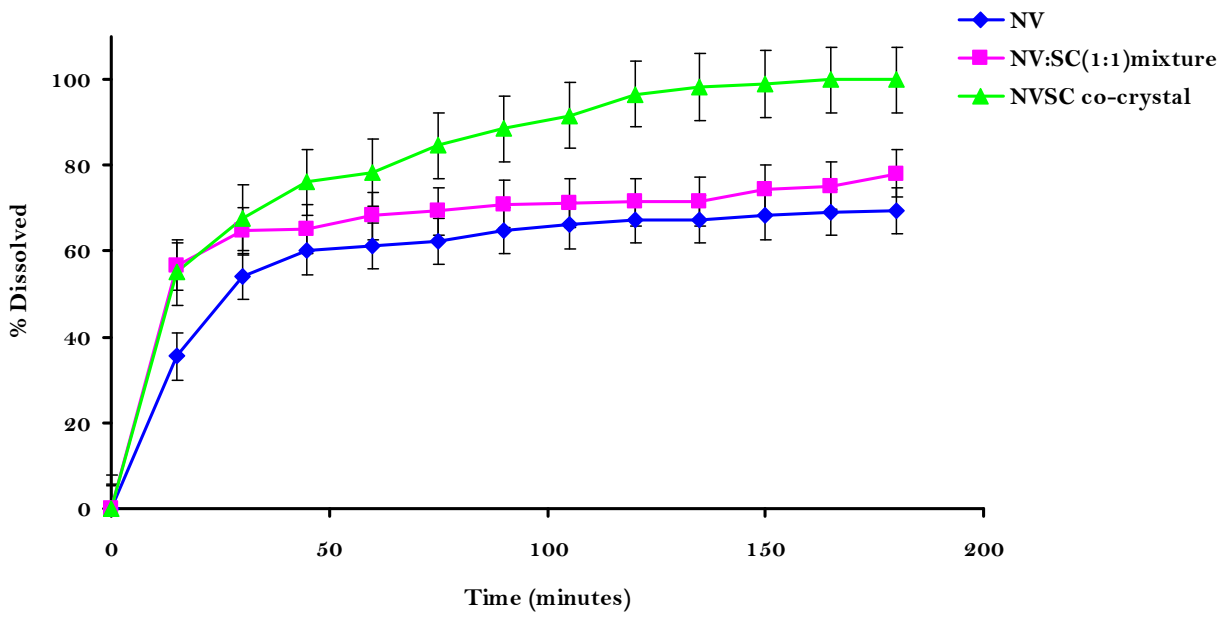

Figure 5.20 Dissolution of NV vs NV:SC (1:1) mixture vs NVSC co-crystal (2:1).

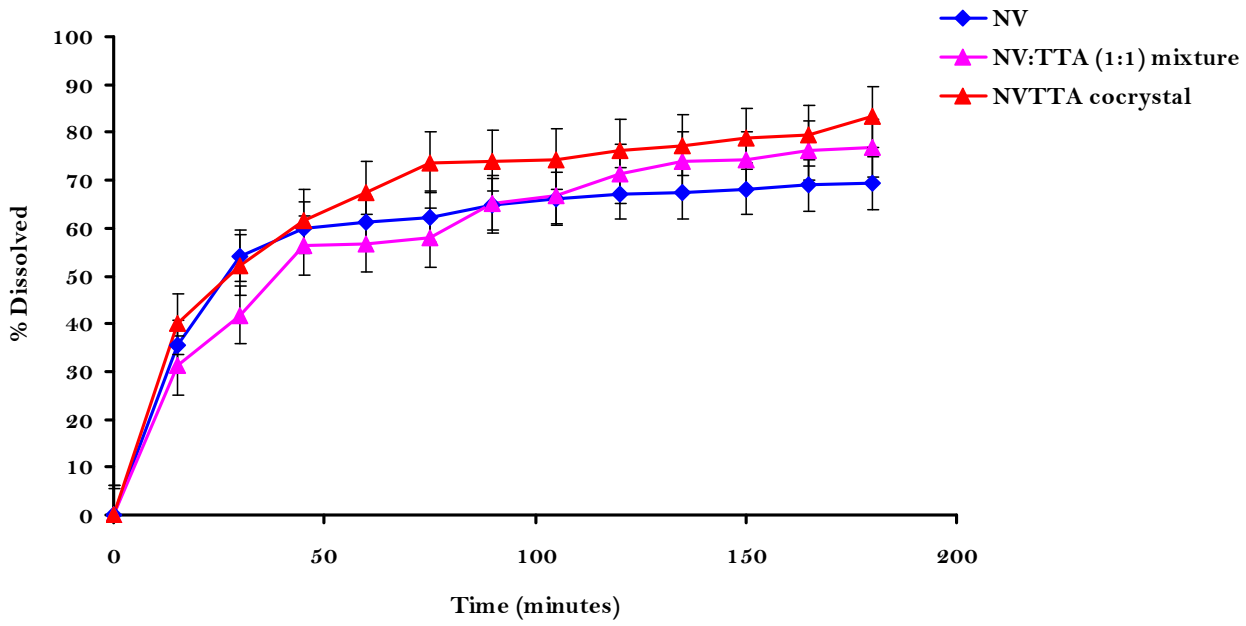

Figure 5.21 Dissolution of NV vs NV:TTA-DL (1:1) mixture vs NVTTA co-crystal (1:1).

For the two co-crystals (Figure 5.22), **NVSC** passed the BP test by displaying 76 % dissolution after 45 min whereas **NVTTA** failed the test with 61.7 % dissolution after 45 min. Initially there is a ~10 % difference in dissolution between **NVSC** and **NVTTA**, but by 105 min we see a dissolution difference of ~20 %.

The melting points of co-crystals **NVSC** and **NVTTA** were established as ~223 and ~228 ºC respectively. Though the m.p. difference is small, the expected trend viz. lower m.p. – higher dissolution rate, is nevertheless borne out by this pair, as predicted earlier in this chapter.

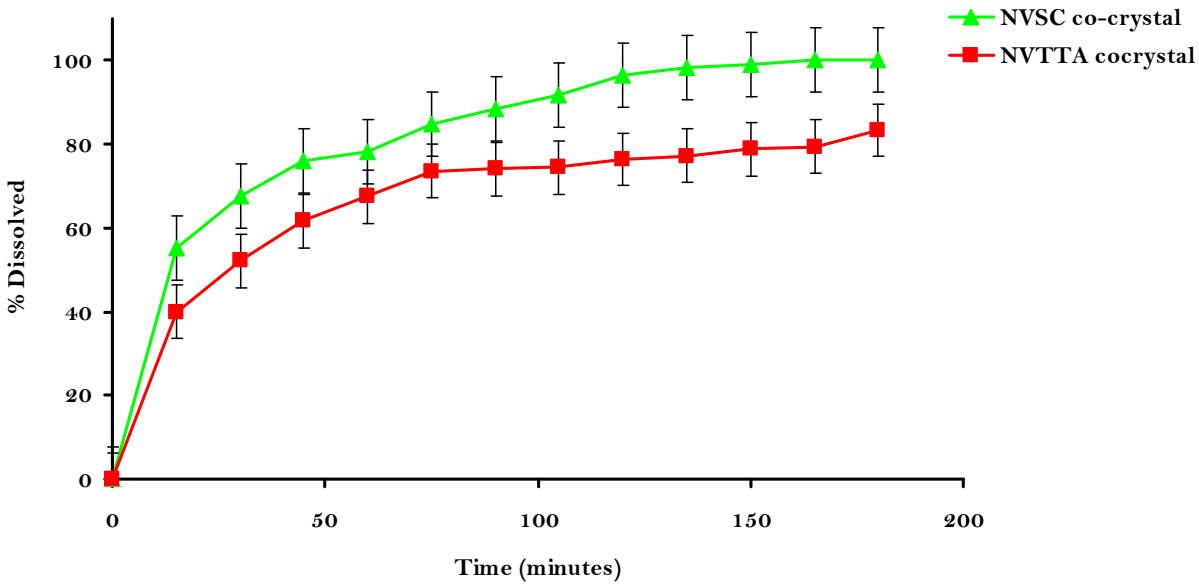

Figure 5.22 Dissolution of NVSC co-crystal versus NVTTA co-crystal.

Statistical methods based on ANOVA were used to determine discrimination in dissolution profiles.[13] Repeated measures Two Way ANOVA were used to determine how dissolution rate was affected by two factors. The percentage dissolved was the dependent variable and time was the repeated factor. Statistically significant dissolution rates between NV untreated and the two NV co-crystals were observed in Two Way ANOVA studies. This was confirmed due to the fact that the P value is <0.0001.

5.9 SOLUBILITY PROFILE OF NV IN THE PRESENCE OF CO-FORMERS

Co-crystallisation, as a rediscovery, poses as a powerful technique to modify key solid-state properties of pharmaceutical compounds such as solubility, stability and dissolution rate.[14] From a supramolecular viewpoint, predictable structural motifs can be introduced by design, offering at least a partial solution to the problem of controlling crystal structure. However, the element of predictability may be misinterpreted as leading to the formation of firstly a single structure and therefore lack of crystal polymorphism and secondly, the control of the dosage regimen. The subject of co-crystal polymorphism was addressed by Porter III et al.,[15] and in this section, we address and question the relevance of the co-crystal supramolecular modification approach with regard to dosage regimen.

The adult dosage regimen for NV is 200 mg daily for 14 days, then 200 mg twice daily. The paediatric dose (age 15 days to adolescence) is 150 mg/m^2 daily for the first 14 days, then 150 mg/m^2 twice daily. The maximum total daily dose is 400 mg. NV is manufactured as a tablet, elixir and suspension dosage form. The side-effects of NV include hepatotoxicity and skin reactions and overdose may result in chest pain, cough, weight loss, and other adverse conditions.

For the co-formers in this study, saccharin is generally used as an artificial sweetener and reports of cancer with minor side-effects such as headaches and diarrhoea (possibly due to the presence of the sulfonamide group) and even weight gain, have appeared even though saccharin may be regarded as a sugar replacement for dietary purposes.[16] The maximum safe dose recommended by WHO is 2.5 mg/day/kg body weight. TTA is regarded as being metabolically inert in man and appears to have no significant side-effects, with an acceptable dose of 0.3 mg/day/kg body weight reported by WHO.[17]

When a dosage regimen for a particular dosage form has been decided upon after clinical trials, it is assumed that this is the most effective dose for maximum pharmacological activity. Each excipient included in the dosage form is carefully selected and its dose is carefully monitored. Upon co-crystallisation, monitoring concentrations of the co-former will undergo the same vigilance. However, to control the excipient dose if co-crystallised (as in this instance SC and TTA with NV) poses a

problem, especially if the excipient presents certain toxic effects at elevated concentrations. A suggestion would be to co-crystallise the established required amount of active ingredient (NV in this instance), then establish a safe dose of excipient (co-formers SC and TTA), then co-crystallise as much active with co-former dose suggested and if more co-former is required for desired effect, an alternative safe excipient (not co-crystallised) should be included in the dosage form.

In this section the aqueous solubility of NV in the presence of co-formers was determined experimentally using the following procedure: A fixed concentration of the co-formers SC and TTA (i.e. exact amount as used for preparation of each co-crystal) was prepared by stirring each of these with solvent (distilled water) in a small glass vial till all the co-former dissolved at 25 °C. For each co-former, NV was added in specific ratio (exact amount used to make co-crystal) until saturation occurred. A further increment was added beyond saturation to ensure turbidity (since undissolved solute was important to ensure saturation) of each sample. Samples were analysed by UV spectrophotometry at 234 nm for NV. Absorbance was monitored at this wavelength in order to eliminate the effects of both SC and TTA, which do not absorb significantly at this wavelength.

A 1 ml sample of the saturated solution was obtained for analysis by separating it from the undissolved solid. Filtration through a 0.45 μm membrane filter followed and precautions were taken to ensure that it was carried out at the temperature of the solubility determination, in order to prevent any change in the equilibrium between dissolved and undissolved solute. The concentration of NV in the saturated solution was determined by UV spectrophotometry at 234 nm. A standard curve of concentration of NV versus absorbance was plotted.

Nevirapine has an aqueous solubility of 0.1 mg/mL at 25 ºC. The solubility enhancement factor for NV, by SC, established by dissolving the API in a 2:1 aqueous solution of the co-crystal former, was 46-fold. By TTA(DL) the enhancement factor was 16-fold at 25°C in a 1:1 aqueous solution of the API and co-crystal former. Table 5.11 indicates that NV aqueous solubility improves in the presence of both co-crystal

formers. The results were further confirmed by the dissolution profiles of both NV:SC and NV:TTA mixtures presented earlier.

Table 5.11 Solubility of the API NV in the presence of co-crystal formers

	Use	Mp/°C	Water solubility (mg/mL) at 25 °C
NV	antiretroviral agent	247-249	0.1 mg/mL
SC	Artificial sweetener	228.8-229.7	3.4 mg/mL
TTA (DL)	antioxidant	206 (*DL*, racemic)	206 mg/mL
NV:SC	-	-	4.6 mg/mL
NV:TTA	-	-	1.6 mg/mL

Almarson and Zaworotko have emphasised that enhanced water solubility is a desirable property of API co-crystals;[18] however, it was found that the enhancements in solubility are greater in API saccharinates (i.e. salts) than in cases where saccharin acts merely as a hydrogen bonded co-crystal former. This was exemplified by the carbamazapine/saccharin co-crystal, which is as insoluble in water as untreated carbamazepine. However, saccharinates of haloperidol, mirtazapine and quinine are freely soluble in water.[11] In the same study, a piroxicam/saccharin co-crystal was used to prove that co-crystals are less soluble than salts when compared with the saccharinates of haloperidol, mirtazapine and quinine.[11] In the present study we find that the NV:SC and NV:TTA mixtures improve the solubility of untreated NV and that SC enhances the solubility of NV three times more than TTA.

Based on the dissolution and solubility enhancement studies, we conclude that the solubility of NV was enhanced in the presence of both SC and TTA. Therefore, both these ingredients may be used as either a co-crystal former or as an excipient in the production of dosage forms. However, the question of whether the co-former solubility is enhanced as well remains unknown. Hence, further studies in this regard are warranted, when the dosage regimen is considered. Furthermore, the solubility and dissolution rate would be greatly dependent on the particle size of the samples included in the study (uniformity of particle size in the present study was indicated in Chapter 2).

5.10 CONCLUSION

Two of the twelve co-formers selected for this study produced co-crystals with nevirapine. These co-crystals were isolated and characterised by thermal and X-ray diffraction methods.

NVSC crystallises in the triclinic space group $P\bar{1}$ with a = 9.5649(5) Å, b = 13.8069(7) Å, c = 13.8726(7) Å, α = 64.090(3)°, β = 79.292(2)°, γ =82.686(2)° with two co-crystal formula units per unit cell. **NVTTA** crystallises in the monoclinic space group $P2_1/c$ with a = 9.8773(2) Å, b = 19.2859(4) Å, c = 9.6971(2) Å, β = 90.665(3)° with four co-crystal formula units per unit cell.

The geometrical features of the nevirapine molecule were found to be essentially the same in both co-crystal **NVSC** and **NVTTA**, despite the fact that the drug molecule interacts with different molecules in these species. Experimental PXRD patterns of the co-crystals were found to be consistent with respective computed patterns, allowing these to serve as reliable references for co-crystal identification.

In considering possible further development of the co-crystals, both saccharin and tartaric acid are listed as GRAS compounds and therefore would not need exhaustive and separate clinical trials, barring perhaps toxicological studies. As a co-crystal former, SC may not be ideal for injectable or drop formulations due to limited water solubility compared to saccharinates. Saccharin is a potent sweetener and it masks the bitter taste of many drugs, which is very useful in paediatric formulations. If the pH is in a reasonable range (i.e. pH 5-6) then injectable forms of the co-crystal would not cause any undue irritation and other undesirable side-effects on the skin.

The most salient feature of the **NVTTA** and **NVSC** co-crystals is that they, by definition, consist of two components, each of which is capable of independent existence, as opposed to saccharinates, which consist of cations and anions, incapable of separate existence.

One can clearly see a place for co-crystals within the pharmaceutical market. On the basis of the limited examples available, some general comments can be made on the physicochemical properties of co-crystals.[19] Melting points are altered for most co-crystals, with approximately 51 % having melting points between those of the API and co-former and 39 % having lower melting points.[19] Correlations with other parameters, such as solubility, are limited and will be complex due to the multi-component nature of co-crystals. In many cases, improved stability, such as resistance to hydrate formation, has been shown for co-crystals. However, general trends are not evident and each system needs to be evaluated to determine if improvements are obtained. Improved solubility for poorly soluble compounds has been achieved using co-crystals. Limited studies suggest that salts will provide a larger increase in solubility if they are available. For poorly soluble neutral compounds, co-crystals are a very feasible approach to improving solubility (as observed in the present study). Co-crystals can provide higher and lower dissolution rates compared to the API. Dissociation is an important consideration in analyzing data from these experiments. It was shown that significant increases in bioavailability are possible with co-crystals, even when dissociation of the co-crystal is known to occur from *in vitro* studies.[19]

Other aspects of development, such as polymorphism and scale-up, will need to be examined for each candidate co-crystal. Processes to produce co-crystals on a large scale will likely require different approaches, such as those based on ternary solubility phase diagrams. Co-crystals will provide additional options for IP, regulatory, and lifecycle management for new and old drugs and will provide additional challenges as they continue through the development process.[19]

To date, no co-crystal drug products appear to be on the market, although there is no doubt that co-crystals are present in pharmaceutical drug pipe-lines and it is only a matter of time before this application becomes a reality. Finally, it should be made clear that no one particular strategy offers a solution for property enhancement of all APIs. Each API must be examined and evaluated on a case-by-case basis in terms of molecular structure and desired final properties.

Given the surge of activity in the field of co-crystals (molecular complexes of an API with one or more solid components), it has become an emerging class of pharmaceutical materials susceptible to design by crystal engineering. This implies that the functional properties of APIs (e.g. solubility and physical stability) can potentially be built in during the solid-state synthesis. The relevance of a potential co-crystal former becomes a crucial issue at this stage, which is clearly demonstrated in this study.

5.11 REFERENCES

1. Data Preparation and Reciprocal Space Exploration, Version 5.1, (Copyright Bruker Analytical X-ray Systems, **1997**)
2. Sheldrick G.M., SHELXS-97, *Program for Crystal Structure Solution*, Institüt für Anorganische Chemie der Universität, Tammanstrasse 4, D-3400 Göttingen, Germany, **1997**.
3. Sheldrick G.M., SHELXL-97, *Program for the Refinement of Crystal Structures*, Institüt für Anorganische Chemie der Universität, Tammanstrasse 4, D-3400 Göttingen, Germany, **1997**.
4. POVRAY, *Persistence of Vision Ray Tracer*, Version 3.6.2, 1991-2003 ©, June **2009**.
5. Cambridge Structural Database and Cambridge Structural Database System, Version 5.30, November **2009**, Cambridge Crystallographic Data Center, University Chemical Laboratory, Cambridge, England.
6. Mui P.W., Jacober S.P., Hargrave K.D., Adams J., *J. Med. Chem.*, **1992**, 35, 201-202.
7. Caira M.R., Stieger N., Liebenberg W., De Villiers M.M., Samsodien H., *Cryst. Growth and Des.*, **2007**, 8, 17-23.
8. Ding J., Das K., Moereels H., Koymans L., Andries K., Janssen P.A.J., Hughes S.H., Arnold E., *Nat. Struct. Biol.*, **1995**, 2, 407-415.
9. Etter M.C., Macdonald, J.C., Bernstein, J., *Acta Crystallogr.*, **1990**, B46, 256-262.
10. Spek A.L., PLATON, *A Multipurpose Crystallographic Tool*, Version 10500 © **1980-2009**.
11. Prashant M.B., Nittala V.R., Rahul B., Desiraju G.R., *Chem. Commun.*, **2005**, 1073-1075.
12. British Pharmacopoeia, British Pharmacopoeia Commission Secretariat, London, UK, **2005**.
13. Gonjari I.D., Karmarkar A.B., Hosmani A. H., *Digest J. Nanomat. Biostruct.*, **2009**, 4, 651-661.
14. Vishweshwar P., McMahon J.A., Bis J.A., Zawarotko M.J., *J. Pharm. Sci.*, **2006**, 95, 499-516.
15. Porter III W.W., Elie S.C., Matzger A.J., *Cryst. Growth Des.*, **2008**, 8, 14-16.

16. Buzzle.Com., Saccharin Side-Effects, *http://www.buzzle.com/articles/saccharin-side-effects.htm*, retrieved 20 November **2010**.
17. WHO 17th Report, FAO/WHO Expert Committee on Food Additives, Geneva, 1974, No.539, retrieved 22 November **2010**. http//:www.inchem.org/documents/jefca/jecmono/vo5le93.htm.
18. Almarsson Ö., Zawarotko M.J., *Int. Pat.* Number, WO 2004/078161 A1, (16/09/**2004**).
19. Schultheiss N., Newman A., *Cryst. Growth and Des.*, **2009,** 9, 2950-2967.

Chapter 6

CONCLUSION

Chapter 6 *presents the concluding remarks of this thesis with recommendations for further studies.*

Three aspects of supramolecular chemistry were investigated in this study, namely polymorphism, cyclodextrin inclusion and co-crystallisation. Firstly, we synthesised and characterised a range of novel 'supramolecularly modified' forms of the pharmacologically active molecules 2-methoxyestradiol (2ME), 2-methoxyestradiol-*bis*-sulfamate (2MES) and nevirapine (NV). Furthermore, we established their thermal stabilities and dissolution properties. In total, the study investigated twelve new compounds of which five were identified by polymorphism studies, five by cyclodextrin inclusion studies and two by co-crystallisation studies. Of these, seven compounds were subjected to single crystal X-ray analysis and their structures were elucidated. Where appropriate, attempts were made to reconcile physical behaviour with crystal structures.

POLYMORPHISM

The drug 2-methoxyestradiol (2-ME), a potent anti-cancer agent with possibly further encouraging pharmacological activities,[1] is available as a capsule (Panzem®) formulation and NanoCrystal® dispersion (NCD) formulation. In the Phase II trial of the NCD formulation it was found that 2ME was well tolerated and had better bioavailability than the capsule formulation.[2] Several structural modifications have been initiated to improve its pharmacological activity. However, the present study was undertaken to highlight the possibility that supramolecular (i.e. non-covalent) modification of 2ME might significantly affect its physicochemical properties and consequently its pharmaceutical characteristics related to delivery. 2ME has decreased stability when compared to derivative molecules and by sulfamoylation,[3] an increased cytotoxic and cytostatic activity, plasma half-life and bioavailability are evidenced. The sulfamoylated analogue of 2ME, 2-methoxyestradiol-*bis*-sulfamate (2MES) was thus included in this study as well.

In the chapter dealing with polymorphism, the author investigated using various isolation techniques, different forms of 2ME and 2MES. Firstly, it should be noted that no previous solid-state characterisation of 2ME or 2MES has been reported in the literature thus far and that the phenomenon of polymorphism in steroidal compounds is

not uncommon. It is reported that 67% of steroidal molecules can occur in different forms given 'due diligence' in attempts to isolate them. This study elucidated the crystal and molecular structures of the starting materials of both 2ME and 2MES accurately by single crystal X-ray determination. Furthermore, 2ME presented a chloroform solvate (**Form III**) by recrystallisation from $CHCl_3$ and an amorphous form (**Form II**) by melt studies. 2MES, in the form of the hemihydrate, after having proven to be very difficult to isolate as a single crystal, was eventually and accurately characterised only after four sets of X-ray intensity data had been collected, the last involving a non-twinned specimen.

Isolation and Characterisation of 2ME Forms I, II and III

The three modifications of 2ME (**Forms I, II,** and **III**) were isolated and characterised by thermal and X-ray diffraction methods. **Form I** was recrystallised from diethyl ether, **Form II** was established as an amorph by DSC melt studies of the melted **Form I,** and **Form III** was recrystallised from chloroform solvent. Both thermal and PXRD analysis showed that **Form I** corresponded very well with the originally synthesised crystalline material. **Form II**, a molten glassy mass, was identified as an amorphous form by both DSC and PXRD analysis. **Form III** was identified as an unstable chloroform solvate, as evidenced by HSM, TGA, PXRD and single crystal X-ray analysis. From the thermal analysis, **Form I** remained relatively stable throughout the heating process with no change until it melted at 185 °C and decomposed at 200 °C. **Form II** (amorphous phase)**,** also identified as an unstable form, became opaque at 112 °C during HSM and DSC analysis, whereupon transition to a crystalline form occurred, the latter melting and decomposing within the same temperature range as the originally prepared **Form I.** This indicated that **Form II,** a metastable form, reverts to the more stable form, **Form I.** **Form III,** the unstable solvated crystal became opaque at 65 °C indicating loss of the chloroform solvent. On heating, the crystal collapsed and the resulting powder then melted and decomposed within a similar temperature range as **Form I, a**gain verifying that **Form I** is the most stable form identified in this study.

The powder X-ray patterns of **Forms I, II** and **III** differed significantly showing that these can serve as references for their identification. The trace for **Form II** had no

peaks, indicating a vitreous phase. Controlled desolvation of **Form III** yielded a powder which displayed the same PXRD pattern as **Form I**, an outcome consistent with HSM analysis.

Form I of 2ME crystallises in the monoclinic space group $P2_1$, with two molecules per unit cell. **Form III** crystallises in the triclinic space group with one formula unit 2ME•2$CHCl_3$ per unit cell. The conformations of the 2ME molecules were found to be identical in both forms. In **Form I,** the 2ME molecules associate as hydrogen bonded dimers which stabilise its layered packing arrangement. In **Form III,** two intermolecular hydrogen bonds appear which, by co-incidence, correspond with two of those identified in **Form I.** These two bonds allowed the formation of continuous ribbons of 2ME molecules in the structure. The 2ME molecule is linked to the chloroform molecules via hydrogen bonding to the ribbon-like arrangement, creating layers between the ribbons. One of the $CHCl_3$ molecules engages in hydrogen bonding to the 2ME layer (bifurcated C-H•••O), while the other is involved in a C-H•••π interaction with the (aromatic) A-ring of the 2ME molecule. No guest-guest interactions are observed within the layers. It was also noted that the layers provided distinct diffusion paths for $CHCl_3$ molecules out of crystals of **Form III** and their presence was consistent with the spontaneous desolvation observed for this solvate when removed from its mother liquor.

Isolation and Characterisation of 2MES hemihydrate (Form I)

2MES hemihydrate was recrystallised from amyl alcohol. Even though only this single form of 2MES (**Form I**) was isolated and characterised, we emphasise the difficulty it presented in its structural elucidation by single crystal X-ray diffraction. The recrystallised 2MES hemihydrate sample did match the original starting material and this was verified by elemental analysis, HSM, TGA, DSC and PXRD. Single crystal X-ray diffraction was essential for establishing the supramolecular interactions in the crystal. From the DSC trace it was evident that the compound spontaneously degrades upon reaching its melting point (175 °C) and it is noteworthy that 2MES hemihydrate discoloured when exposed to light and had to be stored under special conditions to minimise photodegradation.

The PXRD patterns of **Form I** (those of both the originally synthesised material and the material recrystallised from amyl alcohol) were practically indistinguishable and serve as references for this phase.

After several data-collections and structure refinements, **Form I** was eventually found to crystallise in the orthorhombic space group $P2_12_12_1$ with eight 2MES molecules and four water molecules per unit cell. The reason that many data-collections were performed was the need to overcome a crystal twinning problem. **Form I** was classified as a growth twinned crystal and hence X-ray diffraction results from apparently single crystals were quite deceptive. Prior to establishing the true orthorhombic symmetry, computations persistently presented a monoclinic unit cell and a structural model which did not refine satisfactorily. Upon careful examination of the reciprocal lattice, the twinning was revealed and a very thin lamina section was then selected for data-collection and this showed no indication of twinning, yielding the orthorhombic unit cell and the correct space group.

The asymmetric unit (ASU) comprises two 2MES molecules and one water molecule. The molecular structures of the two 2MES molecules were practically identical, with the same geometrical features as the parent steroid 2ME with respect to ring conformations. At each end of the 2MES molecule, there is a sulfamate group rendering the 2MES molecule more soluble in aqueous media than the parent 2ME steroid molecule. The hydrophilic sulfamate groups also engage in extensive hydrogen bonding in the crystal.

In its packing arrangement, 2MES molecules pack head-to-head in a herring-bone style. An individual 2MES molecule bonds with a symmetry-related 2MES molecule at either end through bridging hydrogen bonds mediated by a water molecule. Water molecules are located in isolated sites in the crystal of 2MES hemihydrate, accounting for its thermal stability. The ribbon-like feature observed in the crystal structures of 2ME and its chloroform solvate does not feature here, however.

The basic steroid structure, determined by X-ray analysis, was superimposable for 2ME **Form I, Form III** and 2MES **Form I,** with minimal conformational differences existing, illustrating the rigidity of the steroid backbone.

Experimental PXRD patterns were found to be consistent with computed patterns based on single crystal X-ray diffraction data, allowing these to serve as reliable references for future identification of the respective 2ME and 2MES phases.

Comparative Solubility and Dissolution of 2ME (Forms I and II) with 2MES hemihydrate

The aqueous solubility of 2MES hemihydrate was determined experimentally and was found to be twice that of 2ME, a result which was confirmed by i*n vitro* dissolution studies conducted in aqueous medium at 37 °C. A significant increase in dissolution rate and extent of both 2MES hemihydrate and amorphous 2ME compared to 2ME alone was recorded, with amorphous 2ME being the most significant. After the 3 h dissolution run, both 2MES and amorphous 2ME had twice the dissolution of 2ME alone.

Future Work

The most significant result from this study was the fact that the amorphous 2ME (**Form II**) and 2MES hemihydrate had greater dissolution rates than 2ME (**Form I**). The author recommends that once the capsule (Panzem®) formulation and NanoCrystal® dispersion (NCD) formulation are readily available, a comparative study with these formulations should be carried out. Comparisons should be made with due regard to particle size, form (especially the amorphous form of 2ME) and the desolvated material of 2ME (**Form III**) since desolvation of solvates may improve flowability and modify the average particle size[4] of the original material. However, complete removal of the chloroform must be validated prior to the comparison since chloroform is not a pharmaceutically acceptable solvent. These comparisons would provide much insight into the solubility and wettability aspects of the various solid-state forms and dosage forms currently available for 2ME and 2MES hemihydrate.

CYCLODEXTRIN INCLUSION

Cyclodextrin inclusion of drug molecules into CD cavities results in the improvement of the physicochemical properties of drugs. Such improvements include: improving the stability, taste, odour, solubility and ultimately the bioavailability. With the non-polar cavity available in the CD molecule, inclusion complexes with many hydrophobic guest molecules are facilitated. Our literature review regarding 2ME reported the poor aqueous solubility and dissolution rate of 2ME, which is generally common for steroidal molecules. Thus, the possibility of forming inclusion complexes between 2ME and CDs was considered, with the intention of improving the solubility of 2ME. It was also considered that successful structural elucidation of CD-2ME inclusion complexes might serve as very useful reference structures for those engaged in molecular modelling studies involving CD-inclusion of related steroids. It should be noted that at the beginning of this study, no single crystal X-ray structures of CD-steroid complexes were known. In this study we isolated two such novel crystal structures prepared with the methylated CDs DIMEB and TRIMEB. However, during this study, a report of a single crystal X-ray structure of a steroid appeared but the complex comprised a highly derivatised, charged CD molecule and a modified steroid in the form of its bromide salt,[5] thus representing a very atypical CD-steroid system.

β-CD complex with 2ME

β-CD complexed with 2ME by kneading and by co-precipitation methods and the resulting inclusion complex was designated BCD2ME. Confirmation of water content was by TGA and both TGA and DSC indicated that water loss from this complex was a multi-stage process. X-ray powder diffraction was used to establish complex formation and the complex stoichiometric ratio was established as 2:1 by UV-spectrophotometry. In combination with the principles of isostructurality, the X-ray powder diffraction pattern permitted deduction of the correct crystal system, space group and unit cell data of the new cyclodextrin complex. Isostructurality with a known β-CD complex which contains 4-*t*-butylbenzyl alcohol as guest (CSD refcode KOFJEU) was confirmed.[6] The β-CD molecule in the structure of KOFJEU[6] was used as a trial model for the structural elucidation of BCD2ME. Although the host molecule refined normally, the steroid molecule was severely disordered, preventing its modelling. However, vital information

deduced from the isostructurality of BCD2ME with KOFJEU is that the former complex exists as a dimer whose structure is maintained by O-H•••O hydrogen bonds between the secondary rims of the two host molecules and that a single 2ME molecule is encapsulated within this dimer. Once again, the use of PXRD coupled with isostructurality concepts has been invaluable in identifying genuine CD inclusion complexes in the absence of single crystals and enabling reliable predictions of the crystal parameters.[7]

HPBCD and RAMEB Complexes with 2ME

Both HPBCD and RAMEB complexed with 2ME by kneading each of the CDs with the drug in a 1:1 molar ratio in the presence of water. Both CDs are amorphous and their PXRD traces do not display any sharp peaks: upon complex formation, essentially no change was evident in the resulting PXRD pattern and this was taken as preliminary evidence for inclusion complex formation. FTIR spectra of the complexes confirmed our observations since shifts in certain characteristic bands of the 2ME molecule were indicative of interaction between the CDs and the drug. Finally, the disappearance of the 2ME melting endotherm in DSC traces of putative complexes was taken as further evidence for complex formation.

DIMEB and TRIMEB Complexes with 2ME

The DIMEB and TRIMEB complexes with 2ME (DIB2ME and TRIB2ME respectively) were prepared by co-precipitation methods. TGA was used to determine their respective water contents as 5.1 ± 0.4 H_2O molecules per DIB2ME complex unit and for TRIB2ME the complex:H_2O ratio was 1:1.07. Dehydration of the DIB2ME complex occurred over a broad temperature range and for TRIB2ME not much water loss was observed, which is common for TRIMEB complexes. Both complexes presented a 1:1 CD-2ME stoichiometric ratio. The PXRD technique indicated definite complexation using the co-precipitation method.

For DIB2ME the asymmetric unit (ASU) was determined to consist of one complex unit while for TRIB2ME as many as four independent complex units comprised the ASU. Consequently, solving the TRIB2ME structure was quite challenging owing to the

abnormally large size of the crystallographic asymmetric unit. Also, to refine TRIB2ME anisotropically proved to be very challenging due to limitations of the program SHELXH.[8] After full-matrix least-squares refinement with atoms treated isotropically, a partially anisotropic model was introduced and sequential full-matrix refinement of all four guest molecules and the side-chains of each glucose molecule of the host followed. In the analysis of DIB2ME, one glucose molecule of DIMEB was found to be methylated not only at the O2- and O6- positions, but also at the O3-position, indicating impurity of the parent host used in this instance. The 2ME molecule is found at the secondary rim of the host in both DIB2ME and TRIB2ME with the D-ring of 2ME inserted into the host cavity. For DIB2ME, the primary rims of all the glucose residues are inclined towards the centre of the cavity and the parameters reported indicate that the macrocycle is quite symmetrical, despite the singularity in one glucose ring. In the complex TRIB2ME, molecules A and B in the asymmetric unit have a truncated-cone appearance and molecules C and D deviate slightly from this arrangement. The parameters reported for TRIB2ME indicated that the macrocycle is somewhat distorted. The host conformations in complex units A and B are quite similar but those in units B and C were noted to have distinct differences. The host D presented a somewhat different conformation as well as different host-guest interactions from those in A, B and C.

In the crystal of complex DIB2ME, the water molecules interact with both the host and guest, serving to stabilise the complex. The conformations of the steroid molecules in 2ME, DIB2ME and TRIB2ME were found to be practically identical. However, small variations in guest inclusion were evident. Furthermore, the sterically bulky steroid molecule 2ME, having a fairly sizeable residue (ring-A) that protrudes from the secondary side of the host, was seen to induce new types of CD complex crystal packing arrangements. DIB2ME crystallises in the space group $P2_1$ while TRIB2ME crystallises in the space group P1, both packing arrangements being roughly classed as 'channel-type'. Not surprisingly, neither of these complexes is isostructural with any known DIMEB and TRIMEB complexes. The match between the experimental and calculated PXRD patterns for each of DIB2ME and TRIB2ME was very convincing, indicating the correctness of the single crystal X-ray structural models. Complexation

of 2ME with these CDs definitely resulted in novel complex PXRD patterns that will be incorporated into the reference patterns for isostructurality series. These may well be employed in future identification of isostructural inclusion complexes containing other steroidal guest molecules that are available only in microcrystalline form.

Solubility and Dissolution studies of 2ME and 2MES with CDs

The solubility and dissolution profiles of 2ME and 2MES with CDs were studied using mixtures as well as inclusion complexes. Results were compared with those for the parent compounds 2ME and 2MES. This is the first time that a detailed study of the dissolution profiles of these compounds has been undertaken and the effect of CDs on their dissolution profiles investigated. The main finding was that the aqueous solubility of 2ME was significantly improved via both CD complexation and when 2ME was a component of a physical mixture with the CD. It was determined that all the CDs, except TriEtBCD, improved the aqueous solubility of 2ME while other derivatised CDs viz. RAMEB, HPBCD, DIMEB and TRIMEB, as well as the natural CD, γ-CD, very significantly increased the solubility of 2ME. The methylated CDs proved to be the most effective solubilisers, DIMEB displaying the greatest solubilising effect. The dissolution studies yielded markedly improved profiles for 2ME as mixtures with selected CDs, as complexes prepared by kneading and as complexes prepared by co-precipitation.

Future Work

Phase-solubility studies, developed by Higuchi and Connors,[9] would provide more insight regarding the solubilising influence of the CDs investigated in this study of 2ME. Reduction of drug crystallinity on complexation or solid dispersion with CDs definitely increased the apparent drug solubility and dissolution rate. Thus, CDs, as a result of their ability to form complexes in the dissolution medium, can enhance drug dissolution, even when there is no complexation in the solid state. These data should be viewed in the light of the future work recommended for the polymorphism section of this study, since once again particle size and dosage form variation are of utmost importance when the delivery of the drug is considered. Cyclodextrin inclusion by itself

may allow for better dissolution, but if the incorrect dosage form is chosen, then our purpose is defeated.

Since the present work has revealed new insights into the nature of CD-steroid complex crystal packing, further applications of the available crystallographic data to other included steroids is feasible. As noted earlier, if isostructurality of putative CD-steroid complexes with these known complexes is established, much useful structural information could be extracted from a single experimental PXRD pattern. (The procedure employed to do this was demonstrated earlier in this thesis in the case of the β-CD inclusion complex of 2ME).

CO-CRYSTALLISATION

The final objective of this study was to make co-crystals of nevirapine (NV) with GRAS excipients or compounds that presented themselves as good co-crystal formers. Twelve such co-crystal formers were investigated in this study. Two novel NV co-crystals, containing the GRAS co-formers *rac*-tartaric acid and saccharin, were prepared by co-precipitation methods. As far as the author is aware, these are the first reported examples of co-crystals of NV. Nevirapine, the potent inhibitor of HIV-1 reverse transcriptase, contains an amide function CO–NH and this was exploited in the design of the resulting co-crystals.[10]

Isolation and Characterisation of NVSC and NVTTA Co-crystals

The successful isolation of the co-crystals between NV and saccharin (**NVSC**) and between NV and *rac*-tartaric acid (**NVTTA**) vindicated the original proposal of using GRAS carboxylic acids as potential co-formers. Such co-crystals would not need exhaustive and separate clinical trials, barring perhaps toxicological studies.

TGA did not reveal any solvent in these co-crystals and their melting points were significantly different (223 °C for **NVSC**, 230 °C for **NVTTA**). Both melting points and PXRD traces differed quite significantly from those of the parent API and the co-crystal formers, strongly suggesting co-crystallisation, which was ultimately and definitively proven by single crystal X-ray analysis.

NVSC includes two NV molecules and one saccharin (SC) molecule in the crystal asymmetric unit (ASU) whereas **NVTTA** contains one NV and one TTA molecule in the ASU. Careful crystallographic studies were undertaken to ensure unequivocal location of H atoms that enabled the author to identify these phases as genuine co-crystals rather than salts.

In the ASU of **NVSC**, a pseudo-centrosymmetric hydrogen-bonded NV dimer is present together with a single saccharin (SC) molecule. In **NVTTA**, the ASU comprises one NV molecule and one of the enantiomers of TTA. Supramolecular homosynthon formation involving the CO-NH functions of the two NV molecules occurs in **NVSC**, which features also a supramolecular heterosynthon between NV and SC. In contrast, in **NVTTA** there is a heterosynthon between NV (providing the CO-NH) function and the co-former TTA (providing the –COOH function). This API- co-former association mode is that which was envisaged originally when the author considered using carboxylic acids as potential co-crystal formers with nevirapine.

The well-known "butterfly" conformation[10] of the NV molecule and the adoption of a boat conformation by the seven-membered ring featured in both co-crystal structures. The butterfly shape is essential for the engagement of the molecule at the reverse transcriptase inhibition sites.[11]

In co-crystal **NVSC**, the -NH function of the SC co-former acts as the hydrogen bond donor to a pyridine nitrogen atom on the nevirapine molecule. It is known that SC may alternatively behave as a weak acid when it is co-crystallized with APIs that contain an adequately basic centre and in such cases protonation of the API by saccharin may occur, giving rise to API saccharinate salts.[12] For **NVSC**, a true co-crystal was indeed formed since there was no proton transfer from the SC molecule to the NV molecule.

Dissolution of Co-crystals

Both physical mixtures **NV:SC** and **NV:TTA** as well as the co-crystals **NVSC** and **NVTTA** demonstrated an improved dissolution profile compared to untreated NV. **NVSC** passed the BP test by displaying 76.0 % dissolution after 45 min whereas

NVTTA failed the test with only 61.7 % dissolution after the same period. The melting points of the co-crystals, established as ~223 and ~228 ºC respectively by thermal analysis, were consistent with the predicted behaviour in dissolution experiments, the lower melting solid having a significantly higher dissolution rate.

Future Work

On the basis of the dissolution rate studies, we conclude that SC and TTA may be used either as co-crystal formers or as excipients in the production of dosage forms. However, the question of whether the co-former solubility is enhanced should be investigated when a dosage regimen is considered. This is suggested given the toxicity profiles of high doses of the co-former. Furthermore, the solubility and dissolution rate would be greatly dependent on the particle size of the samples included in the study.

The study of the co-crystallization potential of nevirapine, presented as part of this thesis, has laid the foundation for a more comprehensive programme that should extend to other antiretrovirals and it is suggested that an in-depth investigation of their co-crystal solubility profiles and other pharmaceutically relevant properties (e.g. flowability, compaction) be undertaken. An additional recommendation is that a series of GRAS amides should be considered as an alternative potential series of co-formers for systematic investigation of co-crystallisation with NV. Other aspects of development, such as polymorphism and scale-up, will need to be examined for each candidate co-crystal. Processes to produce co-crystals on a large scale will likely require different approaches, such as those based on ternary solubility phase diagrams. Furthermore IP, regulatory, and lifecycle management for new and old drugs will provide additional challenges as they continue through the development process.

References

1. Ireson C.R., Chander S.K., Purohi A., Perera S., Newman S.P., Parish D., Leese M.P., Smith A.C., Potter B.V.L., Reed M.J., *Br. J. Cancer*, **2004**, 90, 932-937.
2. The Medical News, *Panzem (2-methoxyestradiol) Drug a Possible Candidate for Breast Cancer Treatment*, November, **2007**, retrieved 20 December **2007**. http//www.news-medical.net/news/2007/11/02/32073.aspx?page=2,
3. Vorster C.J.J., Joubert A.M., *Cell. Biochem. Funct.*, **2010**, 28, 412-419.
4. Caira M.R., *In: Topics in Current Chemistry*, Springer-Verlag, Berlin, Heidelberg, **1998**,198, 164-208.
5. McNamara D., Childs S.L., Giordano J., Iarriccio A., Cassidy J., Shet M.S., Mannion R., O'Donnell E., Park A., *Pharm. Res.*, **2006**, 23, 1888-1897.
6. Cambridge Structural Database and Cambridge Structural Database System, Version 5.30, November **2009**, Cambridge Crystallographic Data Center, University Chemical Laboratory, Cambridge, England.
7. Smith V.J., Rougier N.M., de Rossi R.H., Caira M.R., Vico R.V., Buján E.I., Fernández, M.A., Bourne S.A., *Carbohydr. Res.*, **2009**, 344, 2388-2393.
8. Sheldrick G.M., SHELXH, *Program for Crystal Structure Solution*, Institüt für Anorganische Chemie der Universität, Tammanstrasse 4, D-3400 Göttingen, Germany, **1997**.
9. Higuchi T., Connors K.A., *Adv. Anal. Chem. Instr.*, **1965**, 4, 212-217.
10. Caira M.R., Stieger N., Liebenberg W., De Villiers M.M., Samsodien H., *Cryst. Growth and Des.*, **2007**, 8, 17-23.
11. Ding J., Das K., Moereels H., Koymans L., Andries K., Janssen P.A.J., Hughes S.H., Arnold E., *Nat. Struct. Biol.*, **1995**, 2, 407-415.
12. Prashant M.B., Nittala V.R., Rahul B., Desiraju G.R., *Chem. Commun.*, **2005**, 1073-1075.

The Appendix folder on the disk attached to the inside back cover of this thesis contains:

Appendix 1: A full list of the outcomes of recrystallisation of 2ME and 2MES from a range of solvents/solvent mixtures, as well as the results from other methods of polymorph preparation.

Appendix 2: A full list of the outcomes of cyclodextrin inclusion experiments with 2ME.

Appendix 3: A full list of the outcomes of co-crystal formation experiments with NV.

Appendix 4: Supplementary crystallographic information for solved structures in this thesis is saved in a subfolder named according to the designation used in this thesis. The files may be viewed with WORDPAD or NOTEPAD.

Appendix 5: Supplementary crystallographic information for the cyclodextrin complex TRIB2ME. Included is a table with the hydrogen bonds, a table with the primary methoxyl and glycosidic torsion angles, a table with the geometrical parameters of the O4-heptagon in the four independent TRIMEB molecules in the crystal of TRIB2ME and finally a table illustrating the planarity of the O4-heptagons.

Hydrogen bonding interactions for TRIB2ME with symmetry codes

Hydrogen bond	H···A (Å)	D···A (Å)	D-H···A (°)	Symmetry codes
O19A- H19A••• O4A2	2.23	3.062(8)	169	
O19B- H19B ••• O4B1	2.35	3.184(8)	170	
O22B- H22B ••• O20B	2.28	2.722(1)	113	
O19C- H19C ••• O4C2	2.08	2.890(8)	162	
O22C- H22C ••• O20C	2.28	2.695(9)	111	
O19D-H19D ••• O152	2.30	3.095(2)	158	
O22D-H22D ••• O5B5	2.34	2.873(1)	122	-1+x,y,-1+z
O22D-H22D••• O20D	2.27	2.676(1)	110	
C6D6 - H2 ••• O5D5	2.33	3.048(1)	129	
C21A- H21B ••• O6D4	2.58	3.531(1)	163	x,1+y,z
C21A- H21C ••• O3B3	2.54	3.253(1)	130	x,1+y,z
C1A1- H1A1 ••• O3B4	2.58	3.353(1)	134	-1+x,1+y,z
C4A1- H4A1 ••• O6A1	2.46	2.838(1)	102	
C6A1- H6A4 ••• O5A7	2.47	3.277(1)	139	
C9A2- H9A6 ••• O2A2	2.45	3.009(1)	116	
C2A3- H2A3 ••• O5C3	2.51	3.502(1)	171	
C4A3- H4A3 ••• O6A3	2.44	2.803(1)	101	
C5A3- H5A3 ••• O4A4	2.47	2.821(1)	100	
C6A3- H6A8 ••• O5A2	2.37	3.077(1)	128	
C6A3- H6A8 ••• O6A2	2.50	3.463(1)	163	
C7A3-H7AX ••• O3C4	2.57	3.545(1)	174	
C5A4- H5A4 ••• O4A5	2.37	2.802(1)	105	
C6A4- H6A9 ••• O4A4	2.57	2.978(1)	104	
C8A4-H8AY ••• O3B1	2.59	3.492(1)	153	1+x,y,z
C9A4-H9AZ ••• O2A4	2.47	2.955(1)	110	
C4A5-H4A5•••O6A5	2.54	2.887(1)	100	
C5A5- 5A5 ••• O4A6	2.46	2.830(1)	101	
C6A5-H6AZ ••• O5A4	2.30	3.099(1)	137	
C1A6-H1A6 ••• O3A7	2.50	3.118(1)	120	
C5A6-H5A6 ••• O4A7	2.50	2.850(8)	100	
C6A6-H6AB ••• O5A5	2.32	3.072(1)	132	
C8A6-H8AD ••• O2C6	2.51	3.346(1)	143	1+x,y,1+z
C1A7-H1A7 ••• O6A1	2.48	3.306(1)	139	
C9A7-H9AI ••• O2A7	2.54	3.098(2)	116	
C4B -H4B ••• O5B1	2.54	3.467(1)	164	1+x,y,z
C9B1- H9B3 ••• O2B1	2.50	3.013(1)	112	
C1B2- H1B2 ••• O3B3	2.58	3.152(1)	116	
C2B2- H2B2 ••• O5D3	2.52	3.499(1)	166	
C5B2- H5B2 ••• O4B3	2.40	2.778(1)	102	
C6B2- H6B6 ••• O5B1	2.37	3.055(1)	126	
C6B2- H6B6 ••• O6B1	2.43	3.380(1)	161	

C5B3- H5B3 ••• O4B4	2.39	2.814(1)	105	
C8B3- H8B8 ••• O3A2	2.51	3.392(1)	149	1+x,-1+y,z
C9B3- H9B9 ••• O2B3	2.47	2.951(1)	110	
C4B4- H4B4 ••• O6B4	2.55	2.895(1)	100	
C5B4- H5B4 ••• O4B5	2.51	2.868(1)	101	
C6B4- H6BX ••• O5B3	2.28	3.079(1)	137	
C5B5- H5B5 ••• O4B6	2.42	2.823(8)	103	
C6B5- H6BZ ••• O5B4	2.38	3.066(1)	126	
C1B6- H1B6 ••• O6B7	2.50	3.336(1)	140	
C2B6- H2B6 ••• O5D6	2.58	3.540(1)	162	x,y,1+z
C9B6- H9BF ••• O2B6	2.50	3.096(2)	119	
C4B7- H4B7 ••• O6B7	2.42	2.827(1)	104	
C21C - H21I ••• O6D7	2.60	3.521(1)	157	
C51- H5C1 ••• O4C1	2.49	2.845(1)	101	
C7C1- H7C3 ••• O19C	2.49	3.316(1)	142	
C8C1- H8C3 ••• O3C1	2.47	3.055(1)	118	
C1C2- H1C2 ••• O6C2	2.58	2.933(1)	101	
C4C2- H4C2 ••• O2C1	2.48	3.053(1)	116	
C5C2- H5C2 ••• O4C2	2.53	2.873(1)	100	
C6C2- H6C6 ••• O5C3	2.35	3.174(1)	140	
C8C2- H8C4 ••• O3C3	2.60	3.376(1)	136	
C8C2- H8C4 ••• O4C3	2.58	3.127(1)	115	
C9C2- H9C6 ••• O2C2	2.58	3.164(1)	118	
C1C3- H1C3 ••• O6A3	2.58	3.479(1)	149	
C6C3- H6C7 ••• O5C4	2.49	3.321(1)	142	
C1C4- H1C4 ••• O6C4	2.49	2.876(1)	102	
C6C4-H6CX ••• O5C5	2.44	3.229(1)	137	
C1C6-H1C6 ••• O6C6	2.54	2.927(1)	103	
C6C6- H6CB ••• O5C7	2.45	3.175(1)	130	
C9C6- H9CF ••• O2C6	2.54	3.106(1)	117	
C6C7- H6CC ••• O5C1	2.42	3.308(1)	148	
C9C7- H9CI ••• O2C7	2.53	3.125(1)	119	
C18D- H18J ••• O19D	2.09	2.710(3)	120	
C5D1-H5D1 ••• O4D2	2.50	2.868(1)	101	
C6D1-H6D3 ••• O5D7	2.33	3.241(1)	153	
C4D2-H4D2 ••• O6D2	2.47	2.870(1)	103	
C6D2-H6D6 ••• O5D1	2.33	3.086(1)	132	
C6D2-H6D6 ••• O6D1	2.45	3.351(1)	150	
C4D3-H4D3 ••• O6B2	2.47	3.381(1)	151	
C6D3-H6D7 ••• O5D2	2.49	3.323(1)	142	
C8D3-H8D8 ••• O2A2	2.55	3.375(1)	142	x,-1+y,z
C9D3-H9D9 ••• O2D3	2.57	3.150(1)	118	
C1D4-H1D4 ••• O3D5	2.38	3.063(1)	124	

C5D4-H5D4 ••• O4D5	2.44	2.817(1)	102	
C6D4-H6DX••• O5D3	2.36	3.224(1)	145	
C8D4-H8DZ••• O3D4	2.56	3.125(1)	116	
C1D5-H1D5 ••• O22D	2.53	3.308(1)	135	1+x,y,z
C5D5-H5D5 ••• O4D6	2.35	2.750(1)	103	
C9D5-H9DC••• O2D5	2.47	3.083(1)	120	
C4D6-H4D6 ••• O6D6	2.50	2.847(1)	100	
C5D6-H5D6 ••• O4D7	2.44	2.818(1)	101	
C4D7-H4D7 ••• O6D7	2.52	2.881(1)	101	
C6D7-H6DB••• O5D6	2.49	3.176(1)	126	
C321#-H531#••• O2C1	2.55	3.163(1)	121	-1+x,y,z
C328#-H546# ••• O6D3	2.46	3.340(2)	150	
O1-H1•••O6D5				
O19D-H19D•••O1				

Host-Host intermolecular interactions (C-H•••O)
Host-Host intramolecular interactions (C-H•••O)
Guest-Guest intramolecular interactions (C-H•••O) and (O-H•••O)
Host-Guest intermolecular interactions (C-H•••O) and (O-H•••O)
Host-Water interactions (O-H•••O)
Guest-Water interactions (C-H•••O

Principal torsion angles of TRIB2ME

CD	ω(°)a	ω(°)b	Φ(°)	Ψ(°)	Θ_1(°)	Θ_2(°)
A1	-74.4	-	88.7	108.1	49.5	-54.0
A2	62.4	-	102.9	146.3	50.6	-55.8
A3	-80.0	-	95.8	101.2	50.3	-53.2
A4	81.7	-	101.6	152.9	44.6	-60.7
A5	-70.5	-	98.7	142.2	50.7	-54.4
A6	-66.5	-	90.4	97.2	52.2	-57.4
A7	74.8	-	111.9	164.5	44.2	-45.9
B1	59.9	-	102.8	145.8	50.0	-54.3
B2	-78.9	-	95.3	99.0	50.4	-55.3
B3	79.0	-	103.3	151.4	41.6	-59.2
B4	-69.7	-	96.1	142.5	52.2	-55.7
B5	-70.8	-	91.0	103.1	49.9	-58.3
B6	66.5	-	120.4	156.5	46.8	-49.8
B7	-72.6	-	89.8	108.6	49.4	-53.3
C1	65.6	-	106.3	134.0	51.5	-55.7
C2	-72.1	-	92.3	96.7	48.8	-52.7
C3	64.1	-	105.3	156.9	48.4	-50.7
C4	-66.4	-	97.3	126.6	58.3	-54.8
C5	67.7	-	108.7	137.5	51.1	-54.7
C6	-79.3	-	92.6	110.8	47.4	-51.7
C7	65.6	-	104.5	149.4	52.1	-51.8
D1	77.4	-	97.8	139.8	52.9	-57.6
D2	-69.5	-	96.0	123.5	57.6	-53.6
D3	65.9	-	111.7	155.8	49.6	-50.8
D4	-64.6	-	85.4	94.7	46.7	-55.5
D5	75.3	-62.6	102.3	149.9	47.2	-57.8
D6	-75.0	-	97.1	128.0	47.7	-54.3
D7	-67.6	-	98.5	134.6	51.0	-53.5

Geometrical parameters of the O4 polygon for TRIB2ME

Glucose unit	*r*(Å)	*l*(Å)	*a*(°)	*d*(Å)	*t*(°)
A1	5.25	4.49	137.8	0.3362 (0.0042)	-14.0
A2	4.74	4.43	120.5	0.4157 (0.0041)	-10.3
A3	5.25	4.35	131.3	0.1098 (0.0037)	7.4
A4	5.05	4.56	125.8	-0.3712 (0.0041)	14.3
A5	5.14	4.44	124.9	-0.0414 (0.0041)	-20.1
A6	5.08	4.53	135.3	0.4442 (0.0040)	-1.5
A7	4.91	4.12	118.7	-0.2209 (0.0041)	24.2
Mean	***5.06***	***4.42***	***127.8***	***0.2771(0.0041)***	***13.1***
B1	4.83	4.40	120.4	0.4055 (0.0043)	-10.6
B2	5.29	4.37	132.1	0.1440 (0.0039)	5.9

B3	5.00	4.57	126.8	-0.3598 (0.0043)	15.5
B4	5.11	4.49	123.4	-0.0872 (0.0043)	-17.4
B5	5.19	4.51	133.1	0.4609 (0.0040)	-6.2
B6	4.97	4.17	123.3	-0.1719 (0.0042)	26.1
B7	5.09	4.44	134.9	-0.3916 (0.0046)	-12.6
Mean	***5.07***	***4.42***	***127.7***	***0.2887(0.0042)***	***13.5***
C1	4.98	4.45	117.8	0.4079 (0.0044)	0.8
C2	4.61	4.30	126.8	-0.1490 (0.0043)	10.6
C3	5.44	4.49	133.1	-0.2731 (0.0042)	0.2
C4	5.23	4.48	131.7	0.2224 (0.0043)	-15.2
C5	4.78	4.39	118.2	0.2021 (0.0044)	4.9
C6	4.96	4.35	128.7	-0.3067 (0.0046)	15.4
C7	5.50	4.50	139.9	-0.1036 (0.0045)	-20.6
Mean	***5.07***	***4.42***	***127.9***	***0.2378(0.0044)***	***9.7***
D1	5.13	4.55	130.9	-0.0343 (0.0048)	-10.5
D2	4.99	4.52	127.6	-0.0942 (0.0046)	6.1
D3	5.21	4.29	122.5	0.1846 (0.0042)	8.0
D4	5.26	4.44	139.7	-0.0317 (0.0040)	-15.3
D5	4.71	4.39	122.3	-0.1930 (0.0044)	9.3
D6	5.24	4.44	128.2	0.1850 (0.0044)	-3.9
D7	5.23	4.48	127.3	-0.0165 (0.0048)	5.6
Mean	***5.11***	***4.44***	***128.4***	***0.1056 (0.0046)***	***8.4***

Intersaccharidic bond angle, O2(n)···O3(n-1) distances and the tilt angle for TRIB2ME

CD	φ(°)	O2(n)···O3(n-1) (Å)	τ_2(°)
A1	113.6	3.42	+10.20 (0.45)
A2	117.9	3.46	+24.97 (0.41)
A3	116.8	3.31	+15.70 (0.37)
A4	116.5	3.51	+43.34 (0.32)
A5	117.2	3.49	+16.40 (0.37)
A6	115.7	3.49	+9.12 (0.38)
A7	119.6	3.91	+50.23 (0.23)
B1	117.1	3.49	+23.75 (0.41)
B2	116.7	3.33	+15.45 (0.39)
B3	117.0	3.49	+43.79 (0.32)
B4	117.7	3.55	+17.98 (0.38)
B5	116.4	3.41	+9.31 (0.36)
B6	118.9	3.51	+45.53 (0.24)
B7	114.5	3.45	+10.96 (0.48)
C1	115.1	3.23	+34.99 (0.37)
C2	119.1	3.66	-5.99 (0.50)
C3	117.2	3.24	+31.07 (0.26)
C4	116.5	3.27	+24.03 (0.31)

Cyclodextrin inclusion complex preparation with 2ME as potential guest using various methods

Method 1[i]: Neat Grinding for 1 hour		
CD	**Ratio (H:G)**	**Result**
α-CD	1:1	Mixture
β-CD	1:1	Mixture
γ-CD	1:1	Amorphous pattern
DIMEB	1:1	Mixture
TRIMEB	1:1	Mixture
RAMEB	1:1	Mixture
HPBCD	1:1	Mixture
TRIMEA	1:1	Mixture
TRIAcBCD	1:1	Mixture
TRIAcGCD	1:1	Mixture
TRIEtBCD	1:1	Mixture
Method 2[i]: Kneading into paste with water for 1 hour		
CD	**Ratio (H:G)**	**Result**
α-CD	1:1	Mixture
	2:1	Mixture
β-CD	1:1	Mixture
	2:1	Complex
γ-CD	1:1	Mixture
	2:1	Mixture
	3:2	Mixture
DIMEB	1:1	Mixture
TRIMEB	1:1	Mixture
RAMEB	1:1	Complex
HPBCD	1:1	Complex
	2:1	Mixture
	3:2	Mixture
TRIMEA	1:1	Mixture
	2:1	Mixture
TRIAcBCD	1:1	Mixture
TRIAcGCD	1:1	Mixture
TRIEtBCD	1:1	Mixture

Method 3[ii]: Slurry method		
Exp.	**Ratio (H:G)**	**Result**
α-CD		
4°C	1:1	No complex
RT	1:1	No complex
SC	1:1	No complex
60°C	1:1	No complex
4°C	2:1	No complex
RT	2:1	No complex
SC	2:1	No complex
60°C	2:1	No complex
β-CD		
4°C	1:1	No complex
RT	1:1	No complex
SC	1:1	No complex
60°C	1:1	No complex
4°C	2:1	No complex
RT	2:1	Mixture complex and no complex
SC	2:1	Complex
γ-CD		
4°C	1:1	No complex
RT	1:1	No complex
SC	1:1	No complex
60°C	1:1	No complex
4°C	2:1	No complex
RT	2:1	No complex
SC	2:1	No complex
60°C	2:1	No complex
4°C	3:2	No complex
RT	3:2	No complex
SC	3:2	No complex
60°C	3:2	No complex
TRIMEB		
4°C	1:1	No complex
RT	1:1	No complex

SC	1:1	No complex
60 °C	1:1	Complex
DIMEB		
4°C	1:1	No complex
RT	1:1	No complex
SC	1:1	No complex
60°C	1:1	Complex
TRIMEA		
4°C	1:1	No complex
RT	1:1	No complex
SC	1:1	No complex
60°C	1:1	No complex
40°C	1:1	No complex
TRIAcBCD		
4°C	1:1	No complex
RT	1:1	No complex
SC	1:1	No complex
60°C	1:1	No complex
TRIAcGCD		
4°C	1:1	No complex
RT	1:1	No complex
SC	1:1	No complex
60°C	1:1	No complex
TRIEtBCD		
4°C	1:1	No complex
RT	1:1	No complex
SC	1:1	No complex
60°C	1:1	No complex
HPBCD		
4°C	1:1	No complex
RT	1:1	No complex
SC	1:1	No complex
60°C	1:1	No complex
4°C	2:1	No complex
RT	2:1	No complex
SC	2:1	No complex

60°C	2:1	No complex
4°C	3:2	No complex
RT	3:2	No complex
SC	3:2	No complex
60°C	3:2	No complex

[i] Materials prepared using methods 1 and 2 were analysed using PXRD.

[ii] Slurries were made with water at given ratios, stirred for 24 hrs at RT and at 60 ºC for β-CD since β-CD solubility is greater at higher temperatures. Then slow evaporation (RT), rapid cooling (4 ºC), slow cooling (SC) and heating at 60 ºC were employed for crystal growth to occur; resulting crystals were analysed by single crystal X-ray diffraction and thereafter PXRD to determine bulk consistency.